Alma Mater Studiorum – Università di Bologna

DOTTORATO DI RICERCA IN

INGEGNERIA CIVILE E AMBIENTALE

Ciclo XXVI

Settore Concorsuale di afferenza: 08/B1

Settore Scientifico disciplinare: ICAR/07

TITOLO TESI

GEOTECHNICAL CHARACTERIZATION OF MIXED SANDY AND SILTY SOILS USING PIEZOCONE TESTS: ANALYSIS OF PARTIAL DRAINAGE PHENOMENA AND RATE EFFECTS ON THE EXPERIMENTAL SOIL RESPONSE

Presentata da: María Fernanda García Martínez

Coordinatore Dottorato	**Relatore**
Prof. Ing. Alberto Lamberti	**Dott. Ing. Laura Tonni**

Esame finale anno 2014

To my mother

Acknowledgements

First of all I would like to acknowledge the support and guidance I received from my supervisor Dr. Laura Tonni throughout this study. I really admire her tenacity, dedication and achievements in the field of Geotechnical Engineering. At the same time I would like to thank Professor Guido Gottardi for his guidance, encouragement and valuable suggestions. I really appreciate all their helps. The contributions of Dr. Gianfranco Marchi and Dr. Massimo Romagnoli are also greatly appreciated.

I wish to thank all the special people I have met in Bologna during the last three years, from whom I received their friendship and help in the most stressful times.

Finally, I would like to give thanks to my mother, for her unconditional love, support and encouragement throughout my lifetime.

Abstract

The cone penetration test (CPT), together with its recent variation (CPTU), has become the most widely used in-situ testing technique for soil profiling and geotechnical characterization. The knowledge gained over the last decades on the interpretation procedures in sands and clays is certainly wide, whilst very few contributions can be found as regards the analysis of CPT(u) data in intermediate soils.

Indeed, it is widely accepted that at the standard rate of penetration (v = 20 mm/s), drained penetration occurs in sands while undrained penetration occurs in clays. However, a problem arise when the available interpretation approaches are applied to cone measurements in silts, sandy silts, silty or clayey sands, since such intermediate geomaterials are often characterized by permeability values within the range in which partial drainage is very likely to occur. Hence, the application of the available and well-established interpretation procedures, developed for 'standard' clays and sands, may result in invalid estimates of soil parameters.

This study aims at providing a better understanding on the interpretation of CPTU data in natural sand and silt mixtures, by taking into account two main aspects, as specified below:

1) Investigating the effect of penetration rate on piezocone measurements, with the aim of identifying drainage conditions when cone penetration is performed at a standard rate. This part of the thesis has been carried out with reference to a specific CPTU database recently collected in a liquefaction-prone area (Emilia-Romagna Region, Italy).
2) Providing a better insight into the interpretation of piezocone tests in the widely studied silty sediments of the Venetian lagoon (Italy). Research has focused on the calibration and verification of some site-specific correlations, with special reference to the estimate of compressibility parameters for the assessment of long-term settlements of the Venetian coastal defences.

Table of contents

CHAPTER 1: INTRODUCTION

1.1. Background

The cone penetration tests (CPT/CPTu) are widely used in situ testing devices for site characterization. The basic measurements obtained are the cone penetration resistance (q_c), the sleeve friction (f_s) and in the case of CPTu, the pore water pressure (u). During CPT at standard penetration rate of 20 mm/s, it is well accepted that fully drained conditions prevail for sands and fully undrained conditions prevail for clays. However, CPT interpretation in intermediate soils, including silty soils and a large variety of mixed soil types, is a rather complicated task since partially drained conditions may pertain at 20 mm/s. Hence, interpreting properties of intermediate soils with methods developed for either drained or undrained penetration, may induce incorrect estimates of soil parameters.

In recent years, the issue of partial drainage conditions during cone penetration tests has been tackled by several researchers (e.g. Schnaid *et al*., 2004; Randolph and Hope, 2004; Schneider *et al*., 2007), all emphasizing that the preliminary evaluation of drainage conditions is of crucial importance in order to properly interpret the in situ soil response.

As observed by Randolph and Hope (2004), a simple and effective procedure to analyse the effect of partial drainage on piezocone measurements and to detect the transition point from undrained to partially drained and drained responses is to conduct penetration tests at different penetration rates. The influence of penetration rate and soil drainage conditions (horizontal coefficient of consolidation) on the consolidation conditions can be captured by the non-dimensional penetration rate (Finnie and Randolph, 1994), $V = v \cdot d/c_h$, where v is the velocity, d is the diameter of the cone and c_h is the coefficient of consolidation. Normalization of penetration rate and CPTU measurements accounts for data at different depths and enables to derive trend curves of cone penetration resistance and excess pore water pressure. Drained conditions prevail during slow penetration, whereas undrained conditions prevail during rapid penetration. Within this context, experience has been mainly accumulated in centrifuge tests using laboratory reconstituted samples (kaolin clay and silty clay). However, there have been less contributions based on results from field tests and full size penetrometers (e.g. Kim *et al.*, 2008; Tonni and Gottardi, 2009; Schnaid *et al.*, 2010; Suzuki *et al*., 2012).

Over the last decades, the silty soils of the Venetian lagoon (Italy) have been thoroughly investigated. The analysis of the large amount of data collected over the last years at the Treporti test site (Venice), confirmed the great potential of cone penetration test as an in-situ method, especially for stratigraphic profiling of the predominantly silty sediments of the Venetian lagoon. However, the experience gained on the interpretation of piezocone data also revealed significant

limitations of the existing approaches for the characterization of such sediments of the Venetian lagoon, thus suggesting a critical review of empirical and theoretical formulations in relation to their applicability to such soils (Tonni and Gottardi 2011). Indeed, due to the essentially silty nature of such subsoil, partial drainage is very likely to occur during cone penetration at the standard penetration rate (20 mm/s). Accordingly, more suitable site-specific correlations, with special reference to compressibility properties, have been recently proposed (e.g. Tonni *et al*., 2010; Tonni and Gottardi, 2011; Bersan *et al*., 2012; Tonni and Simonini, 2013).

1.2. Aims and objectives

The aims of this research are to provide a better insight into CPTU-based geotechnical characterization of intermediate soils (silts, sandy silts, silty or clayey sands), taking into account that in such intermediate materials partial drainage conditions are very likely to occur during cone penetration. This will be attained by the following objectives:

- Execution of a set of piezocone tests with various penetration rates in silty sand deposits of the Emilia-Romagna Region (Italy).
- Interpretation of such cone penetration data, together with a number of associated dissipation test measurements, according to advanced procedures recently proposed in the literature.
- Interpretation of a set of offshore piezocone tests assembled over the last years at the three Venetian lagoon inlets (Italy), carried out prior to the recent construction of some coastal structures along the coastline. Classification of Venetian sediments from piezocone measurements has been performed using some well-known classification charts.
- Prediction of the long-term response of Venetian coastal defences using a one-dimensional settlement method in conjunction with a secondary compression coefficient profile determined by the available offshore piezocone tests and based on a formulation recently calibrated on field data from a Test Site located in the Venetian lagoon area.
- Modelling of the long-term response of Venetian coastal defences using a finite element approach in conjunction with an appropriate constitutive formulation, specifically intended for simulating the creep behaviour of soft soils (Vermeer and Neher, 1999); calibration of the constitutive parameters using some CPTU-based empirical correlations developed within the research project carried out at the Treporti Test Site.
- Validation of the approach comparing the estimated settlements with vertical displacement measurements provided by a very accurate monitoring system, based on an advanced technique known as Persistent Scatterer Interferometry.

1.3. Outline of the thesis

- **Chapter 1** introduces the background of the research, objectives and outline of the thesis.
- **Chapter 2** presents a review regarding the cone penetration test (CPT) interpretation.
- **Chapter 3** presents the results of a field testing programme of cone penetration test conducted at different penetration rates in liquefaction-prone silty sand deposits of the Emilia-Romagna Region (Italy). Such results are interpreted according to advanced procedures. The drainage (backbone) curves obtained, relating the variation of the normalized penetration resistance or excess pore water pressure with the normalized penetration rate are used to identify the degree of drainage.
- **Chapter 4** introduces a brief description of the interventions for safeguarding Venice from high tides. It describes the geological characteristics of Venice lagoon soil and the geotechnical investigation carried out during the last decades in the area, with special reference to the in situ piezocone campaigns performed at the Treporti Test Site (TTS).
- **Chapter 5** presents the characterization of Venetian silty soils from CPTU carried out at the TTS: soil classification and assessment of soil properties.
- **Chapter 6** extends the investigation and presents a new database of offshore piezocone tests carried out near the three lagoon inlets, in relation to the construction of some coastal defences. The stratigraphic condition of the lagoon basin in these different areas is derived, as well as the relevant geotechnical parameters of the different soil units, with special reference to compressibility properties. The long-term response of such structures is also performed using a 1-D settlement method using two site-specific empirical correlations recently calibrated on Treporti field data to determine the secondary compression coefficient profile. Finally, the approach is validated comparing the estimated settlements with those measured by advanced techniques.
- **Chapter 7** presents a review of the Soft Soil Creep (SSC) model formulation and the numerical results of the modelling of the long-term response of Venetian coastal defences using the finite element code PLAXIS. The SSC model is used for simulating the creep behaviour of such soils and the results are compared with settlement measurements provided by advanced techniques.
- **Conclusions.**

CHAPTER 2: CONE PENETRATION TEST

2.1 Introduction

Over the last few decades, the electronic cone penetration test (CPT) has been established as one of the most widely used in situ methods for site characterization. The CPT major advantages are:

- Quick and near continuous profiling
- Repeatable and reliable data
- Economical
- Strong theoretical background for interpretation

These advantages have led to a continuous increase in the use and application of the CPT worldwide. Nevertheless, the CPT may also have some disadvantages:

- Skilled operators needed
- No soil sampling
- Relatively high fund investment
- Can be restricted in gravel/cemented soils

Despite it is not possible to get soil samples during the test, it is possible to obtain them using CPT pushing equipment. As recommended by Robertson and Cabal (2012) in the Guide to Cone Penetration Testing, it is convenient to first perform several CPT soundings to define the stratigraphic profile and obtain initial estimates of geotechnical parameters and then proceed with selective sampling.

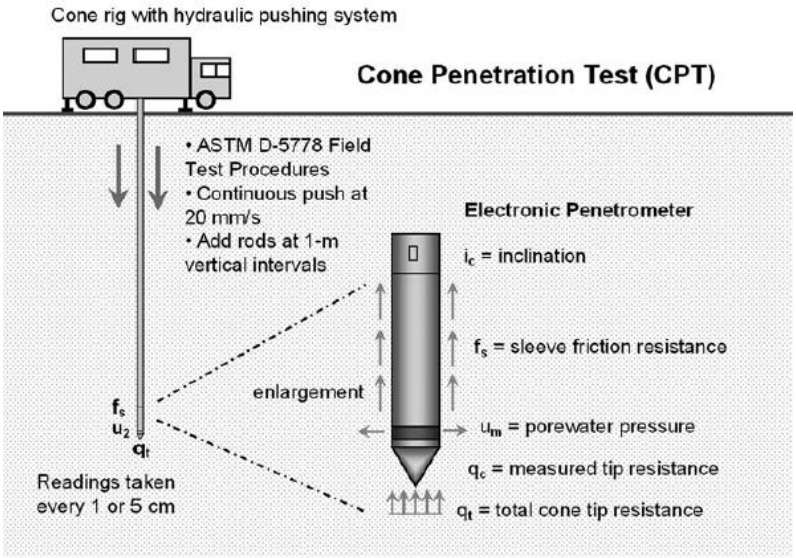

Figure 2.1: CPT per ASTM D 5778 Procedures (from Mayne, 2007*a*)

Important developments have been carried out in the experimental and theoretical knowledge of the process of the CPT penetration and the effect of soil parameters. Since real soils are very complex materials and difficult to be well-captured in a simple model, semi-empirical correlations tend to dominate in practice even though nearly all are well supported by theory (Robertson, 2012).

2.2 Test equipment and Procedures

A CPT system consists of the following components: an electrical penetrometer, a hydraulic pushing system with rods, depth recorder, cable or transmission device and data acquisition system. Most systems used nowadays include pore pressure measurements (i.e., CPTu). The measure of the shear-wave velocity (Robertson *et al.* 1986*b*) is also becoming popular (i.e., SCPTu) and provides a useful insight into correlations between CPT results and soils modulus. Therefore, it is common to see a profile combining cone penetration resistance (q_c), sleeve friction (f_s) and pore pressure (u) and sometimes shear-wave velocity (V_s). Furthermore, if dissipation tests are performed, the consolidation characteristics can be evaluated.

The penetrometers are usually available in two standard sizes: (1) with a base area of 10 cm^2 (diameter = 35.7 mm) and (2) with a base area of 15 cm^2 (diameter = 44 mm). Whereas the 10-cm^2 size is the original standard size, the 15-cm^2 version has been found by numerous commercial companies to be stronger for routine profiling.

Depending on the types of soils being tested, the porous filter is usually located at the apex or midface (u_1 position) or at the shoulder (u_2 position) just behind the cone tip. It can be also positioned behind the sleeve (u_3 position).

The u_2 position is required by international standards for the proper correction of measured cone tip resistance to total resistance (Campanella and Robertson, 1988). The effect of the ambient pore pressure acting on the shoulder just behind the cone and on the ends of the friction sleeve is often referred to as the unequal end-area effect (Campanella *et al.* 1982). Whilst many commercial cones have equal end-area friction sleeves, the unequal end-area effect is always present for the cone resistance and has to be corrected.

This correction can be important in soft-fine grained soils where q_c is low compared to the high pore water pressure u_2 due to the undrained penetration:

$$q_t = q_c + u_2(1 - a) \tag{2.1}$$

where a is the net area ratio determined from laboratory calibration. It typically ranges between 0.70 and 0.85. In sandy soils, where q_c is large relative to pore water pressure u_2, this correction may be insignificant.

Despite the increasing popularity of the CPTu, on on-shore testing the accuracy and precision of pore pressure measurements are not always reliable and repeatable due to loss of saturation of the pore pressure element (Robertson, 2009). Before each cone penetration test, the porous element and sensor must be saturated with silicon oil or glycerin (Campanella *et al*., 1982) and sometimes with grease. However, for onshore projects the cone often penetrates some meters through unsaturated soil before it reaches saturated soil. In this case, the cone pore pressure sensor may be de-saturated because of suction if the unsaturated soil is either clay or dense silty sand. Although the loss of saturation has been minimized by the use of viscous liquids, it has not totally removed the problem.

An additional complication is when the cone penetrates through saturated dense silty and or very stiff overconsolidated clay. In this way, due to the dilative nature of the soil, the u_2 measured can become negative causing loss of saturation in the sensor.

Although it may be difficult to evaluate when the cone is fully saturated, in ground conditions where the soil is mainly soft and the water level is close to the surface it is possible to obtain good pore water pressure measurements (Robertson, 2012).

Despite pore pressure measurements for onshore testing may be less reliable than cone resistance, it is suggested to obtain them. Pore pressure measurements allow correction to q_t for unequal end area effects and provide a qualitative evaluation of drainage conditions during the test and helps in evaluating soil classification (Robertson, 2012). In addition, dissipation tests allow evaluating consolidation characteristics.

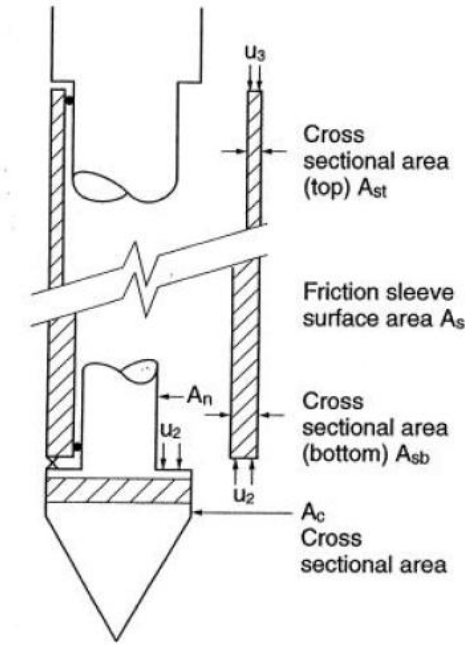

Figure 2.2: Unequal end area effects on friction sleeve and cone tip (from Robertson and Cabal, 2010)

It is well-known that sleeve friction f_s measurements are in general less reliable in comparison to cone resistance in most soft fine-grained soils. The inaccuracy in f_s measurement is mainly due to the unequal end area effects, surface roughness of the sleeve, tolerance in dimensions between the cone and sleeve and load cell design and calibration (Lunne and Andersen, 2007).

In the 1980's subtraction cone designs became popular because of the improved robustness. In subtraction cones the f_s is derived by subtracting the tip load from the total tip force plus sleeve. Nevertheless, in subtraction cone designs any zero load instability of the load cells results in a loss of accuracy in the calculated sleeve friction in soft soils. Hence, for accurate sleeve friction measurements in soft soils, it is recommended that cones have independent load cells (Robertson, 2012). Figure 2.3 shows designs for cone penetrometers using either separated load cells or subtraction load cells.

With good quality control (surface roughness, zero load readings and tolerances) and design (independent load cells and equal end area friction sleeve), accuracy in sleeve friction measurements could be obtained (e.g. Robertson, 2009). However, sleeve friction measurements will be in general less accurate than cone resistance in soft fine-grained materials (Robertson, 2009).

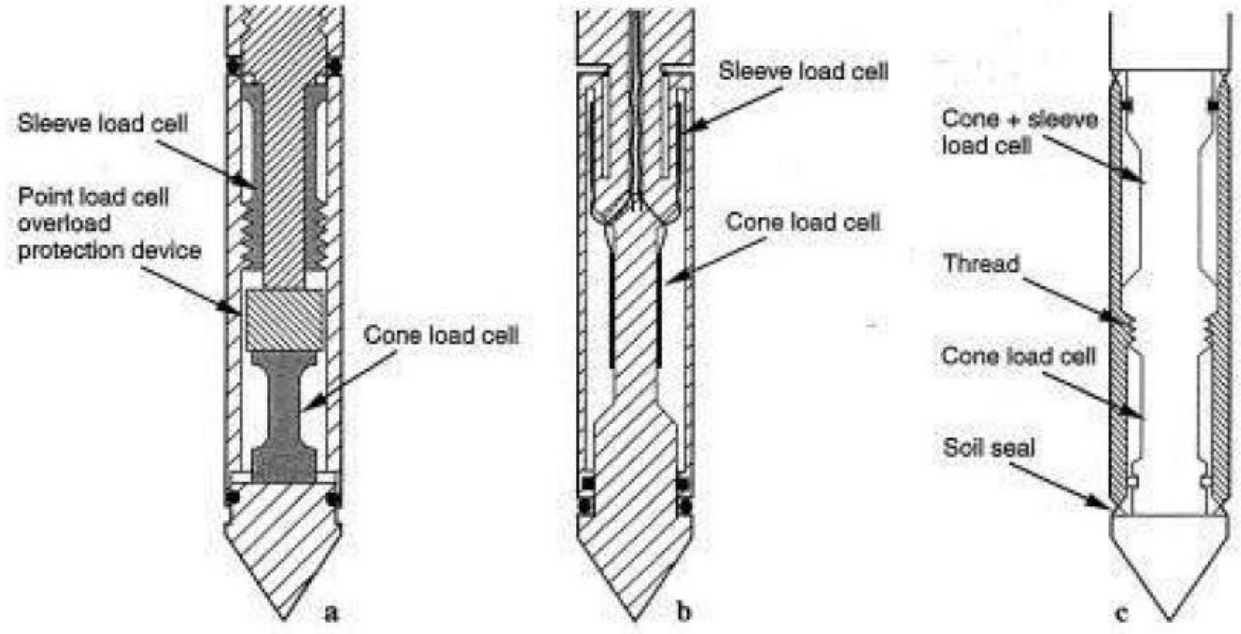

Figure 2.3: Design for CPTs: a) Tip and sleeve friction load cells in compression, b) Tip load cell in compression and sleeve friction load cell in tension, c) subtraction type load cell design (Lunne *et al.*, 1997; Robertson and Cabal, 2012)

2.3 CPT interpretation

2.3.1 Soil type

The parameters obtained from piezocone penetration tests (CPTu) are commonly used to obtain soil stratigraphy and identification of soil type. This has been carried out using charts that associate measured parameters to soil type.

Pioneer charts using cone resistance q_c and friction ratio R_f (=f_s /q_c·100%) were proposed by Schmertman (1978) and Douglas and Olsen (1981). However, the original chart proposed by Robertson *et al*. (1986*a*), based on q_t and R_f (Figure 2.4), became very popular. This non-normalized chart defines 12 soil behaviour type (SBT) zones and uses the corrected cone resistance q_t, which is nearly equal to q_c in coarse-grained soils but in soft fine-grained soils the difference among them would increase.

The normalized chart proposed by Robertson (1990) uses normalized cone resistance Q_t ($=(q_t-\sigma_{v0})/\sigma'_{v0}$) and normalized friction ratio F_r ($=\lfloor f\ /(q_t-\sigma_{v0})\rfloor\cdot 100\%$) and defines 9 zones. The difference between this early charts proposed by Robertson led him to suggest an update on the first chart (e.g. Robertson, 2010*a*), as is shown in Figure 2.5. As can be seen, both are dimensionless and define 9 SBT zones.

These CPT-based classification charts are termed as Soil Behaviour Type (SBT) charts, since the cone responds to the in situ mechanical behaviour of the soil and not to classification based on grain size distribution and soil plasticity carried out on disturbed samples (e.g. Unified Soil Classification System, USCS). Although CPT-based SBT often agrees well with USCS-based classification, differences arise when classifying mixed soils (e.g. Robertson 2009).

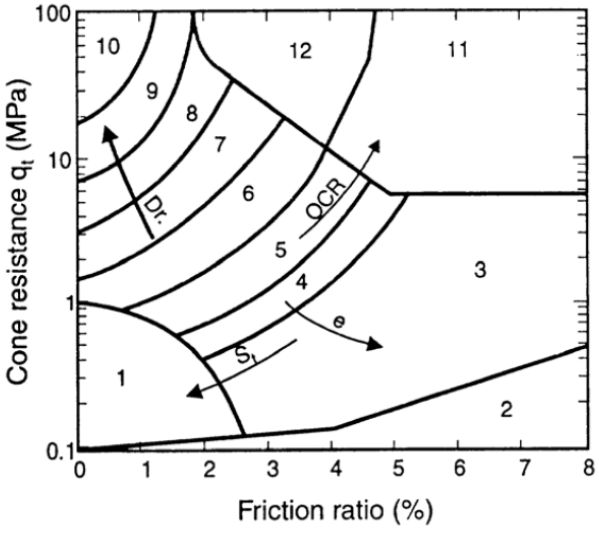

Zone	Soil Behavior Type
1	Sensitive fine grained
2	Organic material
3	Clay
4	Silty Clay to clay
5	Clayey silt to silty clay
6	Sandy silt to clayey silt
7	Silty sand to sandy silt
8	Sand to silty sand
9	Sand
10	Gravelly sand to sand
11	Very stiff fine grained*
12	Sand to clayey sand*

* Overconsolidated or cemented

Figure 2.4: SBT by Robertson *et al.* (1986a)

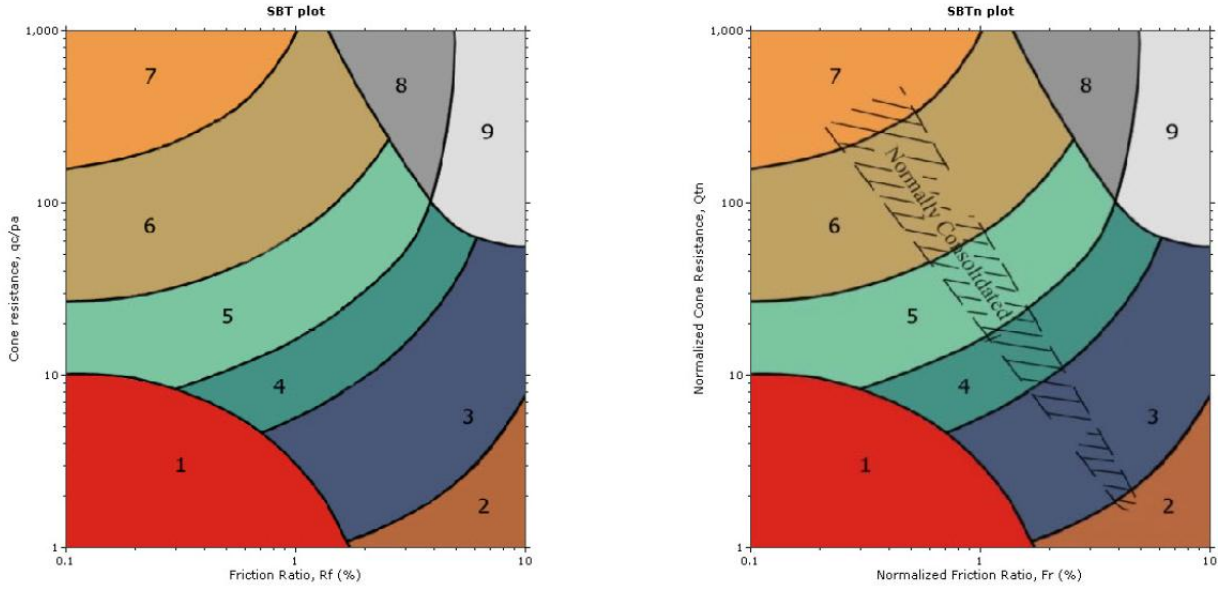

SBT zone	Proposed common SBT description
1	*Sensitive fine-grained*
2	*Clay - organic soil*
3	*Clays: clay to silty clay*
4	*Silt mixtures: clayey silt & silty clay*
5	*Sand mixtures: silty sand to sandy silt*
6	*Sands: clean sands to silty sands*
7	*Dense sand to gravelly sand*
8	*Stiff sand to clayey sand**
9	*Stiff fine-grained**

** Overconsolidated or cemented*

Figure 2.5: Updated SBT charts based a) non-normalized and b) normalized CPT (Robertson 2010*a*; Robertson, 2012)

The normalized cone parameters Q_{t1}, F_r (%) and B_q proposed by Robertson (1990) to estimate soil behaviour type are expressed as follows:

$$Q_{t1} = (q_t - \sigma_{v0}) / \sigma'_{v0} \tag{2.2}$$

$$F_r = \left[f \ / (q_t - \sigma_{v0}) \right] \cdot 100\% \tag{2.3}$$

$$B_q = (u_2 - u_0) / (q_t - \sigma_{v0}) = \Delta u / (q_t - \sigma_{v0}) \tag{2.4}$$

where σ_{v0} is the in situ total vertical stress, σ'_{v0} is the in situ effective vertical stress, u_0 is the in situ hydrostatic water pressure and Δu (= u_2- u_0) is the excess pore pressure.

As mentioned in Robertson (2009), the term Q_{t1} is used, instead of Q_t, to make reference to a stress exponent for stress normalization equal to 1. Further details on stress normalization will be provided in the following paragraphs.

The normalization recommended above was based on theoretical work by Wroth (1984). Robertson (1990) proposed two SBT charts based on either Q_{t1}- F_r (%) or Q_{t1}- B_q (Figure 2.6), but suggested that the Q_{t1}- F_r (%) chart is in general more reliable.

There have been other CPT-based classification charts proposed by other authors such as Olsen and Mitchell (1995), Eslami and Fellinius (1997) and Zhang and Tumay (1999). A description of these charts will not be reported here.

The boundaries between zones in the Q_{t1}- F_r (%) chart are defined by the Soil Behaviour Type index I_c, where I_c is the radius of the essentially concentric circles. Robertson and Wride (1998) modified the definition of the soil behaviour type index, originally identified by Jefferies and Davies (1993), to apply to the Robertson (1990) chart. In this way, I_c was defined as follows:

$$I_c = \left((3.47 - \log Q_t)^2 + (\log F_r + 1.22)^2 \right)^{0.5} \tag{2.5}$$

The contours of I_c on the Robertson (1990) Q_{t1}- F_r chart are shown in Figure 2.7.

As Jefferies and Davies (1993) suggested, the SBT index I_c could also be used to define empirical correlations that vary with soil type. Hence, the SBT index I_c is widely recognized as a powerful concept.

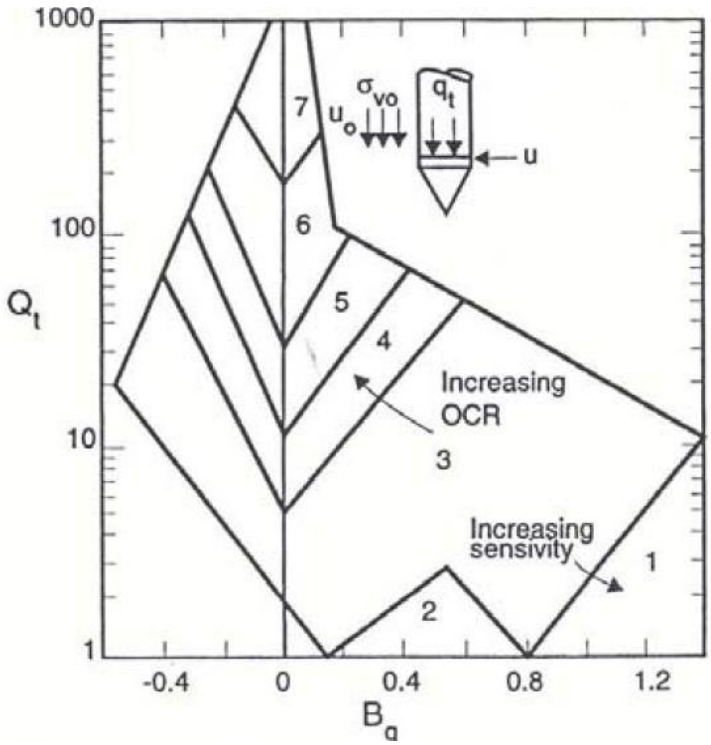

Figure 2.6 : Normalized CPT Soil Behaviour Type (SBTn) chart Q_{t1}-B_q (SBT zones based on Figure 2.5) (Robertson, 1990)

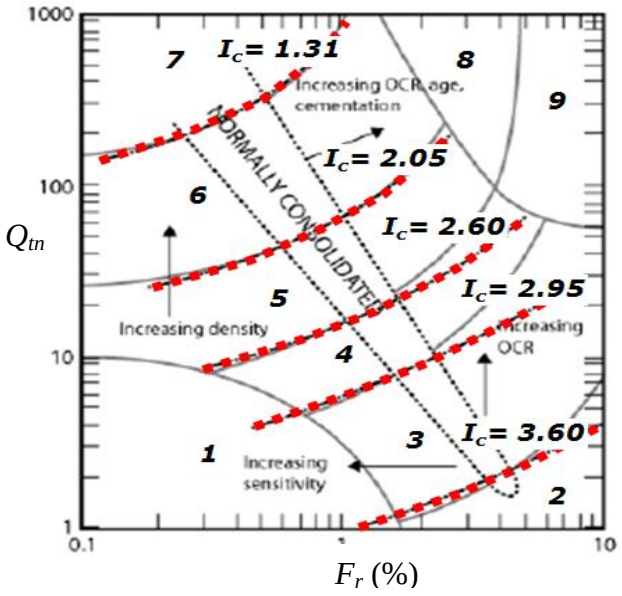

Figure 2.7: Contours of soil behaviour type index I_c on SBTn Q_{tn}- F_r chart (SBT zones based on Figure 2.5) (Robertson, 2009)

Jefferies and Davies (1991) suggested a modified SBTn chart that included piezometric information directly using $Q(1\text{-}B_q)$. Jefferies and Been (2006) noted that it was better to use $Q(1\text{-}B_q)+1$, which proved to be useful when dealing with soft sensitive soils where $B_q > 1$. However, the application of the updated chart (Figure 2.8) can be problematic in very soft soils due to loss of accuracy in q_t. Furthermore, loss of saturation would also complicate the use of this chart. The material type index I_c, which defines the soil type zone boundaries in the chart, is expressed as:

$$I_c = \sqrt{\left(3.47 - \log\left(Q\left(1 - B_q\right) + 1\right)\right)^2 + \left(1.22 + \log\left(F\right)\right)^2} \tag{2.6}$$

Robertson and Wride (1998) and the update by Zhang *et al*. (2002), proposed a normalized cone parameter using a variable stress exponent *n* that varies with SBTn:

$$Q_{tn} = \left[\left(q_t - \sigma_{v0}\right)/\, p_a\right]\left(p_a / \sigma'_{v0}\right)^n \tag{2.7}$$

where $\left(q_t - \sigma_{v0}\right)/\, p_a$ is the dimensionless net cone resistance, $\left(p_a / \sigma'_{v0}\right)^n$ is the stress normalization factor and p_a is the atmospheric pressure. Zhang *et al*. (2002) suggested that the stress exponent could be calculated using the soil behaviour type index I_c, and that index should be obtained using Q_{tn}.

Although there have been several publications (Zhang *et al*., 2002; Idriss and Boulanger, 2004; Cetin and Isik, 2007) regarding the appropriate stress normalization, only that proposed by Robertson (2009) is briefly described herein. A detailed description can be found in Robertson (2009). He suggested the following approach that allows for variable stress exponent with I_c and effective overburden stress:

$$n = 0.381 \cdot I_c + 0.05\left(\sigma'_{v0} / p_a\right) - 0.15 \tag{2.8}$$

where $n \leq 1$.

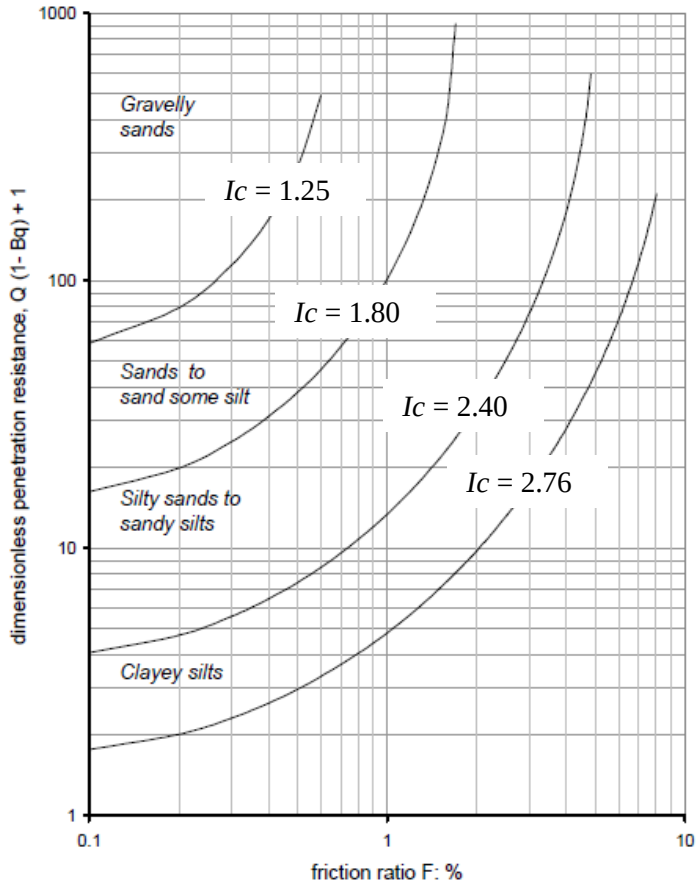

Figure 2.8: Soil type classification $Q(1\text{-}B_q)+1$ - F_r chart (Jefferies and Been, 2006)

For most fine-grained soils, the stress exponent will be equal to 1. On the other hand, when in situ vertical stresses are not high, the stress exponent will range from 0.5 to 0.9 for most coarse-grained soils, whereas at high in situ vertical effective stress (> 1 MPa), *n* tends toward 1 for most soils.

The Schneider et al. (2008) chart. Assessment of data in Q-$\Delta u/\sigma'_{v0}$ space

Schneider *et al*. (2008) proposed a classification chart (Figure 2.9) in terms of Q-$\Delta u/\sigma'_{v0}$ and stated that assessment of data in Q-$\Delta u/\sigma'_{v0}$ space was superior to Q-B_q space. Their study focused on separating the influence of overconsolidation ratio (*OCR*) from that of partial consolidation on normalized piezocone parameters, which both tend to increase the normalized cone resistance Q and decrease the pore pressure parameter B_q, leading to the potential overlap of soil types in Q-B_q classification charts and uncertainty in assessing whether penetration is drained, undrained or partially drained (Schneider *et al*., 2008).

For offshore projects in general, and onshore projects with soft fine-grained soils and ground water level close to the surface, the proposed chart can be very useful. Nevertheless, for onshore projects where the CPTu pore pressure could not be reliable due to loss of saturation of the cone sensor, the application of the chart can be problematic (Robertson 2012).

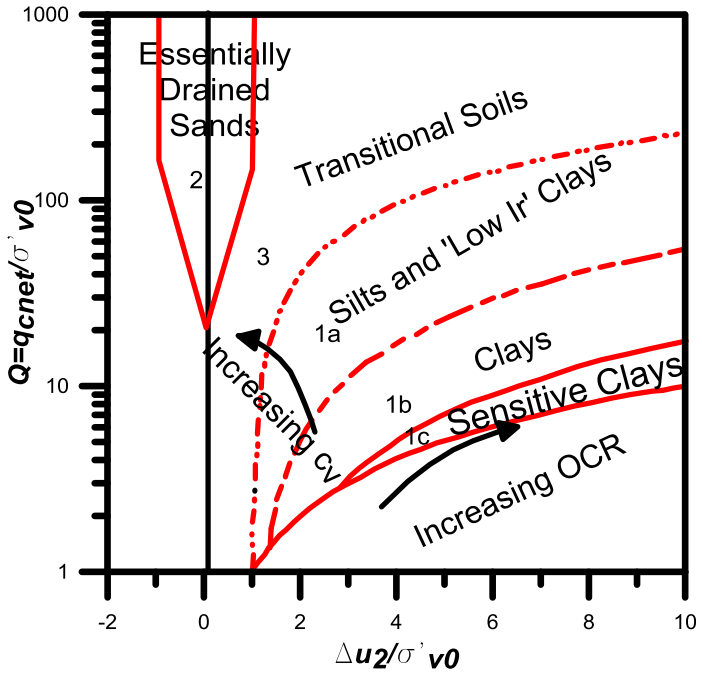

Figure 2.9: Soil classification chart according to the approach proposed by Schneider *et al.* (2008)

2.3.2 Drained CPT penetration

During cone penetration at standard rate (v = 2 cm/s), fully drained conditions prevail for coarse-grained soils and most of the geotechnical parameters are based on drained behaviour.

2.3.2.1 Stiffness

The use of the seismic CPT (SCPT) allows direct measurement of shear-wave velocity V_s. The shear wave velocity is measured during pauses in the CPT using a downhole technique, leading to a continuous profile of V_s.

Although direct measurement of V_s is preferable to estimates, where they can not be obtained, relationships with cone penetration resistance and soil behaviour type index I_c can be useful. Based on SCPT profiles, Figure 2.10 shows a set of contours of normalized shear-wave velocity V_{s1} developed by Robertson (2009) on the Q_{tn}-F_r chart, for Holocene and Pleistocene age and mostly uncemented soils. The V_{s1} is expressed as:

$$V_{s1} = V_s \left(p_a / \sigma'_{v0} \right)^{0.25} \text{ (m/s)} \tag{2.9}$$

The contours of V_{s1} in Figure 2.10 are related to Q_{tn} (Robertson, 2009):

$$V_{s1} = \left(\alpha_{vs} Q_{tn} \right)^{0.5} \tag{2.10}$$

$$\text{or } V_s = \left[\alpha_{vs} \left(q_t - \sigma_v \right) / p_a \right]^{0.5} \tag{2.11}$$

where α_{vs} is the shear-wave velocity cone factor that can be estimated using:

$$\alpha_{vs} = 10^{\left(0.55 I_c + 1.68\right)} \text{ (m/s)}^2 \tag{2.12}$$

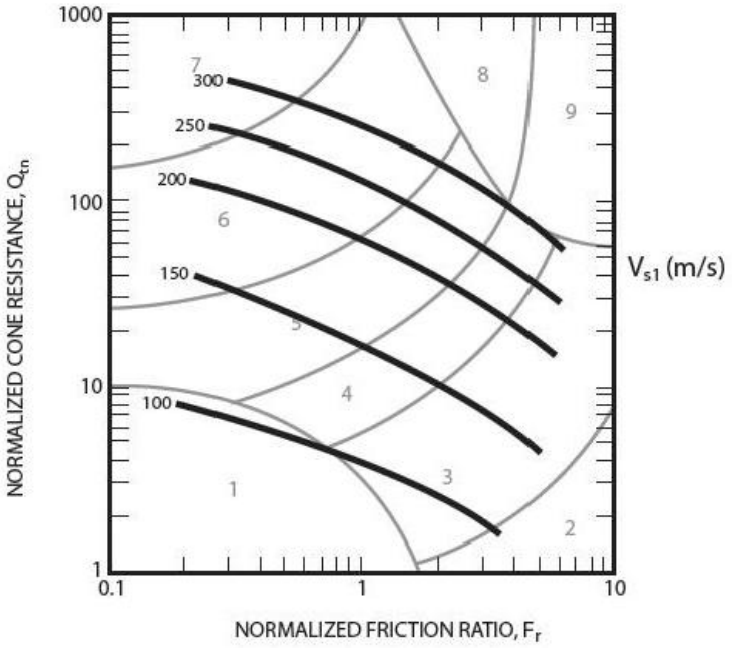

Figure 2.10: Contours of normalized shear-wave velocity, V_{s1} on normalized SBTn Q_{tn}-F_r chart (Robertson, 2009)

The V_s is a direct measure of the small strain shear modulus G_0 and is determined using the equation:

$$G_0 = \rho V_s^2 \tag{2.13}$$

where ρ is the mass density of the soil.

Using the V_{s1} contours and n = 0.5 (for most coarse-grained soils), Robertson (2009) defined a small strain shear modulus, G_0, for young, uncemented soils:

$$G_0 = (\rho / p_a) \cdot \left[10^{(0.55 I_c + 1.68)}\right] \cdot (q_t - \sigma_{v0}) \tag{2.14}$$

Where p_a is the atmospheric pressure and ρ/p_a is expressed in $(s/m)^2$.

Being G_0 the maximum shear modulus for small strains, it should be soften to an appropriate strain level for design purposes. As Robertson (2009) stated, for some applications engineers require the estimate of the Young's modulus E'. The Young's modulus is related to the shear modulus G by the following relationship:

$$E' = 2(1+\upsilon)G \tag{2.15}$$

where the Poisson's ratio (υ) ranges from 0.1 to 0.3 for most soils in drained conditions. Therefore, $E' \sim 2.5G$ for most coarse-grained soils.

Following Fahey and Carter (1993), a simple approach to estimate the amount of softening can be used:

$$G/G_0 = 1 - f(q/q_{ult})^g \tag{2.16}$$

where f and g are constants that depend on soil type and stress history, q is the applied load, q_{ult} is the ultimate or failure load and q/q_{ult} is the degree of loading. Fahey and Carter (1993) and

Mayne (2005) recommended that f = 1 and g = 0.3 are appropriate values for uncemented soils that are not highly structurated. For low to moderate degrees of loading (0.2-0.3), the ratio G/ G_0 ranges from 0.30 to 0.38. In this way, the Young's modulus for application in simplified elastic solutions is approximately $E' \sim 0.8G_0$.

For low risk projects, Robertson (2009) suggested to estimate E' for uncemented, predominately silica-based soils of either Holocene or Pleistocene age (when $I_c < 2.6$) using the following equation:

$$E' = 0.8(\rho / p_a) \cdot \left[10^{(0.55 I_c + 1.68)}\right] \cdot (q_t - \sigma_{v0}) \tag{2.17}$$

2.3.2.2 In situ state

Robertson and Campanella (1983) showed that relative density is not a reliable parameter to evaluate the in situ state due to variations in compressibility for sands. Sands with high compressibility result in lower cone resistance for the same relative density compared with sands with low compressibility.

Research has shown that the state parameter ψ (Been and Jefferies, 1985), based on critical state conditions, is a relevant parameter suitable to describe the in situ state of sands. According to Been and Jefferies, the state parameter ψ is defined as the difference between the current void ratio (e) and the critical state void ratio (e_c) at the same effective stress. As ψ links the effects of void ratio and effective stress in a unique way, it seems to be an appropriate index for describing soil behaviour compared to the relative density.

Been *et al*. (1986; 1987) first investigated the possibility of evaluating ψ using CPT/CPTu. They considered a number of calibration chamber test results primarily on clean sands, so as to develop a simple method for assessing the soil state.

Further research has shown that the inverse problem of evaluating the state from CPT measurements is complex and depends on several soil parameters. Jefferies and Been (2006) show how the inverse problem can be aided using numerical modelling. A detailed description of the evaluation of soil state using CPT is provided in Jefferies and Been (2006).

Based on a large amount of data, including field and chamber test as well as analytical/numerical results, Robertson (2009) estimated contours of state parameter on the SBTn Q_{tn}-F_r chart for uncemented Holocene age soils.

Based on a large database of liquefaction case histories, Robertson and Wride (1998) suggested a correction factor K_c to correct the normalized cone resistance Q_{tn} to an equivalent clean sand value ($Q_{tn,cs}$).

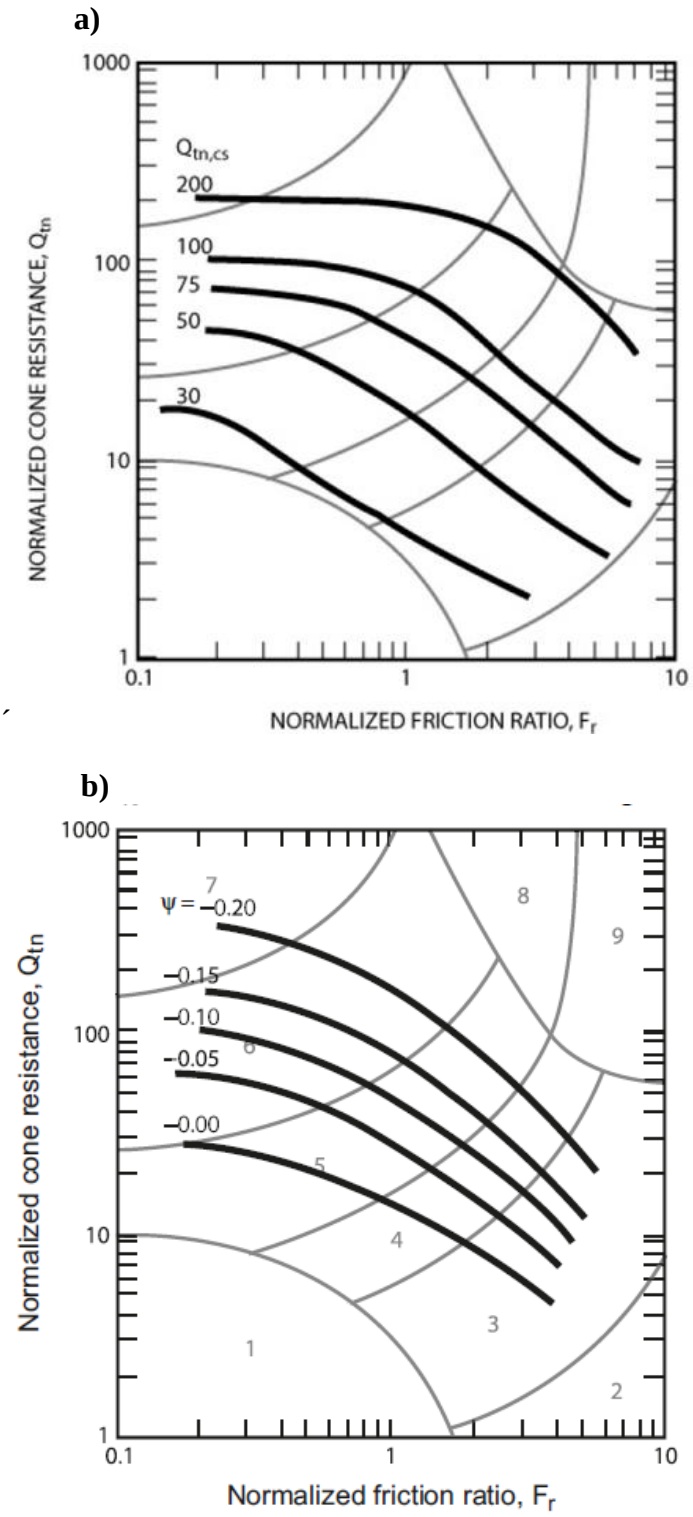

Figure 2.11: a) Contours of clean sand equivalent normalized cone resistance, *Qtn,cs*, based on Robertson and Wride (1998) liquefaction method (Robertson, 2009) and b) Contours of estimated state parameter ψ for uncemented Holocene age-soils (Robertson, 2009)

The correction factor, which is a function of grain characteristics (combined influence of fines content, mineralogy and plasticity), is applied when $I_c > 1.64$. Robertson (2010*b*) observed a strong similarity between the contours of the clean equivalent cone resistance $Q_{tn,cs}$ (Figure 2.11*a*) and the contours of ψ (Figure 2.11*b*). Accordingly, the following simplified and approximate relationship to estimate the state parameter for a wide range of sandy soils was proposed:

$$\psi = 0.56 - 0.33 \log Q_{tn,cs} \tag{2.18}$$

2.3.2.3 Shear strength

Robertson and Campanellla (1983) suggested a correlation to estimate the peak friction angle (ϕ') for uncemented, unaged, moderately compressible, predominately quartz sands based on calibration chamber test results.

$$\tan\phi' = \frac{1}{2.68}\left[\log\left(\frac{q_c}{\sigma'_{v0}}\right) + 0.29\right] \tag{2.19}$$

Kulhawy and Mayne (1990) suggested an alternate relationship for clean, rounded, uncemented quartz sands, and assessed the relationship using field data:

$$\phi' = 17.6 + 11\log(q_{t1}) \tag{2.20}$$

where $q_{t1} = (q_t / p_{atm})/(\sigma'_{v0} / p_{atm})^{0.5}$.

Jefferies and Been (2006) showed a strong link between ψ and ϕ' for a wide range of sands. Accordingly, it is possible to link $Q_{tn,cs}$ with ϕ'using:

$$\phi' = \phi'_{cv} - 48\psi \tag{2.21}$$

where ϕ'_{cv} is the constant volume or critical state friction angle depending on mineralogy (Bolton, 1986), usually about 33 degrees for quartz sands but can be as high as 40 degrees for feldespathic sand. Hence, substituting Equation (2.18) into (2.21), the relationship between $Q_{tn,cs}$ and ϕ' becomes:

$$\phi' = \phi'_{cv} + 15.84\left[\log Q_{tn,cs}\right] - 26.88 \tag{2.22}$$

The advantage of using Equation (2.22) is that it includes the importance of grain characteristics and mineralogy, that are reflected in ϕ'_{cv} and soil type (Robertson, 2010*b*).

2.3.2.4 Brief introduction to soil liquefaction evaluation: The Robertson and Wride (1998) method

Most of the existing work on soil liquefaction has been related to cyclic softening, mainly cyclic liquefaction. Cyclic liquefaction requires undrained cyclic loading, such as earthquake loading. Deformations during cyclic loading will depend on the magnitude and duration of the cyclic loading, the density of the soil and the extent to which shear stress reversal develops. If extensive shear reversal occurs, the effective stress state can reach the point of essentially zero effective stress. When the condition of essentially zero effective stress is reached, large deformations can result. However, when cyclic loading stops, the deformations generally stabilize (Robertson and Wride, 1998).

Cyclic liquefaction can take place in almost all saturated coarse-grained soils provided the magnitude and duration of the cyclic loading is sufficiently large. Fine-grained soils can also un-

dergo cyclic softening if the applied cyclic shear stress is close to the undrained shear strength. However, deformations in this case will be generally small due to the cohesive strength at low effective stress (see Robertson and Wride, 1998; Robertson and Cabal, 2012 for details).

Prof. Seed and his co-workers developed an exhaustive SPT-based approach to estimate the potential for cyclic liquefaction for level ground conditions due to earthquake loading. The approach requires an estimation of the cyclic stress ratio (CSR) profile induced by a design earthquake and the cyclic resistance ratio (CRR) of the ground. If CSR > CRR, cyclic liquefaction can occur.

Seed and Idriss (1971) developed a simplified method to estimate CSR based on the maximum ground surface acceleration (a_{max}) at the site. The expression for CSR is given by:

$$CSR = \frac{\tau_{av}}{\sigma'_{v0}} = 0.65\left[\frac{a_{\max}}{g}\right]\left(\frac{\sigma_{v0}}{\sigma'_{v0}}\right)r_d \tag{2.23}$$

where τ_{av} is the average cyclic shear stress, g is the acceleration due to gravity, σ_{v0} and σ'_{v0} are the total and effective vertical overburden stress, respectively and r_d is a stress-reduction factor which is dependent of depth. The stress reduction coefficient r_d was originally introduced by Seed and Idriss (1971). More recently, Idriss and Boulanger (2004) proposed the following relation:

$$r_d = \exp\left[\begin{array}{l}\left(-1.012 - 1.126\sin\left(\frac{z}{11.73} + 5.133\right)\right) \\ + \left(0.106 + 0.118\sin\left(\frac{z}{11.28} + 5.142\right)\right)M\end{array}\right] \tag{2.24}$$

where z is depth in metres and M is moment magnitude. As the uncertainty in r_d increases with increasing depth, Equation (2.24) should only be applied for depths less than about 20 m.

The approach based on the SPT has many problems, mainly due to the inconsistent nature of the SPT (Robertson and Wride, 1998). On the other hand, due to the continuous, reliable and repeatable nature of the CPT, several correlations have been proposed to estimate CRR (e.g. Robertson and Campanella, 1985; Stark and Olson, 1995; Idriss and Boulanger, 2003).

Based on discussions at the National Center for Earthquake Engineering Research (NCEER) workshop held in 1996, Robertson and Wride (1998) recommended the following CPT correlation for sand:

$$CRR_{7.5} = 93\left[\frac{(q_{c1N})_{cs}}{1000}\right]^3 + 0.08 \qquad \text{if} \qquad 50 \le (q_{c1N})_{cs} < 160 \tag{2.25}$$

$$CRR_{7.5} = 0.833\left[\frac{(q_{c1N})_{cs}}{1000}\right] + 0.05 \qquad \text{if} \qquad (q_{c1N})_{cs} < 50 \tag{2.26}$$

where $(q_{c1N})_{cs}$ is the normalized cone penetration resistance (q_{c1N}) corrected to an equivalent clean sand value. The normalized cone resistance (q_{c1N}) is obtained by a simple iterative stress normalization procedure that depends on the soil behaviour type index (see Robertson and Wride, 1998 for details). More recently, Robertson (2009) updated the stress normalization to allow for a variation of the stress exponent with SBTn index I_c and effective overburden stress (see Section 2.3.1).

Figure 2.12 shows the recommended correlation (updated by Roberston, 2009). The field observation data used to compile the curve plotted in the figure were based on the following:

- Holocene age, clean sand deposits;
- Level or gently sloping ground;
- Magnitude M = 7.5 earthquakes;
- Representative average CPT values for the layer examined;
- Depth range from 1 to 15 m, 85% for depths < 10 m

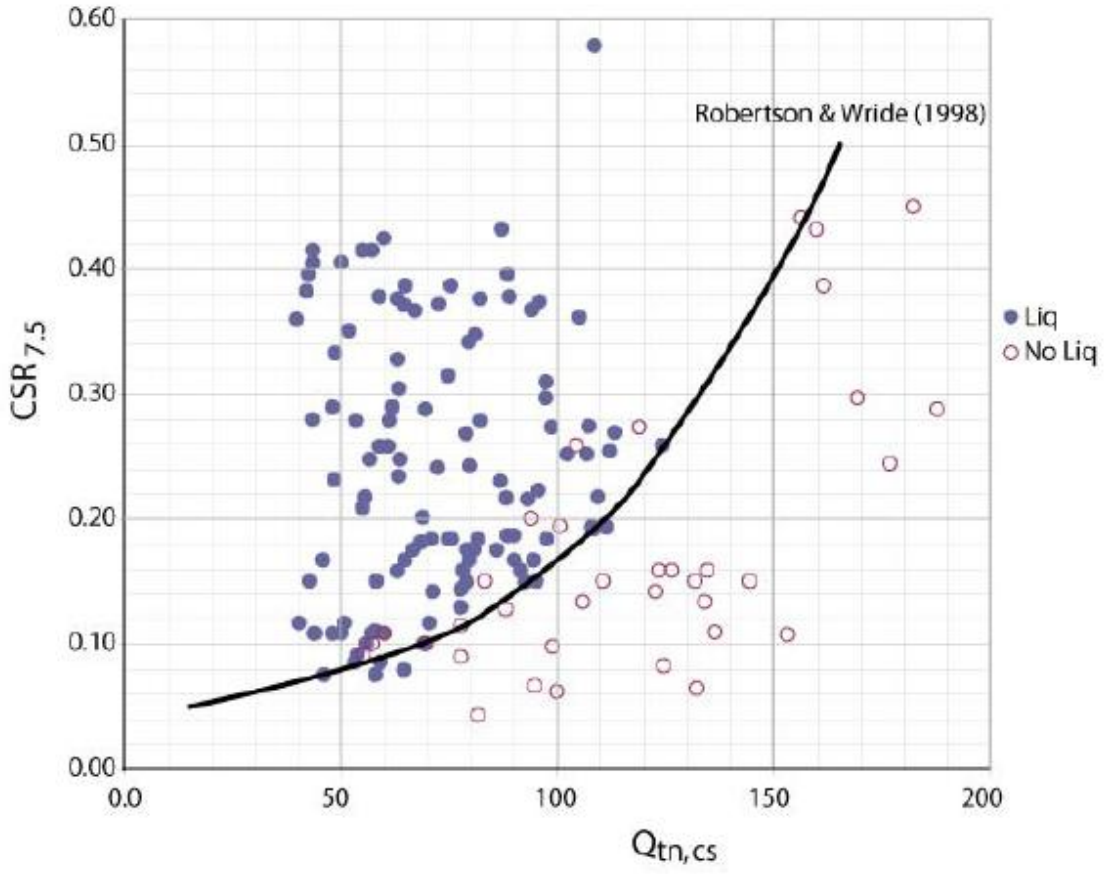

Figure 2.12: $CRR_{7.5}$ from CPT normalized clean sand equivalent cone resistance (updated by Robertson, 2009) (figure from Robertson and Cabal, 2012)

As Robertson and Wride (1998) remarked, attention should be paid when extrapolating CPT correlation to conditions outside the above. However, the correlation can be conservative when applied to all measured CPT values in variable deposits, where a small amount of data could show possible liquefaction.

Based on the approach suggested by Robertson and Fear (1995), Robertson and Wride (1998) proposed estimating an equivalent clean sand using a correction factor K_c in the following way:

$$\left(q_{c1N}\right)_{cs} = K_c q_{c1N} \tag{2.27}$$

where the correction factor K_c is a function of the soil behaviour type index I_c. The methodology proposed by Robertson and Wride (1998) to estimate $CRR_{7.5}$ from CPT is summarized in Figure 2.13.

As Robertson and Wride (1998) suggested in their work, when $I_c > 2.6$, samples should be obtained and evaluated using other criteria (e.g. Marcuson *et al*., 1990).

Finally, the factor of safety against cyclic liquefaction is given by:

$$FS = \frac{CRR_{7.5}}{CSR} MSF \tag{2.28}$$

where *MSF* is the Magnitude Scaling Factor to convert the $CRR_{7.5}$ for $M = 7.5$ to the equivalent CRR for the design earthquake. Idriss (1999) recommended the following expression for *MSF*:

$$MSF = 6.9 \exp\left(\frac{-M}{4}\right) - 0.058 \tag{2.29}$$

$$MSF \leq 1.8 \tag{2.30}$$

At any depth, if CSR is greater than the estimated CRR (adjusted to the same magnitude), cyclic softening (liquefaction) is possible (Robertson and Wride, 1998).

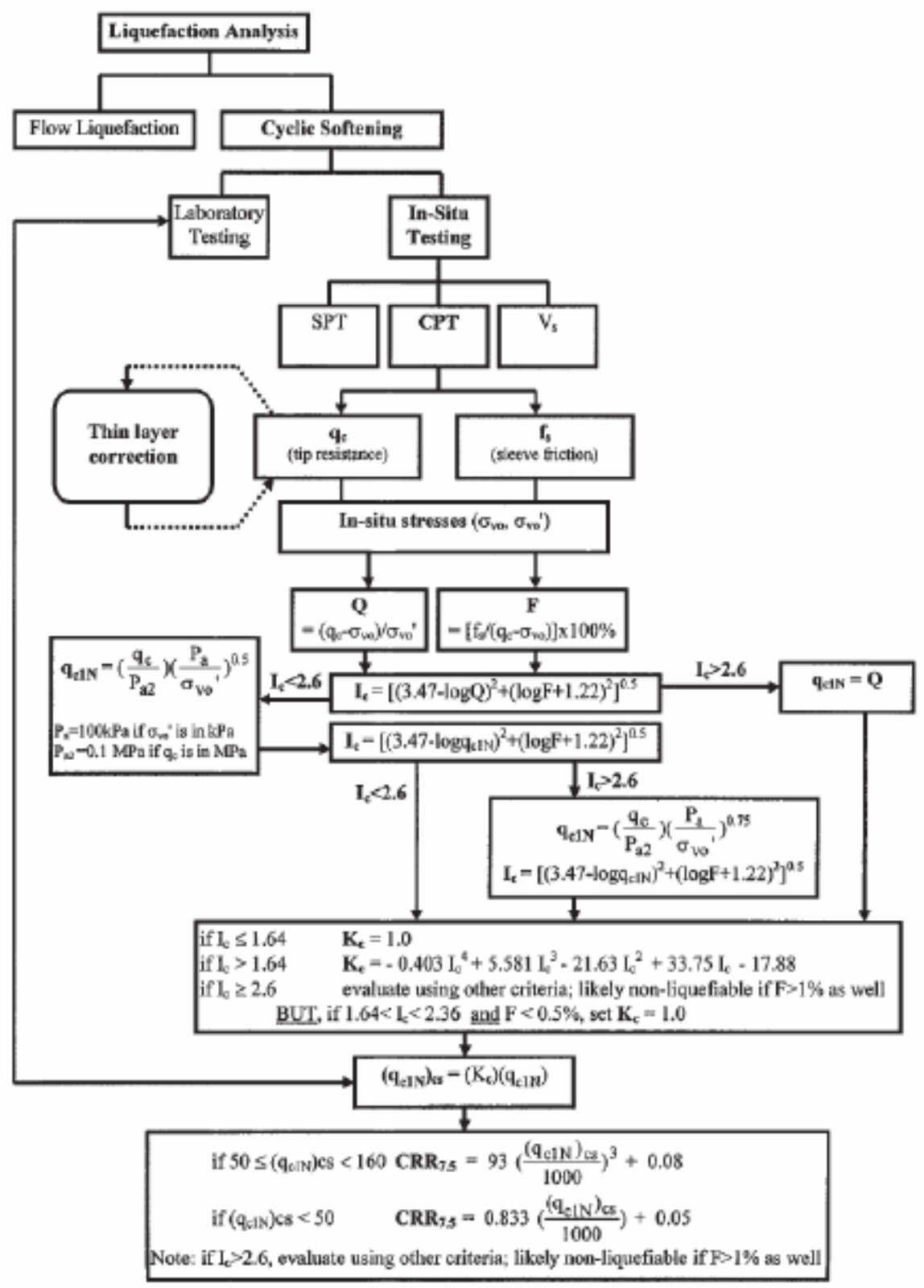

Figure 2.13: Flow chart to evaluate cyclic resistance ratio ($CRR_{7.5}$) from CPT (Roberson and Wride, 1998)

2.3.3 Undrained CPT penetration

It is generally accepted that at the standard penetration rate, undrained penetration occurs in fine-grained soils and most of the geotechnical parameters are based on undrained behaviour.

2.3.3.1 In situ state and undrained shear strength

The in situ state for fine-grained soils is usually defined in terms of *OCR*. The *OCR* is defined:

$$OCR = \frac{\sigma'_p}{\sigma'_{v0}} \tag{2.31}$$

where σ'_p is the maximum past effective consolidation stress and σ'_{v0} the present effective overburden stress. This definition is appropriate for mechanically overconsolidated soils where the removal of overburden stress has been the only change the soils have experienced. Nevertheless, for cemented or aged soils the *OCR* is the ratio of the yield stress σ'_y and σ'_{v0}.

Kulhawy and Mayne (1990) suggested the well-known method to estimate *OCR* and yield stress in fine-grained soils:

$$OCR = k(q_t - \sigma_v)/\sigma'_{v0} = kQ_{t1} \tag{2.32}$$

or

$$\sigma'_p = k(q_t - \sigma_{v0}) \tag{2.33}$$

where k is the preconsolidation cone factor.

Kulhawy and Mayne (1990) showed that an average value of k = 0.33 can be assumed, with a range varying from 0.2 to 0.5. Higher values of k are recommended in aged, heavily overconsolidated clays. The Kulhawy and Mayne approach is valid for Q_t < 20.

Ladd and Foott (1974) empirically developed the following relationship, relating the peak undrained shear strength, s_u with *OCR*:

$$s_u/\sigma'_{v0} = (s_u/\sigma'_{v0})_{OCR=1}(OCR)^m = S(OCR)^m \tag{2.34}$$

The peak undrained shear strength s_u is estimated using:

$$s_u = (q_t - \sigma_{v0})/N_{kt} \tag{2.35}$$

$$\text{or } s_u/\sigma'_{v0} = \left(\frac{q_t - \sigma_{v0}}{\sigma'_{v0}}\right)(1/N_{kt}) = Q_{tn}/N_{kt} \tag{2.36}$$

where N_{kt} is the cone factor that varies from 10 to 20, with an average of 14. For normally consolidated fine-grained soil, the undrained shear strength ratio $(s_u/\sigma'_{v0})_{OCR=1}$ ranges from 0.2 to 0.3 (Jamiolkowski *et al*., 1985), with an average value of 0.22 in direct simple shear.

According to this, using N_{kt} linked to soil sensitivity via F_r and assuming S = 0.25, ϕ' ~ 26° and m = 0.8 for most sedimentary clays, silts and organic fine-grained soils, Robertson (2012) suggested:

$$OCR = (2.625 + 1.75 \log F_r)^{-1.25} (Q_{t1})^{1.25} \tag{2.37}$$

Based on the assumption that the sleeve friction measures the remolded shear strength of the soil, $s_{u(r)} = f_s$ (e.g., Lunne *et al*. 1997), the remolded undrained shear strength ratio is expressed as:

$$s_{u(r)} / \sigma'_{v0} = f_s / \sigma'_{v0} = (F_r Q_{tn}) / 100 \tag{2.38}$$

By combining Equations (2.36) and (2.38), assuming N_{kt} = 14, soil sensitivity can be estimated:

$$S_t = s_u / s_{u(r)} = 7.1 F_r \tag{2.39}$$

In this way, Robertson (2009) represented the remolded shear strength ratio contours on the normalized SBTn chart (Figure 2.14). As sensitivity increases, the contours move toward region 1, identified as " sensitive fine-grained soils". However, as Robertson (2009) remarks, the contours of $(s_{u(r)} / \sigma'_{v0})$ should be interpreted as guide, as any lack of accuracy in f_s measurements will influence the result.

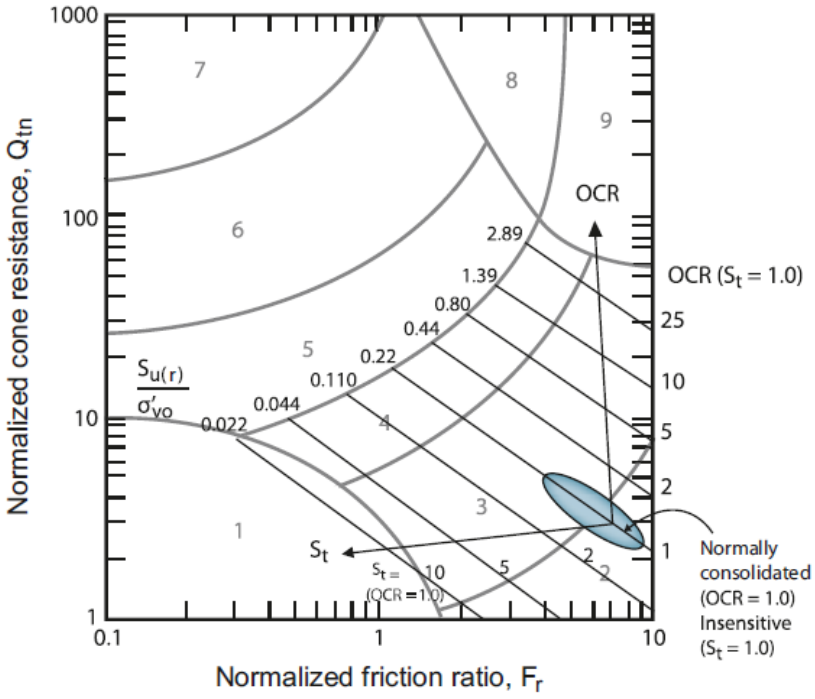

Figure 2.14: Contours of remolded undrained shear strength ratio $(s_{u(r)} / \sigma'_{v0})$ and trends in the OCR and soil sensitivity on SBTn chart (Robertson, 2009)

As recommended by Robertson, for moderate to high risk projects, site-specific correlations should be developed based on consistent values of the undrained shear resistance and the *OCR*.

2.3.3.2 Constrained modulus

The one-dimensional constrained tangent modulus, *M*, (Lunne *et al*. 1997), is used to estimate settlements at the end of primary consolidation:

$$M = \frac{1}{m_v} = \frac{(1+e_0)\cdot \ln 10 \cdot \sigma'_z}{C_{c/r}} \tag{2.40}$$

where m_v is the equivalent oedometer coefficient of compressibility, e_0 is the initial void ratio and $C_{c/r}$ is the compression index, either C_c or C_r, depending on σ'_{v0}.

Existing correlations between *M* and cone resistance typically have the form:

$$M = \alpha_M (q_t - \sigma_{v0}) \tag{2.41}$$

where α_M is the constrained modulus cone factor.

Mayne (2007*a*) showed that α_M varied with soil type and net cone resistance with values from 1 to 10, with low values applying to soft clays. Robertson (2009) suggested that α_M varies with Q_{tn} and proposed the following simplified correlation:

When $I_c > 2.2$ (fine-grained soil) use:

$$\alpha_M = Q_{tn} \quad \text{when } Q_{tn} \leq 14 \tag{2.42}$$

$$\alpha_M = 14 \quad \text{when } Q_{tn} > 14 \tag{2.43}$$

When $I_c < 2.2$ (coarse-grained soil) use:

$$\alpha_M = 0.03\left[10^{(0.55I_c+1.68)}\right] \tag{2.44}$$

Robertson (2009) remarked that estimates of *M* can be improved with further information such as plasticity index and natural water content, where α_M can be lower in soils with high water content and in organic soils.

2.3.3.3 Coefficient of consolidation from monotonic dissipation tests

In a CPTu test performed in saturated clays and silts, large excess pore water pressures are generated during penetration of piezocone. Once penetration is stopped, these excess pressures will decay with time and finally reach equilibrium conditions which correspond to hydrostatic values (Mayne 2002).

How rapidly the pore pressures dissipate depends on the permeability (k) as well as the horizontal coefficient of consolidation (c_h). In silty sands excess pore pressures may dissipate in a few minutes whereas fat plastic clays may dissipate in 2 o 3 days.

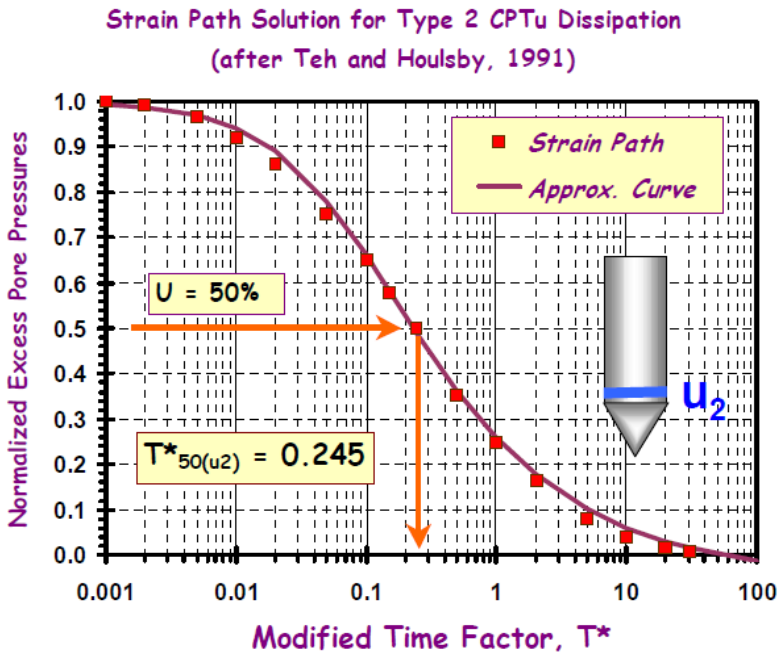

Figure 2.15: Modified time factors for u_2 monotonic porewater dissipations (Mayne, 2002)

During cone penetration the primary direction of pore water flow is horizontal, resulting in the rate of dissipation being more controlled by the horizontal coefficient of consolidation, c_h, than by the vertical coefficient of consolidation, c_v.

Soft to firm clays and silts will generally show monotonic pore pressure decays (readings always decrease with time). In these cases, the strain path method (Teh and Houlsby, 1991) may be used to determine c_h:

$$c_h = \frac{T^* r^2 \sqrt{I_r}}{t_{50}} \tag{2.45}$$

where T^* is the modified time factor, r is the probe radius, I_r (= G/s_u) is the rigidity index and t is the measured time usually taken at 50% equalization. For the particular case of 50% of consolidation, T^* = 0.245 for the type 2 of piezocone element (shoulder u_2).

2.4 Partially drained conditions on cone penetration testing

Drained or undrained conditions are required depending on desired measurements of interest for design (i.e., drained or undrained soil properties). Interpreting geotechnical parameters of 'intermediate'soils such as clayey sands and silts, silts and silty clays with the cone penetration test is a difficult task since partially drained conditions are likely to exist at the standard penetration rate of 2 cm/s.

However, the fact that the penetration velocity affects the cone resistance q_c for such 'intermediate' soils was not considered when standards were prepared for the CPT (Kim *et al*., 2008). Hence, correlations developed for sands (drained conditions at v = 2 cm/s) or for clays (undrained conditions at v = 2 cm/s) will not be suitable for soils in which partially drained conditions prevail at standard penetration rate. The uncertainty concerning the degree of drainage complicates the interpretation of geotechnical parameters.

It is well known that varying the penetration velocity drainage conditions of the advancing penetrometer can be modified. For soils investigated up to now, the tip resistance of an advancing penetrometer generally increases as the rate of penetration has reduced sufficiently for partial consolidation to occur. At very high rates of penetration, where conditions are fully undrained, viscous effects dominate and cause the tip resistance to increase with velocity. Hence, there is a transition point from undrained to partially drained conditions where viscous and partial consolidation effects equalize, showing a minimum resistance (Chung *et al*., 2006).

The influence of penetration velocity v and soil drainage properties (horizontal coefficient of consolidation) on the consolidation conditions can be captured by a normalized velocity V defined by Finnie and Randolph (1994):

$$V = \frac{v \cdot d}{c_h} \tag{2.46}$$

where v is the penetration velocity, d is the penetrometer diameter and c_h is the coefficient of consolidation. Finnie and Randolph (1994) suggested transition points of $V < 0.01$ for drained response and $V > 30$ for fully undrained response.

The majority of research to date has been mainly carried out in laboratory using centrifuge tests and reconstituted specimens clays (e.g., House *et al*., 2001; Randolph and Hope, 2004; Chung *et al*., 2006; Lehane *et al*., 2009). Schneider *et al*. (2007) tested normally consolidated and overconsolidated specimens of clay and silty clay. Jaeger *et al*. (2010) presented the results of variable penetration rate CPT in an intermediate soil (75% sand, 25% kaolin) performed in centrifuge. Oliveira *et al*. (2011) performed centrifuge tests with variable penetration rates in silty tailings.

Figure 2.16 shows the results of Jaeger *et al*. (2010). They observed that *Q* monotonically decreased as normalized velocity, *V*, increased from 0.01 to 160. However, no viscous effects were observed in their sand-kaolin experimental data. The figure also includes the results provided by Schneider *et al*. (2007).

The variation of *Q* with *V* clearly differs for the four soil types investigated. Whereas there is a clear difference in the variation of *Q* with *V* for the normally consolidated kaolin (NC kaolin) and the lightly overconsolidated silica flour-bentonite (LOC SFB), the overconsolidated kaolin (OCR kaolin) and the overconsolidated silica flour-bentonite (HOC SFB) exhibit similar trends. The normalized velocity at which *Q* is minimum is approximately 100 for the kaolin and the SFB soils tested.

By contrast, very few contributions are based on results from field scale tests and full size penetrometer. Kim *et al*. (2008) performed CPT at various penetration rates ranging from 20 to 0.01 mm/s in saturated clayey silt and silty clay soils. Tonni and Gottardi (2019) showed the results of two piezocone tests carried out at non-standard penetration rates (15 mm/s and 40 mm/s) performed in Venetian silty soils (Figure 2.17). Schnaid *et al*. (2010) presented piezocone results in gold and bauxite tailings carried out at penetration rates corresponding to 1 mm/s, 2 mm/s and 20 mm/s. Suzuki *et al*. (2012) presented the results of piezocone test performed in silty soils at rates that varied by five order of magnitude from 0.002 mm/s to 20 mm/s. Poulsen *et al.* (2013) carried out CPTs at 0.5, 1, 5, 20 and 60 mm/s in silty soils.

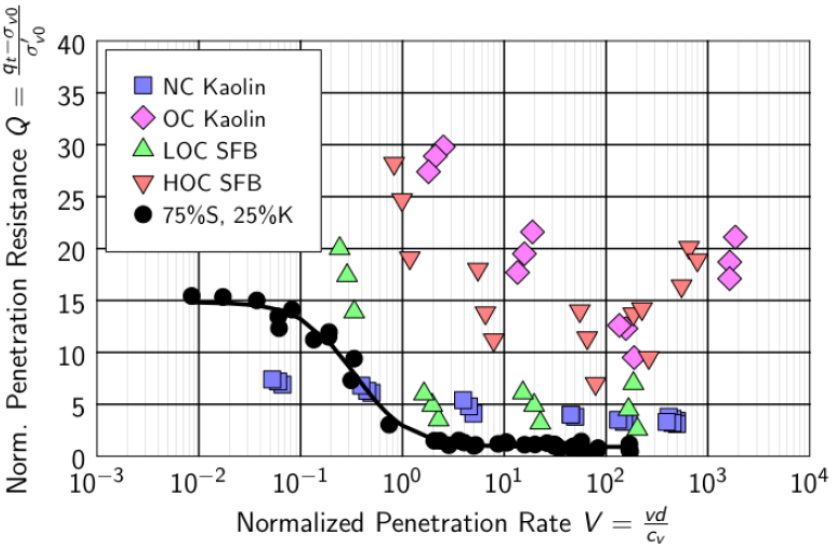

Figure 2.16: Effect of normalized penetration velocity on normalized penetration resistance in five materials: intermediate soils (75% sand, 25% kaolin mixture) data from Jaeger *et al*. (2010) and lightly and heavily overconsolidated silica flour-bentonite (SFB), and normally consolidated and overconsolidated kaolin data from Schneider *et al*. (2007). (Jaeger *et al*., 2010)

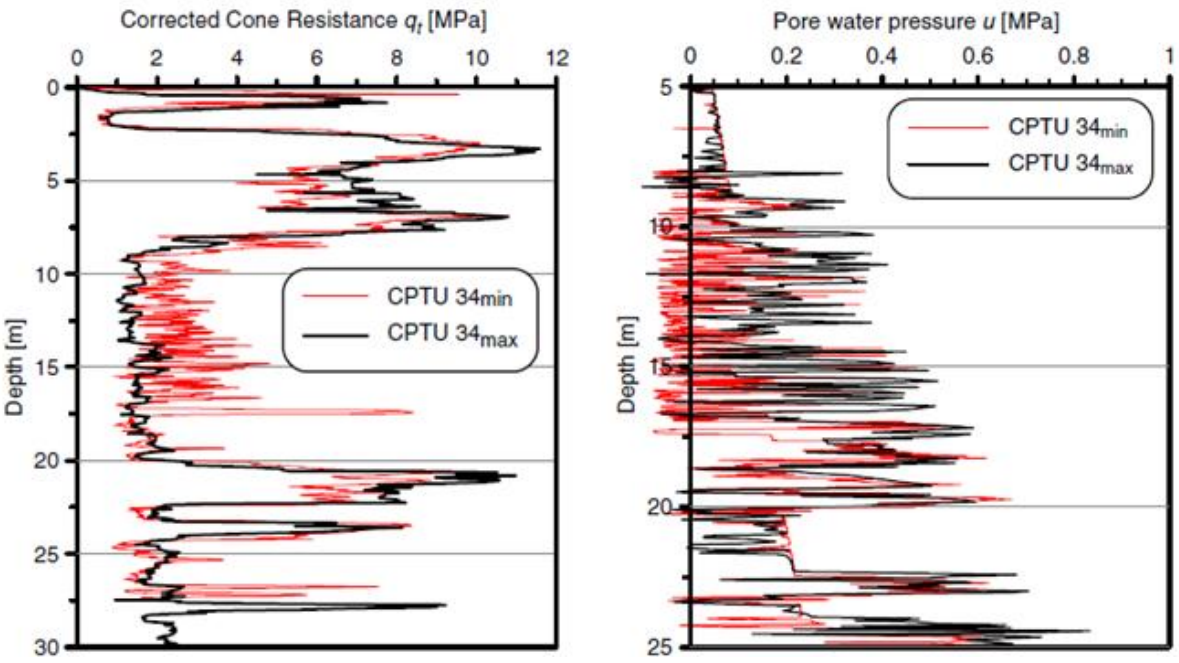

Figure 2.17: Comparison between a) cone resistance and b) pore water pressure of adjacent in situ CPTU tests performed at different penetration rates (Tonni and Gottardi, 2009)

Figure 2.18 shows the results from Kim *et al.* (2008) obtained conducting CPTUs with different penetration rates in two layers. The figure evidences how the cone resistance depends on the penetration rate. For the silty clay layer, the transition from undrained to partially drained occurs at a penetration rate of 0.2 mm/s, whilst it occurs at 1 mm/s for the clayey silt. This highlights the fact that the change in drainage condition is dependent on soil type (Poulsen *et al.*, 2011).

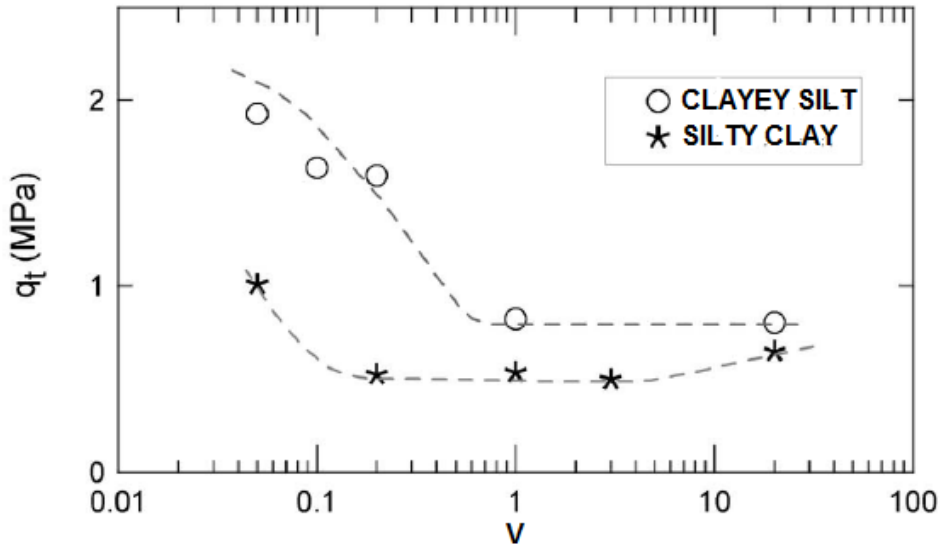

Figure 2.18: Effect of penetration rate on average cone penetration resistance q_t (Kim *et al.*, 2008)

Backbone curve equation

Randolph and Hope (2004), among others, based on studies performed in centrifuge using kaolin, presented backbone curves relating the variation of the normalized penetration resistance or excess pore pressure with the normalized penetration rate. Figure 2.19 shows the backbone curve reported by Randolph and Hope (2004), where the net cone resistance q_{cnet} is normalized by a reference value (undrained value $q_{cnet,ref}$). The normalized net cone resistance shows a gradual transition for $V < 30$. The backbone curves are of the form:

$$\frac{q}{q_{ref}} = \left(a + \frac{b}{1 + cV^{d}}\right)\left\{1 + \frac{\mu}{\ln 10}\left[\sinh^{-1}(V/V_o) - \sinh^{-1}(V_{ref}/V_o)\right]\right\} \tag{2.47}$$

where q_{ref} is the minimum undrained tip resistance measured as proposed by House *et al*. (2001), V_{ref} is the undrained normalized velocity, V_o is the normalized velocity at which viscous effects start to decay, μ is the rate parameter and a, b, c and d are parameters.

As Randolph (2004) remarked, the resulting curve fits may be used either to evaluate whether a given penetration test is partially drained or not, or to obtain a value for the consolidation coefficient of a particular soil by matching the transition point to an appropriate backbone curve.

House *et al*. (2001) suggested that the transition point for partially drained conditions may be evaluated varying the penetration velocity over a depth range. This procedure is referred as *twitch* test. At a given depth the penetration rate was successively halved, from an initial value down to a low value, and the penetrometer advanced by 1 or 2 diameters of the probe in each step. Following this approach, Randolph (2004) conducted a *twitch* cone test in a soft clay in Western Australia (Figure 2.20). The penetration rate was halved after each ~2 cone diameters, from an initial rate of 20 mm/s down to 0.02 mm/s before going back to the standard rate.

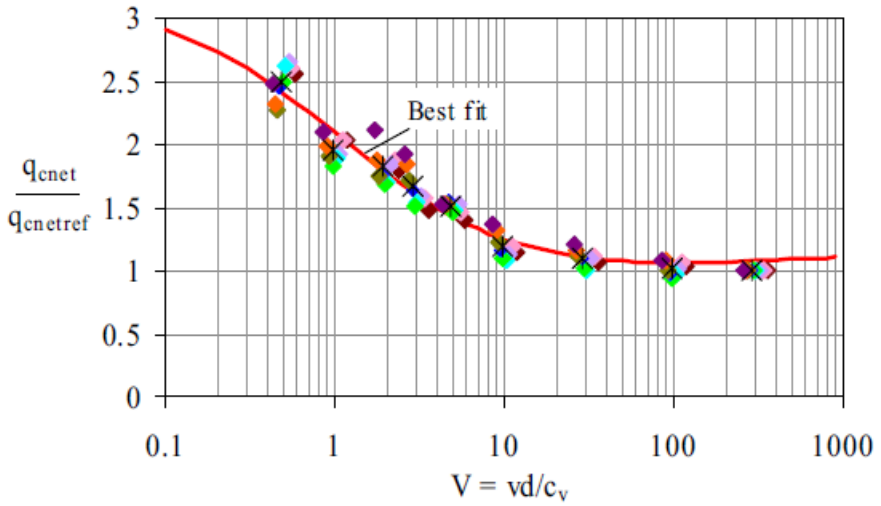

Figure 2.19: Effect of normalized penetration rate on cone resistance (Randolph and Hope, 2004)

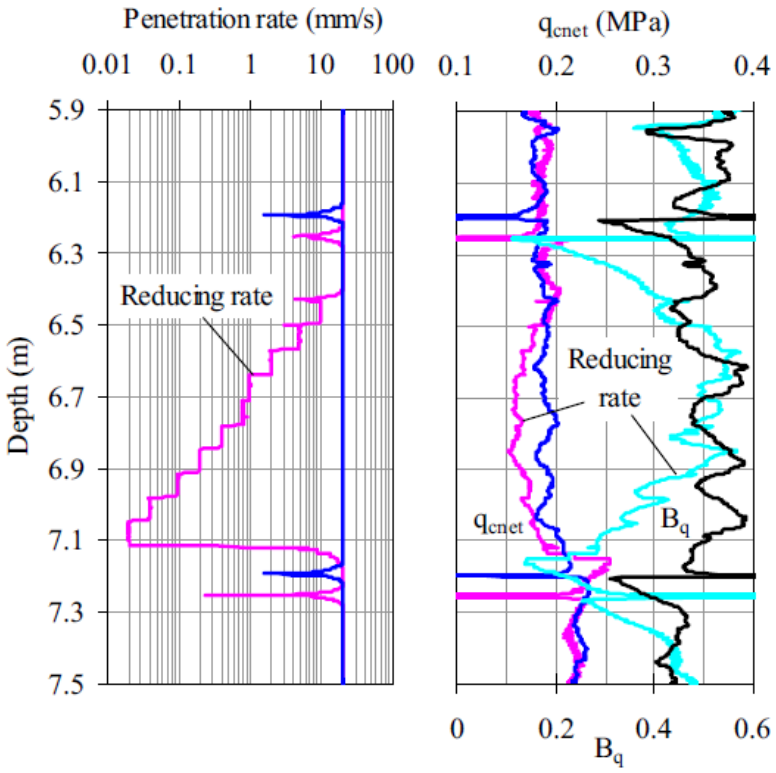

Figure 2.20: Standard and *twitch* tests in soft clay (Randolph, 2004)

As can be seen in Figure 2.20, initially, as the penetration rate reduces, the cone resistance decreases due to reduced viscous effects. Below 6.9 m the cone resistance starts to increase again towards the profile for the standard test.

Figure 2.21 shows the results of cone *twitch* test fitted using Equation (2.47), with the parameters *a*, *b*, *c* and *d* based on those proposed by Randolph and Hope (2004). The horizontal position of the data (*V*) were adjusted by varying the coefficient of consolidation (c_v) in order to give the best fit to the backbone curve (see Randolph, 2004 for details).

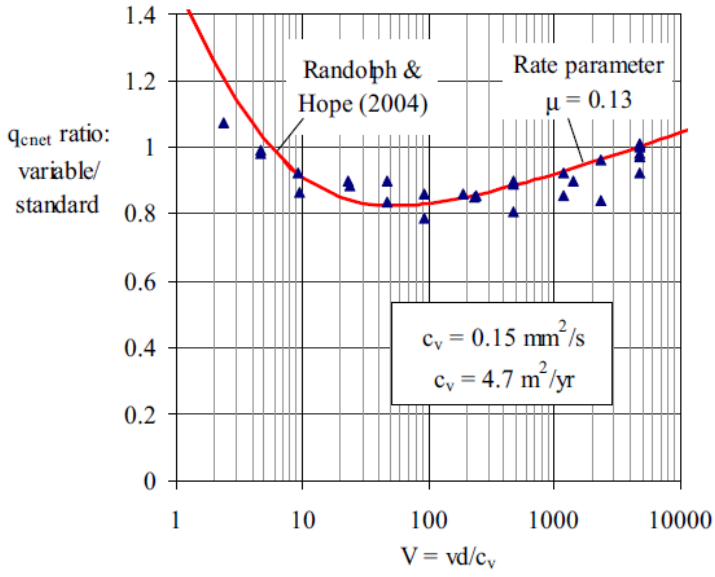

Figure 2.21: Fitting results of cone twitch test (Randolph, 2004)

Oliveira *et al*. (2011) presented in their work a set of centrifuge tests with variable penetration rates performed with a soil classified as silty tailings and an analytical approach to the backbone curve equation:

$$\frac{q_c}{q_{c,und}} = 1 + \frac{b-1}{1+\left(\frac{v \cdot d}{n \cdot c_v}\right)^{\frac{4c}{b-1}}} \tag{2.48}$$

where q_c is the cone penetration resistance, $q_{c,und}$ is the minimum undrained tip resistance and b, c and n are parameters. No increase in resistance due to viscous effects is considered. Figure 2.22 shows the best fit of data based on Equation (2.48).

DeJong and Randolph (2012) analyzed the effect of partial consolidation on normalized cone resistance and normalized excess pore pressure as a function of V in numerical and experimental data for contractive soils. The fitted curves through the data in Figure 2.23*a* and 2.23*b* are of the form, respectively:

$$\frac{\Delta u_2}{\Delta u_{2ref}} \approx 1 - \frac{1}{1+\left(V / V_{50}\right)^c} \tag{2.49}$$

$$\frac{Q}{Q_{ref}} \approx 1 + \left(\frac{Q_{drained} / Q_{ref} - 1}{1+\left(V / V_{50}\right)^c}\right) \tag{2.50}$$

where Δu_{2ref} is the initial excess pore pressure for undrained penetration, Q_{ref} is the Q value during undrained penetration, $Q_{drained}$ is the Q value under fully drained conditions, V_{50} is the normalized velocity corresponding to the penetration velocity at which 50% of the excess pore pressure for undrained penetration is mobilized and c is the maximum rate of change of the function with V. The dashed lines in Figure 2.23 are approximate bounds of other published data (Kim *et al*., 2008; Jaeger *et al*., 2010; Schnaid *et al*., 2010).

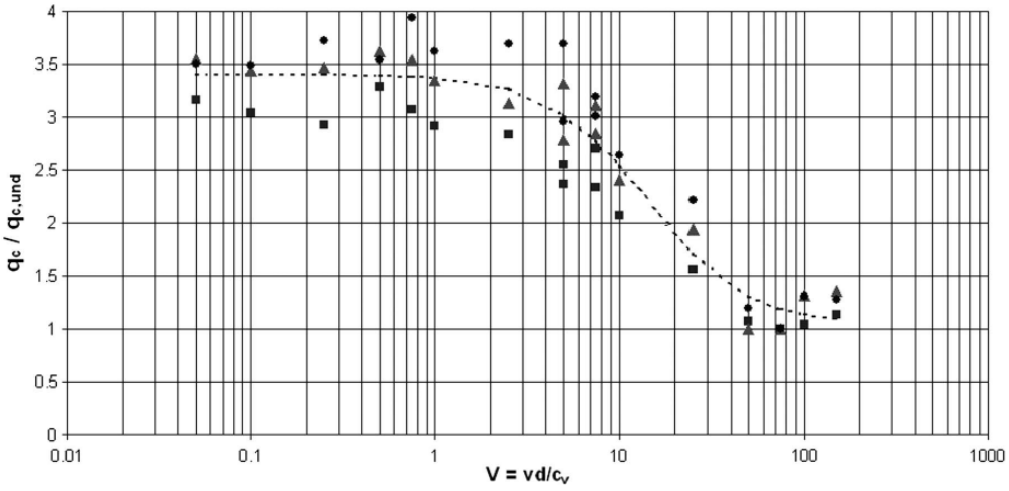

Figure 2.22: Normalized velocity V versus normalized cone tip resistance and backbone curve (Oliveira *et al*., 2011)

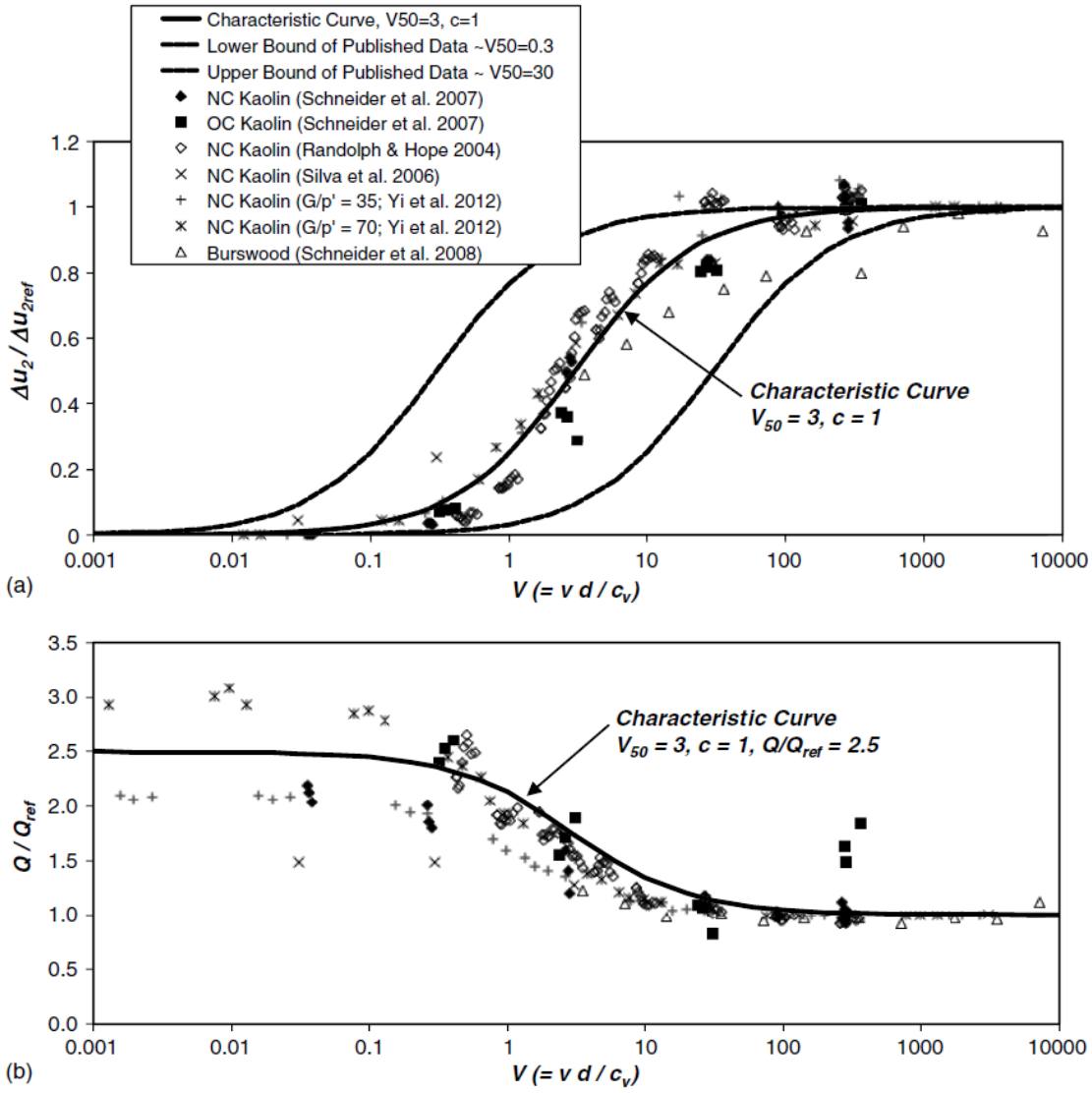

Figure 2.23: a) Normalized velocity V versus normalized Δu_2 ; b) normalized velocity V versus normalized Q (De-Jong and Randolph, 2012)

CHAPTER 3: VARIABLE RATE CPTU IN SILTY SAND DEPOSITS

3.1 Introduction

Over the last decades cone penetration testing, with or without pore pressure measurements (CPTU/CPT), has become the most widely used in-situ testing technique for stratigraphic profiling and site characterization. The amount of knowledge so far gained on the interpretation of CPT/CPTU in sands and clays, in terms of fundamental mechanics of cone penetration, soil classification charts and both theoretical and empirical correlations for the estimate of soil parameters, is undoubtedly wide.

However, a problem may arise when the existing interpretation approaches, developed for "standard" clays and sands, are evaluated for analysing cone penetration measurements in silts or other complex soil mixtures, such as sandy silts, silty or clayey sands. Indeed, these intermediate geomaterials are often characterized by permeability values within the range in which partial drainage is very likely to occur at the standard penetration rate of 20 mm/s, hence the application of the available and widely-known interpretation procedures, based on a stiff distinction between drained and undrained conditions, may result in invalid estimates of soil parameters.

In recent years, the issue of partial consolidation during cone penetration has been discussed in a number of contributions (e.g. Schnaid *et al*., 2004; Randolph, 2004; Schneider *et al*., 2007), all showing the importance of a preliminary assessment of drainage conditions in order to properly interpret the in situ soil response.

Figure 3.1: Satellite view of the villages of Mirabello and San Carlo and location of the test sites

Following the pioneering work of Randolph and Hope (2004), piezocone tests (CPTU) carried out at different penetration rates are now widely recognized as a simple and effective way to analyse the effect of partial drainage on penetrometer measurements and to detect the transition point from undrained to partially drained and drained responses.

In the context of non-standard penetration rate tests, the available experimental studies have mainly dealt with centrifuge physical models and laboratory reconstituted specimens of normally consolidated kaolin clay or silty clay (e.g. Randolph and Hope, 2004; Schneider *et al*., 2007; Lehane *et al*., 2009; Oliveira *et al*., 2011). Contrariwise, very few contributions (Kim *et al*., 2008; Tonni and Gottardi, 2010; Schnaid *et al*., 2010; Suzuki *et al*., 2012) are based on results from field scale tests and full size penetrometer. As Poulsen *et al.* (2011) remarked, the interpretation of field tests is, however, more difficult because of inhomogeneous soil stratigraphy.

This Chapter presents the results of a set of variable rate piezocone tests recently carried out at Mirabello and San Carlo (Figure 3.1), two small villages located in the eastern part of the River Po alluvial plain, close to the historical city of Ferrara (Northern Italy). In this area, extensive liquefaction-induced ground effects, including surface fractures, sand craters and abundant ejection of sands from both fractures and water wells, were observed after the mainshock (M = 6.1) of the seismic sequence that struck a wide portion of the Emilia Region since mid-May 2012.

In this study attention has been strictly focused on the analysis of piezocone measurements collected within the sandy silts and silty sands forming the upper 10 m of the two sites subsoil and the different soil response in relation to the different penetration rates is discussed. Special emphasis is given to the interpretation of dissipation tests and the recent approach developed by DeJong and Randolph (2012) is applied to experimental data in order to determine the horizontal coefficient of consolidation c_h.

Figure 3.2: a) Ground fractures and associated sand ejection observed at Mirabello industrial area after the 20th May earthquake; b) damages in the centre of the village (Courtesy of Prof. G. Vannucchi, University of Florence, Italy)

3.2 Site details

The subsurface geology of the Emilia earthquake epicentral area is characterized by the presence of compressional structures of the Apennines that are covered by marine and continental clastic deposits of the Po Plain. The surficial Holocenic deposits, due to fluvial aggradation of both Po river and its Apennine tributaries, mainly consist of silts and clays, with interbedded sand levels associated with ancient riverbeds or flooding events. An extensive overview of the geology of this area can be found elsewhere, e.g Lo Presti *et al.* (2013). It is worth observing here that the villages of Mirabello and San Carlo were founded upon the levees of an abandoned reach of a local watercourse (Reno River) which was subjected in late 1700 to an artificial diversion in order to avoid recurrent flooding.

The earthquakes of May 20, 2012 and May 29, 2012 caused locally important and extensive liquefaction phenomena. The coseismic site effects were mainly observed along the paleo-Reno River, where Sant'Agostino, San Carlo, Mirabello and Vigarano Mainarda are situated.

At the time of the 20th May event, great amount of ejected sands from ground cracks and high water fountains were observed by local inhabitants, thus suggesting the material was ejected with high pressure, unusual for events of this magnitude and depth. That leads to think that the liquefied layer is located at a low depth. In fact, as confirmed by local geology, the source unit consist of a sand layer at 7m to 8 m from the surface, having a thickness that varies between 1.5 m to 4 m.

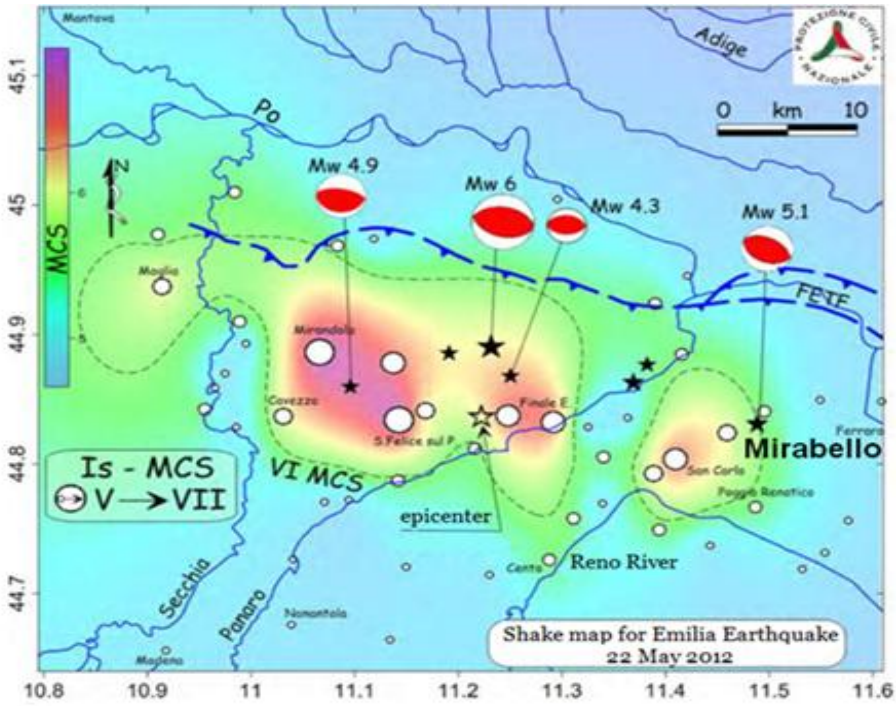

Figure 3.3:Shake map for the Emilia earthquake (Courtesy of L. Martelli, Servizio Geologico, Sismico e dei Suoli, Emilia Romagna Region)

3.3 Piezocone testing programme

3.3.1 Mirabello Site

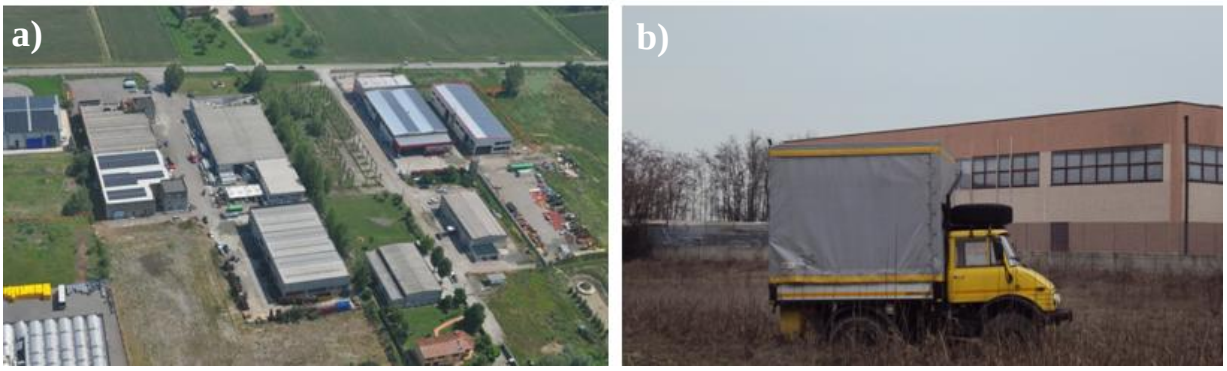

Figure 3.4: a) Overview of the Test Site; b) CPT truck

The piezocone tests performed in the first campaign were carried out in a warehouse industrial area located just outside the centre of Mirabello. Here, diffuse liquefaction phenomena, with some local intense effects, occurred and caused major damages to industrial buildings, as shown in Figure 3.2*a*. The experimental programme included 5 adjacent CPTU, performed along verticals located within a 2 m distance so as to avoid any possible uncertainty in the data interpretation due to horizontal spatial variability. The adopted cone penetration rates *v*, held constant in each test, were equal to 10, 20, 40, 80 and 130 mm/s.

The penetration device used was a standard cone (35.7 mm diameter having a corresponding cross sectional area A_c = 10 cm^2 and sleeve area A_s = 15 cm^2). The equipment enables continuous measurement of the cone resistance q_t, the sleeve friction f_s and the pore pressure u. The porous filter is located at the shoulder (Position 2) just behind the cone tip. Data are logged at about 1 second intervals, with a standard penetration rate of 20 mm/s. The equipment was also provided with an inclinometer.

Despite penetration tests have been assumed to be performed at constant rate, soil heterogeneity and capabilities of the equipment in keeping the velocity constant caused variations of penetration rates in the range of ±30% of the average value. In addition, as can be appreciated from Figure 3.5, the set-up between CPTU pushes causes noticeable changes in the velocity, recording incremental values which may be in the order of the average value or even bigger. This is more evident as the penetration rate that has to be reached increases. Piezocone measurements obtained at these points were not taken into account.

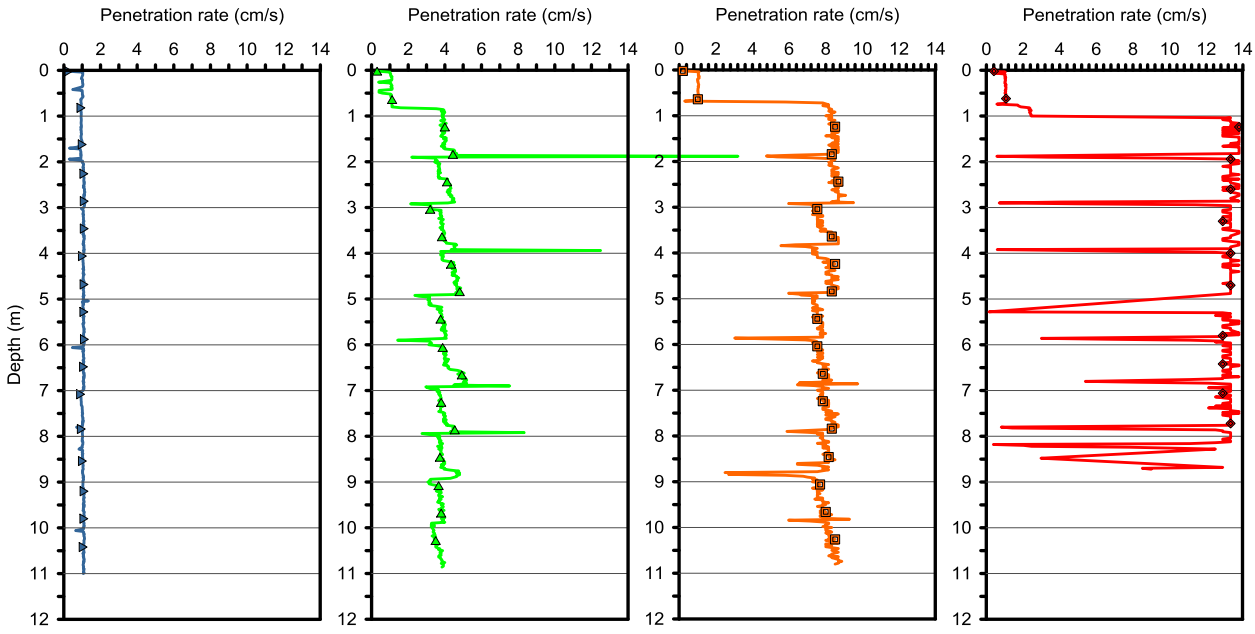

Figure 3.5: Range of penetration rate during piezocone tests.

Figure 3.6 shows the corrected cone resistance q_t, the pore pressure u and the sleeve friction f_s measurements from the first test CPTU-0, performed at standard v = 20 mm/s, taken to 20 m depth. Such profiles detail an alternation of sand and silt mixtures from ground level to approximately 8 m in depth, with local thin lenses of finer sediments, followed by a predominantly clayey unit.

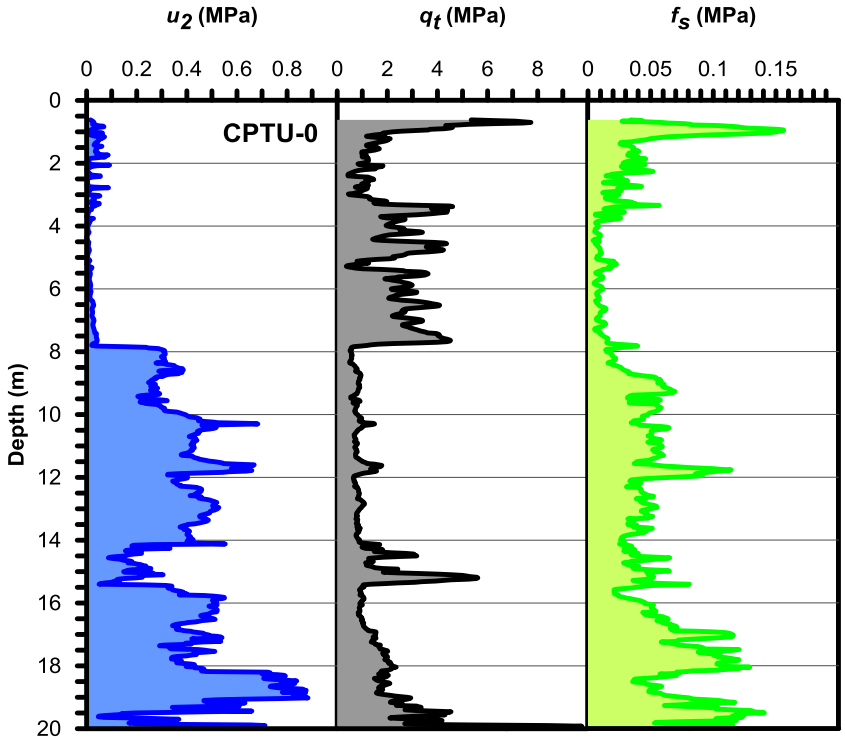

Figure 3.6: CPTU-0 log profiles (2 cm/s)

This stratigraphic condition is clearly described by the well-known and newly revised piezo-cone-based classification framework proposed by Robertson (2009), aimed at identifying the in situ soil behaviour type (SBTn). As shown in Figure 3.7, the upper 4 meters of the Mirabello subsoil mainly consist of an alternation of silty sands/sandy silts (SBTn = 5), silts (SBTn = 4) and silty clay (SBTn = 3); from 4 to 8 m in depth, sediments turn out to be somewhat coarser (sands/silty sands), with occasional presence of clay and organic soils; below 8 meters, sediments are classified as clay-silty clay.

Results from classification approach developed by Schneider *et al*. (2008) are also plotted in Figure 3.7. According to such classification framework, data from groundwater level to 8 m fall in domains 2 and 3. The former includes sands whereas the latter includes a wide variety of mixed soil types. From 8 m to 14 m, sediments are classified as clays (zone 1b) with presence of silts from 8.75 to 9.75 n. At depths greater than 14 m, the stratigraphic profile is characterized by alternated layers of transitional soils and silts (zones 3 and 1a) and clays (zone 1b).

The complete set of piezocone measurements obtained from the non-standard penetration rate tests (CPTU A, B, C, D) is plotted in Figure 3.8. Data were collected in Spring 2013, after a period of heavy rainfall causing the water table to raise close to the ground surface ($z_w \approx 1$ m). By contrast, CPTU-0 was carried out a few months before, when the water table was located at approximately 3.5 m in depth.

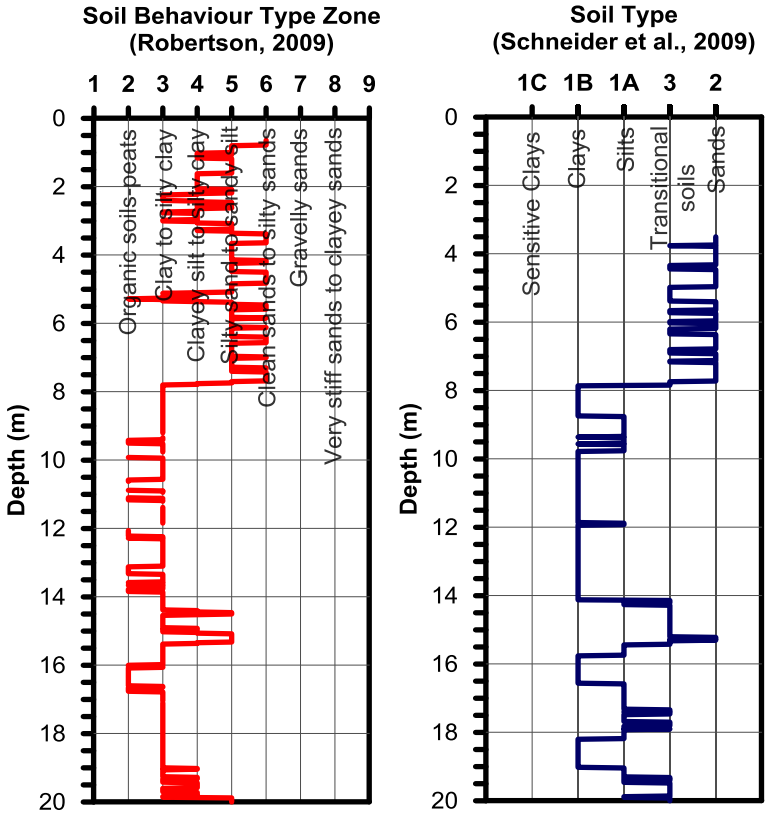

Figure 3.7: CPTU-based classification methods applied to CPTU-0

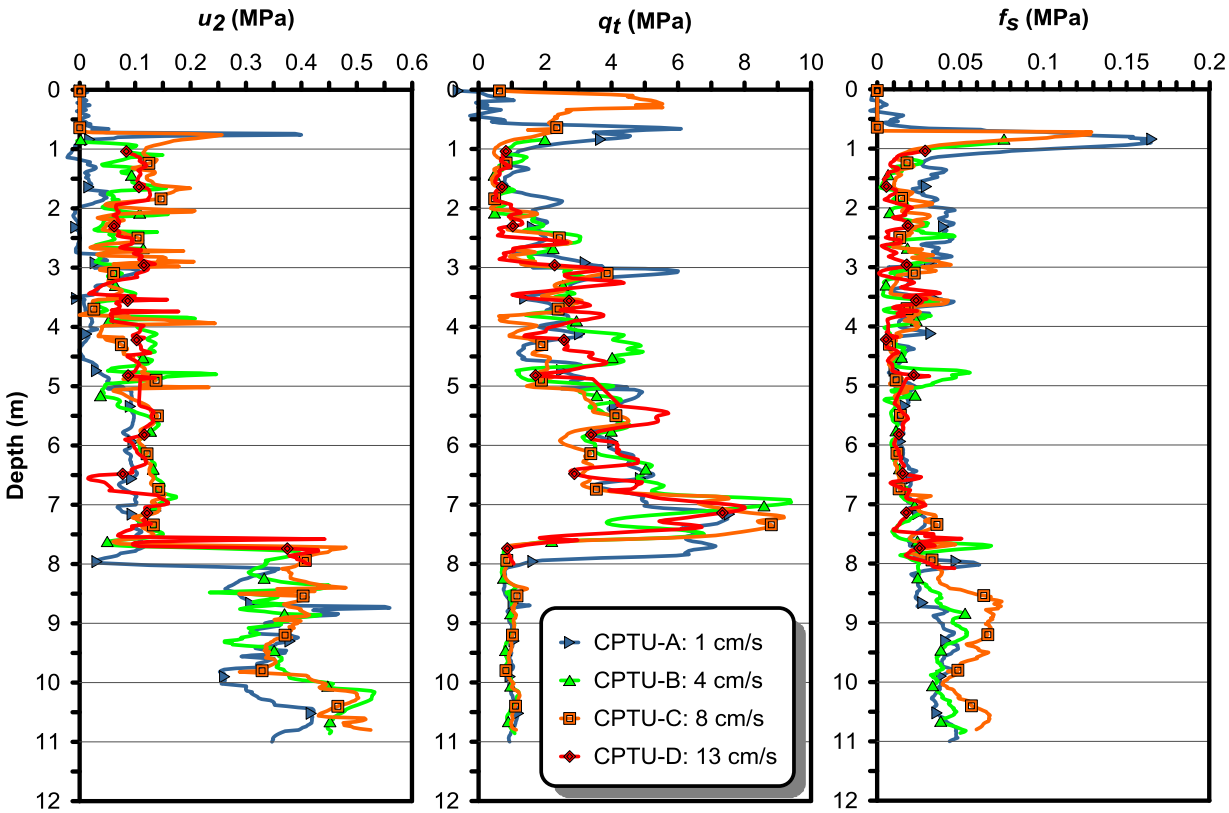

Figure 3.8: Piezocone profiles of adjacent tests at different penetration rates at Mirabello Site

The attention was focused on the shallow sand and silt mixtures, 8 m thick, initially detected by the standard CPTU-0, hence the non-standard tests were stopped at a depth of about 11 m. In particular, piezocone data from thin soil layers within 5.3 and 6.4 m in depth were thoroughly examined.

It must be observed that some local variations at the Mirabello Site may have some effects on the results and should be taken in consideration when comparing q_t and u_2 profiles obtained from adjacent CPTU tests.

Dissipation tests

As explained in Chapter 2, one of the advantages of the piezocone test is that it can be used to evaluate the coefficient of consolidation of the ground. At the beginning of the dissipation test the magnitude of the excess pore pressures generated depend on the drainage conditions during penetration.

At Mirabello Site, dissipation tests were performed in tests B, C and D at a depth approximately 5.8 m (Figure 3.9). These dissipation tests show monotonic porewater decays with the logarithmic of time, generally associated to normally consolidated geomaterials. The well-known method proposed by Teh and Houlsby (1991) was applied herein for the estimate of the horizontal coefficient of consolidation c_h .

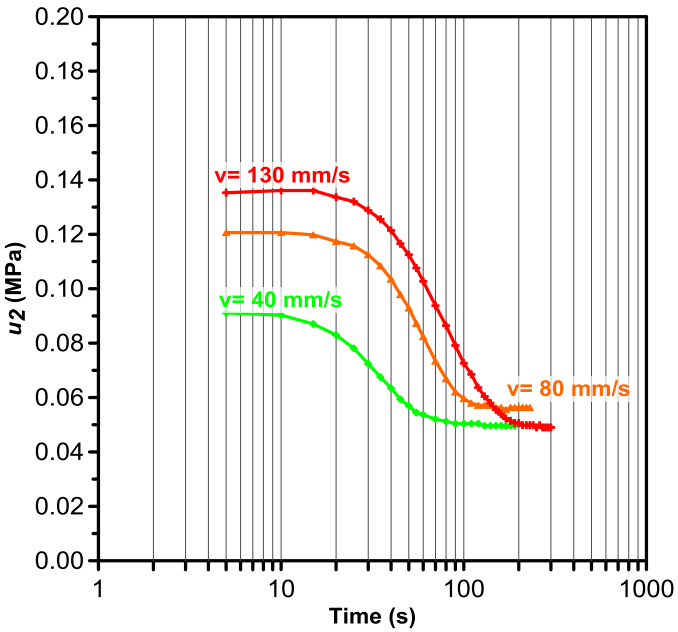

Figure 3.9: Dissipation curves carried out at a depth of 5.8 m, for different penetration rate tests

According to this approach, the process of dissipation is described in terms of a modified time factor, T^*, given by the following equation:

$$T^* = \frac{c_h t}{r^2 \sqrt{I_r}} \tag{3.1}$$

where t is the measured time, r is the radius of the probe and I_r (= G/τ_{max}) is the rigidity index. Such modified time factor accounts for the influence of the shear stiffness on the process of consolidation. For the particular case of 50% consolidation, the modified time factor T^* is equal to 0.245.

As Mayne (2007*b*) stated, for drained loading the shear strength is given by $\tau_{max} = c' + \sigma'_{v0} \cdot \tan\phi'$, where $c' = 0$ can be applicable in most cases. On the other hand, for undrained loading, is given by $\tau_{max} = c_u = s_u$, where s_u is the undrained shear strength.

If the penetration can be assumed to occur under undrained conditions, the peak undrained shear strength is estimated using:

$$s_u = \frac{(q_t - \sigma_{v0})}{N_{kt}} \tag{3.2}$$

where N_{kt} is the cone factor that varies from about 10 to 20.

In an attempt to get a better insight into the problem, s_u has been assessed using the cone resistance profile obtained from the piezocone test performed at v = 80 mm/s and N_{kt} has been assumed equal to 20. It is worth observing that the undrained shear strength calculated in this way for such intermediate soils is quite high ($s_u \approx 0.16$ MPa; $s_u / \sigma'_{v0} \approx 2.6$). Besides, there is a significant uncertainty in the assessment of s_u using this relationship which was in turn developed

for fine-grained soils in fully undrained conditions. For this reason, τ_{max} has been finally obtained using $\tau_{max} = \sigma'_{v0}.\tan\phi'$.

In order to evaluate the angle of shear resistance, two different relationships have been used. The one proposed by Robertson and Campanella (1983),

$$\phi' = \arctan\left[\frac{1}{2.68}\left(\log\left(\frac{q_c}{\sigma'_{v0}}\right) + 0.29\right)\right] \tag{2.19}$$

and the one proposed by Kulhawy and Mayne (1990),

$$\phi' = 17.6 + 11\log(q_{t1}) \tag{2.20}$$

where $q_{t1} = (q_t / p_{atm}) / (\sigma'_{v0} / p_{atm})^{0.5}$. These correlations provided very similar estimates of ϕ' and a mean value of 34º was adopted as representative for such intermediate soils.

In terms of stiffness, the maximum shear modulus was obtained by means of down-hole testing. The down hole test used for this purpose was carried out near the city centre of Mirabello. A mean value of G_0 = 77.4 MPa ($V_s \approx$ 200 m/s) was considered representative for the range of depths of interest.

Considering that the ratio G/G_0 ranges from 0.3 to 0.38, the shear modulus G was estimated and a reasonable value of $I_r = G/\tau_{max}$ = 380 was used to calculate the horizontal coefficient of consolidation following Teh and Houlsby (1991). Table 3.1 provides the values estimated. Further remarks on the determination of c_h in relation to different degrees of drainage during cone penetration will be provided in Section 3.6.

Table 3.1: Summary of the horizontal coefficients of consolidation values for silty soils, according to Teh & Houlsby (1991).

Test	Depth m	v mm/s	t_{50} s	c_h m^2/s
CPTU4	5.86	40	32	$4.7 \cdot 10^{-5}$
CPTU8	5.84	80	54	$2.8 \cdot 10^{-5}$
CPTU13	5.82	130	72	$2.1 \cdot 10^{-5}$

As it can be observed in the table above, the values of c_h deduced from the dissipation test, are reasonably close to each other. Although the coefficient of consolidation is known to be stress-dependent, the c_h values calculated above are adopted as representative values for the range of depths selected for this analysis (5.3 m – 6.4 m).

3.3.2 San Carlo Site

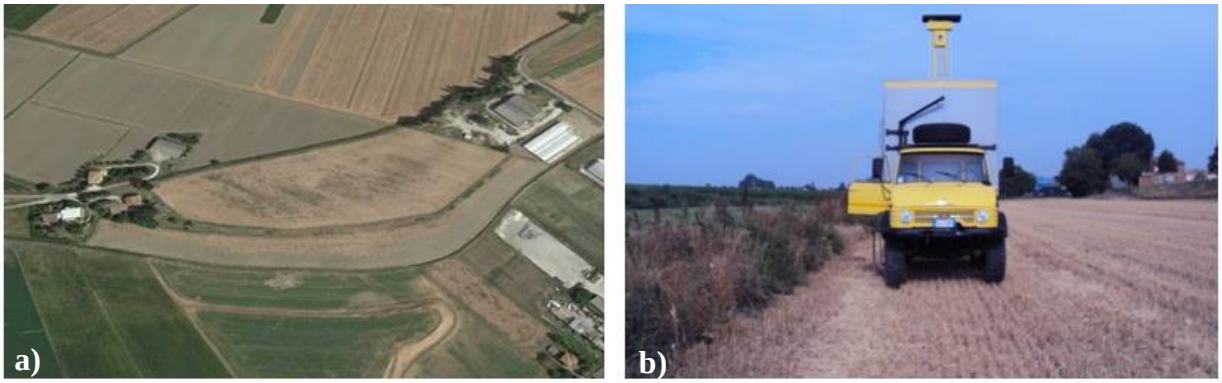

Figure 3.10: a) Overview of the Test Site (from Google earth); b) CPT truck

Figure 3.11: Sand deposits along the abandoned reach of a local watercourse (image taken from the website panoramio.com)

The experimental programme carried out at San Carlo included 3 adjacent piezocone tests, conducted in close proximity to each other (at a distance apart of 1.5-2 m). The tests were performed at constant penetration rates of 10, 20 and 80 mm/s. Nevertheless, the velocity profiles revealed once again the difficulty in keeping the velocity constant particularly at high penetration rates.

It is worth observing here that the characteristic sedimentary infilling of river plains, involving alternation of high and low permeability layers with evident lateral heterogeneity, complicates the soil units correlation even between adjacent piezocone test profiles.

Figure 3.12 shows the profiles of corrected tip resistance q_t, pore water pressure u_2 and sleeve friction f_s measured in a standard CPTU (v = 20 mm/s) at San Carlo, taken to 20 m depth. The groundwater was encountered at approximately 1.5 m from the ground surface. The water table fluctuation may be explain the fact that the shallowest layers seem to be lightly overconsolidated.

Pore pressures are almost zero or even negative up to 7.3 m . As Robertson (2012) remarked, when a cone is pushed through saturated dense silty sand, the u_2 measured can become negative

due to the dilative nature of the soil in shear, resulting in small air bubbles coming out of solution in the cone sensor pore fluid and loss of saturation in the sensor. Beneath this layer, when the cone is pushed through the clay unit, these air bubbles can go back into solution and the cone becomes saturated again. As can observed in Figure 3.14, at z ≈ 7.5 m, u_2 values sharply increase.

As in the Mirabello campaign, classification of San Carlo sediments from piezocone data has been performed using the classification charts proposed by Schneider *et al.* (2008) and Robertson (2009). Based on the latter classification framework (Figure 3.13), the upper 4 meters of San Carlo subsoil mainly consist of clean sands to silty sands (SBTn = 6); from 4 to 7.5 m in depth, sediments turn out to be somewhat finer (SBTn = 5), with some lenses of sands (SBTn = 6). Below 7.5 m, soils are classified as clay-silty clay (SBTn = 3), being interbedded with a silty layer (STBn = 4 and SBTn = 5) between depths of 18-19 m.

Results from classification approach developed by Schneider *et al*. (2008) are also plotted in Figure 3.13. It is worth observing that as Robertson (2012) stated, the application of the Schneider *et al* chart can be problematic when applied to onshore CPTU where the pore pressure measurements may not be reliable, due to loss of saturation. According to such classification framework, data from groundwater level to 4 m fall in domain 2 (sands). From 4 m to 7.5 m, sediments are classified as transitional soils (zone 3) with presence of a thin layer of sand (zone 2) at approximately 7 m. Below 7.5 m, the stratigraphic profile is characterized by an alternation of silts (zone 1a) and clays (zone 1b), with the presence of thin layers of coarser materials being more evident at depths greater than 16 m.

With the aim of assessing drainage conditions during penetration, two further tests were performed at non standard rates of v = 10 mm/s and v = 80 mm/s. In Figure 3.14 data from tests CPTU-min, CPTU-st and CPTU-max, carried out at v = 10 mm/s, v = 20 mm/s and v = 80 mm/s respectively, are plotted. Once again, the attention was focused on the shallow sandy mixtures from 4 to 7.5 m in depth. Therefore, the non standard tests were stopped at a depth of about 9 m.

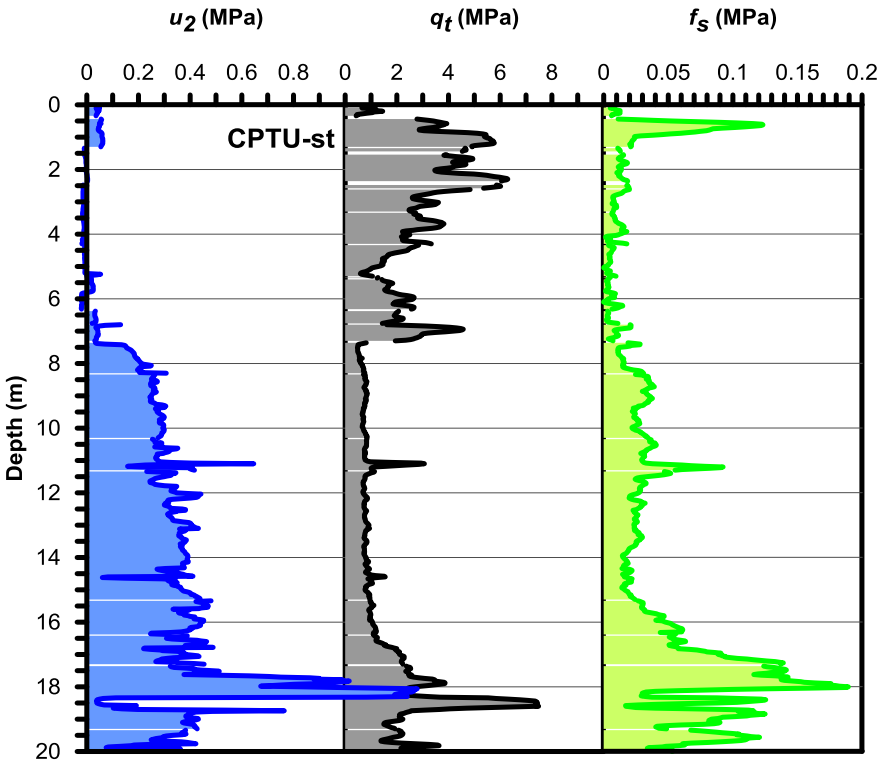

Figure 3.12: CPTU-st log profiles (2cm/s)

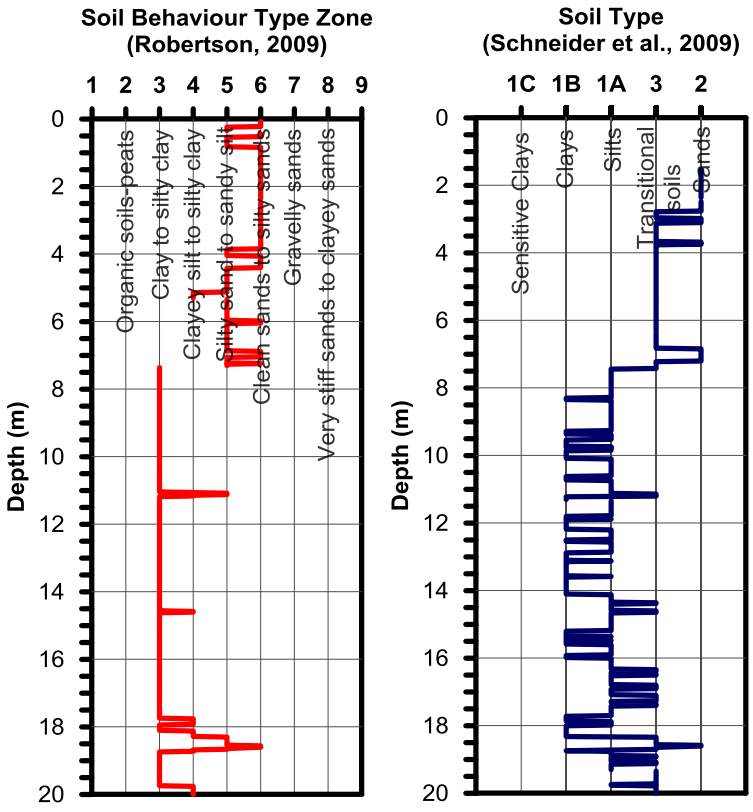

Figure 3.13: CPTU-based classification methods applied to CPTU-st

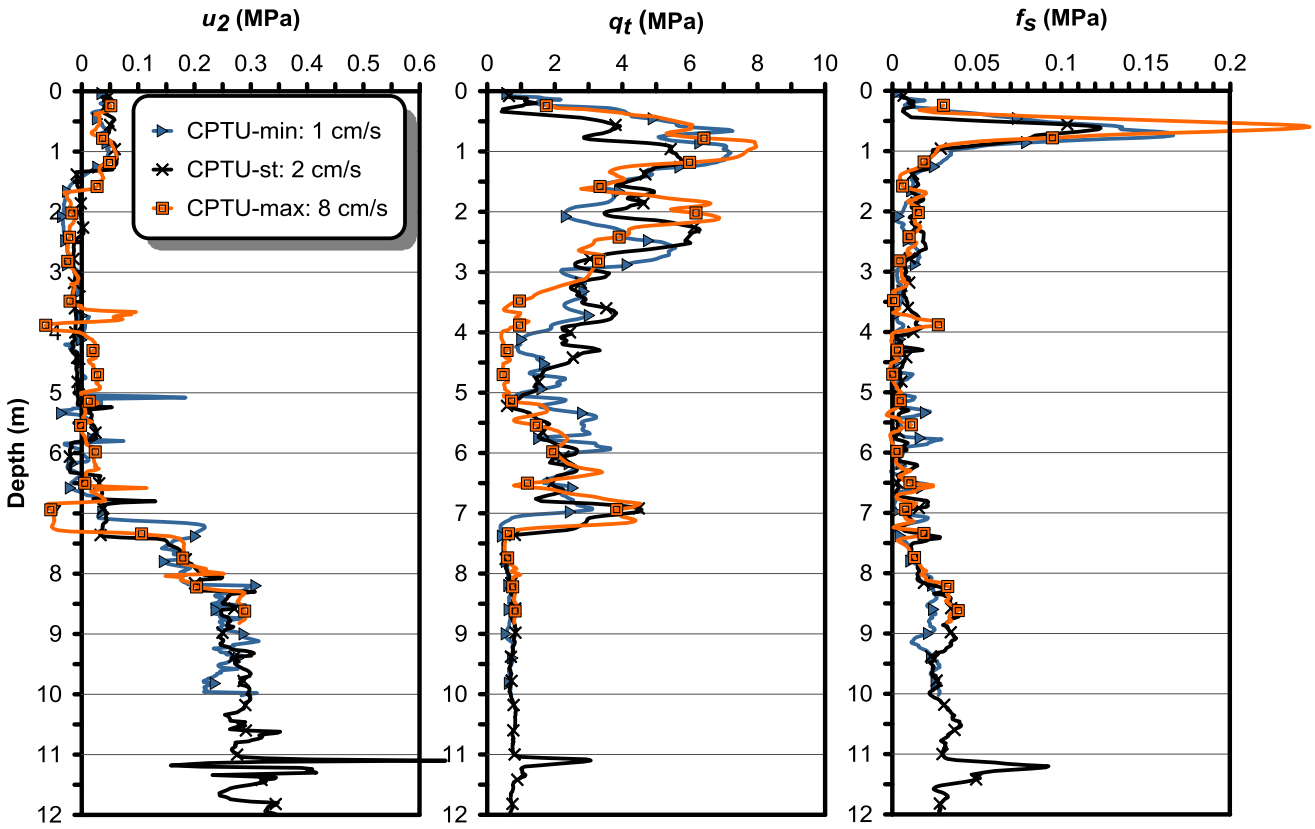

Figure 3.14: Piezocone profiles of adjacent tests at different penetration rates at San Carlo Site

Dissipation tests

Dissipation test were also performed at San Carlo site to study the consolidation characteristics of the silty sediments. When negative u_2 penetration pore pressures are observed in unusual situations, it is strongly recommended to perform dissipation tests. If a soil is a sand or sandy silt, full dissipation should occur within 5 minutes (Schneider *et al*., 2008).

Figure 3.15 shows the results of the dissipation test carried out at a depth of 5.8 m for CPTU-min. At this depth, the penetration (v = 10 mm/s) was stopped and the decay of the excess pore pressures was measured. It can be observed that pore pressures start as negative and then increase towards the hydrostatic values. Nevertheless, the test was stopped before this condition were reached.

Dissipation tests performed during the other two penetration tests did not show any recognizable behavioural patterns and probably due to errors in pore pressure measurements, are not reported here.

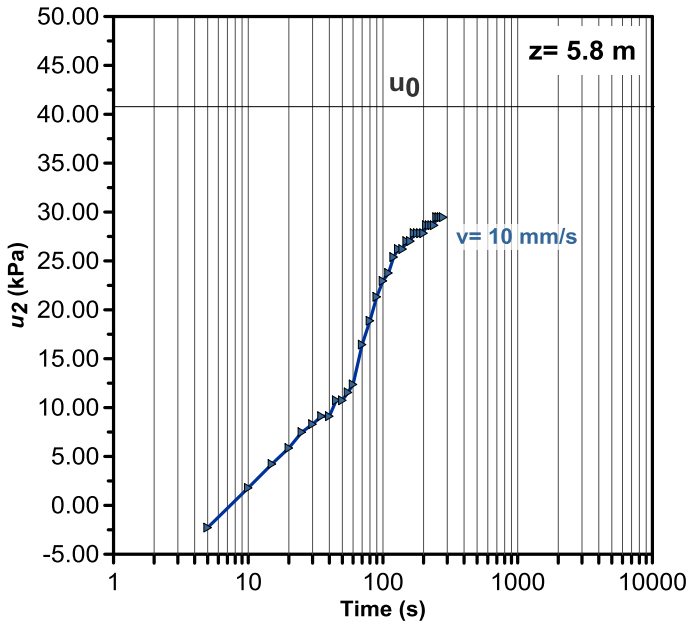

Figure 3.15: Dissipation curves carried out at a depth of 5.8 m, for CPTU-min

3.4 Assessing soil liquefaction potential

The standard cone penetration test (CPT) sounding at Mirabello was used for the assessment of soil liquefaction potential (see Chapter 2) according to the CPT-based approach proposed by Robertson and Wride (1998). A detailed description of the approach can be found in Robertson and Wride (1998).

The magnitude (M_w) adopted in the analysis is equal to 6.14, derived from the ZS9 seismic source zone mode (Meletti *et al.*, 2008). The expected horizontal PGA on rock with 10% probability of exceedance in 50 years is assumed equal to 0.15g and the stratigraphic amplification factor (S_s) is taken equal to 1.5 for a soil supposed to correspond to class C.

The soil behaviour type index I_c (Figure 3.16*a*) was calculated using normalization techniques proposed in Robertson and Wride (1988), based on iterative procedures. Figure 3.16*b* shows the results of applying the correlation proposed between the soil behaviour type index I_c and apparent fines content FC (%). Although the correlation is approximate, is a useful guide for this study purposes.

For soils with I_c > 2.6, samples should have been obtained and evaluated using other criteria as such proposed in Robertson and Wride (1998). However it is reasonable to assume that soils with I_c > 2.6 (FC > 35%) are not liquefiable. In this way, for profile points with I_c > 2.6, cyclic liquefaction has been not evaluated.

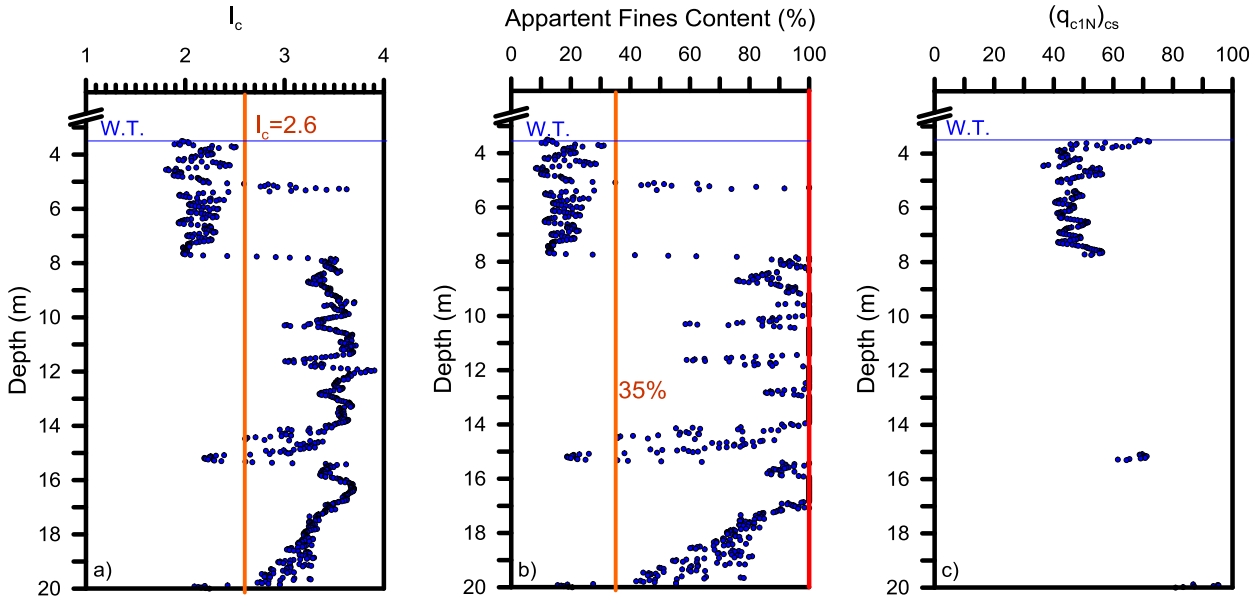

Figure 3.16: Application of the CPT method to CPTU-0 (Mirabello) for estimating a) Soil type index (Ic), b) apparent fines content (FC) and c) equivalent clean sand normalized penetration resistance

Then, the normalized cone penetration resistance corrected for overburden stress (q_{c1N}), obtained by an iterative process, has been corrected for grain characteristics using a correction factor K_c $\left(q_{c1N,cs} = K_c \cdot q_{c1N}\right)$, which is a function of the soil behaviour type index I_c. The equivalent clean sand normalized penetration resistance $(q_{c1N})_{cs}$ (Figure 3.16*c*) was used to estimate the cyclic resistance ratio (CRR).

Finally, the factor of safety (FS) profile within the silty sands was obtained comparing the cyclic stress resistance (CSR) from the earthquake to the CRR profile for the soil deposit, adjusted to the same magnitude. The FS (Figure 3.17) from 4 to 8 m turns out to be below 1.0, thus confirming the susceptibility of these sediments to cyclic liquefaction.

Due to the factor of safety can be used to predict if a layer can liquefy or not, but not to predict degrees of severity, the liquefaction potential index (LPI) proposed by Iwasaki *et al*. (1982) and after modified by Sonmez (2003) was used to estimate the severity categories. As these researchers suggested, damage to structures tends to be severe if the liquefiable layer is thick, shallow and the FS is quite less than 1.

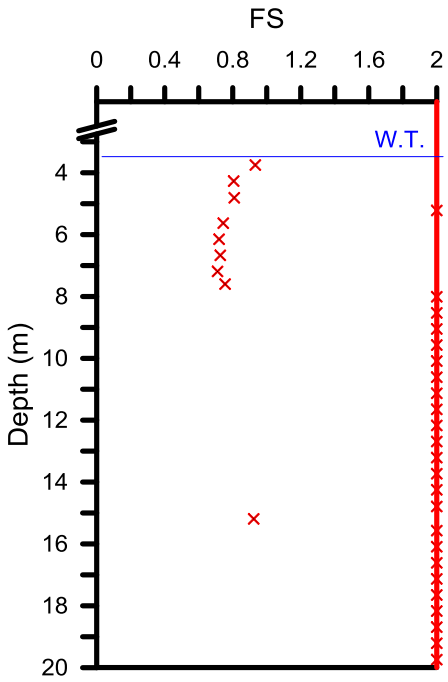

Figure 3.17: Factor of safety against liquefaction of Mirabello subsoil

As surface manifestations of liquefaction at greater depths than 20 m are unusually reported, the computation of LPI was limited to depths ranging from 0 to 20 m. The original definition of the LPI was expressed as follows:

$$LPI = \int_0^{20m} F(z) \cdot w(z) \cdot dz \tag{3.3}$$

in which

$$F(z) = 1 - F_L \quad \text{for } F_L \leq 1; \tag{3.4}$$

$$F(z) = 0 \quad \text{for } F_L > 1; \tag{3.5}$$

$$w(z) = 10 - 0.5z \quad \text{for } z < 20\text{m}; \tag{3.6}$$

$$w(z) = 0 \quad \text{for } z > 20\text{m} \tag{3.7}$$

where z is the depth (m) of the midpoint of the soil layer. Liquefaction potential categories proposed by Iwasaki *et al.* (1982) are tabulated in Table 3.2.

Table 3.2: Liquefaction potential categories proposed by Iwasaki *et al.* (1982)

Liquefaction index (LPI)	Liquefaction potential
0	Very Low
0 < LPI ≤ 5	Low
5 < LPI ≤ 15	High
15 < LPI	Very high

Table 3.3: Liquefaction potential categories proposed by Sonmez (2003)

Liquefaction index (LPI)	Liquefaction potential
0	Non liquefiable ($F_L \geq 1.2$)
0 < LPI ≤ 2	Low
2< LPI ≤ 5	Moderate
5 < LPI ≤ 15	High
15 < LPI	Very high

Nevertheless, as Sonmez and Gokceoglu (2005) stated, non-susceptible areas could not be distinguished based on this categories. In addition, the "moderate" category was not listed in Table 3.2. Details on the limitations of the LPI and severity categories defined by Iwasaki *et al.* (1982) are provided in Sonmez (2003). To overcome this limitations, Sonmez (2003) modified the $F(z)$ term present in the equation of LPI as follows:

$$F(z) = 0 \quad \text{for} \quad F_L \geq 1.2; \tag{3.8}$$

$$F(z) = 2 \cdot 10^6 e^{-18.427 F_L} \quad \text{for} \quad 1.2 > F_L > 0.95; \tag{3.9}$$

$$F(z) = 1 - F_L \quad \text{for} \quad F_L < 0.95 \tag{3.10}$$

and introduced new categories into the classification proposed by Iwasaki *et al.* (1982), shown in Table 3.3.

Finally, Figure 3.18 shows the cumulative LPI values from 0 to 20 m in depth obtained from CPTU-0 at Mirabello Site. The LPI values mainly increase from 8 m up to the groundwater table, ranging from LPI = 0 to LPI = 6 respectively.

Finally, it is worth observing that, despite a substantial lack of contributions on this issue, partial consolidation might probably affect the evaluation of soil liquefaction susceptibility from CPTU. However, the common use of a correction factor related to fines content, together with a stress normalization of q_t that depends on the soil behaviour type index, allows accounting for the intermediate nature of the sediments and therefore implicitly includes in some way the effect of partial drainage on the liquefaction analysis. Indeed, the results obtained in this study on the Mirabello piezocone data, using the Robertson and Wride method, are fully consistent with the observed liquefaction phenomena.

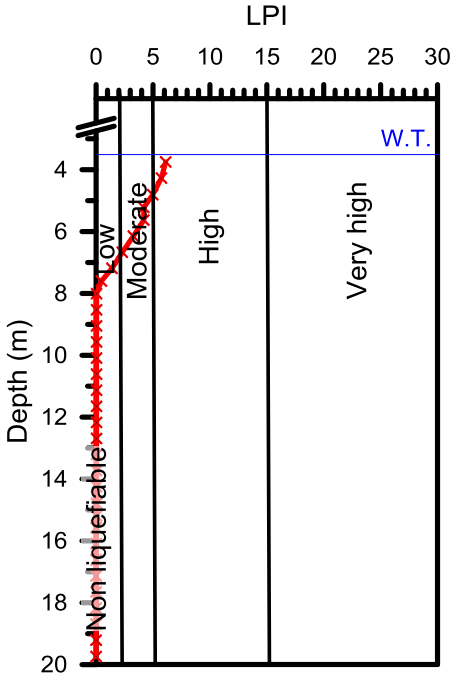

Figure 3.18: LPI in the soil column using CPTU-0 from Mirabello Site

3.5 Analysis of penetration rate effects

3.5.1 Mirabello Site

Despite a certain difficulty in interpreting field data in comparison with other published centrifuge test results, the accurate analysis of piezocone profiles plotted in Figure 3.8 reveals a general slight decrease of q_t together with an increase of u when the penetration rate v varies from 10 mm/s to 80 mm/s. By contrast, a gain in cone resistance is observed when the penetration velocity is equal to the maximum value v = 130 mm/s. A similar effect, which is likely to be attributed to viscous phenomena, has been reported by other authors for field, calibration chamber CPTs or centrifuge testing performed on fine soils under undrained conditions (e.g. Powell and Quarterman, 1988; Randolph, 2004).

In order to get a better insight into the rate effects within the silty sands, Figure 3.19 shows the profiles of corrected tip resistance, q_t, and pore pressure, u_2, measured in the non-standard tests, from 5.3 to 6.4 m in depth. It can be seen that generally u_2 increases and q_t reduces as the cone velocity increases from 10 mm /s to 80 mm/s. In contrast, at 130 mm/s, the q_t values are in general higher than those observed at 80 mm/s and the u_2 values reduce, thus confirming the observations made in the above paragraph.

According to such experimental results, it seems reasonable to assume that a penetration rate equal to 80 mm/s, where q_t is minimum, corresponds to a fully undrained behaviour with negligible viscous effects. Additional tests, performed at cone velocities within the range 80÷130 mm/s, could undoubtedly help in identifying more accurately the transition point to fully undrained conditions.

The collected data between 5.3 and 6.4 m have been plotted in terms of v. Points in Figure 3.20 have been obtained calculating the average of the measured q_t, u_2 and f_s values within thin homogeneous soil layers. As evident from the graphs, the cone resistance at v = 10 mm/s is approximately 20% higher in comparison with its minimum value assumed at v = 80 mm/s, whilst at a higher penetration rate (v = 130 mm/s), the cone resistance significantly increases (≈30%) due to viscous effects. On the other hand, the pore pressure u_2 increases from 10 mm/s to 80 mm/s. It should be also pointed out that these silty sand sediments showed u_2 reducing from 80 mm/s to 130 mm/s.

The trend behaviour of f_s is somewhat similar to that observed for q_t, although it is well-known that sleeve friction measurements are generally less reliable in comparison to cone resistance and pore pressure measurements.

The way in which different penetration rates may affect the in situ soil response is also illustrated in Figure 3.21 with reference to the rather sophisticated classification chart developed by

Schneider *et al.* (2008). The approach, based on the normalized variables $Q = (q_t - \sigma_{v0})/\sigma'_{v0}$ and $\Delta u/\sigma'_{v0}$, was primarily derived to aid in separating whether cone penetration is drained, undrained or partially drained, hence it is recognized as superior to other classification frameworks when evaluating piezocone measurements in clayey silts, silts, sandy silts and transitional soils.

The data points from the non-standard tests CPTU-A, CPTU-B and CPTU-C, collected from 5.3 to 6.4 m, were plotted in such soil classification chart. The figure shows that the points fall in the domain of transitional soils, with a tendency to move towards the "essentially drained" behaviour when the adopted cone velocity *v* corresponds to the minimum value (10 mm/s).

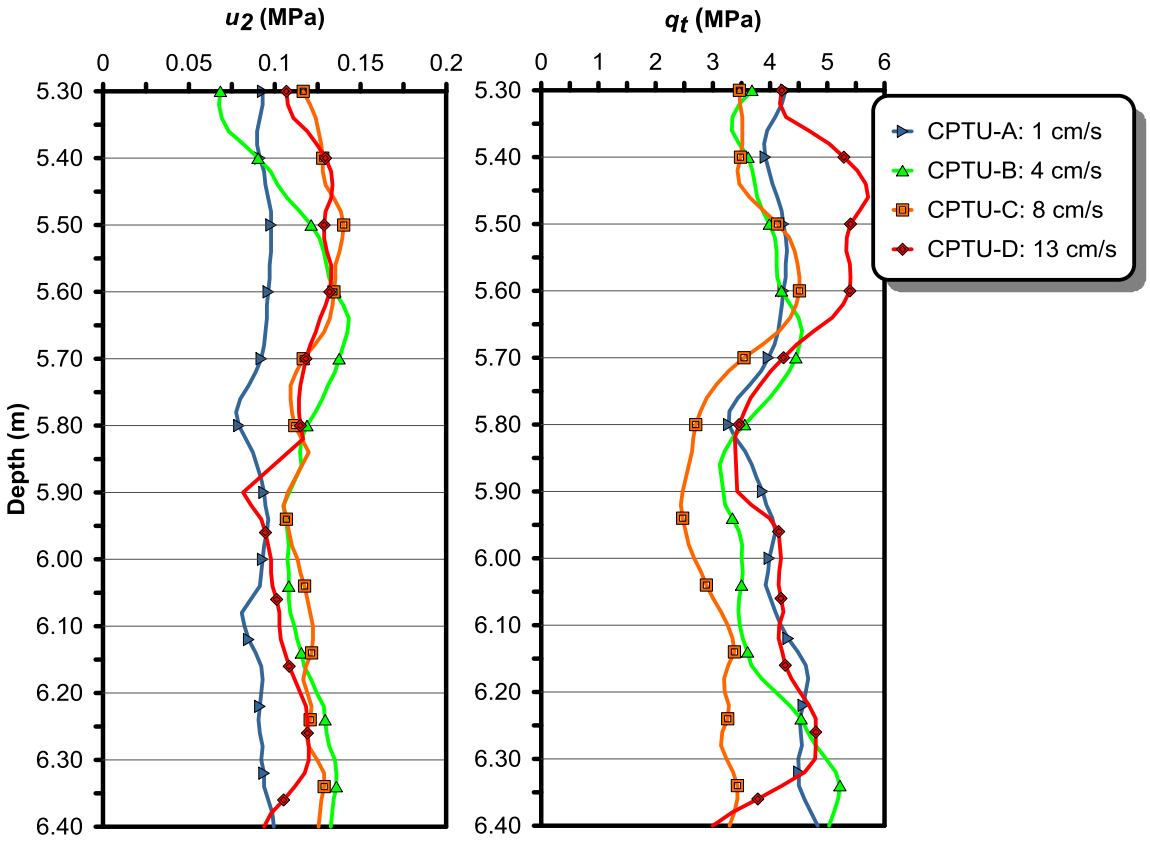

Figure 3.19: Comparison for the rate tests from 5.3 to 6.4 m

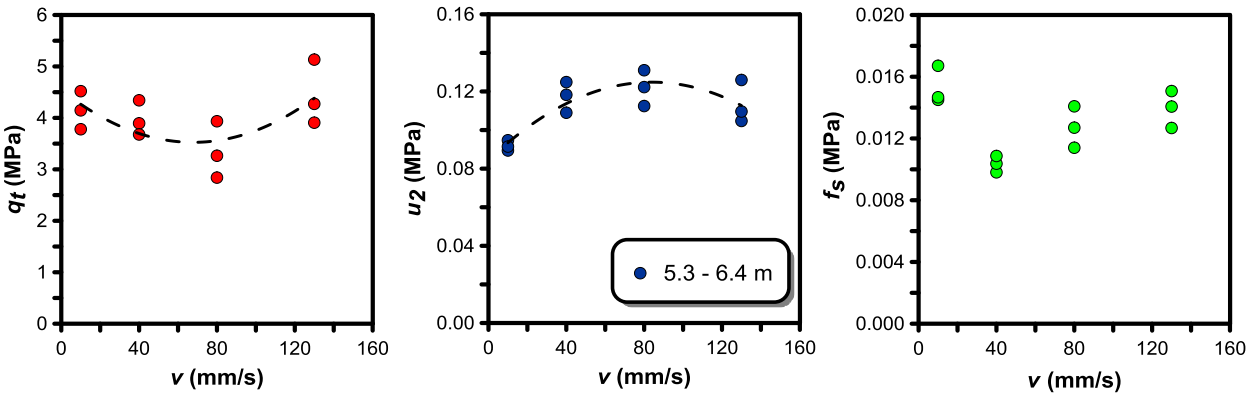

Figure 3.20: Effect of penetration rate on the cone resistance, q_t, pore pressure u_2 and sleeve friction f_s measurements

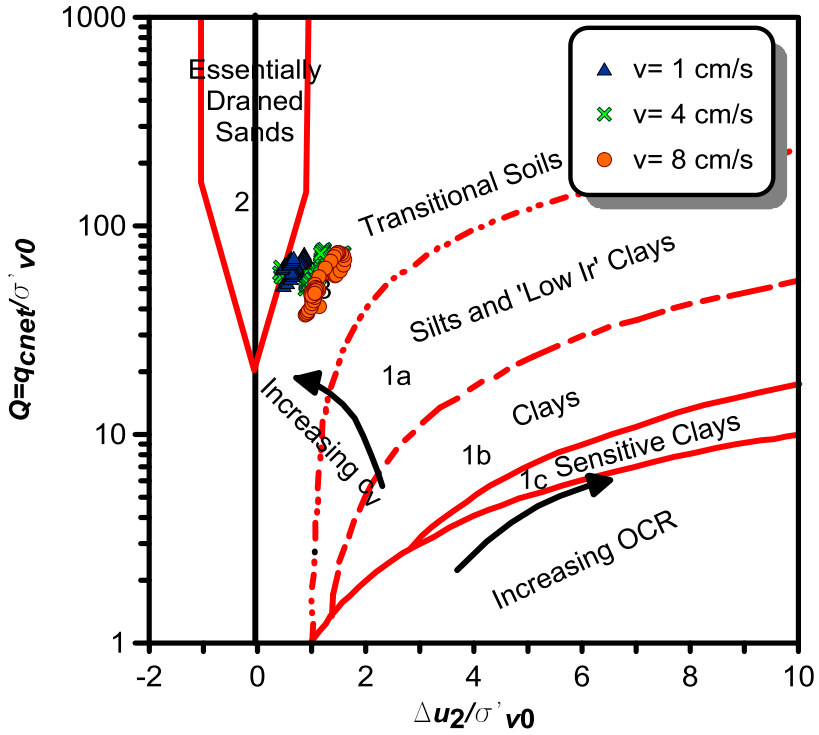

Figure 3.21: Effect of penetration rate on soil classification in the Schneider *et al.* (2008) chart

Drainage characterization curve

Dimensionless parameters were used to compare the cone penetration measurements from the available non standard penetration rates. Finnie and Randolph (1994) defined a dimensionless velocity V of the form:

$$V = \frac{v \cdot d}{c_h} \tag{2.46}$$

where v is the penetration velocity (mm/sec), d is the diameter of the penetrometer (35.7 mm) and c_v is the vertical coefficient of consolidation (mm^2/sec).

The influence of the normalized velocity on the excess pore pressure ratios ($\Delta u/\sigma'_{v0}$) is shown in Figure 3.22 together with the curves provided by Schneider *et al.* (2007), obtained by fitting model CPTU data from beam centrifuge tests in normally consolidated and overconsolidated specimens of kaolin clay and silty clay.

The trend lines from Schneider *et al.* (2007) manifest that pore pressure response of silty soils clearly differs from that of kaolin. The excess pore pressure ratios measured in the silty soils increase with V up to approximately 15 but then reduce reaching negative values above $V \approx$ 100. A similar trend was observed in silty sediments from Mirabello (5.3 to 6.4 m), which reached a maximum $\Delta u/\sigma'_{v0}$ at $V \approx 100$ and then showed a slightly negative slope beyond this value. Nevertheless, due to the largest normalized velocity being limited to $V \approx 165$, it was not possible to observe if higher normalized rates would have induced negative Δu.

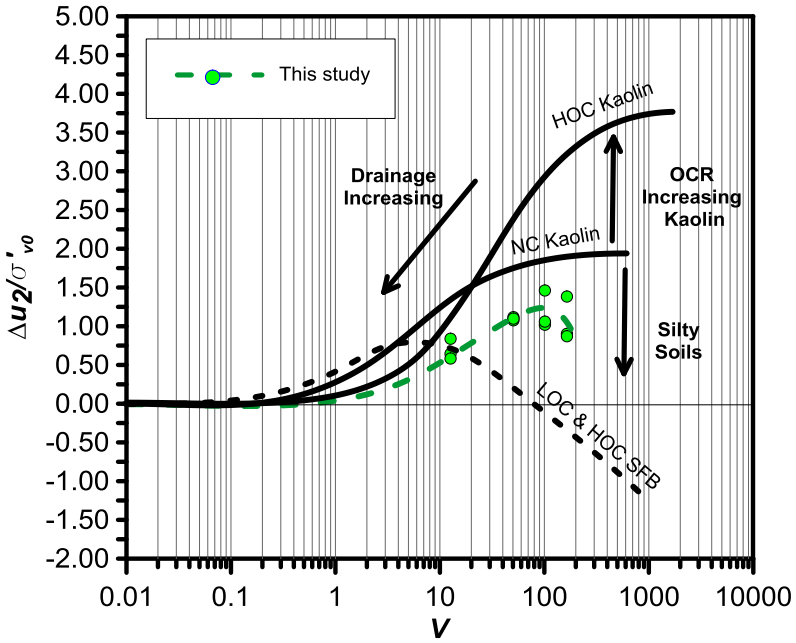

Figure 3.22: Effect of normalized velocity on normalized excess pore pressure, $\Delta u_2/\sigma'_{v0}$ and comparison with the curves provided by Schneider *et al.* (2007)

According to the approach originally proposed by Randolph and Hope (2004) and recently revised by DeJong and Randolph (2012), CPTU measurements were analysed in terms of the normalized variables $\Delta u_2/\Delta u_{2ref}$ and Q/Q_{ref} plotted against the normalized cone velocity V, where Δu_{2ref} and Q_{ref} are the reference excess pore pressure and normalized cone resistance for undrained penetration (v = 80 mm/s) respectively.

The applicability of this approach is shown in Figure 3.23. It must be emphasized that points were obtained by calculating the average of the $\Delta u_2/\Delta u_{2ref}$ and Q/Q_{ref} values within thin layers from 5.3 to 6.4 m in depth.

Figure 3.23*a* evidences a "saddle" behaviour around a minimum Q/Q_{ref} value at $V \approx 100$ (v = 80 mm/s), with higher values at lower normalized velocities due to partial consolidation and also higher Q/Q_{ref} at higher V due to viscous rate effects.

The dataset clearly exhibits two regions, which are considered to correspond to partially drained penetration for $V < 100$ and undrained penetration for $V > 100$. Unfortunately, due to the very slow penetration rate required for fully drained conditions, the minimum normalized velocity at which partially drained conditions may start has not been individuated.

Finally, ignoring rate effects that lead to an increasing resistance with higher normalized velocities, the trend curves $\Delta u_2/\Delta u_{2ref}$ - V and Q/Q_{ref} - V have been obtained using the equations proposed by DeJong and Randolph (2012):

$$\frac{\Delta u_2}{\Delta u_{2ref}} \approx 1 - \frac{1}{1 + \left(V / V_{50}\right)^c} \tag{2.49}$$

$$\frac{Q}{Q_{ref}} \approx 1 + \frac{Q_{drained}/Q_{ref} - 1}{1 + (V/V_{50})^c} \tag{2.50}$$

where the V_{50} is the normalized velocity corresponding to the penetration velocity at which one-half of the excess pore pressure for undrained penetration is mobilized. This coefficient is fairly sensitive to soil stiffness. In fact, decreasing I_r would result in curves shifted to the right and with that, increasing V_{50} values. On the other hand, the exponent c is the maximum rate of change in $\Delta u_2/\Delta u_{2ref}$ with V. $Q_{drained}/Q_{ref}$ in Equation (2.50) represents the ratio between the drained and undrained normalized cone resistance.

Despite the few points available, it was possible to define a *backbone* curve (Figure 3.24) for the silty sediments examined. The best fit has been obtained using least-squares approach, based on the difference between the normalized excess pore pressure (or Q/Q_{ref}) and the *backbone* curve for each data point. As a result, V_{50}, c and $Q_{drained}/Q_{ref}$ have been set equal to 10.38, 1.83 and 1.74 respectively. Besides, the value of c_h adopted for determining V has been set equal to $2.8 \cdot 10^{-5}$ m^2/s. obtained from the Teh and Houlsby (1991) method, mentioned in Section 3.3.1.

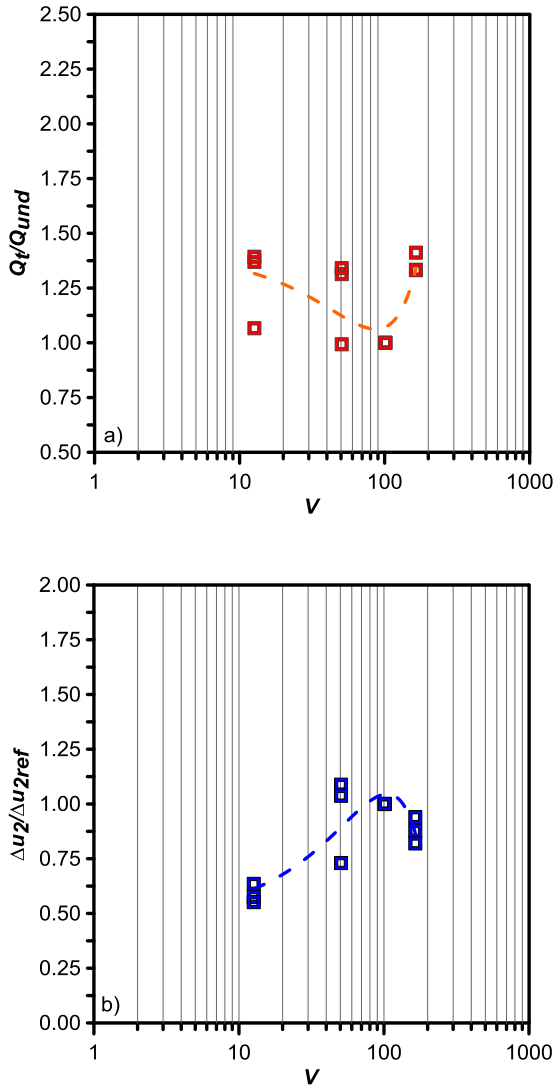

Figure 3.23: Effect of penetration rate a) on Q/Q_{ref} ; b) and on $\Delta u_2/\Delta u_{2ref}$

It turns out that drained cone penetration, corresponding to $\Delta u_2/\Delta u_{2ref}$ <0.05, occurs at V less than 2, whereas undrained conditions ($\Delta u_2/\Delta u_{2ref}$ < 0.90) occur at a normalized velocity of about 40 or higher. Furthermore, given the very slow penetration rate required for fully drained penetration, the ratio $Q_{drained}/Q_{ref}$ is very difficult to determine in the field.

Following DeJong *et al.* (2013), Figure 3.25 presents a chart that relates the coefficient of consolidation, velocity and normalized velocity. When performing standard piezocone tests, it is desirable to assess whether partial drainage is occurring and to change the velocity in order to obtain drained or undrained cone measurements. For a given c_h, obtained from pore pressure dissipation data, the associated normalized velocity for the standard rate 20 mm/s can be estimated. If V is between 2 and 40, partial drained conditions prevail and the penetration rate should be changed depending on measurements desired for design and equipment limitations.

Finally, the *backbone* curves obtained by Schneider *et al*. (2007), Oliveira *et al.* (2011) and DeJong and Randolph (2012) are plotted together in Figure 3.26 with that obtained in the present study.

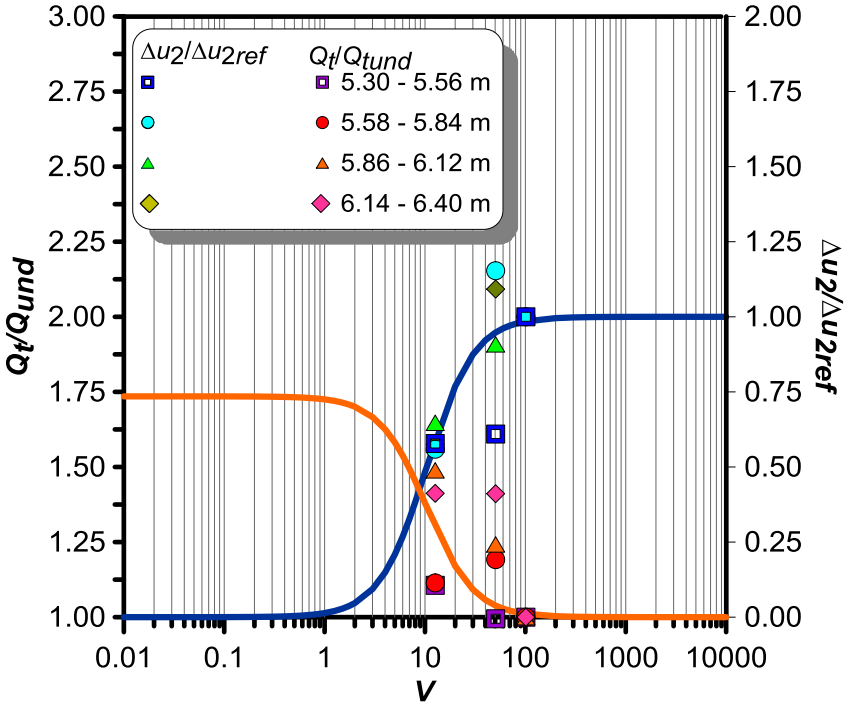

Figure 3.24: Effect of V on Q/Q_{ref} and $\Delta u_2/\Delta u_{2ref}$ ignoring rate effects and respective backbone curves

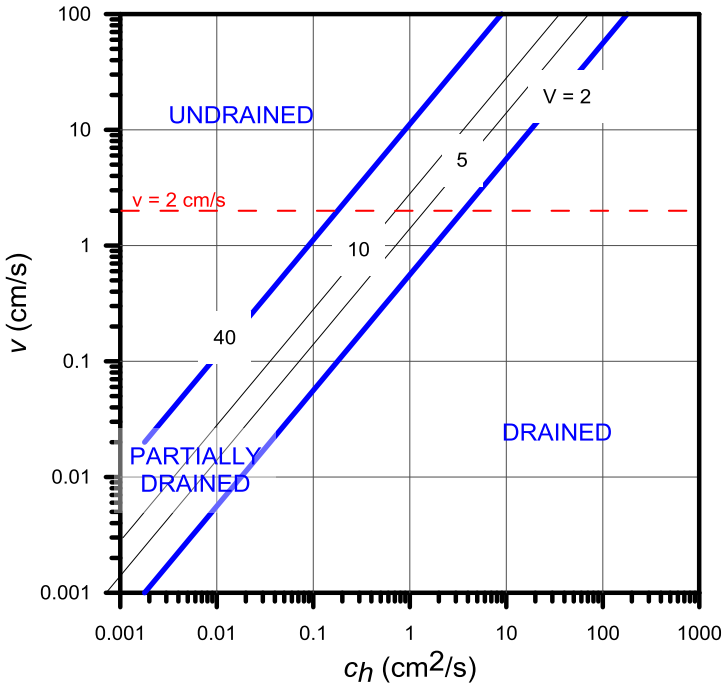

Figure 3.25: Selection of penetration rates depending on desired drainage conditions

Schneider *et al*. (2007) tested in centrifuge a mixture of 95% silica flour and 5% bentonite (SFB) with the *OCR* varying between 2 and 6 and the coefficient of consolidation varying from $4.4 \cdot 10^{-8}$ to $16.8 \cdot 10^{-8}$ m^2/s. Oliveira *et al*. (2011) presented centrifuge variable rate penetration tests using cone penetrometers. The silty soils tested had a coefficient of consolidation $c_v = 1.4 \cdot 10^{-6}$ m^2/s. DeJong and Randolph (2012) provided a *backbone* curve obtained from experimental and numerical data from different authors for normally consolidated kaolin. The respective curves were fitted within the framework of Equation (2.49) and constants V_{50} and c are shown in Table 3.4.

All *backbone* curves presented in Figure 3.26 seem to have similar maximum rate of change in $\Delta u_2/\Delta u_{2ref}$ with V (c constant), with the exception of the curve obtained from Schneider *et al.* (2007), which presented very high c value. Soil type also seems to affect the differences observed in constant V_{50}. Nevertheless, the spread of the limited number of experimental data from Mirabello can be reasonably captured by V_{50} values that vary between those observed in DeJong and Randolph (2012) and in Oliveira *et al*. (2011), 3 and 15 respectively.

Table 3.4: Constant values based on Equation (2.49)

Test	V_{50}	c
Schneider *et al.* (2007)	0.92	6.93
Oliveira *et al.* (2011)	15	1.67
DeJong & Randolph (2012)	3	1

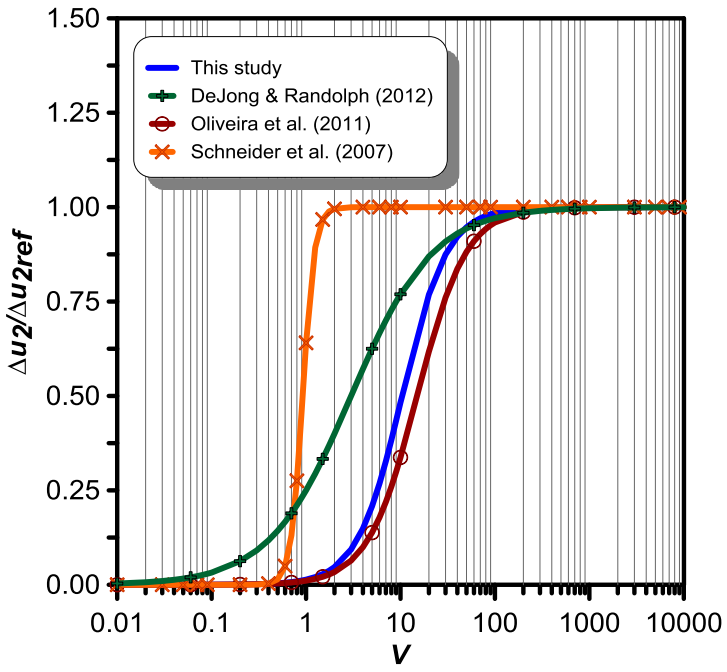

Figure 3.26: Backbone curves showing effect of V on normalized Δu_2

3.5.2 San Carlo Site

The CPTU response of the silty sands from 4.5 to 6.5 m were investigated for a range of cone velocities. Figure 3.27 shows the profiles of corrected tip resistance, q_t, and pore pressure, u_2, measured in CPTU-min (v = 10 mm/s), CPTU-st (v = 20 mm/s) and CPTU-max (v = 80 mm/s), from 4.5 to 6.5 m in depth.

Interpreting these results is quite difficult because the silt is rarely uniform. However, as can be observed in Figure 3.27, u_2 values at 10 mm/s and 20 mm/s are comparable. This values generally vary between -25 kPa to 25 kPa. This is consistent with the similar trends also observed in the q_t profiles at these rates. On the other hand, at v = 80 mm/s the u_2 values generally tend to be higher than those measured at lower velocities, varying between 0 and 25 kPa, The q_t profile at v = 80 mm/s is rather more difficult to interpret and it can be partly due to horizontal spatial variability of the subsoil.

The simplest way to examine drainage conditions is by plotting the cone resistance, pore pressure and sleeve friction against penetration rate. Points in Figure 3.28 have been obtained calculating the average of the measured values within thin homogeneous soil layers (about 25 cm thick). The cone resistance for a penetration rate between 10 and 20 mm/s decreases whereas the pore pressure is almost constant. From 20 mm/s to 80 mm/s, the u_2 values slightly increase, whilst q_t apparently decreases. However, the scatter of q_t at 80 mm/s and the lack of data points between v = 20 mm/s and v = 80 mm/s makes difficult to be certain that the cone resistance at this penetration rate is the minimum resistance corresponding to fully undrained conditions. The trend behaviour of f_s is similar to that observed for q_t, although it is widely recognized that sleeve friction measurements are less reliable.

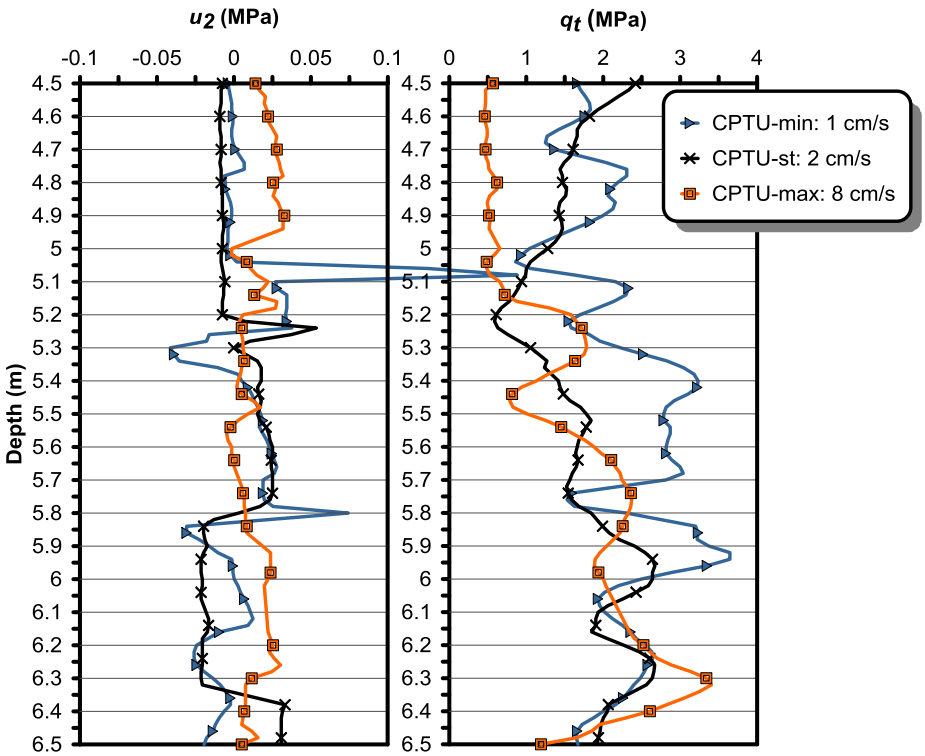

Figure 3.27:. Comparison for the rate tests from 4.5 to 6.5 m

The influence of partial drainage for soil classification was also examined. As in the case of Mirabello tests, the CPTU results from San Carlo were plotted in the classification chart proposed by Schneider *et al*. (2008). As can be observed in Figure 3.29, data points (4.5-6.5 m) fall in the domain of transitional soil, with negative Δu and tending to increase Q as the adopted velocity decreases, moving vertically towards the "essentially drained behaviour".

As long as the soil layer is below the groundwater level and the piezocone filter element is saturated and the sensor does not lose saturation during penetration, the soil classification chart based on Q and $\Delta u/\sigma'_{v0}$ can be reliable in separating drainage conditions when positive pore pressures are measured (Schneider *et al*., 2008).

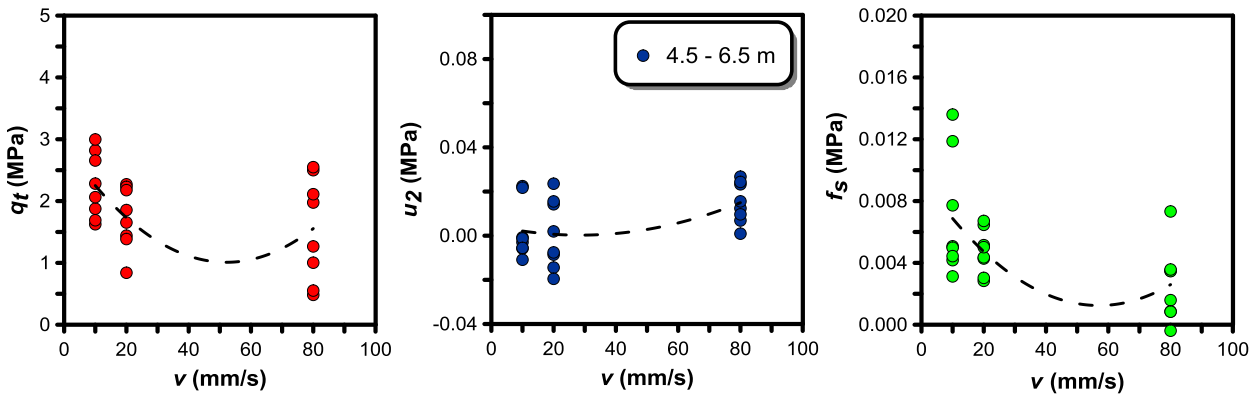

Figure 3.28: Effect of penetration rate on the cone resistance q_t, pore pressure u_2 and sleeve friction f_s measurements

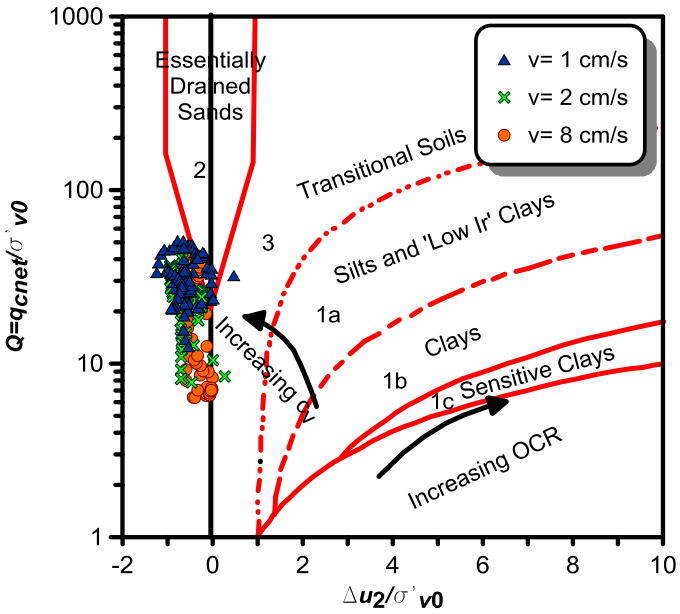

Figure 3.29: Effect of penetration rate on soil classification in the Schneider *et al*. chart

However, due to difficulties in maintaining the cone sensor saturated in dilatants deposits, the application of this chart can be problematic. In this way, the classification chart proposed by Robertson (2009) that uses the friction ratio F_r (%), has been also used to examine the influence of penetration rate when penetration becomes partially drained. As can be seen in Figure 3.30, data points generally show a decrease in F_r (%) and increase in Q_{tn} as penetration velocity reduces. However, the increase in Q_{tn} from approximately 5.4 to 6.5 m in depth at v = 80 mm/s, leads to an overlap of soil types.

Finally, the uncertainties in interpreting the way in which penetration rate affect the soil response of such silty soils, did not allow to define any drainage curve within the framework of Equations (2.49) and (2.50). In spite of this observation, following Randolph and Hope (2004), data points were plotted in the q/q_{ref} - V space, where q_{ref} is the reference cone resistance measured at v = 80 mm/s, and compared with the *backbone* curves obtained by other authors, already mentioned in Section 3.5.1. The coefficient of consolidation was reasonably assumed equal to c_h = $3 \cdot 10^{-5}$ m/s.

Data points from Figure 3.31 show that q/q_{ref} vary between a wide range of values and the maximum rate of change in q/q_{ref} with V would be very high, comparable to that shown from data from Schneider *et al.* (2007). This could be due to the big dispersion of the points.

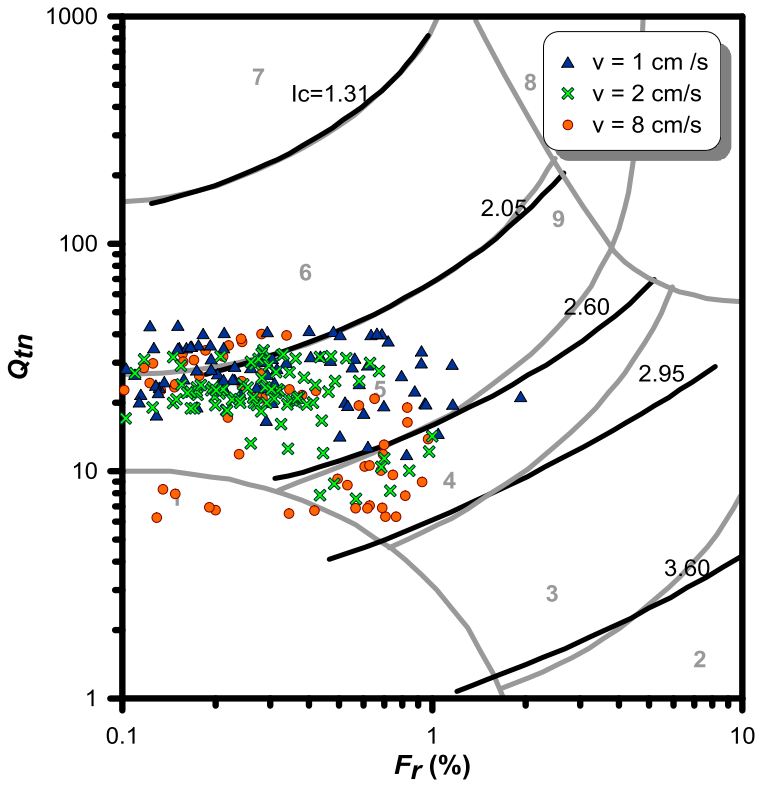

Figure 3.30: Effect of penetration rate on soil classification in the Robertson (2009) chart

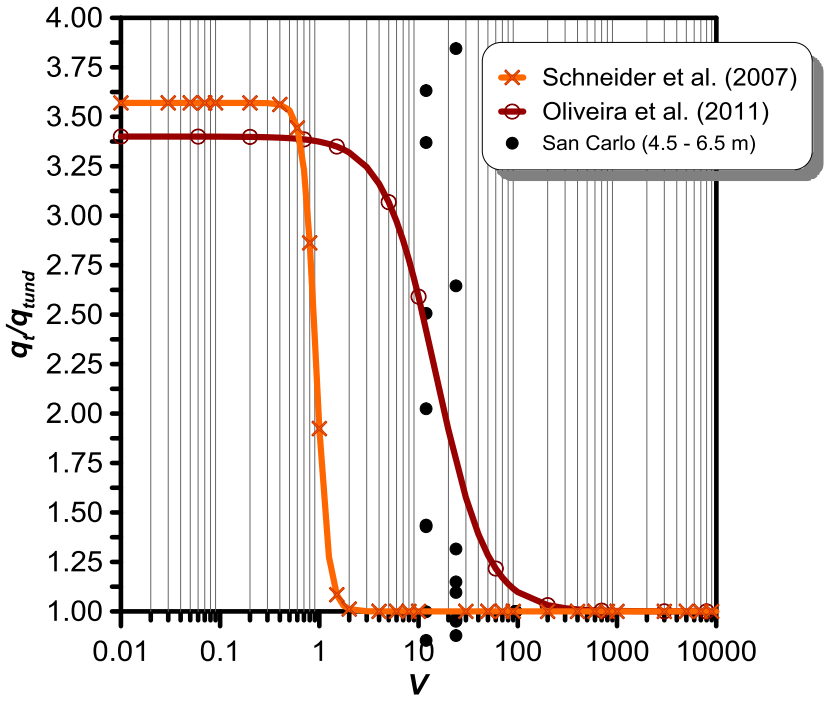

Figure 3.31: Backbone curves showing effect of V on normalized q_t

3.6 Some remarks on the evaluation of the coefficient of consolidation

The influence of the extent of partial consolidation on excess pore pressure dissipation

Dissipation tests are widely performed in soils in which CPTU penetration occurs under conditions of partial drainage to evaluate the coefficient of consolidation. However, it is well-known that partial drainage during cone penetration reduces the initial excess pore pressure in comparison with a fully undrained soil response, hence the application to dissipation tests of widely recognized interpretation methods, based on the assumption of perfectly undrained conditions, can result in inaccurate estimate of the horizontal coefficient of consolidation, c_h.

As DeJong and Randolph (2012) remarked in their work, the initial excess pore water pressure measured at the beginning of the dissipation test varies depending on the consolidation conditions around the advancing cone. They showed the numerical results from Silva *et al*. (2006) plotted as $\Delta u_2/\Delta u_{2ref}$ in Figure 3.32*a*, where Δu_{2ref} is the reference initial excess pore pressure for undrained penetration, and as $\Delta u_2/\Delta u_{2max}$, which represents the conventional approach used in practice and where Δu_{2max} is the maximum excess pore pressure within each respective curve. As can be observed, the dissipation curves normalized by this conventional way ($\Delta u_2/\Delta u_{2max}$) are shifted to the right, producing curves with higher t_{50} values and the magnitude of that shift in the $\Delta u_2/\Delta u_{2max}$ curve increases as the initial $\Delta u_2/\Delta u_{2ref}$ value decreases (DeJong and Randolph, 2012). Furthermore a similar pattern of behaviour was observed in experimental data for NC kaolin from Schneider *et al*. (2007) (Figure 3.32*b*).

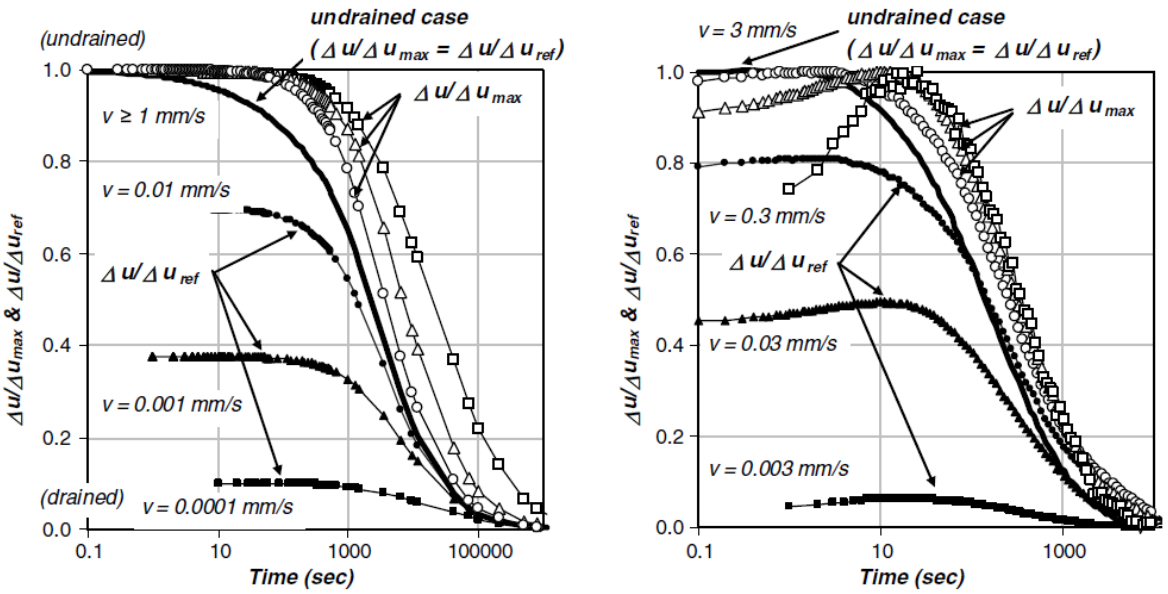

Figure 3.32: a) Dissipation curves from numerical results from cavity expansion analysis for NC kaolin using data from Silva *et al*. (2006); b) Dissipation curves from experimental data for NC kaolin from Schneider *et al*. (2007) (figure from DeJong and Randolph, 2012)

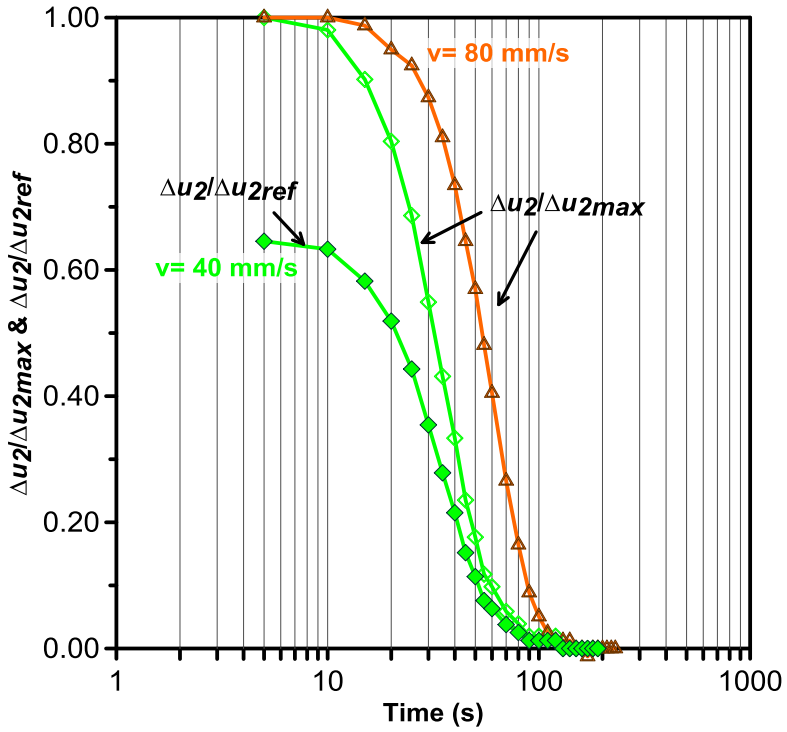

Figure 3.33: Dissipation curves from experimental data from Mirabello Site

Accordingly, DeJong and Randolph remarked that interpretation of the c_h from the $\Delta u_2/\Delta u_{2max}$ curves in Figure 3.32 using the well-established Teh and Houlsby (1991) method would produce incorrect estimates of c_h, decreasing systematically as the degree of partial consolidation during penetration increases.

Figure 3.33 shows normalized dissipation curves from experimental data for intermediate soils from Mirabello Site. Here, the Δu_{2ref} is the initial excess pore pressure for undrained penetration at v = 80 mm/s. In this case, an opposite response is obtained compared to that observed by DeJong and Randolph for the numerical results for NC kaolin. In fact, the $\Delta u_2/\Delta u_{2max}$ curve following cone penetration at v = 40 mm/s is shift to the left with respect to the dissipation curve following undrained penetration (v = 80 mm/s), producing smaller t_{50} values.

A new approach for estimation of c_h

Following Teh and Houlsby (1991), DeJong and Randolph (2012) developed a procedure for the evaluation of c_h, accounting for different drainage conditions. The characteristic curve for monotonic dissipation following undrained penetration can be expressed as follows:

$$U = \frac{\Delta u}{\Delta u_{ref}} \approx \frac{1}{1+\left(T^*/T^*_{50}\right)^b} \tag{3.11}$$

where the modified time factor is defined as $T^* = c_h t/\left(r^2\sqrt{I_r}\right)$ and the modified time factor at which 50% excess pore pressure remains is T^*_{50} = 0.245; the b exponent that best captures the rate of change is 0.75. Table 3.5 shows the modified time factors at various stages of dissipation.

Table 3.5: Time factor (u_2 position) at different stages of dissipation (Teh and Houlsby, 1991)

U	T^*	T^*/T^*_{50}
0.8	0.038	0.155
0.7	0.078	0.318
0.6	0.142	0.580
0.5	0.245	1.000
0.4	0.439	1.792
0.3	0.804	3.282
0.2	1.600	6.531

During partially drained penetration, the initial U_0 (=$\Delta u_2/\Delta u_{2ref}$) for a given V corresponds to a modified time factor $T^*_0 = T^*_{50}\left(1/U_0 - 1\right)^{1/b}$. DeJong and Randolph (2012) provided a direct relationship between a modified time factor T'_f, associated with a given percentage f of excess pore pressure dissipation referred to the initial U_0 in partial drainage conditions and the normalized rate V:

$$T'_f = \frac{t \cdot c_h}{r^2\sqrt{I_r}} = T^*_{50}\left(\frac{1}{(1-f)U_0} - 1\right)^{1/b} - T^*_0 = T^*_{50}\left[\left(\frac{1}{(1-f)U_0} - 1\right)^{1/b} - \left(\frac{1}{U_0} - 1\right)^{1/b}\right] \tag{3.12}$$

Substituting the extent of partial dissipation during penetration (U_0) from Equation (2.49) into Equation (3.12), a direct relationship between T'_f and V is established. The horizontal coefficient of consolidation c_h is finally obtained from T'_{50}, on the basis of an assumed value of the rigidity index I_r.

Figure 3.34 shows the relationship between t_{50} and c_h, taking V_{50} = 3 and c =1 from DeJong and Randolph (2012) results, v = 2cm/s, a cone radius r = 17.85 mm (d = 35.7 mm) and for rigidity index value of 100. The relationship for the fully undrained conditions by Teh and Houlsby (1991) is also plotted for reference. As can be deduced from the figure, the trends coincide during undrained conditions (t_{50} > 100s). However, as the degree of partial consolidation during penetration increases, the curves diverge and the c_h estimated using the well-known Teh and Houlsby (1991) procedure would provide underestimated c_h values.

The application of this method using the parameters obtained for the case of Mirabello analysis (V_{50} = 10.38, c =1.83 and I_r = 380) provided a curve for v = 2 cm/s shifted upward on the graph compared to that given by DeJong and Randolph. As DeJong and Randolph (2012) remarked in their work, if $b < c$, a minimum t_{50} is reached at high c_h, after which, as c_h increases, t_{50} increases again. This would lead to a non-unique value of c_h. For V_{50} = 10.38, c =1.83, I_r = 380 and v = 2 cm/s, $t_{50,min}$ is equal to 69 seconds. Hence, for t_{50} < 69s, it has not been possible to deduce a 'corrected' coefficient of consolidation using the proposed method.

It is reasonable to suppose that the error in interpretation of c_h (and I_r) from dissipation tests at Mirabello site may have contributed to inaccurate estimate of V_{50}. However, as already mentioned, the spread of data is well-captured by variations of V_{50} proposed in the literature.

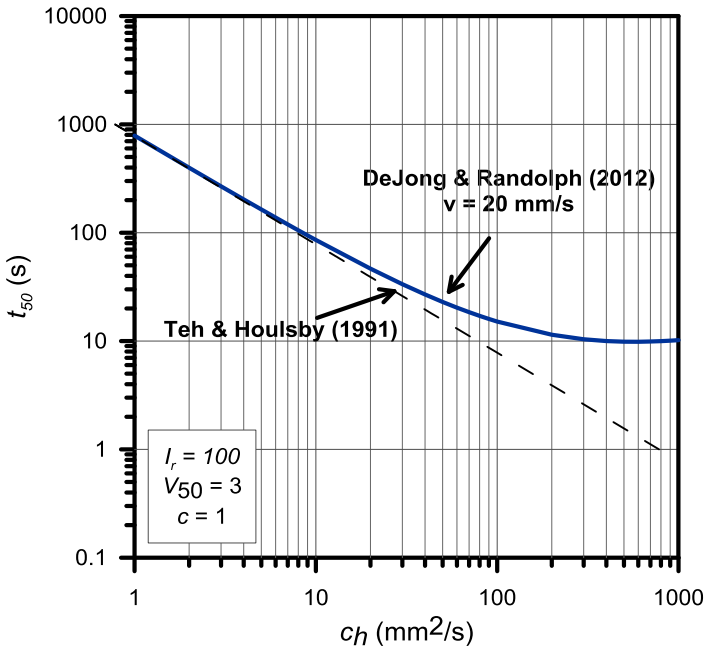

Figure 3.34: Variation in t_{50} with consolidation coefficient for V_{50} = 3 and c = 1 (curve from DeJong and Randolph, 2012)

CHAPTER 4: THE VENICE LAGOON

4.1. Introduction

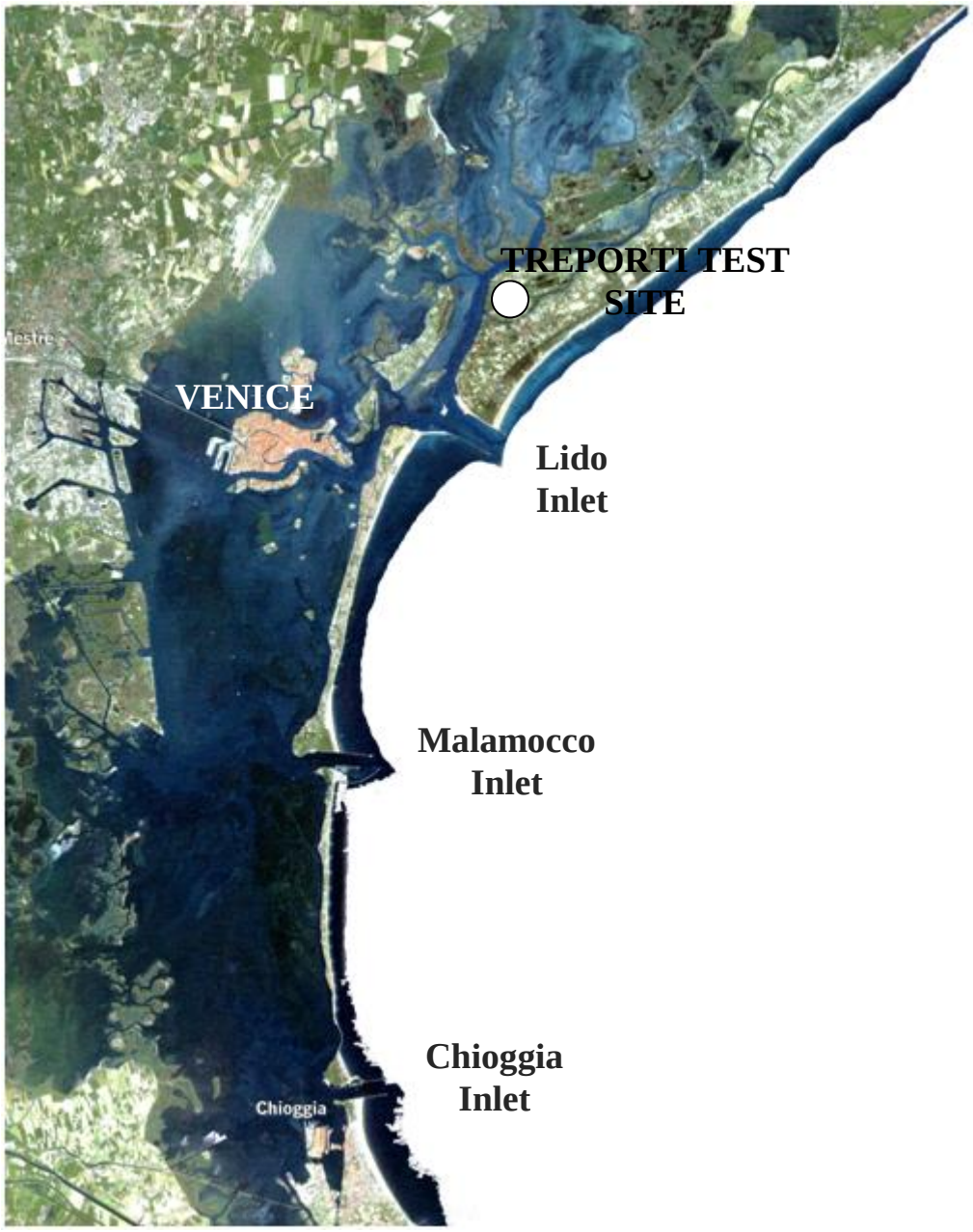

Figure 4.1: Satellite view of the Venetian lagoon with its three inlets and location of Treporti Test Site (from Tonni and Simonini, 2013)

The Venetian Lagoon (Italy) or *Laguna Veneta* is a 550 km^2 enclosed bay of the Adriatic Sea in which the historical city of Venice is situated. It is the largest wetland in the Mediterranean basin. Around 8% is land, including Venice and smaller islands. The land system of the area is made up of dry land, natural or artificial. Lido, Malamocco and Chioggia are the three inlets that connect the lagoon to the Adriatic Sea (see Figure 4.1).

The whole Venetian coastal environment as well as the invaluable historical patrimony of Venice are subject to high variations in water level which have grown gradually more frequent and higher since early 1900's.

In general, tide levels depend on astronomical, geophysical and meteorological factors. The first one results from the movement and alignment of celestial bodies, mainly the Moon. The phenomenon of high water (*acqua alta*) mainly occurs between autumn and spring, when the astronomical tides are accentuated by the Sirocco and the Bora seasonal winds. The geophysical factor principally depends on the geometric shape of the lagoon basin. The meteorological factor is associated to many variables, such as precipitation, the strength and direction of winds, etc.

Two additional natural factors that contribute to the phenomena of high water are the subsidence, i.e. the natural lowering of the soil level and eustasy, i.e. the continuous rise of the level of the sea. The effects of these phenomena have increased because of the man-induced factors, caused by the use of lagoonal water for industrial uses and global warming.

The measures of sea level in Venice are in reference to the hydrographic station located nearby the *Basilica di Santa Maria della Sallute*. With a tide of +110 cm, more than 10 % of the city is blocked with water. When tides are more than +120 cm and 140 cm height, respectively 40% and more than 60% of Venice is flooded (Jamiolkowski *et al*., 2009).

During the last century, the episodes of tides equal to or greater than +80 cm have increased. High tides mainly occur during fall and winter (about 80% of the occurrences are between October and February), disturbing the lives of inhabitants and causing significant damage to the architectural heritage ("Problems: High waters"). This phenomenon has been triggered not only by the eustasy and natural subsidence, but also since mid 1920s by additional subsidence due to extraction of ground water (see Figure 4.3). In the early 1970s, the groundwater pumping was forbidden and the ground level rebounded by approximately 20 mm. Then the subsidence came back to its natural trend (Jamiolkowski *et al*., 2009).

Figure 4.2: Venice, 1st December 2008 (image taken from the website salve.it)

Over the last decades, a number of engineering solutions, including both nearshore and offshore structures, have been constructed in order to protect human activities of the whole Venetian coastal environment as well as the invaluable historical and artistic heritage of Venice from sea storms, high tides and recurrent flooding.

Between the 19th century and the first decades of the 20th century, long jetties were built at the inlets connecting the lagoon to the Adriatic Sea (Figure 4.1). In the early 1990's, a long-term safeguarding project was approved which involved the morphological restoration of the coast line, the erosion mitigation, the reinforce of the existing jetties, the oil tankers traffic reduction and the fishing farms re-opening (Jamiolkowski *et al*., 2009).

In relation to the ambitious project known as MOSE (MOdulo Sperimentale Elettromeccanico, *Experimental Electromechanical Module*), consisting on a mobile barriers system for the temporarily closure of the lagoon inlets, from 2003 to 2007, the existing jetties were reshaped, new breakwaters were built in front of the inlets and a small island was realized within the Lido inlet.

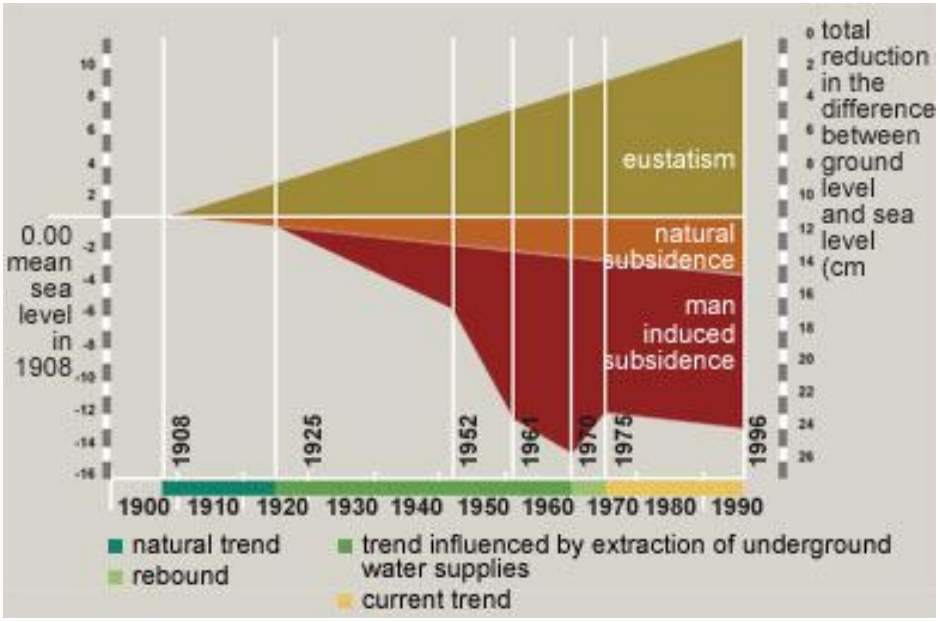

Figure 4.3: Eustatic ride of the sea level and natural subsidence (image taken from the website salve.it)

4.2. Venetian Lagoon sediments

The Venice Lagoon sits upon the Adriatic plate in a basin located between the Alps and the Apennine chains. It is underlain by approximately 800 m of Quaternary deposits. During the Quaternary the area underwent alternating periods of marine regressions and transgressions. Hence, continental and marine sediments coexist. The upper 50-70 m-thick deposits are characterized by a complex interbedding of sands, silty clays and silts, which occurred in the last glacial period of Pleistocene (Würm). The top Würmian layer is composed of a rather stiff silty clay, commonly referred to as *caranto*. Moving from the mainland towards the shoreline, the caranto lies at depths from about 5 m to 12 m below m.s.l. and shows thicknesses that range from a few centimetres to a few meters. Other overconsolidated layers may be found at greater depths probably due to temporaneous oscillations of the sea level during the Würmian period (Cola and Simonini, 2002).

The shallowest deposits, from ground level to 5-10 m below mean sea level (m.s.l), are due to the Holocene. The Holocene architecture is rather complex due to the geological history combined with human intervention (Madricardo *et al*., 2007; Donda *et al*., 2008; Tosi *et al*., 2009*a*).

Since XII century, the main engineering activities involved improvements in communication between the lagoon and sea and conservation of the city insularity (Colombo, 1986). Between 15th and 17th century, rivers such as Brenta, Piave and Sile were diverted into extensive canals around the periphery in order to avoid infilling and robust stone-walls to protect the channel and island banks against erosion were constructed. The shape of the lagoon inlets has been also steadily modified: after the second world war, a navigable channel (*Oil Channel*) was carved through the lagoon to allow the large oil tankers to reach the industrial area of Porto Marghera. This channel linked the sea to the coastal line, running through the harbour in Malamocco inlet. All these human interventions caused a continuous reduction of sediment balance (Simonini *et al*., 2007).

Subdivisions of the Quaternary System

System	Series	Stage	Age (Ma)
Quaternary	Holocene		0-0.0117
	Pleistocene	Tarantian	0.0117-0.126
		Ionian	0.126-0.781
		Calabrian	0.781-1.806
		Gelasian	1.806-2.588
Neogene	Pliocene	Piacenzian	Older

Table 4.1: Subdivisions of the Quaternary System

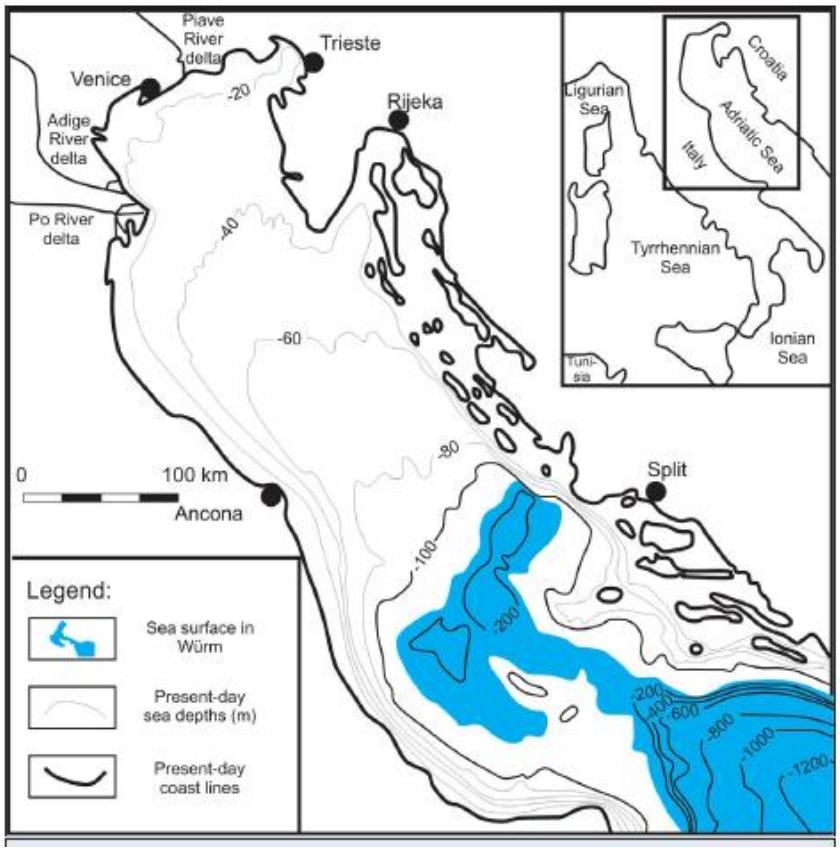

Figure 4.4: Boundaries of Adriatic Sea during Würm (Correggiari *et al.*, 1996; Velić and Malvić, 2011)

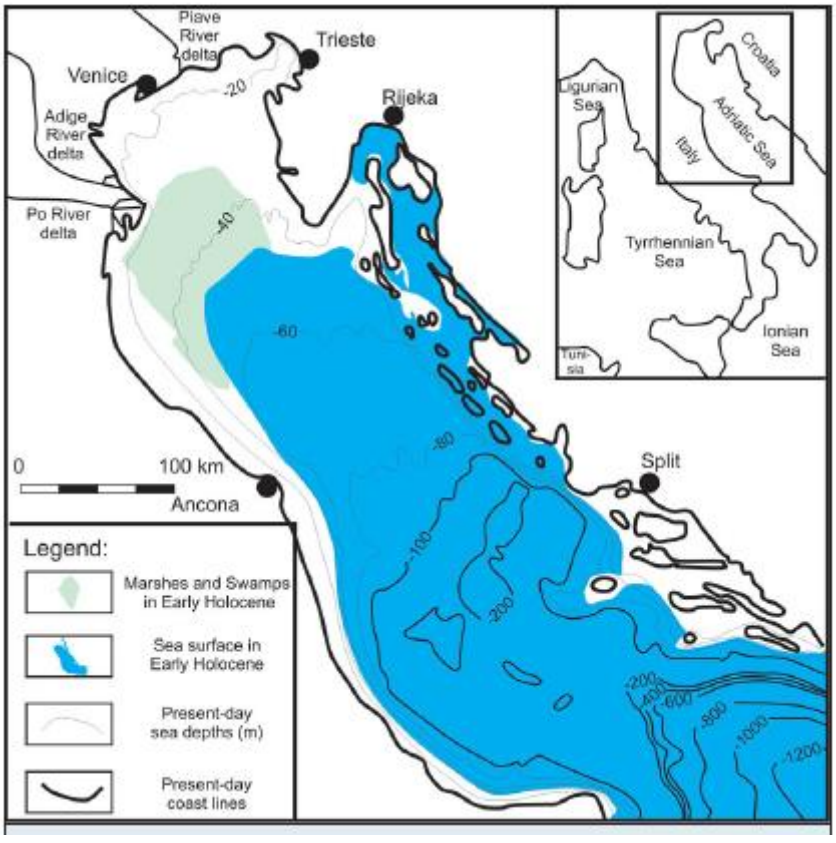

Figure 4.5: Boundaries of Adriatic Sea in beginning of Holocene (Correggiari *et al.*, 1996; Velić and Malvić, 2011)

Regarding grain-size distribution, 95% of Venetian sediments can be grouped into three classes (Cola and Simonini, 2002): medium-fine sands (SP-SM), silts (ML), and very silty clays (CL), according to the unified soil classification System. The remaining 5% may be classified as organic clay and peat.

Sands are predominantly composed of silicates and carbonates, the latter in the forms of detrital calcite and dolomite crystals, especially at higher depths (Favero *et al*., 1973). Sits and silty clays, originated from mechanical degradation of sands, have a content of non-active clay minerals, not exceeding beyond 20%, which are mainly composed of illite with minor quantities of chlorite, kaolinite and smectites (Curzi, 1995; Cola and Simonini, 2002).

4.3. Site characterization

Over the last decades, the shallow Pleistocene sediments underlying the Venetian lagoon have been thoroughly investigated. First in the 1970s, in relation to the regional land subsidence and then in the late 1980s, within the context of the system of interventions presented to safeguard Venice, including mobile gates at the inlets. Geotechnical investigations were performed to obtain stratigraphic conditions along with the cross sections of the inlets and to estimate relevant geotechnical properties for a preliminary selection of the mobile gates foundations. Between 2001 and 2004, additional and more exhaustive investigations were also integrated in order to accomplish a proper foundation design (Jamiolkowski *et al*., 2009).

From the large amount of data collected over approximately 40 years, it turned out that the Venetian subsoil conditions consist of a complex assortment of interbedded normally consolidated or slightly overconsolidated silts, medium-fine silty sands and silty clays.

Despite grain size heterogeneity, research has shown that these sediments have a common mineralogical composition and that their mechanical behaviour is mostly controlled by intergranular friction (Cola and Simonini, 2002). Furthermore, as a consequence of their predominantly silty nature and high heterogeneity, undisturbed soil sampling is rather difficult to achieve, hence geotechnical characterization must essentially rely on in situ testing.

In order to gain a better understanding of such intermediate soils, research was focused on some selected trial tests sites, considered as representative of the Venetian subsoil, especially in relation to the foundation design of the gates.

The first test site was located at the Malamocco inlet. A series of investigations, including boreholes, dilatometer (DMT), piezocone (CPTU), cross hole tests (CHT) and self-boring pressurement (SBPM) were performed on contiguous verticals at the Malamocco Test Site (MTS) (Cola and Simonini, 1999, 2002; Ricceri *et al*., 2002). These site investigation campaigns were mainly aimed at calibrating the empirical correlations between the soil classification and CTPU and DMT measurements, including their seismic versions SCPTU and SDMT (Ricceri *et al*., 2002).

The extensive laboratory investigations completed at MTS (Cola and Simonini 2002; Biscontin *et al*. 2001; 2006) confirmed the highly heterogeneous nature of the subsoil. Thus, in order to determine the simplest properties with a certain degree of accuracy, a relative large number of tests were required. Furthermore, because of high silty content and the low-structured nature, the sediments resulted very sensitive to stress relief and disturbance owing to sampling, thus influencing negatively assessment and reliability of laboratory tests (Jamiolkowski *et al*., 2009).

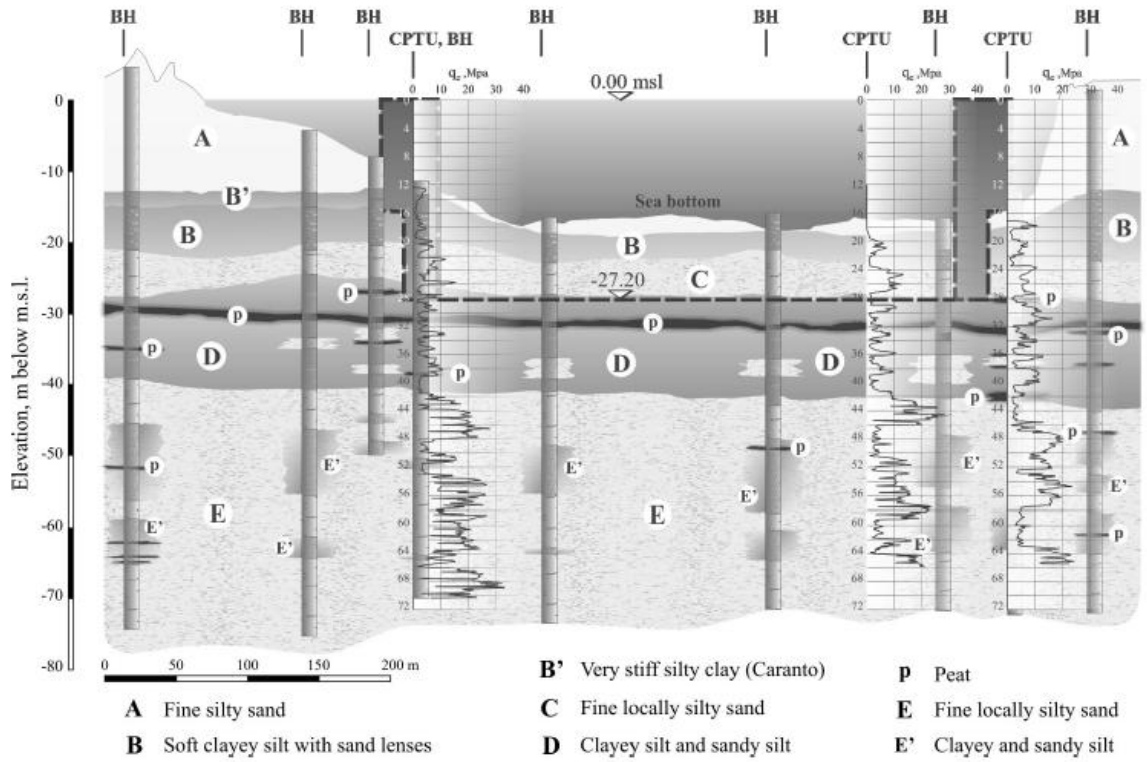

Figure 4.6: Soil profile at the Malamocco inlet (Jamiolkowski *et al*., 2009)

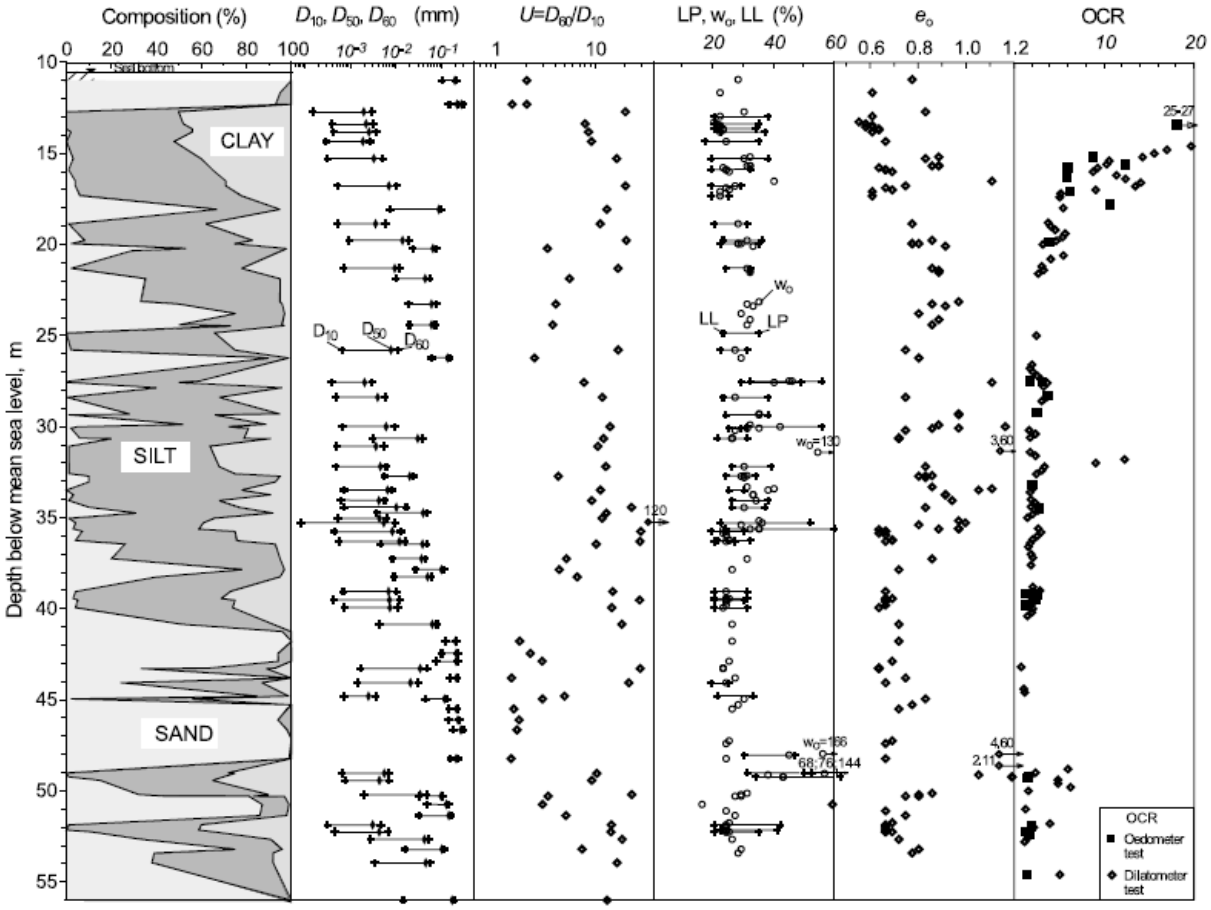

Figure 4.7: Soil profile, basic properties and stress history at the Malamocco Test Site (Cola and Simonini, 2002)

A new representative test site was then located outside Treporti, an old fishermen village, located at the inner border of the lagoon, close to the Lido inlet (see Figure 4.1). The research programme was carried out by the Italian Universities of Padova, Bologna and l'Aquila with the aim of the better understanding the behaviour of the silty sediments forming the shallowest layers of the Venetian lagoon subsoil (Gottardi and Tonni, 2004; 2005).

The aim of the Treporti Test Site (TTS) was to assess directly in situ the stress-strain-time properties of such heterogeneous soils. The research programme, consisting of a detailed geotechnical characterization of the subsoil using in-situ tests, boreholes and high quality laboratory tests, included also the construction of a vertical-walled cylindrical test bank (see Figure 4.8). The embankment, which had a diameter of 40 m and a total height of 6.7 m, was progressively built in order to load the ground uniformly up to 107 kPa (Simonini, 2004; Gottardi and Tonni, 2004; 2005).

The experimental programme was performed in four phases, depending upon the different loading conditions related to the bank presence. The "first phase" was intended to give an initial description of the subsoil, paying special attention to the detection of the most compressible layers within the area. Afterwards, a the "second phase" was carried out just beneath the circular area of the loading bank that was to be built. The bank construction started on September 2002 and ended on March 2003. When completed, a number of tests were performed from the top of the embankment itself in the so-called "third phase". The last campaign was carried out four years later, after the gradual removal of the bank (Tonni and Gottardi, 2010; 2011).

The ground beneath the test bank was heavily instrumented (see Figure 4.8*c*) with the aim of periodically measuring main geotechnical quantities in consequence of the loading-bank construction (Simonini, 2004): pore pressure in fine-grained soils by means of Casagrande and vibrating wire piezometers, induced total stresses by means of load cells, horizontal displacements with depth using inclinometers, surface settlements through a GPS equipment and routine surveying methods, deep vertical settlements by rod extensometers and vertical strains with depth by means of sliding deformeters. The latter is a device for the measurement of soil axial strains along a vertical or inclined direction.

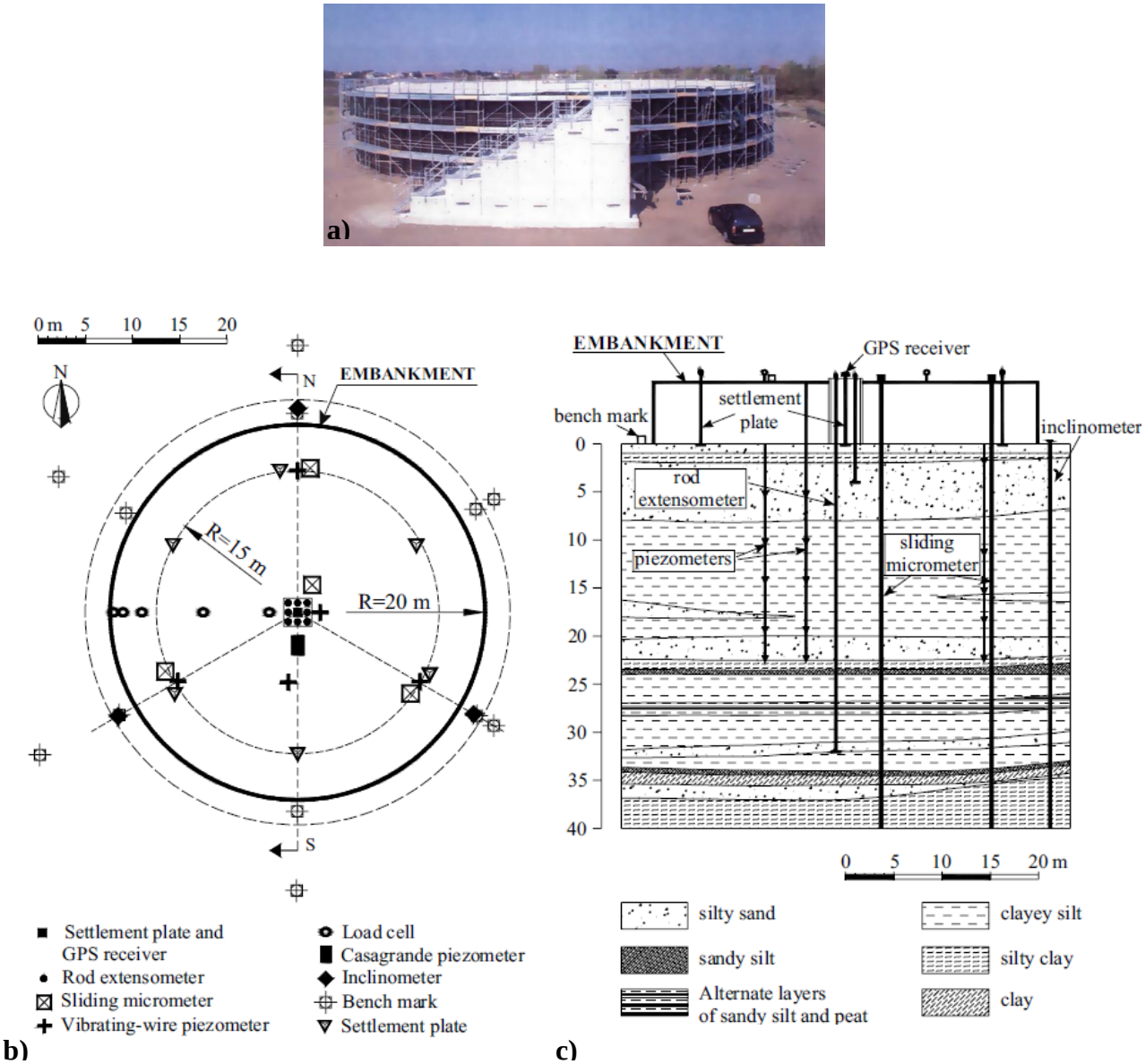

Figure 4.8: a) Treporti test embankment; b) location of the monitoring instrumentation; c) cross-section of trial embankment and soil profile (Simonini, 2004; Simonini *et al.* 2007)

4.3.1. The Treporti Test Site

Preliminary investigation

The "first phase" of the in situ campaign was carried out by means of 7 piezocone tests (CPTU from 1 to 7 in Figure 4.9) and 2 mechanical penetrometer (CPT A and B in Figure 4.9). No dissipation tests were performed in this phase.

The standard CPTU tests were performed by the Soil Mechanics Laboratory of the University of Bologna by means of an integrated electronic piezocone, manufactured by Delft Geotechnics, with 200 kN of nominal thrust. The equipment provides continuous measurement of q_c (cone resistance), f_s (sleeve friction) and u_2 (pore pressure measured behind the cone tip). Data were logged at about intervals of 1 second. The equipment included also an inclinometer that al-

lows depth correction in relation to the possible deviation of push rods (Tonni and Gottardi, 2004).

Figure 4.10 shows an example of the corrected cone resistance (q_t) and pore pressure (u_2) profiles of CPTUs located along the west-east cross section. Cone resistance profiles of CPT A and B are also plotted. The water level is very close to the ground level, according to the nearby canal level and subjected to local tidal excursions, about ± 0.5 m twice a day. Figure 4.10 demonstrates the very heterogeneous nature of the subsoil. A silty sand is detected from ground level to 6-7 m in depth. Then it follows a rather dense alternation of sandy to clayey silts. Such variation is particularly evident in the u_2 profile, where the pore pressure rarely follows up the hydrostatic level, frequently falls below it, but never developing high Δu (= $u_2 - u_0$) values. Rather large friction ratio values occasionally observed, indicate the presence of thin layers of peat and organic soils (Gottardi and Tonni, 2004).

Between depths of 7-8 m and 20 m, it is identified a potentially more compressible fine-grained unit, mainly composed of silts. However, its thickness it is not constant throughout, being interbedded with a clean sand layer variable in thickness. In Figure 4.10, the interbedded sand is detectable in CPTU 6 and CPTU B and becomes rather significant in CPTU 1, CPTU 5 and CPTU 7, whilst in tests CPTU 2 and CPTU 3 (not shown here) the whole layer from 8 to 20 m in depth can be considered a unique silty layer. In this way, the NW corner of the site area was selected as the most suitable location of the loading bank.

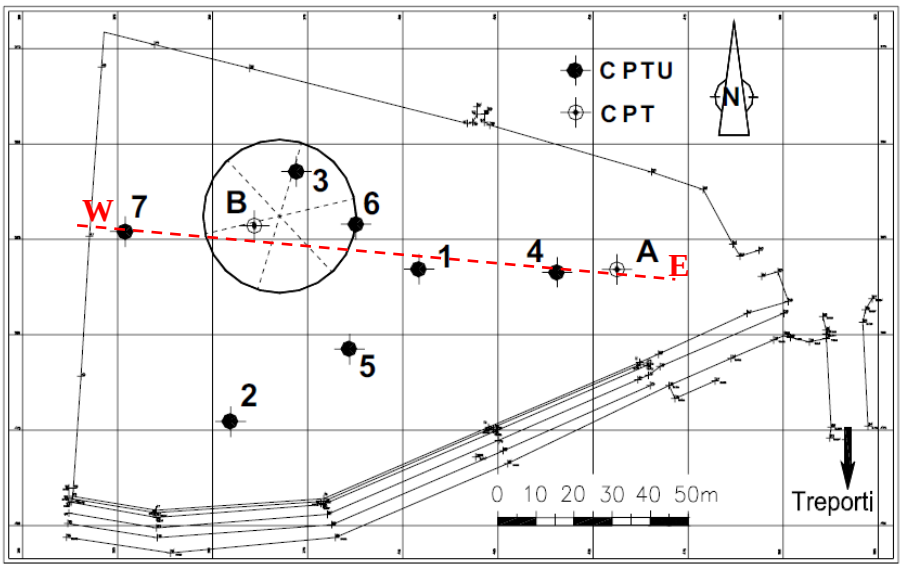

Figure 4.9: Plan of the testing area and location of the penetrometer tests of the "first phase" (Tonni and Gottardi, 2004)

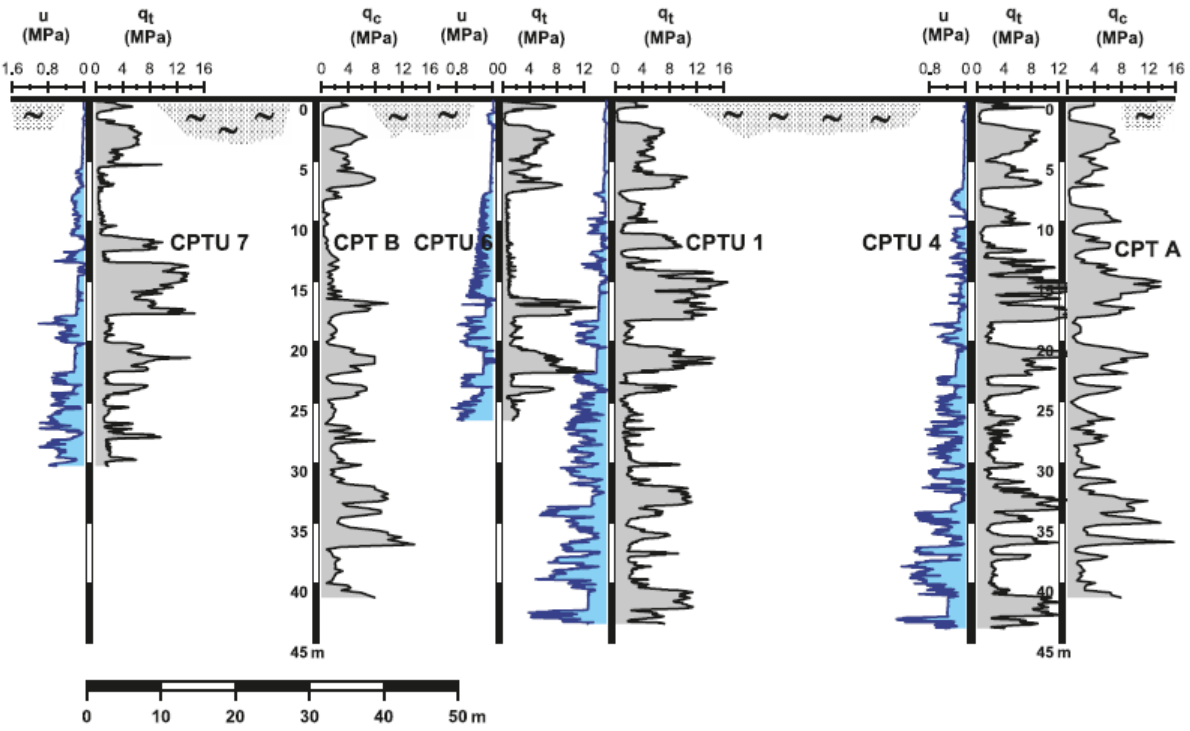

Figure 4.10: Cross section W-E of the test site area (Tonni and Gottardi, 2011)

A typical Treporti soil profile with the basic physical properties from ground surface to 25 m in depth is shown in Figure 4.11, as provided by laboratory tests performed on samples from borehole S3, located within the circular area selected for the location of the embankment. In the plot showing the soil grading (%), the silt and sand fractions predominate (in this case represent on average 42% and 44% of the tested materials respectively). Mean values of the plasticity index (PI) and liquid limit (w_L) turn out to be 13.31% and 36.53%, respectively. Activity (A = PI/ % clay particles) of the clay part ranges from 0.20 to 0.50, thus confirming that the fine-grained sediments are in general nonactive (Tonni and Gottardi, 2011).

Such features as the piezocone response at the TTS yielded information in good agreement with that obtained at the MTS and reported in Ricceri *et al*. (2002), thus leading to consider the TTS as representative of the typical Venetian subsoil (Tonni and Gottardi, 2011).

Second-phase characterization

The site investigation programme carried out in a "second phase" geotechnical characterization of the subsoil below the test bank, consisted of 10 piezocone and 10 flat dilatometer (see Marchetti *et al.*, 2004), 2 standard mechanical CPT and 4 60 m deep boreholes. Furthermore, 3 seismic cone tests (Mayne and McGillivray, 2004) and 3 seismic dilatometer tests (Marchetti *et al*., 2004; Mayne and McGillivray, 2004) were subsequently carried out.

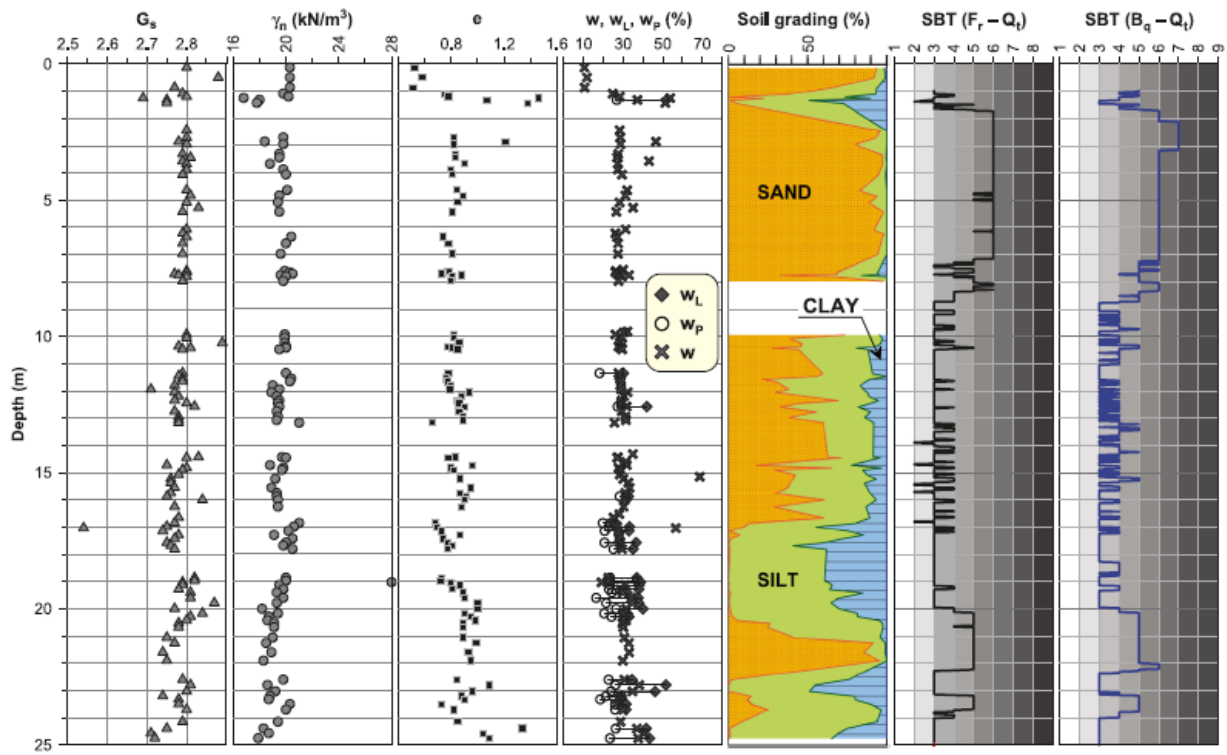

Figure 4.11: Basic physical soil properties (G_s: grain specific gravity; γ_n: in situ soil unit weight; e: void ratio; w: water content) at TTS, grading characteristics, and CPTU-based classification using Robertson's (1990) soil behaviour type charts (Tonni and Gottardi, 2011)

All these tests were located within a circular area of 45 m diameter. The CPTUs and DMTs were located in the same positions, numbered from 11 to 20 in Figure 4.12. All tests were driven as deep as possible, depending on the maximum thrust available, typically to about 42 m (Gottardi and Tonni, 2004).

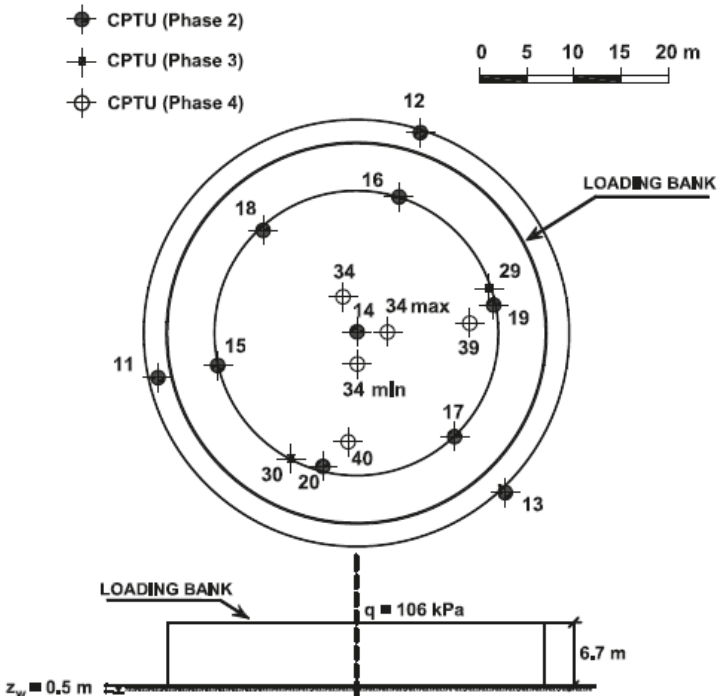

Figure 4.12: Location of the CPTU beneath the loaded area (Tonni and Gottardi, 2009)

Results from the CPTU 14, located in the centre of the loaded area, are shown in Figure 4.13. The soil lithology from the relevant deep borehole is also shown for comparison.

Figure 4.14 reports CPTU results (cone resistance and pore pressure profiles) from two cross sections, drawn along the selected diameters 11-19 and 20-12 (see Figure 4.12). It is interesting to observe in Figure 4.14*a* the presence of a clean sand located approximately between depths of 14 m and 18 m, which moving Eastwards tends to progressively disappear.

All set of tests carried out in the area confirm its stratigraphic conditions, specially with reference to the presence of a compressible silty layer from 8 to 20 m in depth.

Dissipation tests were also performed in this phase to estimate the consolidation characteristics of fine-grained soils (see Chapter 5).

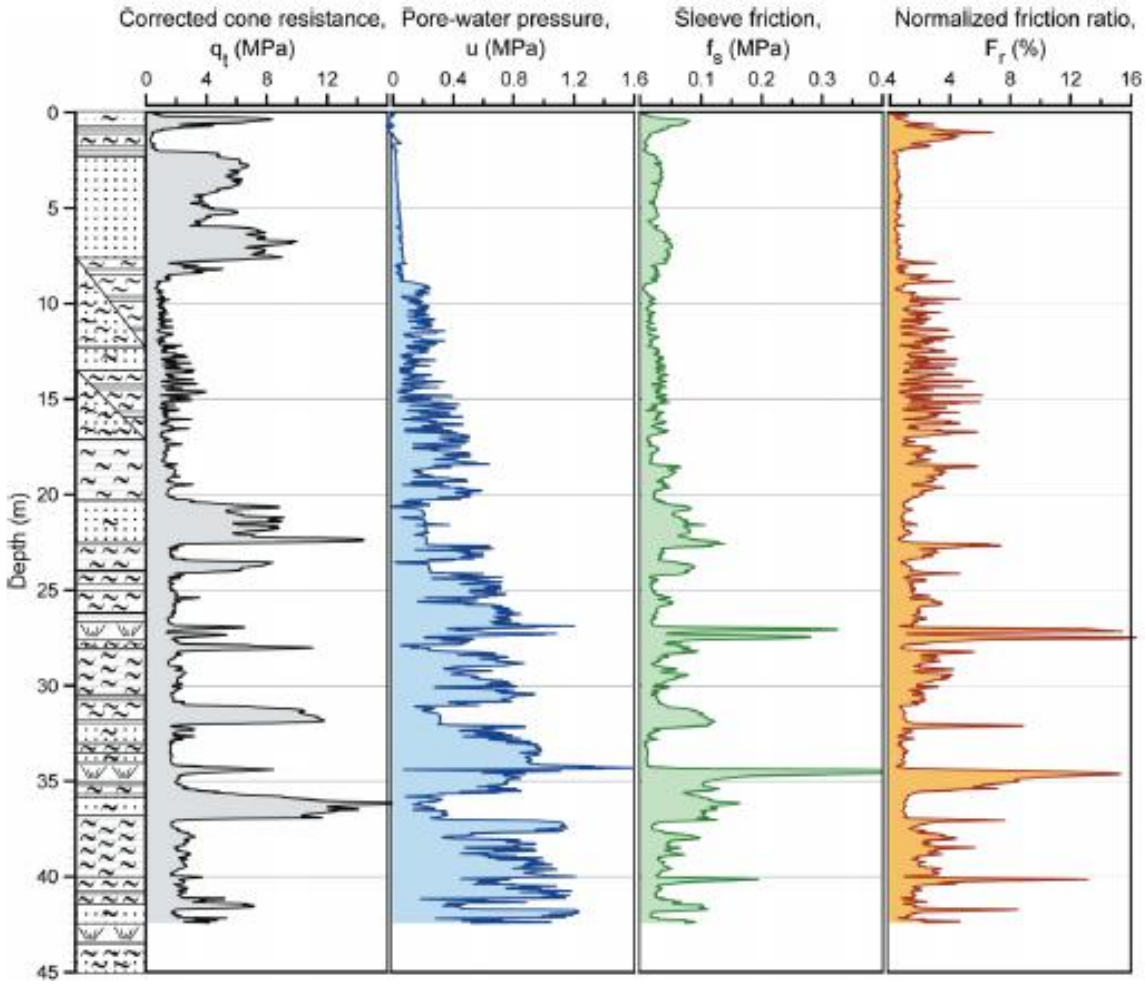

Figure 4.13: CPTU 14 log profiles (Tonni and Gottardi, 2011)

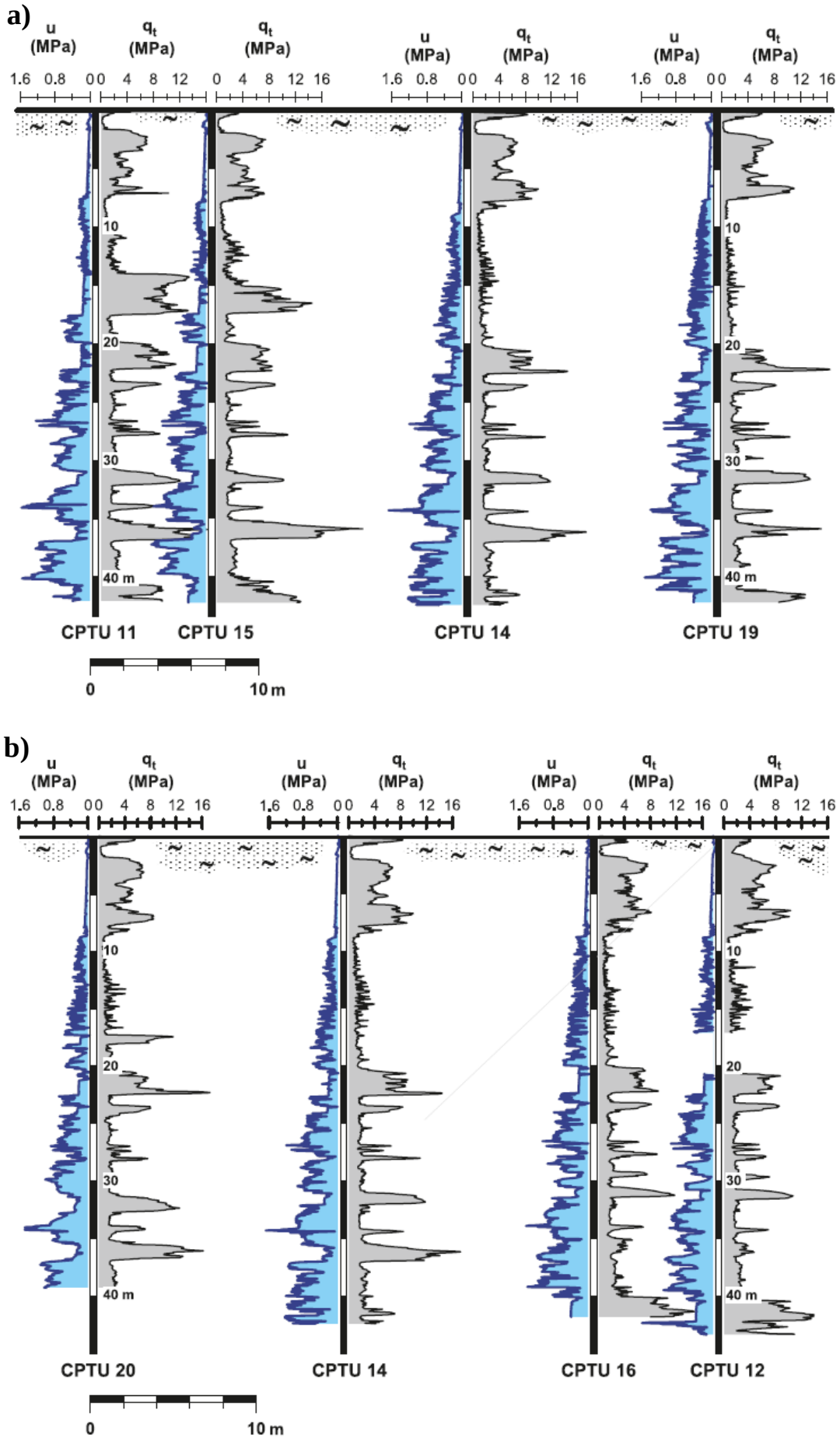

Figure 4.14: Cross section along the embankment diameter directions a) 11-19; b) 20-12 (Tonni and Gottardi, 2011)

Final campaigns

In May 2003, after the end of the test bank construction the so-called third phase was carried out from the top of the bank itself. In addition to DMTs, two further piezocone tests labelled as CPTU 29 and CPTU 30 were performed (see Figure 4.12). The aim was to study the effect of the stress level increase in the foundation subsoil due to the embankment presence (Tonni and Gottardi, 2011).

The sliding deformeters installed beneath the bank (Figure 4.8*c*) measured soil axial displacements along a vertical during its construction and for almost four years after the end of construction as well as throughout the gradual removal of the bank (from June 2007 to March 2008). The results from the sliding deformeters will be reported in Chapter 5.

The final campaign was launched in April 2008, after the complete removal of the loading bank. It included piezocone tests CPTU 34, CPTU 39 and CPTU 40, close to selected verticals already investigated in both second and third campaigns. Besides, two further piezocone tests (CPTU 34min and CPTU 34max) were performed near the centre of the loaded area at non-standard velocities (0.15 cm/s and 4 cm/s respectively). The purpose of performing these non-standard piezocone tests was to examine drainage conditions during penetration, which is of crucial interest in such intermediate soils (Tonni and Gottardi, 2009).

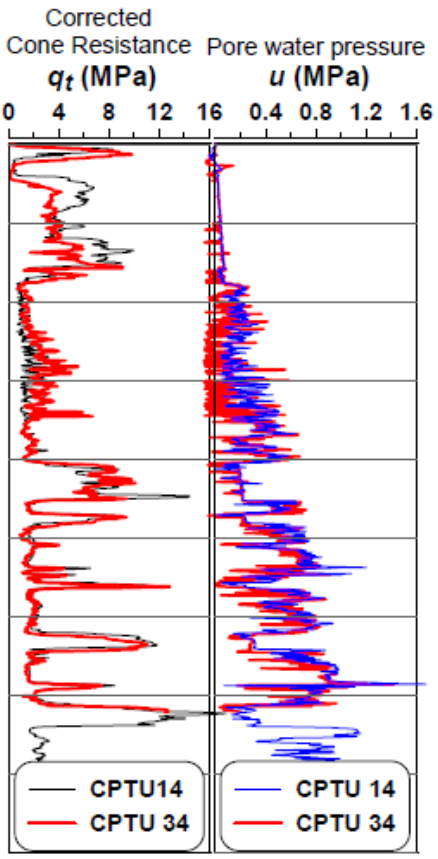

Figure 4.15: Comparison of second and fourth phase piezocone tests (Tonni and Gottardi, 2010)

4.4. The MOSE mobile barriers

The MOSE mobile barriers system is part of a the interventions to protect the city of Venice (Italy) and the Venetian Lagoon from flooding. The project consists in a series of caissons embedded under the sea bottom at the three inlets, Lido, Malamocco and Chioggia, and housing flap gates which are able to temporarily isolate the Lagoon from the Adriatic Sea during high tides (Jamiolkowski *et al*., 2009).

The mobile barriers together with the complementary measures, such as coastal reinforcement and the raising up of the lagoon banks, pavements and sidewalks, define an extremely efficient and functional system of defence.

Background

The history of the project for the MOSE goes back to the first half of the 1970s. The first Special Law 171/73 established the principle that the problem of safeguarding Venice was a matter of "priority national interest" ("Mose system").

In 1975 the State Ministry of Public Works issued an international call for tender to determine the most appropriate solution to guarantee the defence of the Venetian Lagoon from high waters. However, the procedure was closed without choosing a single project from among those presented. The Ministry therefore acquired all the proposals presented and gave them to a group of experts commissioned to prepare a project that would cover all the measures necessary to preserve the hydrogeological balance of the lagoon and mitigate high waters (the "Progettone" of 1981).The second Special Law (Law No. 784/1984) of Venice took shape under a committee for policy, coordination and control of the safeguarding activities known as the "Comitatone" and entrusted to design and implement the measures to a single body, the *Consorzio Venezia Nuova*.The *Consorzio Venezia Nuova* presented in 1989 a complex system of interventions under a project named Riequilibrio E Ambiente (the REA, "Rebalancing and the Enviroment" Project) which included mobile barriers at the inlets to control tides in the lagoon. It provided an abstract design and was finally approved by the Higher Council of Public Works in 1994. In 1998 the first environmental impact study was accepted and then improved in 2002. Construction began simultaneously in 2003 at all the three lagoon inlets and is expected to be completed by 2016 ("Mose system"; "MOSE Project, Venice, Venetian Lagoon, Italy").

Floodgates and components

A total of 78 gates, divided into four barriers, are being laid at the seabed. At the Lido inlet, there will be two rows of gates composed of 21 and 20 elements linked by an artificial island. At the Malamocco and Chioggia inlets, there will be one row of 19 and 18 gates respectively.

Figure 4.16: First MOSE manoeuvres (image taken from the website salve.it)

The gates consist of metal box-type structures. When a tide of more than 110 cm height is expected, compressed air pumped into the structure raising up the barriers to the surface of the water isolating the lagoon from the Adriatic Sea. The gates are hollowed at the bottom in order to allow the blowing of compressed air. However, in normal tidal conditions, they will be filled with water and rest in their housing structures (see Figure 4.17) ("MOSE Project, Venice, Venetian Lagoon, Italy").

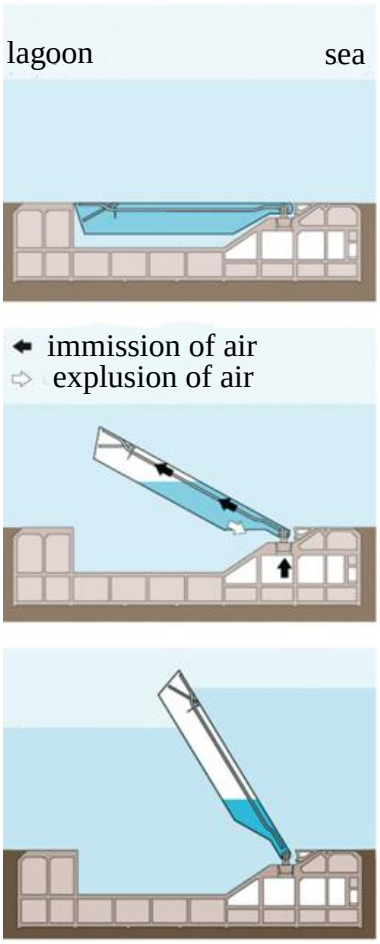

Figure 4.17: Gate movement (image taken from the website salve.it)

CHAPTER 5: CHARACTERIZATION OF VENETIAN SILTY SOILS FROM CPTU

5.1 Introduction

Sediments forming the upper 100 m of the Venetian lagoon basin consist of a chaotic system of interbedded normally consolidated or slightly overconsolidated silts (ML), medium-fine silty sands (SP-SM) and silty clays (CL) (Cola and Simonini, 2002).

As mentioned in Chapter 4, a representative test site of such subsoil was located outside Treporti (North Eastern lagoon) and a comprehensive geotechnical characterization was carried out by means of several in situ tests, mainly piezocone and flat dilatometer, boreholes and undisturbed sample extraction in addition to high-quality laboratory testing programme (Gottardi and Tonni, 2004).

A full-scale geogrid-reinforced vertical-walled cylindrical test bank was progressively built (from September 2002 to March 2003 in 13 steps of 0.5 m) and continuously monitored for the following 4 years keeping the relevant geotechnical quantities under control, such as pore water pressure, induced total stresses, surface vertical displacements and horizontal displacements and vertical strains with depth (Gottardi and Tonni, 2004). Monitoring went on as well during the gradual removal of the bank, from June 2007 to March 2008. Figure 5.1 shows a scheme of the construction history of the embankment and the associated settlements measured in the centre (S3) and at the edge of the bank by other three multiple micrometers (S1, S2 and S4).

The extensive CPTU programme was performed in four different phases, i.e before the construction (phases 1 and 2), after the end of bank construction (phase 3) and after the completion of the gradual removal of the loading-bank (phase 4) (Tonni and Gottardi, 2009; 2010; 2011). In Figure 5.1 is also shown the location of CPTUs performed before the test bank construction.

A typical piezocone log profile of the Venetian lagoon subsoil is depicted in Figure 5.2. It shows the corrected cone resistance (q_t), the sleeve friction (f_s) and the pore pressure at position 2 (u_2) from the initial test CPTU 20 together with the soil grading plot. Such profiles confirm a highly stratified system, with a top fine clean sand layer of 6-7 m of thickness, followed by clayey silts interbedding sandy silts. In this figure are also superimposed for comparison data from the adjacent CPTU 40, performed in the final phase. As can be observed, due to overconsolidation, q_t and f_s from CPTU 40 generally increase and excess pore pressures are very low or even negative, especially within the silty layer from 8 to 20 m depth (Tonni and Gottardi, 2009; 2010).

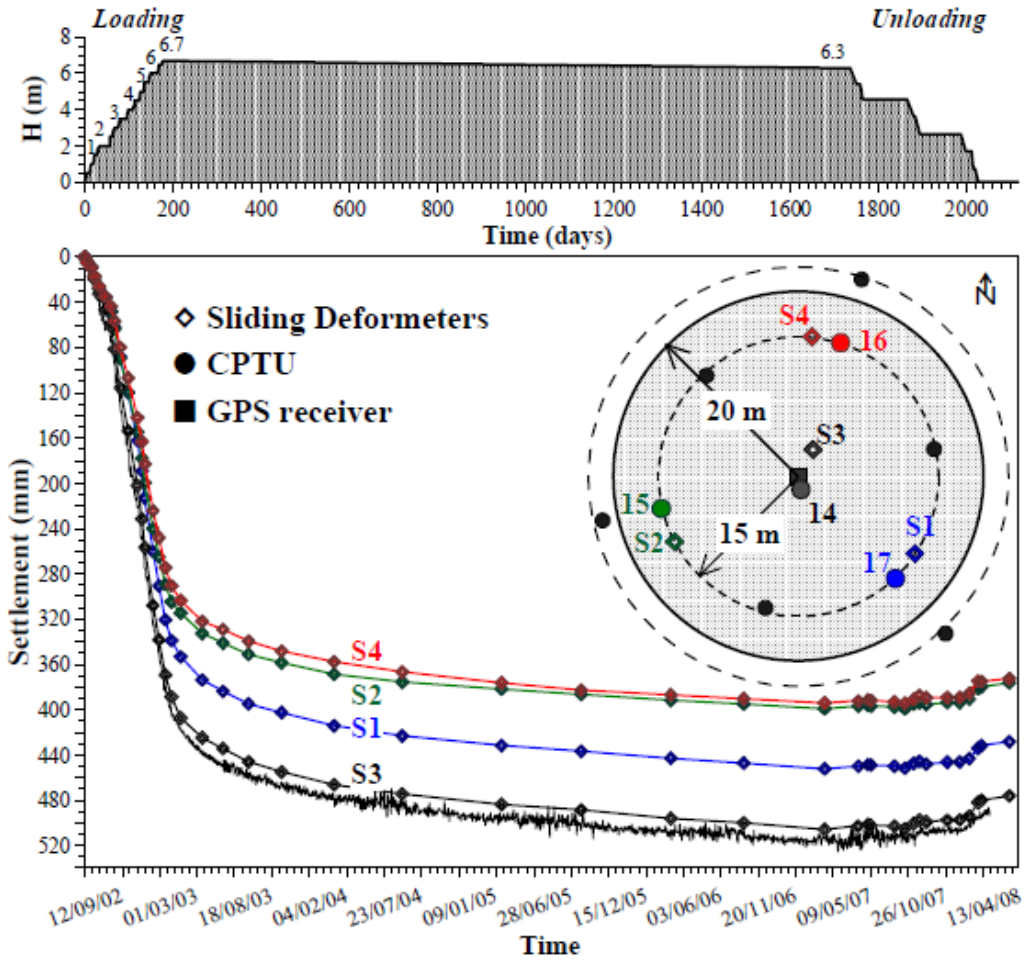

Figure 5.1: Construction history of the test bank, measured settlements beneath the loaded area and location of the piezocone testing campaigns (Bersan *et al*., 2012)

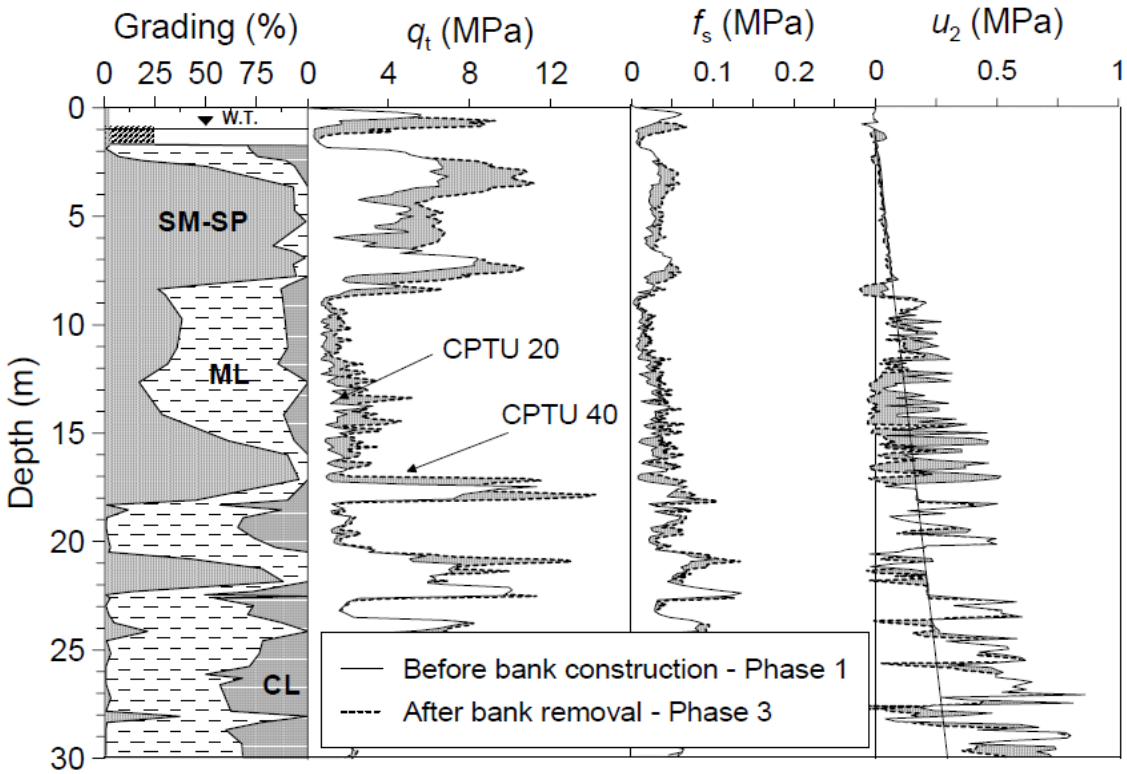

Figure 5.2: CPTU profile before bank construction (continuous line) and after embankment removal (dotted line) (Tonni *et al*., 2010)

5.2 Soil classification

Soil classification from piezocone measurements has been performed using the well-known Soil Behaviour Type (SBT) charts proposed by Robertson (1990), including all CPTU measurements normalized with respect to vertical stress (Q_t, F_r and B_q). Figure 5.3*a,b* shows the application of these charts to CPTU 20. Most points fall in zones 3, 4, 5 and 6, which include a wide range of soils (from clays-silty clays to silty sands). Comparing this results with the grain-size distribution from laboratory tests revealed a certain inaccuracy of the SBT charts when applied to silts, which generally fall in both the silt mixtures and clay zones (Tonni *et al*., 2010).

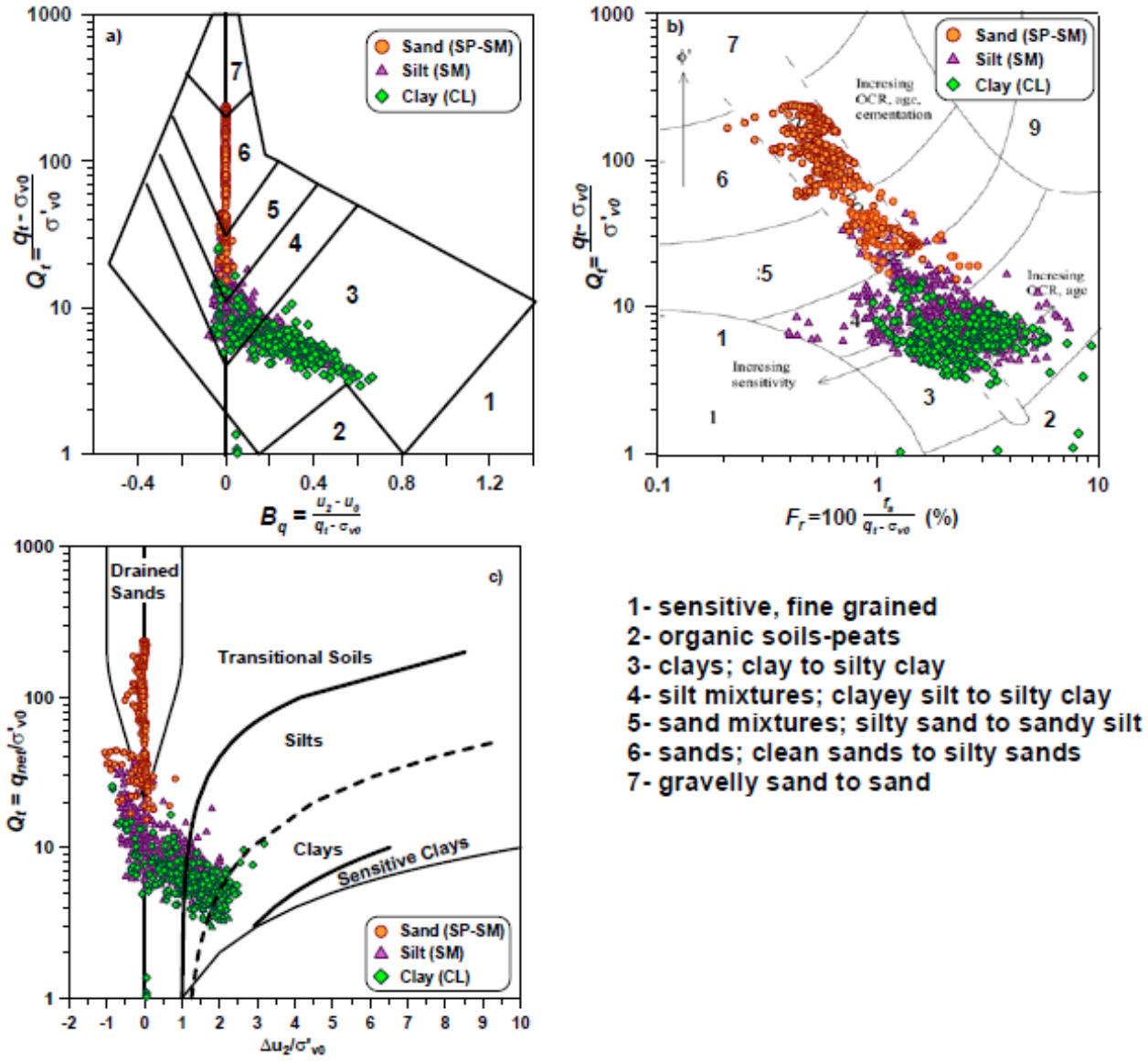

Figure 5.3: Soil classification from CPTU 20 using charts proposed by: a,b) Robertson (1990) and c) Schneider *et al*., (2008) (Tonni *et al*., 2010)

Results from the more sophisticated classification approach developed by Schneider *et al*. (2008) are also plotted in Figure 5.3*c*. It is based on the normalized piezocone parameters Q_t and $\Delta u_2/\sigma'_{v0}$ rather than Q_t and B_q, and was primarily derived to aid in separating whether penetration is drained, undrained or partially drained. However, as Tonni *et al*. (2010) remarked, this approach does not provide further details for classification of Venetian sediments.

In spite of the dense alternation of different grain-sized soils, the following units can be identified (Gottardi and Tonni, 2004):

- very soft silty clay from ground level to 2 m in depth;
- medium-fine sand from 2 m to approximately 8 m in depth;
- silt with thin layers of sandy to clayey silt from 8 to 20 m in depth;
- dense clean sand interbedded within the silty unit (not everywhere);
- silty sand;
- at depths greater than 24 m, alternate layers of silty sand, sandy silt, and clayey silt, with occasional presence of peat.

5.3 Compressibility characteristics

Compressibility characteristics of Treporti subsoil has been evaluated using field data, by means of four sliding deformeters installed beneath the bank, one in the centre and three symmetrically distributed along a 30 m diameter concentric circumference (see Figure 5.1).

The sliding deformeter is a device used for the measurement of soil axial strains along a vertical or inclined direction. Such equipment can monitor, every metre and down to 57 m in depth, distance variations with a precision of ± 30 μm (Kovari and Amstad, 1982).

Figure 5.4 plots the local vertical displacements measured by the sliding deformeters S1, S2, S3 and S4. Two different curves refer to the end of construction of the embankment (March 2003) as well as just before starting the gradual removal (April 2007). Besides, superimposed to the displacements plots are the corrected cone resistance profiles of the adjacent piezocone tests.

As can be observed in Figure 5.4, larger vertical strains are detected in the shallow silty clay layer and within the silty unit, from 8 to 20 m depth., whereas contribution of soils deeper than 25-30 m seems negligible. As expected, the sliding deformeter located close to the centreline (S3) measured the largest displacements.

In addition, due to the horizontal spatial variability of the Treporti subsoil, the process of deformation did not occur symmetrically with respect to the centreline. In fact, the dense clean sand present at times within the silty unit, may have affected the deformation measured between 8 m and 20 m depth (Bersan *et al*., 2012).

It is worth mentioning that comparing the horizontal displacements provided by the inclinometers located just outside the bank and vertical displacements measured by the sliding deformeters (S1, S2 and S4), it appeared that the total vertical displacement is one order of magnitude greater than the maximum horizontal displacement, thus confirming that the process of deformation prevalently developed in the vertical direction (see Simonini *et al*., (2007) for further details).

Furthermore, the pore pressure monitoring exhibited a quite high rate of consolidation, comparable with the test bank construction time. Therefore, it can be assumed that settlements due to primary consolidation developed contemporary with the embankment construction (Simonini, 2004; Gottardi and Tonni, 2005; Simonini *et al*., 2007).

The differential displacements plotted as a function of the effective vertical stress σ'_v represent an effective way to describe the subsoil deformation throughout the loading process. As an example, Figure 5.5 depicts a few of the typical ε_v - logσ'_v curves derived from vertical strain measurements obtained from the sliding deformeter located beneath the centre of the loading bank, between 6 and 23 m depth. In this case, 1-D loading conditions can be accepted.

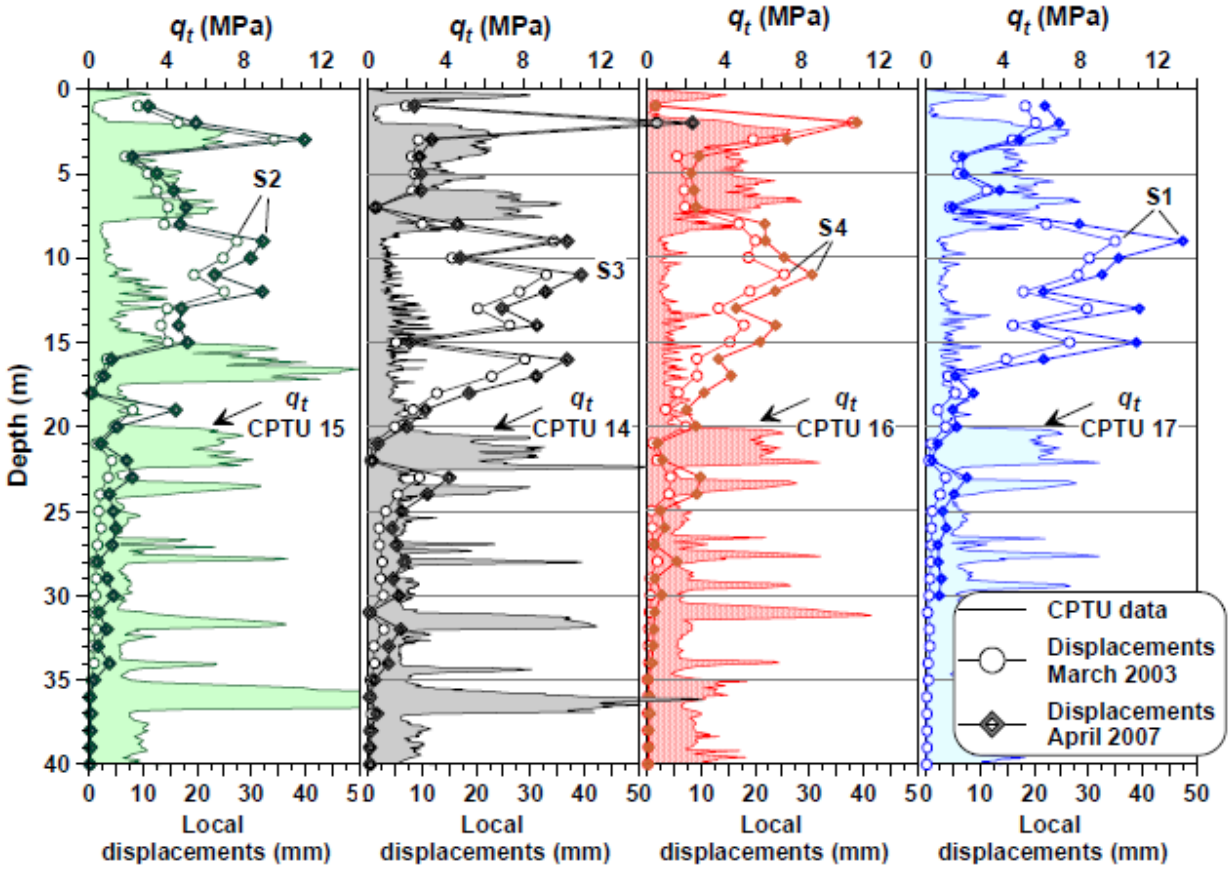

Figure 5.4: Local vertical displacements recorded at different dates by the sliding deformeters S1, S2, S3 and S4, together with cone resistance (q_t) profiles from adjacent piezocone tests (Bersan *et al*., 2010)

Curves in Figure 5.5 exhibit a shape similar to that observed in ε_v - logσ'_v plots obtained from oedometer tests. As evident from figure, the curves are somewhat straight and flat at the beginning of the loading phase. Then, it is followed by a sharp variation of curvature. Hypothesizing that no important delayed deformation as a consequence of the consolidation should occur along with the process of loading, Simonini (2004) remarked that the slope change observed can be interpreted in terms of yielding stress σ'_Y , which can be in turn assumed that the classical preconsolidation stress was $\sigma'_p \approx \sigma'_Y$.

Therefore, such interpretation of the field data confirmed that Venetian lagoon sediments are essentially normally consolidated or slightly overconsolidated, with *OCR*-values ranging from 1.1 to 2. The slightly overconsolidated state may be due to ageing effects in conjunction with the pore pressure oscillations induced by the tides (Simonini, 2004).

The latter part of the stress-strain curves in due to the deformation occurred at constant vertical stress (from March 2003 to April 2007). As already mentioned, primary consolidation basically took place during the loading test construction. Hence, settlements obtained after the embankment completion are most likely to be attributed to secondary compression (Bersan *et al*., 2012).

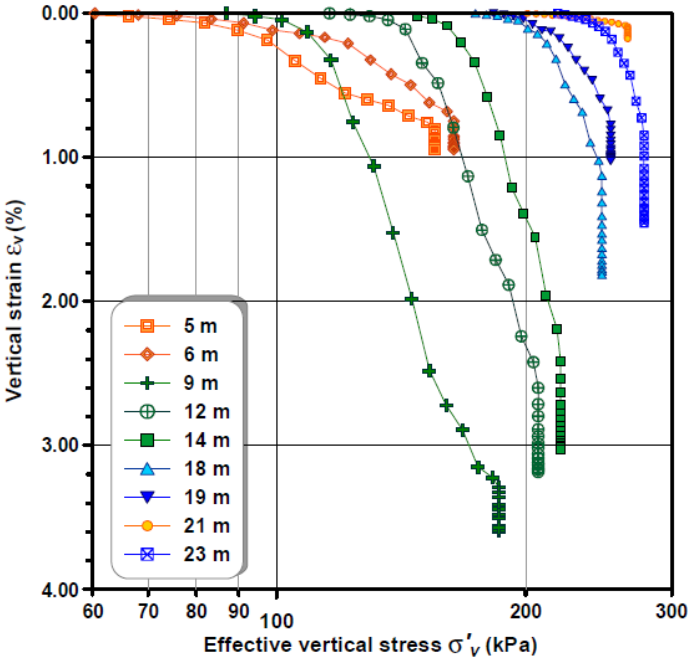

Figure 5.5: Field axial strains plotted versus effective vertical stress (Bersan *et al*., 2012)

As secondary settlements can not be clearly separated from primary consolidation, in the Treporti analysis was adopted the widely-accepted assumption of treating primary and secondary components separately.

Figure 5.6 shows the vertical strain (ε_v) – logarithm of time (log*t*) curves obtained by the sliding deformeter S3 during loading and stationary stages. As it is clear from the graphs, the latter part of the curves (deformation at constant vertical stress), is generally found to be sloping and approximately linear (Bersan *et al*., 2012).

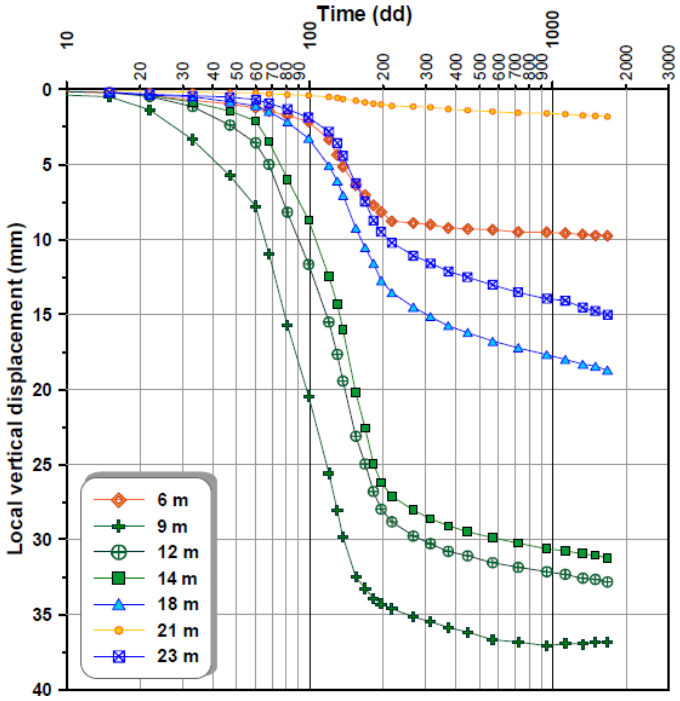

Figure 5.6: Vertical displacements beneath the centreline of the loaded area versus time (Bersan *et al*., 2012)

Constrained modulus

Compressibility of the upper 20 m sediments, expressed in terms of the constrained modulus *M*, has been evaluated using the soil vertical strain data provided at 1 m intervals by the sliding deformeter located beneath the centre of the loading area (S3). In this case, 1-D loading conditions apply.

$$M = 1/m_v = \delta\sigma_v / \delta\varepsilon_v \quad (5.1)$$

Previous interpretation of vertical strains induced by the embankment showed that the use of the well-established empirical correlations (Lunne and Christophersen, 1983; Kulhawy and Mayne, 1990) based on a net distinction between drained and undrained conditions, revealed limitations of such correlations to provide any reliable description of the compressibility properties of the silty soils of the Venetian lagoon (Tonni and Gottardi, 2011). However, Tonni and Gottardi (2011) showed that the semiempirical relationship proposed by Senneset *et al*. (1988) for silty soils of the North Sea, provided reliable moduli of intermediate soils.

Tonni *et al.* (2010) provided a site specific correlation for the 1D modulus on loading (M_L), for both coarse and fine Venetian sediments, taking the vertical strains measured soon after the embankment completion as a reference (Figure 5.7). The formulation proposed is given by:

$$M = 2.3(q_t - u_2) \quad (r^2 = 0.93) \quad (5.2)$$

On the other hand, Tonni and Gottardi (2011) proposed a correlation in terms of the SBT index, I_c (Robertson and Wride, 1998). They showed that the introduction of I_c could provide a unified approach to estimate the compressibility characteristics for a wide range of soils.

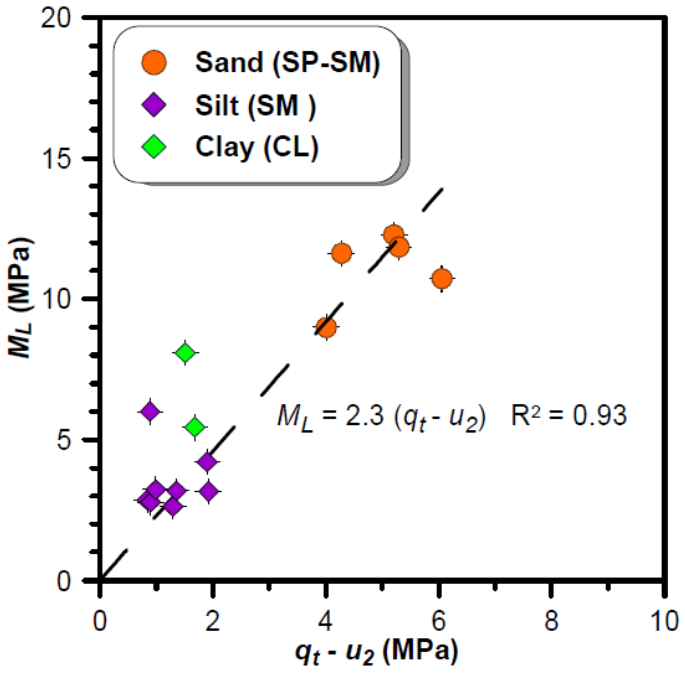

Figure 5.7: Constrained modulus as a function of q_t-u_2 (Tonni *et al*., 2010)

$$M = 1.35 I_c \left(q_t - \sigma_{v0}\right) \tag{5.3}$$

where $I_r = \sqrt{\left(3.47 - \log Q\right)^2 + \left(1.22 + \log Fr\right)^2}$.

Coefficient of secondary compression

Over the last three decades, most of the research on the time-dependent behaviour of soils has been carried out on the one-dimensional compression of cohesive soils. The formulations proposed for clays can be assigned to two approaches, Hypothesis A and Hypothesis B (Ladd *et al.* 1977, Jamiolkowski *et al.* 1985), which consider alternative conjectures about the combination of primary and secondary consolidation during the excess pore pressure dissipation. However, in spite of the substantial contributions on this topic, there are still controversial opinions on the mechanisms that control creep during primary compression (Tonni and Simonini, 2013). For a general review see Mesri (2003) and Leroueil (2006).

In Figure 5.8, the typical *S*-shaped consolidation curve in the semi-logaritmic plane *e-log*t for a generic loading step in oedometer test is shown. In common practice it is accepted to treat secondary consolidation separately from primary consolidation although it is widely recognized that the phenomenon takes place from the beginning of loading (Ŝuklje 1957, Bjerrum 1967, Leroueil *et al*. 1985).

Secondary compression is typically characterized by the coefficient $C_{\alpha\varepsilon}$ (or $C_{\alpha e}$ in *e-log*t plane) which is determined from the slope of the straight line portion of the vertical strain (ε_z) - logarithm of time (*log*t) curve obtained from oedometer tests:

$$C_{\alpha\varepsilon} = \frac{\Delta\varepsilon_v}{\Delta \log t} = \frac{\Delta e}{(1+e_p)\cdot \Delta \log t} = \frac{C_{\alpha e}}{1+e_p} \tag{5.4}$$

where e_p is the void ratio at the start of the linear portion of the experimental *e-log*t curve. Although there is experimental evidence that $C_{\alpha\varepsilon}$, may change with time, the most common approach is to assume that $C_{\alpha\varepsilon}$,(or $C_{\alpha e}$) is independent of time.

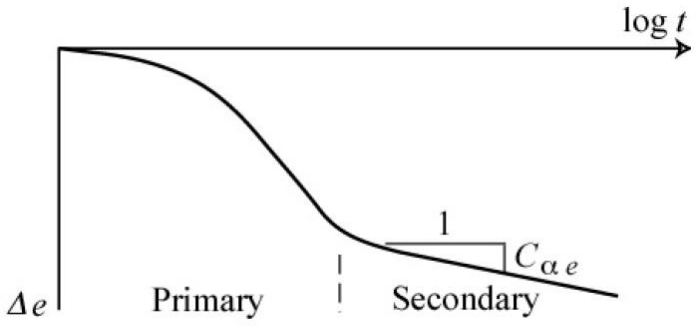

Figure 5.8: S-shaped compression curve in semilogarithmic plot

It must be emphasized that although the time-dependent behaviour of sands and silts has been not traditionally taken into account in the classical settlement calculation, there is experimental evidence that the creep phenomenon in granular soils is not negligible. In relation to the confining stress level, time-dependent behaviour of coarse-grained materials can assume two alternative characteristics. In fact, at low confining stresses the deformations are caused rearrangement over time owing to sliding and rolling between sand particles, whereas at high confining pressures the deformations are related to continuous fracturing and deformation of grains (Augustesen *et al*. 2004).

As already mentioned, the final part of the ε_v –log*t* curves in Figure 5.6 is due to deformation that occurs after the test bank construction, fitted by a straight line whose slope is assumed to be defined by the secondary compression coefficient $C_{\alpha\varepsilon}$. As Bersan *et al*. (2012) remarked in their work, based on field results, C_α seems to slightly change with time (Figure 5.6). In fact, such observation had been also confirmed by other researchers, either in laboratory or in the field. Indeed, Leroeuil *et al*. (1985) reported a general nonlinear strain-time response based on long-term creep tests and observed that the curves for overconsolidated specimens showed a continuously increasing slope with the log*t* after end of primary consolidation. On the other hand, normally consolidated specimens showed a continuously decreasing slope, similarly to Treporti field results.

The coefficient of secondary compression ($C_{\alpha\varepsilon}$) of the Treporti sediments was derived from data associated to the early stages of the secondary compression process. $C_{\alpha\varepsilon}$ in silts turned out to vary between 0.0025 and 0.0052, with a mean value of approximately 0.0046, whilst in sands, it varied in the range 0.00058-0.00093. Figure 5.9*b* provides the computed values of $C_{\alpha\varepsilon}$ and $C_{\alpha\varepsilon}^{*}$, where the latter refers to 3-D deformation conditions, obtained from the curves associated to the sliding deformeters S1,S2 and S4. Besides, in Figure 5.9*a* are plotted the values of the compression ratio $C_{c\varepsilon}\left(=\Delta e/\left(\left(1+e_0\right)\cdot\Delta\log\sigma'_v\right)=C_c/\left(1+e_0\right)\right)$, obtained from curves depicted in Figure 5.5 by calculating the slope of the straight line describing compressibility in the NC domain. The values referred to 3-D conditions, namely the *modified* compression ratio $C_{c\varepsilon}^{*}$, obtained from the curves derived from strain measurements at S1, S2 and S4, have also been plotted.

The effects of the effective vertical stress on the secondary compression coefficient C_α have been investigated by several researchers in literature. Mesri and Godlewski (1977) suggested that a unique relationship exists between C_α and C_c through the secondary compression stage, and that relationship provides a simple method for calculating secondary settlement (e.g. Mesri, 1987; Mesri *et al*., 1994). According to Mesri and Godlewski (1977), the ratio C_α/C_c is approximately a constant for a wide variety of natural soils and it varies in the range 0.025-0.06.

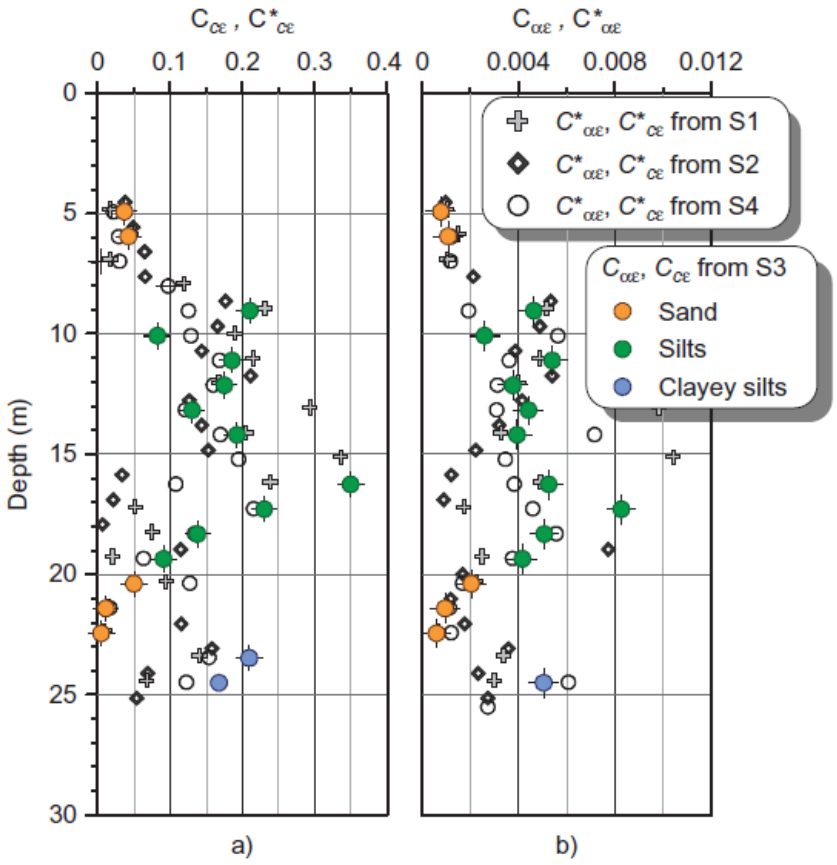

Figure 5.9: a) Back-calculated $C_{c\varepsilon}$ and $C_{c\varepsilon}^*$ values from four sliding deformeters; b) back-calculated $C_{\alpha\varepsilon}$ and $C_{\alpha\varepsilon}^*$ values from four sliding deformeters (Tonni and Simonini, 2013)

Following this approach, Bersan *et al.* (2012) showed that the ratio $C_{\alpha\varepsilon}/ C_{c\varepsilon}$ obtained for the Venetian lagoon sediments lies within a narrow range of 0.02-0.04, even when the ratio $C_{\alpha\varepsilon}^*/ C_{c\varepsilon}^*$ is considered. Only in the coarse-grained sediments from 20 to 22 m depth exceeded the upper limit of 0.04.

The pioneering research (Bersan *et al*., 2012; Tonni and Simonini, 2013) carried out on the Treporti long-term settlement data has provided an attempt to relate the secondary compression coefficient $C_{\alpha\varepsilon}$, as obtained from sliding deformeter measurements, to the CPTU data collected in Treporti Test Site, expressed in terms of the corrected cone resistance q_t. The approach is based on the experimental evidence that, in Venetian soils, frictional response governs both cone resistance and secondary compression, hence empirical correlations between $C_{\alpha\varepsilon}$ and q_t are likely to be a useful alternative on the classical laboratory tests for the estimate of creep characteristics.

Furthermore, in an attempt to provide more significant relationships using dimensionless variables in CPT-based correlations (Wroth 1988), Bersan *et al*. (2012) proposed an expression for $C_{\alpha\varepsilon}$ in terms of the dimensionless normalized cone resistance Q_{tn} $\left(=\left(q_t-\sigma_{v0}\right)/\, p_a\cdot\left(p_a/\sigma'_{v0}\right)^n\right)$, as defined by Robertson (2009). In this approach, an iterative nonlinear stress normalization procedure, accounting for the stress level in the soil class effects, was applied to the corrected cone resistance q_t in order to determine Q_{tn} (see Chapter 2).

Figure 5.10 shows the trend between $C_{\alpha\varepsilon}$ and Q_{tn}. Superimposed on the plot are also the values of $C_{\alpha\varepsilon}^{*}$ obtained from the sliding deformeters S1, S2 and S4. Assuming a log-log relationship, the equation of the best fit regression line in Figure 5.10, based on the data from the sliding deformeter S3 (centreline), is given by:

$$C_{\alpha\varepsilon} = 0.03 \cdot (Q_{tn})^{-0.89} \tag{5.5}$$

with R^2 = 0.83. It should be noted here that the use of a variable stress exponent n that depends on both stress level and the well-known soil behaviour type index I_c (see Equation (2.8)), provided better estimates of $C_{\alpha\varepsilon}$ also in comparison with the dimensionless cone resistance Q_{t1} (n = 1) (Bersan *et al.*, 2012).

As Tonni and Simonini (2013) remarked in their work, the correlations proposed previously (relating $C_{\alpha\varepsilon}$ to q_t or Q_{tn}), did not take into account partial drainage phenomena during the cone penetration in Venetian silty soils. Accordingly, in an attempt to account in some way for the different pore pressure response in relation to the drainage conditions around the advancing cone, it was suggested a power function expression for $C_{\alpha\varepsilon}$ in terms of the normalized cone tip resistance Q_{tn} and the excess pore pressure ratio $\Delta u/\sigma'_{v0}$.

The multiple regression analysis was performed in a log-log format and for the data collected over the centreline of the loading bank, the least square analysis gave the following relationship:

$$C_{\alpha\varepsilon} = 0.077 \cdot (Q_{tn})^{-1.14} \cdot \left(1 + \frac{\Delta u}{\sigma'_{v0}}\right)^{-0.74} \quad (R^2 = 0.86) \tag{5.6}$$

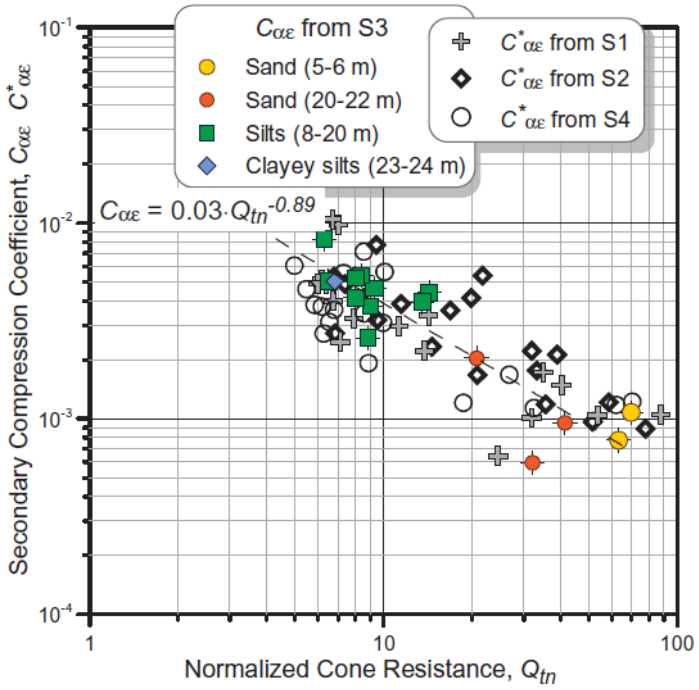

Figure 5.10: In situ $C_{\alpha\varepsilon}$ as a function of Q_{tn} (Bersan *et al.*, 2012)

5.4 Consolidation analysis

In the "second phase" and in the "third phase" of the testing programme carried out at the Treporti Test Site, several dissipation tests were performed in order to evaluate the consolidation characteristics of fine-grained soils, expressed in terms of the coefficient of consolidation c_h. Figure 5.11 shows representative dissipation curves, which describe the pore pressure (position 2) trend with time in the predominantly silty unit. The figure also shows the trends obtained at depths below 24 m, where alternate layers of silty sand, sandy silt and clayey silts prevail. As evident from Figure 5.11, the decay of excess pore pressures occurs rapidly, taking approximately 1000 s in the silty layer and a little longer in the deepest ones.

The coefficient of consolidation was derived from the pore pressure dissipation data using the well-known and widely used procedure proposed by Teh and Houlsby (1991), already briefly described in Chapter 2. A rigidity index, I_r, of 50 was assumed and a time factor, T^*, corresponding to 50% degree of consolidation was considered in order to determine c_h for Venetian soils. The values of c_h are reported in Table 5.1. As can be appreciated, in the upper part of the silty unit, c_h can be assumed equal to 10^{-5} m^2/s whereas below 17 m in depth it decreases by one order of magnitude. A value of 10^{-7} m^2/s was found only in a few cases.

However, as Tonni and Gottardi (2011) remarked, the Teh and Houlsby (1991) method for interpreting dissipation tests is based on the assumption of fully undrained response during penetration, which may be questionable in the Venetian silty soils.

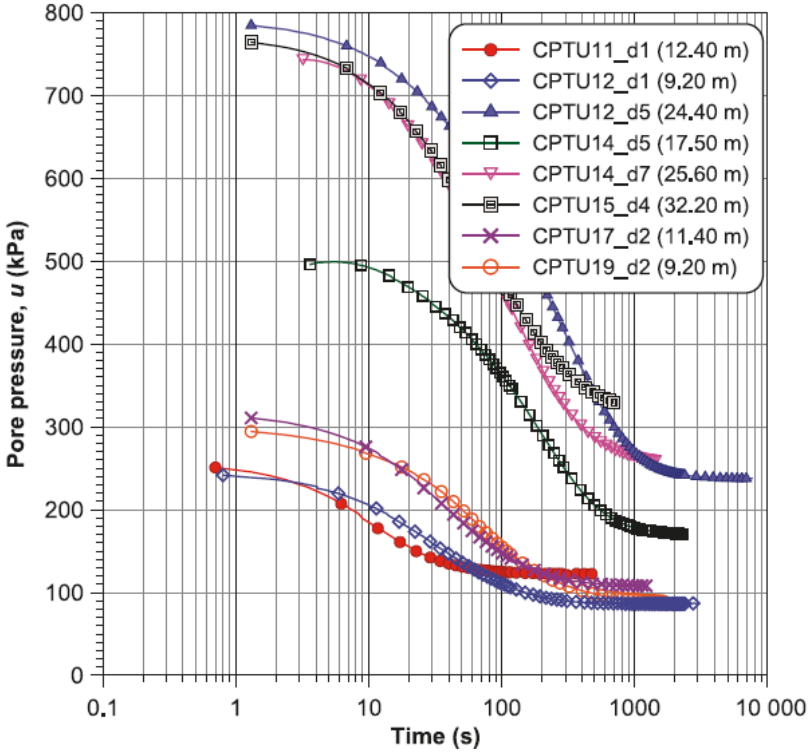

Figure 5.11: Pore pressure trend with time (Tonni and Gottardi, 2011)

Table 5.1: Horizontal consolidation coefficients from CPTU dissipation tests (Tonni and Gottardi, 2011)

Test	Depth (m)	c_h (m^2/s)
11_D1	12.40	5.9×10^{-5}
12_D1	9.20	2.1×10^{-5}
12_D5	24.40	3.7×10^{-6}
14_D5	17.50	4.1×10^{-6}
14_D7	25.60	7.0×10^{-6}
14_D8	30.00	3.8×10^{-6}
14_D9	34.30	4.3×10^{-6}
15_D3	26.00	8.4×10^{-7}
15_D4	32.20	8.6×10^{-6}
16_D3	18.80	2.1×10^{-6}
16_D4	24.30	5.4×10^{-6}
17_D2	11.40	2.0×10^{-5}
19_D2	9.50	1.0×10^{-5}
20_D3	18.35	4.5×10^{-6}
29_D6	25.80	9.5×10^{-7}
29_D8	33.40	7.1×10^{-6}

Note: c_h, coefficient of consolidation.

5.5 Stress level effects

The CPTU programme carried out in Treporti and organized into different phases of the loading history, by first performing tests prior to the bank construction, followed by tests performed from the top of the bank after its completion and by some additional tests carried out four years later, at the end of the bank removal. This provided the opportunity of analyzing the stress level effect on the in situ response of the Venetian lagoon sediments (Tonni and Gottardi, 2011).

As an example, Figure 5.12 shows a comparison between piezocone profiles obtained from piezocone tests labelled as CPTU 19 and CPTU 29, performed in the second and third testing campaigns respectively and located at a distance of 15 m from the centre of the loaded area. The analysis is limited to the upper 20 m, since at greater depths the loading bank presence seems to have less significant effects on measurements.

Figure 5.12*a* shows the influence of the stress increment as a consequence of the load in the corrected cone resistance (q_t). This influence appears particularly evident in the sandy layer from 2 m to approximately 8 m in depth. Furthermore, Figure 5.12*b,c,d* also provides a comparison of CPTU 19 and CPTU 29 profiles in terms of three different stress normalization procedures applied to the recorded q_t values.

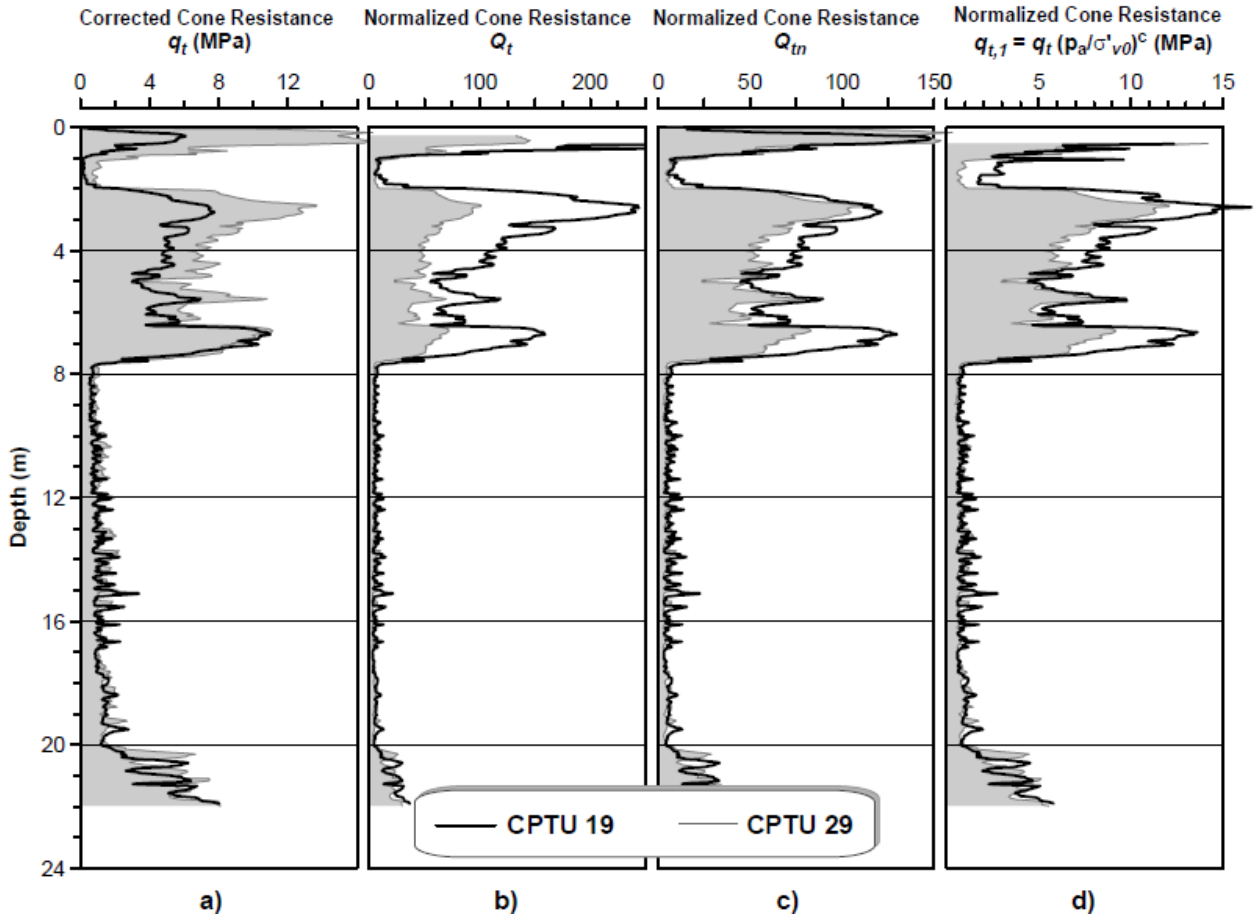

Figure 5.12: Stress normalization of CPTU 19 and CPTU 29 data (Tonni *et al.*, 2011)

Depending on which overburden stress normalization procedure is used, different interpretations of cone penetration data may result. Indeed, profiles of the normalized cone resistance Q_t, based on a linear stress normalization scheme (Wroth, 1984; Robertson, 1990), show a significant difference within the sandy layer, despite void ratio changes induced by the loading bank can hardly explain a similar variation (Tonni and Gottardi, 2011). This result is mostly due to an inappropriate overburden stress normalization procedure, which seems to be appropriate for cohesive soils, but not for cohesionless (Cetin and Isik, 2007).

Such result is not observed when using more advanced techniques, based on iterative nonlinear stress normalization procedures. In fact, when data are interpreted in terms of the dimensionless normalized cone resistance Q_{tn}, defined by Robertson (2009), accounting for the stress level and the soil class effects, better agreement between normalized data referring to CPTU 19 and CPTU 29 can be observed (Figure 5.12*c*).

An analogous response was observed using the variable normalization procedure (Figure 5.12*d*) proposed by Moss *et al*. (2006). Accordingly, the normalized tip resistance $q_{t,1}$ is given by:

$$q_{t,1} = \left(\frac{p_a}{\sigma'_{v0}} \right)^c \cdot q_t \tag{5.7}$$

where c is the tip normalization exponent, determined from the q_t and the friction ratio R_f $\left(= 100 \cdot f_s / q_t\right)$ by means of an iterative procedure.

Figure 5.12*c,d* confirms the effectiveness of both variable normalization approaches that account for the non-linear, soil type-dependent effect of overburden stress on CPTU measurements. The slight differences in profiles when passing from the pre-loading to post-loading phases are consistent with the expected variations in void ratio and the basically normally consolidated state of sediments (Tonni *et al*., 2011).

In situ state parameter

It has been widely recognized the use of the state parameter ψ (Been and Jefferies, 1985), referred to critical state conditions, as a meaningful parameter to represent the in situ state of sandy soils (see Chapter 2).

Tonni *et al*., (2011) provided in their study an attempt to assess the in situ state of Treporti sediments using two different methods recently proposed in the literature. A preliminary evaluation of ψ was obtained using the approximate relationship developed by Robertson (2010*b*). Figure 5.13 shows the contours of the state parameter ψ (red continuous lines) on the SBT chart Q_{tn} – F_r developed by Roberston. He observed a strong similarity with the contours of the contours of ψ and the contours of the clean sand equivalent cone resistance $Q_{tn,cs}$. Robertson and Wride (1998) suggested the concept of a clean sand equivalent cone resistance, which would represent

the equivalent clean sand resistance for CPT results in silty sands, and proposed a correction factor, K_c, to correct normalized cone resistance (Q_{tn}) in silty sands to an equivalent clean sand value ($Q_{tn,cs}$). The correction factor is a function of grain characteristics of the soil that can be estimated using the soil behaviour type index I_c. According to such method, the following simple expression was eventually proposed:

$$\psi = 0.485 - 0.314 \log Q_{tn,cs} \tag{5.8}$$

However, the application of Equation (5.8) to adjacent tests CPTU 19 and CPTU 29, did not seem to capture any change of ψ due to the loading bank construction. In fact, points plotted in Figure 5.13, which correspond to values associated to the upper sandy unit from 2 m to 8 m depth, overlap each other. Similar results were obtained using CPTU 20 and CPTU 30 data (Tonni *et al*., 2011).

An alternative method applied to Treporti sediments is that proposed by Jefferies and Been (2006). Using this approach, the state parameter ψ was evaluated by a combination of laboratory and in situ tests. The expression for ψ (Jefferies and Been, 2006) is given by:

$$\psi = -\frac{\ln\left(\frac{Q_p}{k'\left(1-B_q\right)}\right)}{m'} \tag{5.9}$$

where B_q is the pore pressure parameter and Q_p is the tip resistance normalized by mean stress p'_0:

$$Q_p = \frac{q_t - p_0}{p'_0} \tag{5.10}$$

while parameters k' and m' are functions of soil type that according to Jefferies and Been, can be expressed in terms of the critical stress ratio M and the slope λ_{10} of the critical state line in the e-$\log_{10} p'$ space by the following approximate relationships:

$$k'/M = 3 + 0.85/\lambda_{10} \tag{5.11}$$

$$m' = 11.9 - 13.3\lambda_{10} \tag{5.12}$$

In order to first evaluate p'_0 and thus Q_p, the lateral earth pressure coefficient at rest K_0 is needed. This was obtained from interpretation of the dilatometer test (DMT) carried out in Treporti, using common correlations proposed in the literature. For these purposes, dilatometer tests located close to CPTU 19 and CPTU 20 were considered.

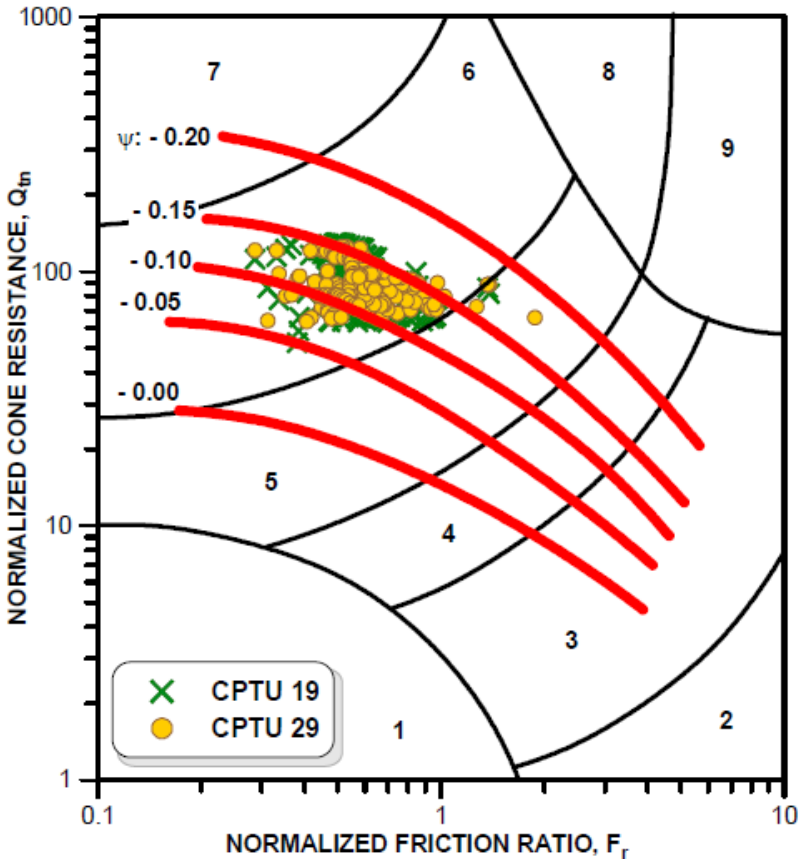

Figure 5.13: Evaluation of ψ prior to the loading bank construction (using CPTU 19) and after its completion (using CPTU 29) using Equation (5.8) (Tonni *et al*., 2011)

On the other hand, the critical state parameters ϕ'_{crit} and λ_{10} were obtained using correlations proposed by Cola and Simonini (2002), developed on the basis of a large amount of experimental data on Venetian sediments. They provided an expression for ϕ'_{crit} and λ_{10}in terms of a grain size index, I_{GS}, defined as the ratio between the non-uniformity coefficient U and the mean particle diameter D_{50}. Reliable values of I_{GS} were obtained from laboratory tests performed on soil samples from Treporti Test Site.

Figure 5.14 shows the profile of the estimated state parameter ψ, obtained by the application of the Jefferies and Been method to both CPTU 19 and CPTU 29 (from 2 m to 22 depth). As can be seen, ψ is negative, thus confirming the dilative behaviour of Venetian soils. Comparing the two curves, it is observed a shift of the ψ profile towards negative values as a consequence of the stress increments induced by the embankment (Tonni *et al*., 2011).

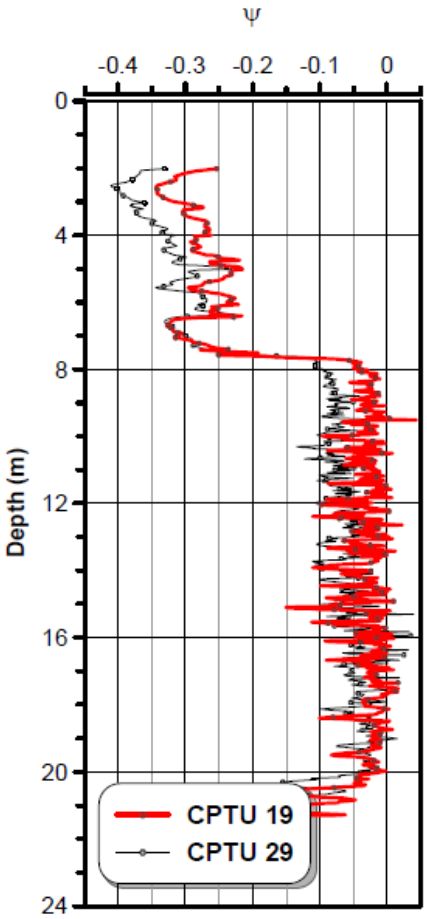

Figure 5.14: Profiles of ψ obtained from interpretation of CPTU 19 and CPTU 29 data (Tonni *et al*., 2011)

5.6 Stress history

Following Simonini (2004), a first estimate of the preconsolidation pressure σ'_p of the silty layers was obtained by interpreting the sharp variation of curvature observed in the $\varepsilon_v - \log\sigma'_v$ curves of Figure 5.15. The figure refers to the field axial strains measured by the sliding deformeter S3 (centreline), at 1 m intervals, from 9 to 20 m. The stress increments at every depth were calculated according to the elastic theory.

Accordingly, the *OCR* prior the bank construction turned out to range between 1.1 and 1.3, thus confirming that Venetian sediments are in general slightly overconsolidated (Simonini *et al*., 2007). The *OCR* values after the bank removal could be back-calculated from the stress history applied through the test bank. The load effect is more significant in the shallowest 15 m.

Such *OCR*s were compared with estimates obtained from the application of the well-known relationship calibrated on clays proposed by Powell *et al.* (1988). However the application of Powell's formula provided rather unrealistic predictions (Tonni and Gottardi, 2009).

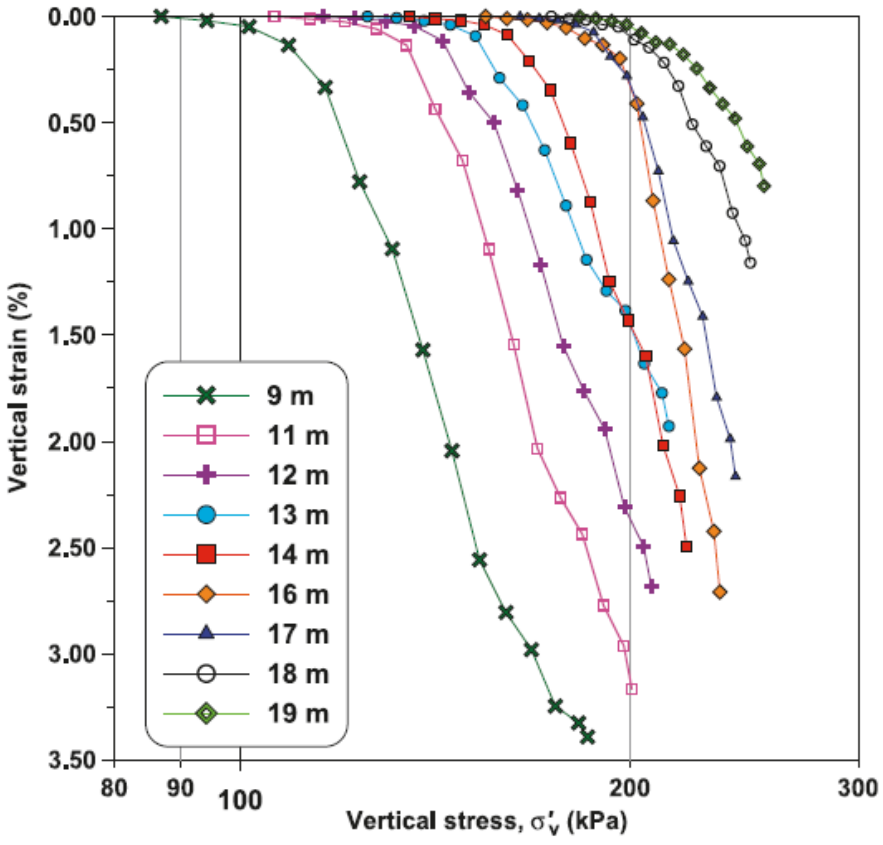

Figure 5.15: Field axial strains from 9 to 20 m in depth vs stress increment (Tonni and Gottardi, 2011)

In an attempt to get more reliable *OCR* values, a site-specific correlation for Venetian soils, including a dependence on the friction ratio F_r, was suggested (Tonni *et al*., 2010):

$$OCR = 0.038 \cdot F_r \cdot \left(\frac{q_t - u_2}{\sigma'_{v0}} \right)^{1.21} \tag{5.13}$$

with $R^2 = 0.92$.

Figure 5.16 shows the predictions of *OCR*s applying Equation (5.13) to the test CPTU 34, carried out in the last campaign.

Based on the approach originally suggested by Mayne (1991), a new site-specific correlation, similar to that developed by Simonini (2004), was eventually proposed for Venetian soils in Tonni and Gottardi (2011):

$$OCR = 0.91 \cdot \left(\frac{q_t - u}{\sigma'_{v0}} \right)^{0.23} \tag{5.14}$$

where the two constants were determined as best fit of *OCR* values that referred to post-bank removal conditions.

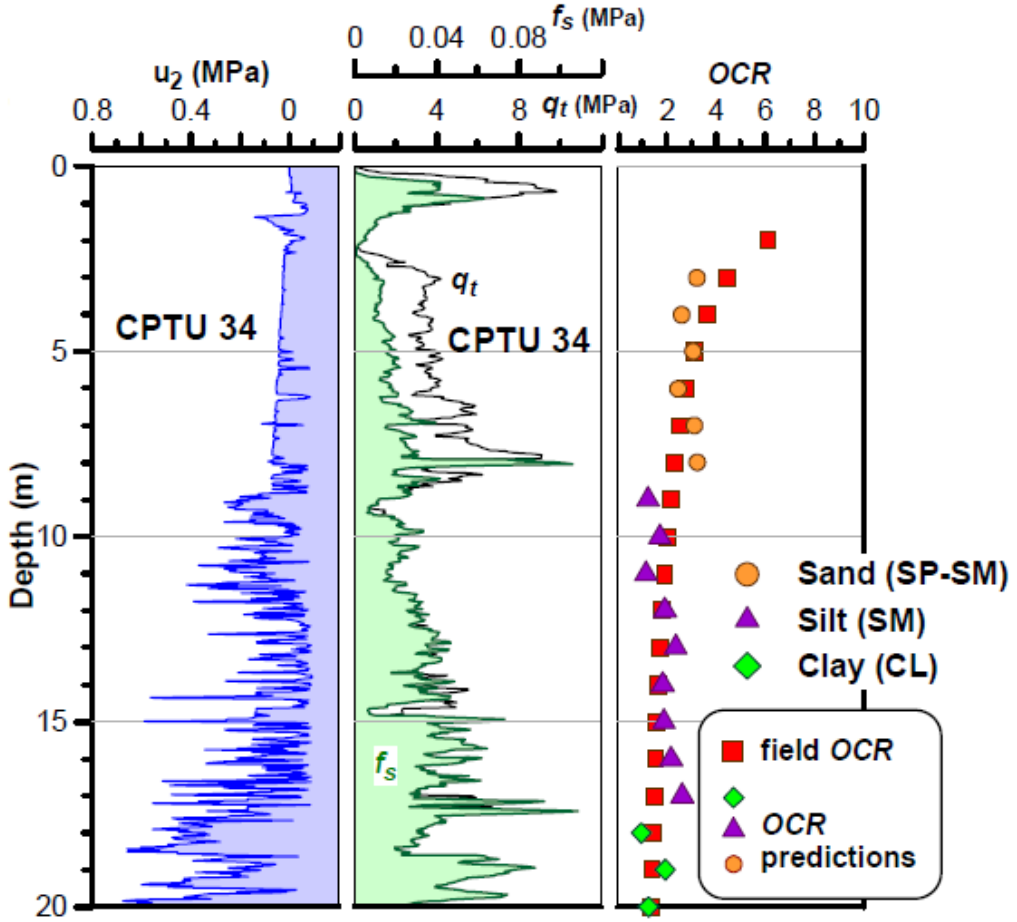

Figure 5.16: *OCR* predictions (after bank removal) for different soils using Equation (5.13) (Tonni *et al*., 2010)

5.7 The issue of partial drainage in Venetian silty soils

The issue of drainage degree detection during cone penetration in Venetian sediments was analysed (Tonni and Gottardi, 2009; Tonni and Gottardi, 2010) from the perspective of two interpretation procedures, proposed by Schnaid *et al.* (2004) and Randolph and Hope (2004).

The first approach proposed by Schnaid *et al.* (2004) as a development of the pioneering work of High *et al.* (1994), is based on plotting the normalized cone resistance Q_t versus the pore pressure parameter B_q together with the undrained strength ratio s_u/σ'_{vo}. Figure 5.17 shows the application of this method to CPTU 14 and CPTU 34 data from 7.7 to 20 m depth (predominately silty layer). A cone factor N_{kt} equal to 15 was used to transform q_t to undrained shear strength. Most point in the figure in the range where $B_q < 0.3$, which corresponds to the zone in which partial drainage prevails when testing NC soils at a standard rate of penetration. As observed by Tonni and Gottardi (2009), the calculated undrained strength ratio (s_u/σ'_{vo}) showed values in general significantly higher than those commonly accepted (0.2-0.3; e.g. Ladd *et al.*, 1977) for NC or slightly OC soils and exhibits substantial scatter and that suggested that deviation from this pattern is basically related to partial drainage conditions.

On the other hand, due to the undergone compression and overconsolidation, data from CPTU 34, again referable to the silty unit, show a more pronounced dilative behaviour, with even negative excess pore pressures.

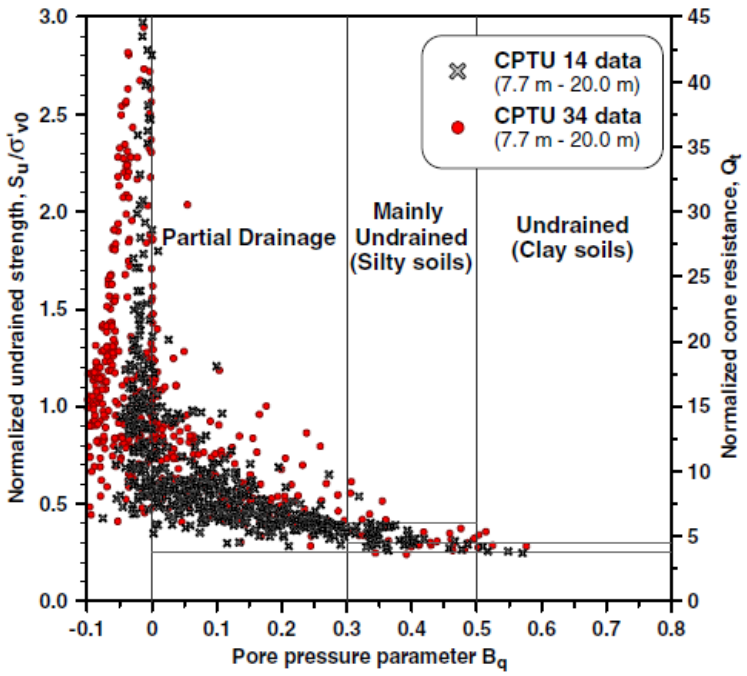

Figure 5.17: Soil classification from CPTU 14 addressing drainage conditions during cone penetration (Tonni and Gottardi, 2009)

With regard to the second approach, tests at non standard penetration rates were considered as a simple way to identify the transition point from undrained to partially drained response.

The final piezocone campaign at TTS included two tests (CPTU 34_{min} and CPTU 34_{max}) performed near the centre of the loaded area at non-standard rates, i.e v = 0.15 cm/s and v = 4 cm/s respectively (Tonni and Gottardi, 2009). Figure 5.18 shows cone resistance (q_t) and pore pressure (u) profiles of tests CPTU 34_{min} and CPTU 34_{max}. As evident from figure, a general increase in q_t and a decrease in u can be observed within the silty unit (from 7 to 20 m depth) when the penetration velocity is lower than the standard (v = 0.15 cm/s).

In Figure 5.19 data from the standard test CPTU 34 and those carried out at non-standard velocities (CPTU 34_{min} and CPTU 34_{max}) were represented in terms of B_q versus the normalized penetration rate $V = v \cdot d / c_v$ defined by Finnie and Randolph (1994), where d is the probe diameter and c_v is the coefficient of consolidation. In the figure are also depicted the curves provided by Schneider *et al*. (2007), obtained by fitting model CPTU data from beam centrifuge tests in normally consolidated and overconsolidated specimens of kaolin clay and silty clay. However, discrepancies between data from Treporti and the trend lines provided by Schneider *et al*. (2007) are evident. This could be partly due to uncertainties about the evaluation of the coefficient of consolidation, which was estimated using well-established procedures based on the assumption of purely undrained behaviour during penetration, which may not apply to such intermediate soils (Tonni and Gottardi, 2010).

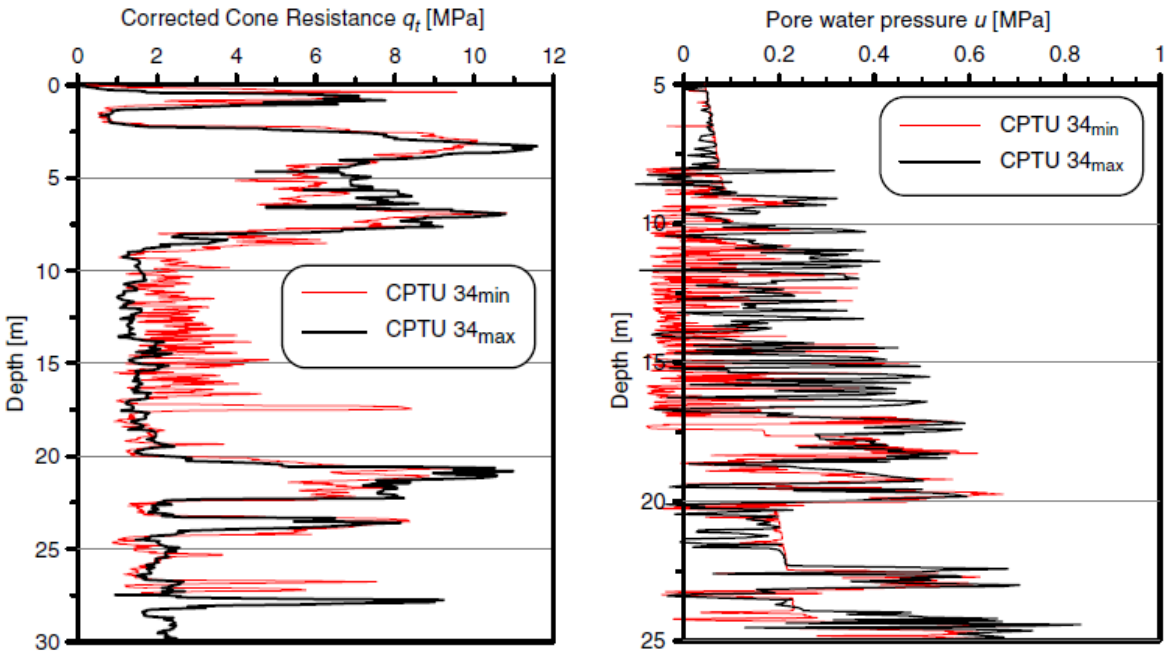

Figure 5.18: Comparison between a) cone resistance and b) pore water pressure of adjacent CPTU tests performed at different penetration rates (Tonni and Gottardi, 2009)

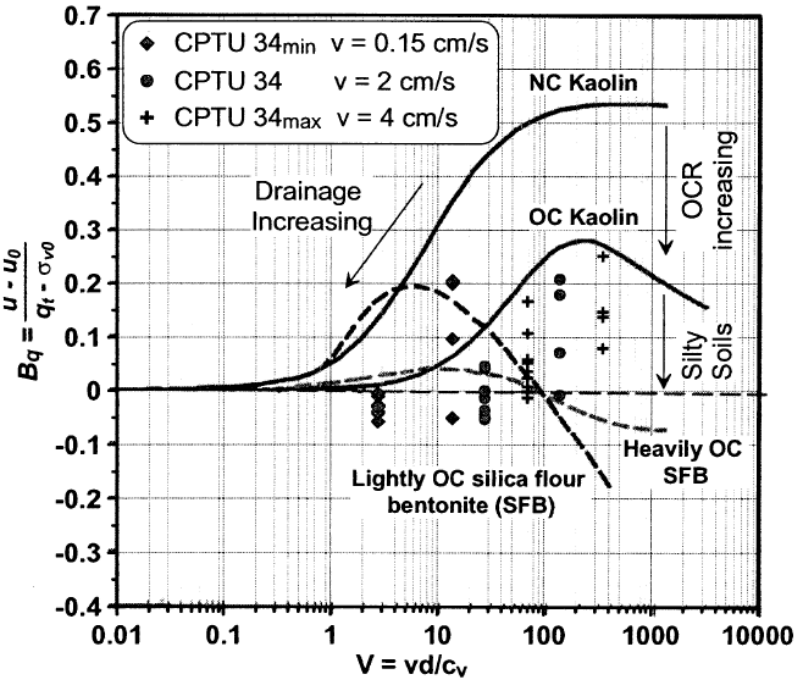

Figure 5.19: Effect of normalized penetration rate on excess pore pressure ratio and comparison with the curves provided by Schneider *et al.* (2007) (Tonni and Gottardi, 2010)

CHAPTER 6: PREDICTING LONG-TERM SETTLEMENTS OF COASTAL DEFENCES OF THE VENETIAN LAGOON

6.1 Introduction

In the last 50 years, the historical city of Venice (Italy) has been affected by a significant increase in the frequency of flooding, as a consequence of the eustatic sea level rise coupled with natural and man-induced subsidence phenomena. Different engineering solutions, including both nearshore and offshore structures, have been developed over the years in order to protect human activities of the whole coastal environment as well as the invaluable historical and artistic heritage of the city from sea storms, high tides and recurrent flooding.

First in the late 19th century, several long jetties were built at the three inlets (Lido, Malamocco, Chioggia) connecting the lagoon to the Adriatic Sea (Figure 6.1). More recently, in 2003, the Italian Government officially approved the MOSE project for the construction of mobile barriers designed to close the three lagoon inlets of Lido, Malamocco and Chioggia when tides are higher than 110 cm. Such project included a number of additional protection measures, such as the reinforcement and extension of the existing jetties together with the construction of a small island, new breakwaters and harbours.

In order to preserve both integrity and effectiveness, a fundamental issue in the design of such structures is represented by the estimate of both short-term and particularly long-term settlements, being the unexpected or underestimated lowering in the structure height a probable cause of flooding. Indeed, the extensive geotechnical investigation campaigns and the large amount of research carried out over more than two decades on the one-dimensional compression of the Venetian lagoon soils have shown that these heterogeneous, predominantly silty sediments exhibit a considerable time-dependent deformations governed by creep phenomena. As evident, a similar mechanical behaviour has significant implications on settlement predictions.

Movements of such structures have been monitored using an advanced technique known as *Persistent Scatterer Interferometry* (PSI), based on satellite-borne remote sensors. As explained in Tosi *et al.* (2012), the method is based on the identification and exploitation of individual radar reflectors, or persistent scatterers (PS), that remain coherent over long time intervals so as to develop displacement-time series. A significant advantage of PSI is represented by the possibility of detecting displacements with very high spatial and temporal resolution. According to ENVISAT ASAR and TerraSAR-X satellite images acquired from April 2003 to December 2009 and from March 2008 to January 2009 respectively, displacements of Venetian coastal structures turned out to range from a few mm/year for breakwaters and jetties older than 10 years to a maximum of 50-70 mm/year in the case of new or recently reshaped structures. Details on the

whole PSI monitoring performed from Lido to Chioggia inlets can be found in Tosi *et al*. (2012).

In this Chapter attention has been focused first on soil classification of Venetian sediments from piezocone tests located along the new breakwaters and in the artificial island, and carried out prior to the their construction.

Finally, the long-term response of Venetian coastal defence structures has been performed using a one-dimensional settlement method in conjunction with a secondary compression coefficient $C_{\alpha\varepsilon}$ profile determined from piezocone test data. The approach is based on a formulation recently calibrated on field data assembled during approximately 6 years at the Treporti Test Site (TTS, Venice), within an extensive research.

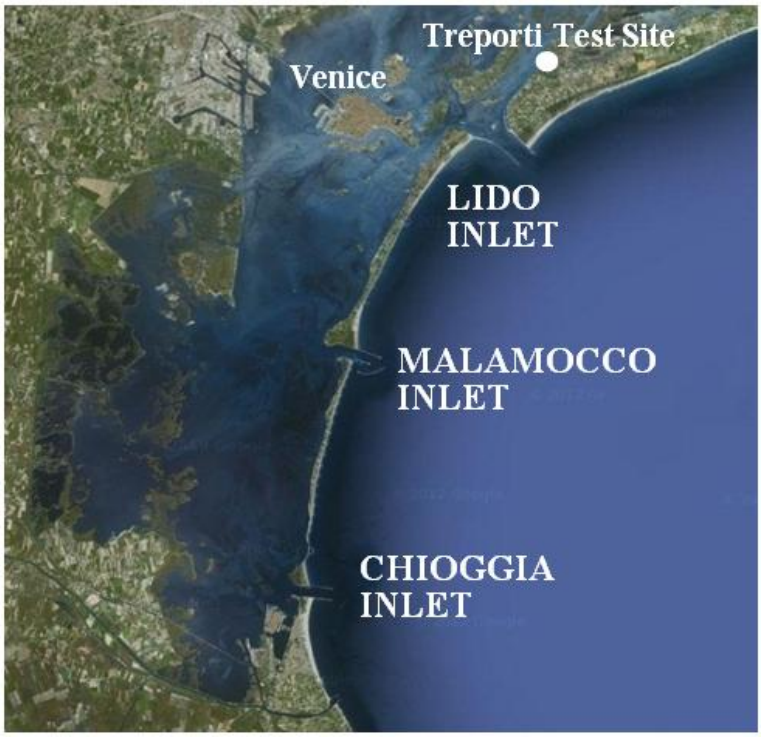

Figure 6.1: Satellite view of the Venetian lagoon

6.2 Persistent Scatterer Interferometry monitoring

The Persistent Scatterer Interferometry (PSI) is a radar-based remote-sensing technique to measure and monitor land deformation. PSI is an advanced class of differential interferometric Synthetic Aperture Radar techniques (DInSAR) based on data acquired by spaceborne SAR sensors. The PSI techniques can be used with data that come from terrestrial or airbone SAR sensors. Nevertheless, the spaceborne SAR sensors are the most important PSI data source (Crosetto *et al*., 2009).

As Crosetto *et al*. (2009) remarked, there are two main differences between DInSAR and PSI techniques: the first one is the number of SAR images processed (PSI uses typically more than 20 series of SAR images), and the other difference is the implementation of appropriate data modelling and analysis methods that permit to get the following outcomes:

1) the time series of the deformation;
2) the average displacement rates over the period covered;
3) the component of the atmospheric phase of each SAR image and;
4) the residual topographic error.

PSI allows getting a global vision of the deformation process occurring in an extensive area, keeping at the same time the ability to measure individual features, like structures and buildings. For further details see Crosetto *et al*. (2005).

Since the early 2000s, PSI has been widely employed in the Venice Lagoon, with the main purpose of monitoring land subsidence which is however one of the major environmental phenomena threatening this coastal area (Teatini *et al*., 2007, 2010; Strozzi *et al*., 2009; Tosi *et al*. 2009*b*).

According to ENVISAT and TerraSAR-X satellite images acquired from April 2003 to December 2009 and from March 2008 to January 2009 respectively, long-term displacements of coastal structures along the Venice littoral turned out to range from a few mm/year for breakwaters and jetties older than 10 years to a maximum of 50-70 mm/year in the case of recently reshaped or new structures. Details on the whole PSI monitoring performed from Lido to Chioggia inlets are provided in Tosi *et al.* (2012).

The Inlets of the Venice Lagoon

Displacements of Venetian coastal structures are monitored by PSI using ENVISAT and TerraSAR-X images. As remarked in Tosi *et al.* (2012), the number of PS detected by ENVISAT is much lower than that distinguished by TerraSAR-X due to the higher spacial resolution of the former and the loss of signal coherence during the longer ENVISAT acquisition period caused by structural changes of the reflectors.

According to Tosi *et al*. (2012) settlement rates on the order of 1-2 mm/year are measured along the coastal strips and are due to the natural subsidence in the study areas. Larger rates are induced by subsoil heterogeneity or buildings constructed or reshaped in recent times.

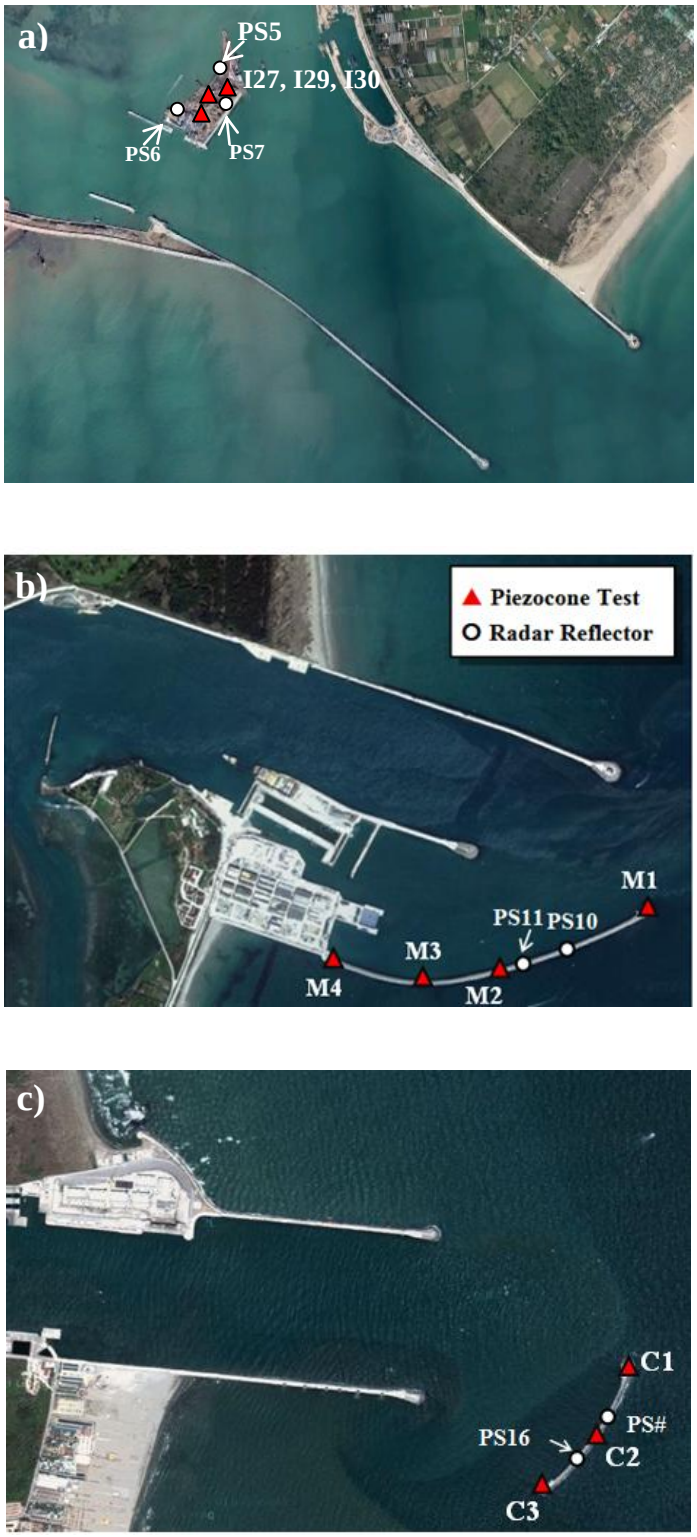

Figure 6.2: Satellite view of the a) Lido inlet; b) Malamocco inlet and c) Chioggia inlet and location of the piezo-cone tests and radar reflectors (Persistent Scatterer, PS)

At the Lido inlet (Figure 6.2*a*), the offshore portion of the southern jetty shows settlement rates less than 2-3 mm/year whereas rates rise up to 70 mm/year toward the root due to the re-shape of the structure. On the other hand, the breakwater containing the new artificial island has consolidation rates greater than 5 mm/year. The refuge harbour constructed on the north side of the Lido inlet subsides at rates on the order of 20-40 mm/year with the exception of the central part which is rising by nearly 10 mm/year.

The PSI outcome shows that at the Malamocco inlet (Figure 6.2*b*), the major displacements characterize only the new structures whereas the old jetties appear almost stable. Outside the inlet, the new 1280 m-long breakwater shows settlement rates that vary in the range 5-25 mm/year, with the higher rates observed close to the seaward edge of the structure.

At the Chioggia inlet (Figure 6.2*c*), the offshore portion of the existing jetties remained essentially unchanged. In the north side of the inlet a new harbour was recently constructed. The new structure shows settlement rates of about 40 mm/year. Uniform settlements of about 15 mm/year are observed in the offshore breakwater.

6.3 The piezocone database

The stratigraphic condition of the lagoon basin in this area as well as the relevant geotechnical parameters of the different soil units have been derived from a number of piezocone tests carried out prior to the construction of the new breakwaters outside the Malamocco and Chioggia inlets and the artificial island at the Lido inlet (Figure 6.3).

The site investigation campaign included:

- Three piezocone tests performed at the inlet of Lido (CPTUs I27, I29 and I30). Such tests were carried out within the area of the recently constructed artificial island. The precise location is unknown by this author.
- Four piezocone tests carried out at the site of Malamocco (CPTUs from M1 to M4). The tests covered the length of the external breakwater.
- Three piezocone tests performed at the Chioggia inlet (CPTUs C1, C2 and C3). As in the previous site, the tests were located along the length of the breakwater.

All tests were pushed to about 60 m below the sea level. Two tests, I29 and I30 from Lido, were only pushed to about 30 m depth.

All the CPTU profiles confirm the highly stratified system, characterized by alternated layers of silty sands, silts and silty clay. This is also confirmed by previous studies performed at different sites of the Venetian lagoon. The pore pressure profiles usually describe a slightly contractive response, with generally relative low values of excess pore pressures Δu.

A large amount of research has been carried out on the interpretation of the CPTU data collected in the inlets. The effectiveness of some well-known piezocone-based classification framework proposed by Robertson (1990), Been and Jefferies (2006), Schneider *et al*. (2008) and Robertson (2009) have been discussed.

Special attention has been paid to the assessment of the secondary compression of the Venetian sediments. In this context, the predictive capability of the formulation recently calibrated on field data from Treporti Test Site (Venice) has been evaluated.

Figure 6.3: View of the a) Lido inlet, b) Malamocco inlet and c) Chioggia inlet and location of the piezocone tests (images taken from the website salve.it)

6.4 Soil Classification

Classification of Venetian sediments from piezocone data has been performed using some well-known soil classification charts, implying the assessment of data in Q_{t1} - B_q (Robertson, 1990), Q (1-B_q)+1 - F_r (%) (Jefferies and Been, 2006), Q_{t1} - $\Delta u_2/\sigma'_{v0}$ (Schneider *et al*., 2008) and Q_{tn} - F_r (%) (Robertson, 2009) spaces.

6.4.1 Malamocco: external breakwater

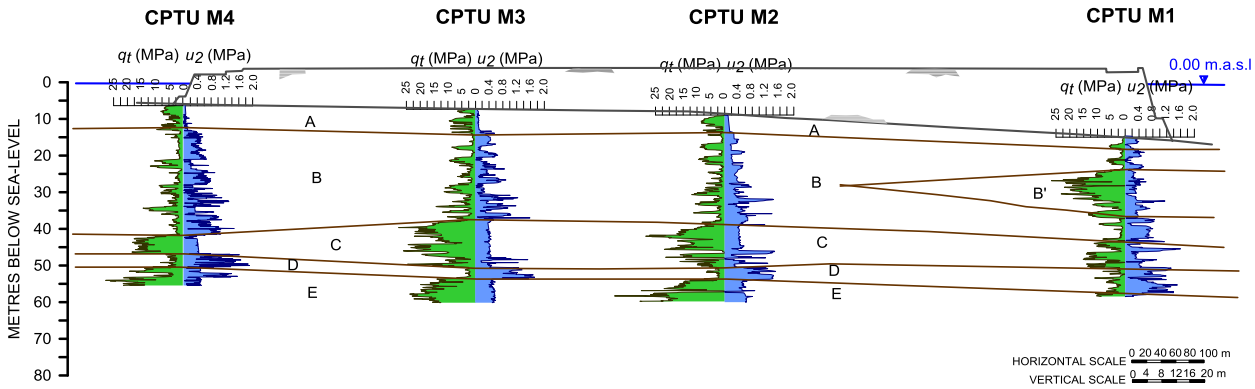

Figure 6.4: Cross section of the test-site area

Figures 6.5, 6.7, 6.9 and 6.11 show the corrected cone resistance q_t, the pore pressure u_2 and the sleeve friction f_s from the four available tests CPTU M1, M2, M3 and M4. A highly stratified system can be immediately identified from these profiles.

Results from the application of the charts to CPTU data from Malamocco are shown in Figures 6.6, 6.8, 6.10 and 6.12. From these figures, cases *a* and *d* report data from CPTU in terms of Q (1-B_q)+1, Q_{tn} and F_r (%), on the classification charts proposed by Jefferies and Been (2006) and Robertson (2009), respectively. Relevant points generally fall in zones which include soils ranging from clays – silty clays to clean sands – sandy silts. Mainly differences between them are observed when applied to shallow coarse-grained materials, in which $B_q \approx 0$ and the stress exponent is close to 0.5 in the clean sand region (see stress exponent profile in Figure 6.13).

Besides, as Robertson (2012) stated, in soft soils, where q_t is small compared to u_2, the difference q_t - u_2 is very small and lacks accuracy and reliability. Hence, in the Jefferies and Been chart, where $Q_{t1}(1-B_q)+1$ is the effective cone resistance (q_t - u_2) normalized by σ'_{v0}, the applicability of the chart can be problematic.

- CPTU M1

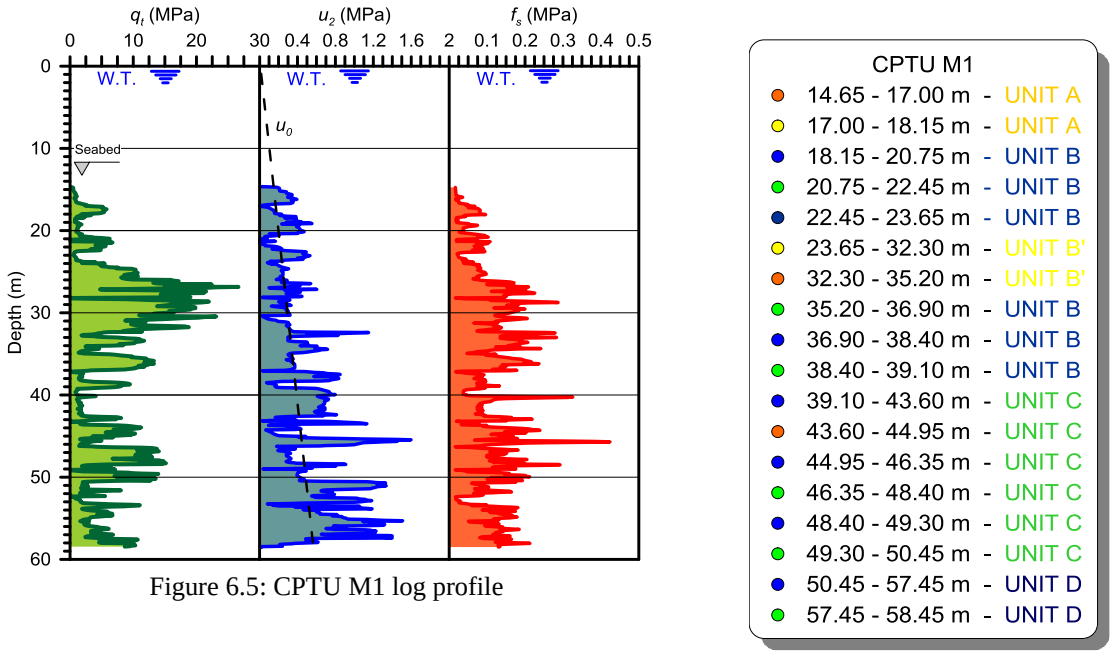

Figure 6.5: CPTU M1 log profile

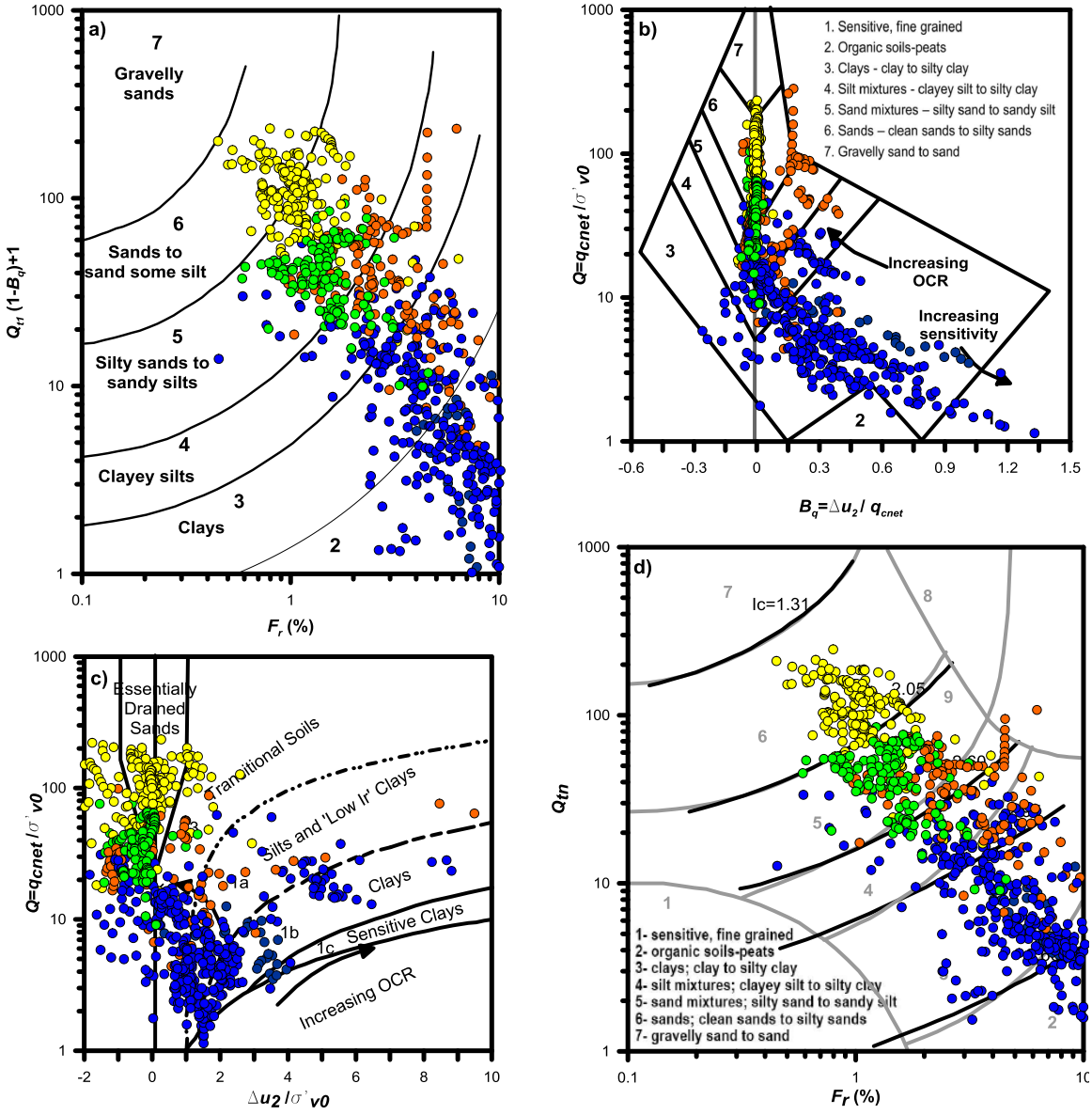

Figure 6.6: Soil classification according to the approaches proposed by: a) Jefferies and Been (2006); b) Robertson (1991); c) Schneider *et al.* (2008) and d) Robertson (2009) applied to test M1

- CPTU M2

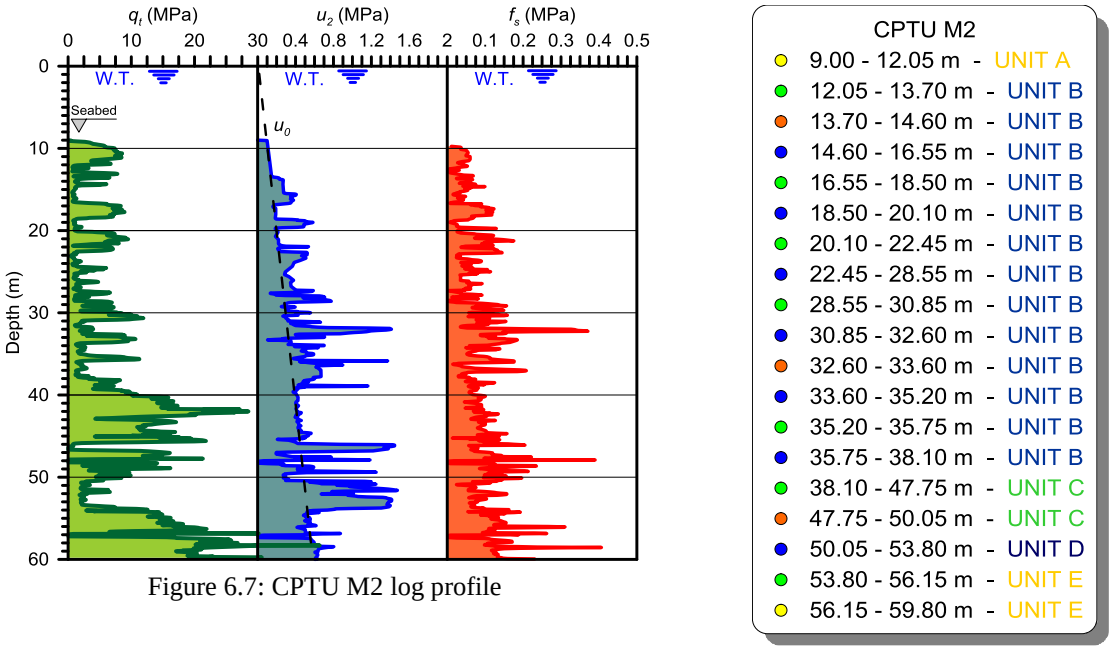

Figure 6.7: CPTU M2 log profile

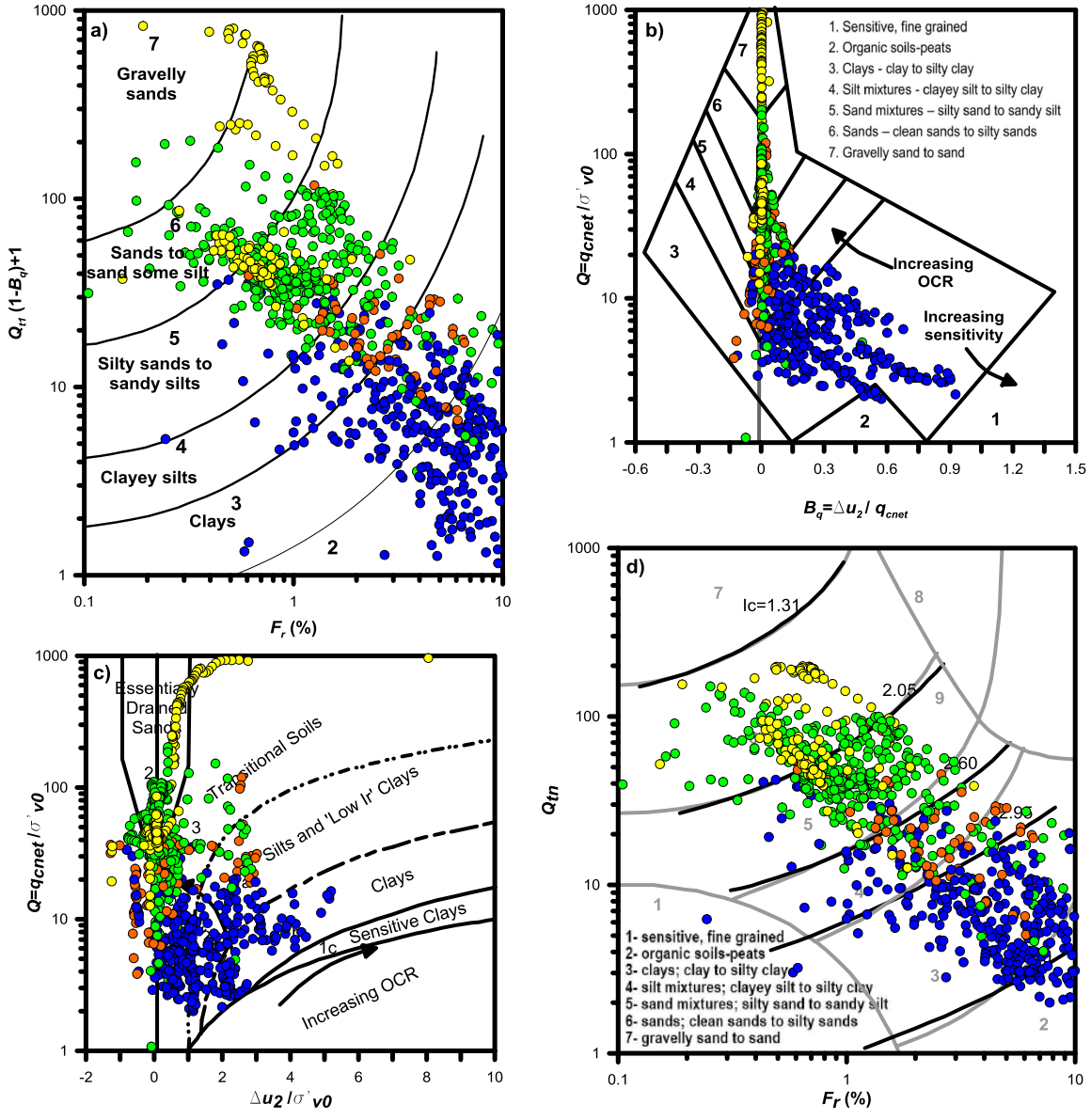

Figure 6.8: Soil classification according to the approaches proposed by: a) Jefferies and Been (2006); b) Robertson (1991); c) Schneider *et al.* (2008) and d) Robertson (2009) applied to test M2

- CPTU M3

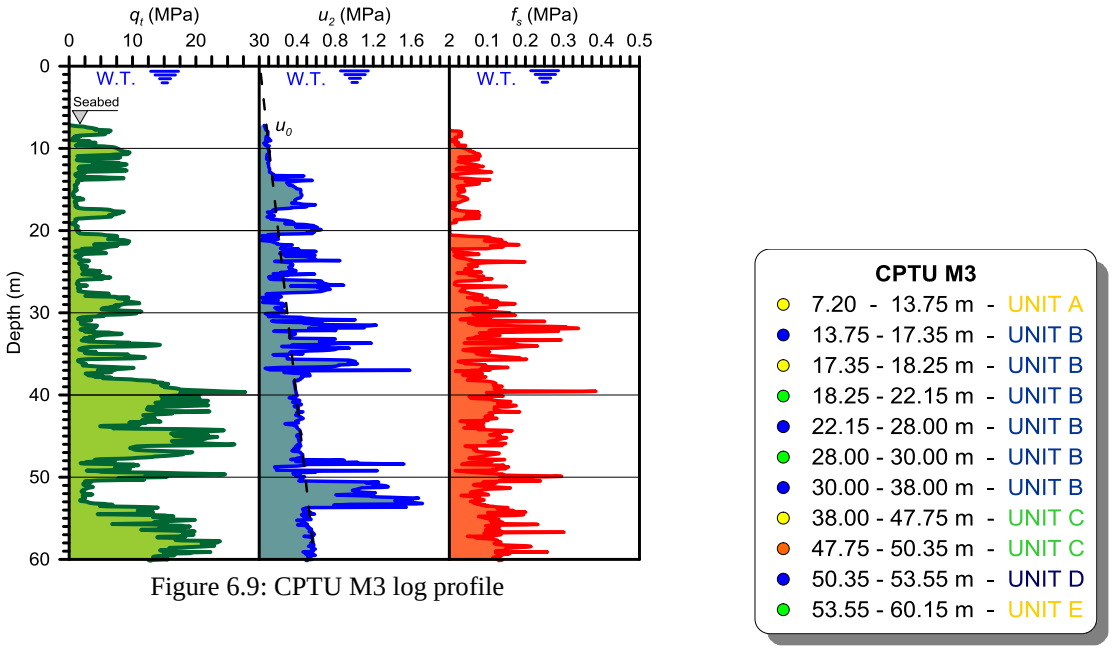

Figure 6.9: CPTU M3 log profile

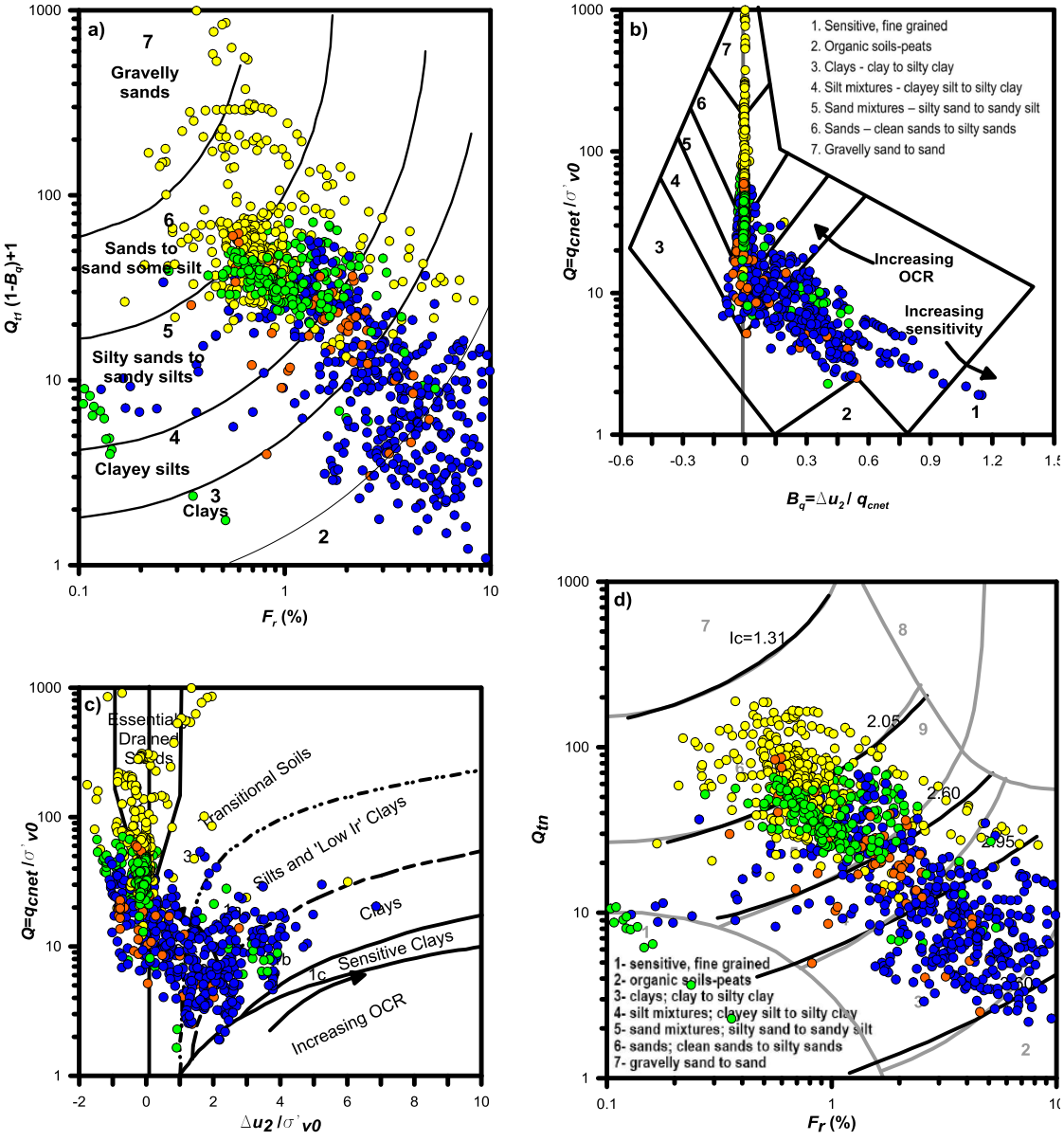

Figure 6.10: Soil classification according to the approaches proposed by: a) Jefferies and Been (2006); b) Robertson (1991); c) Schneider *et al.* (2008) and d) Robertson (2009) applied to test M3

- CPTU M4

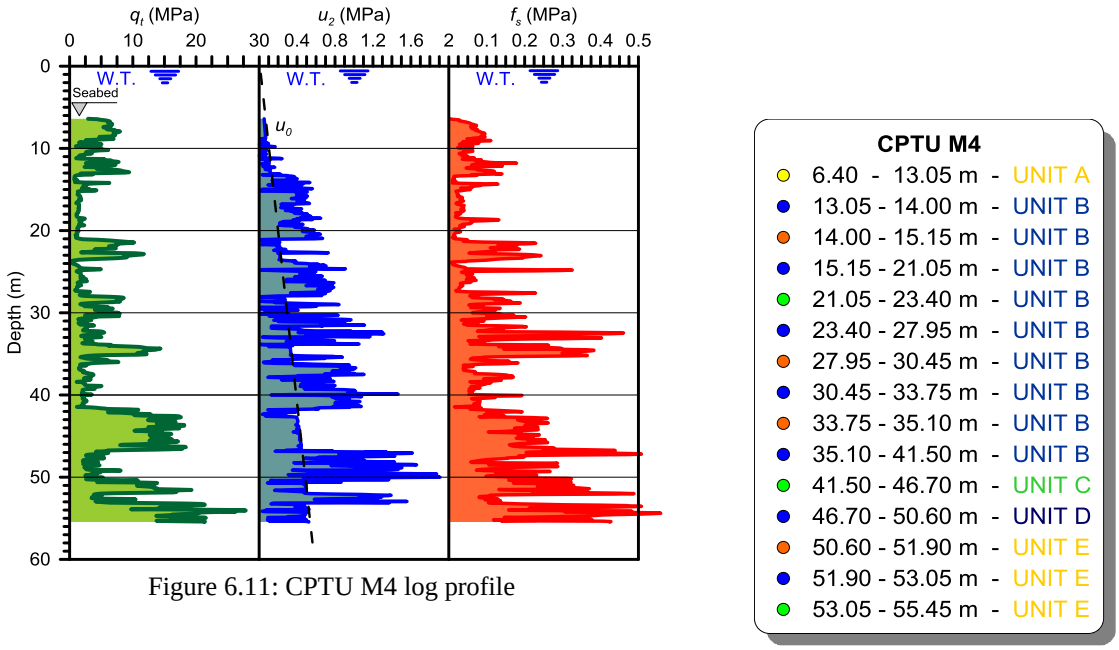

Figure 6.11: CPTU M4 log profile

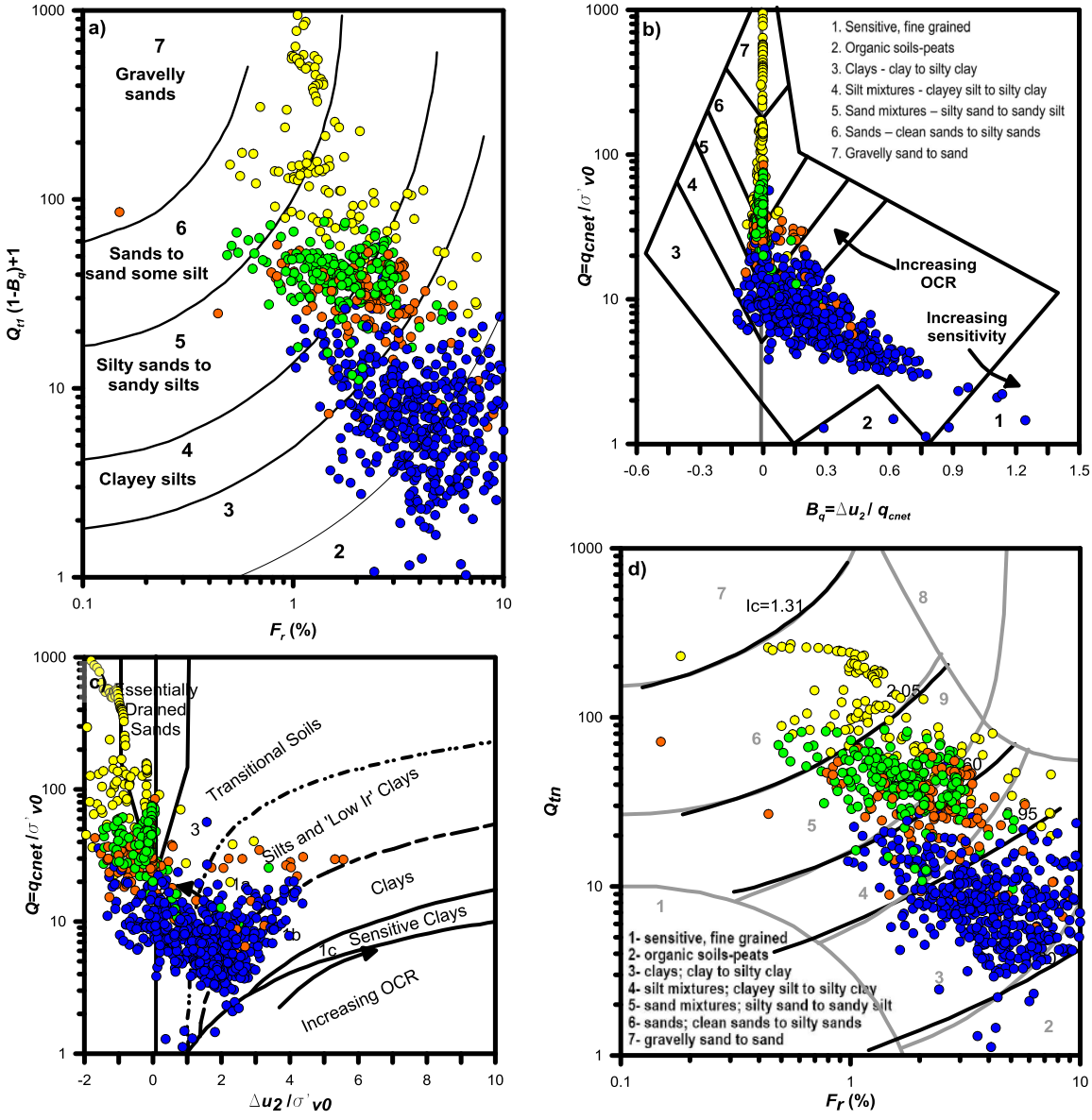

Figure 6.12: Soil classification according to the approaches proposed by: a) Jefferies and Been (2006); b) Robertson (1991); c) Schneider *et al*. (2008) and d) Robertson (2009) applied to test M4.

According to the SBTn profiles shown in Figure 6.13, the Robertson's (2009) approach seems to predict a more pronounced clay-like behaviour (zone 3) in comparison with the stratigraphic profiles obtained from nearby boreholes (not shown here).

Cases *b* from Figures 6.6, 6.8, 6.10 and 6.12 report data in terms of Q and B_q on the classification chart proposed by Robertson (1990). The application of this chart to CPTUs show that most of the points fall in zones 3 to 6. Data tend to indicate that as Q increases (or *OCR*), B_q tends to decrease.

The chart proposed by Schneider *et al*. (2008) applied to CPTU data is shown in Figures 6.6, 6.8, 6.10 and 6.12 (cases *c*), based on the normalized piezocone parameters Q and $\Delta u_2/\sigma'_{v0}$. According to such classification framework, a large number of the CPTU data fall in domains 1a – 2, most of them falling in zone 3, which includes a wide variety of mixed soil types. The application of the method to CPTUs is useful for separating whether penetration in drained, undrained, or partially drained.

Although soil classification in $Q - B_q$ space and Q - $\Delta u_2/\sigma'_{v0}$ space are analogous, the first one provides further detail for classification of clayey soils. Nevertheless, when focusing on separating the influence of *OCR* from that of partial consolidation on normalized CPTU parameters, soil classification in Q - $\Delta u_2/\sigma'_{v0}$ space is the most suitable.

Figure 6.14 illustrates the different trends of increasing *OCR* for clay data from CPTU M1 (19.35 to 20.15 m) in both soil classification charts. The Robertson's approach shows that as Q increases, B_q tends to decrease, whereas in the Q - $\Delta u_2/\sigma'_{v0}$ space the data show small changes in $\Delta u_2/\sigma'_{v0}$.The trends of Q increasing and B_q decreasing with OCR have been also plotted in Figure 6.15. Predictions of *OCR* have been obtained using an empirical relationship proposed by Tonni and Gottardi (2011) calibrated on data from Treporti Test Site (see Chapter 5, Equation (5.14)), which relates the *OCR* to the effective cone resistance (q_t-u_2) normalized by σ'_{v0}.

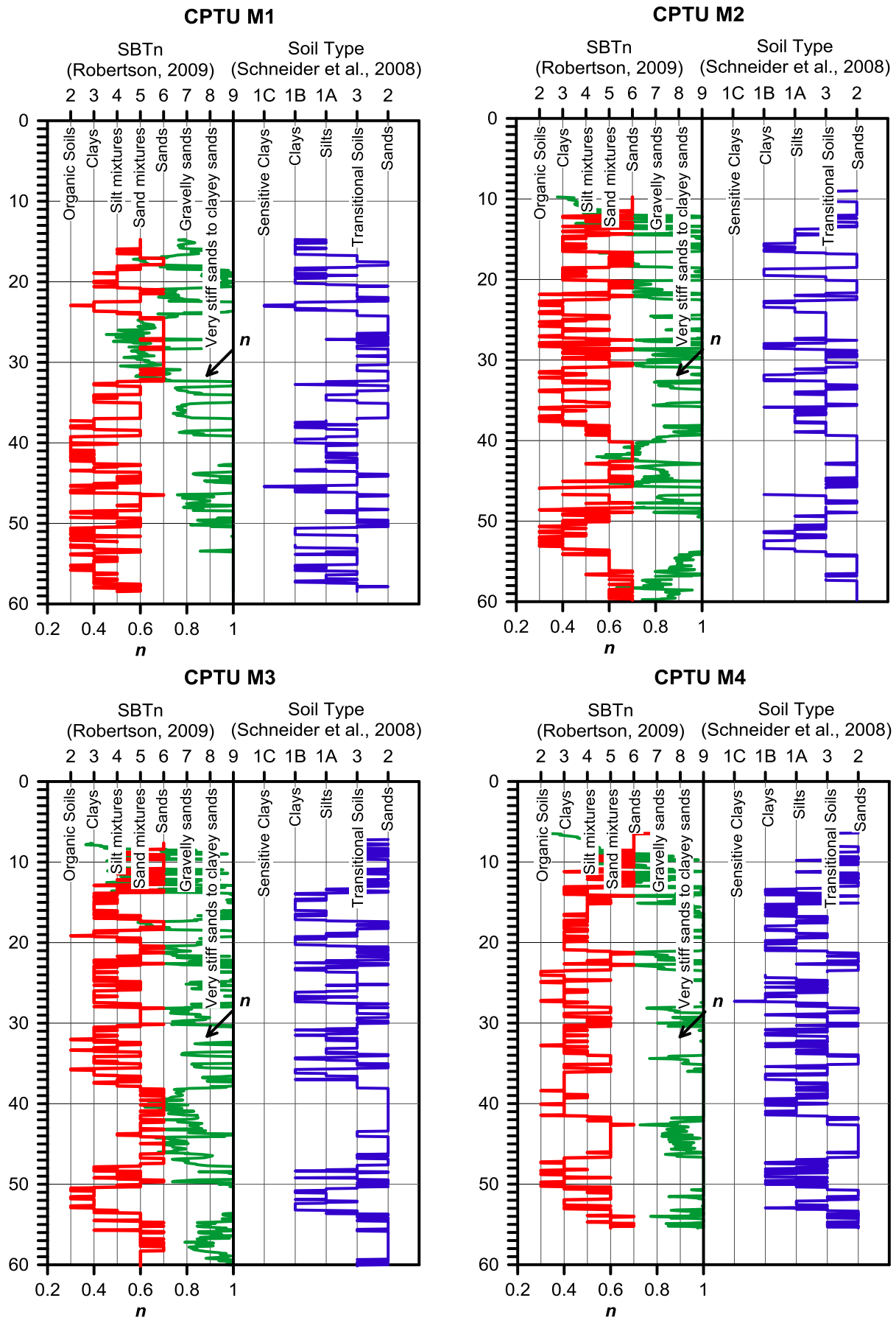

Figure 6.13: Schneider *et al*. (2008) and Robertson (2009) classification methods applied to Malamocco tests and stress exponent profiles

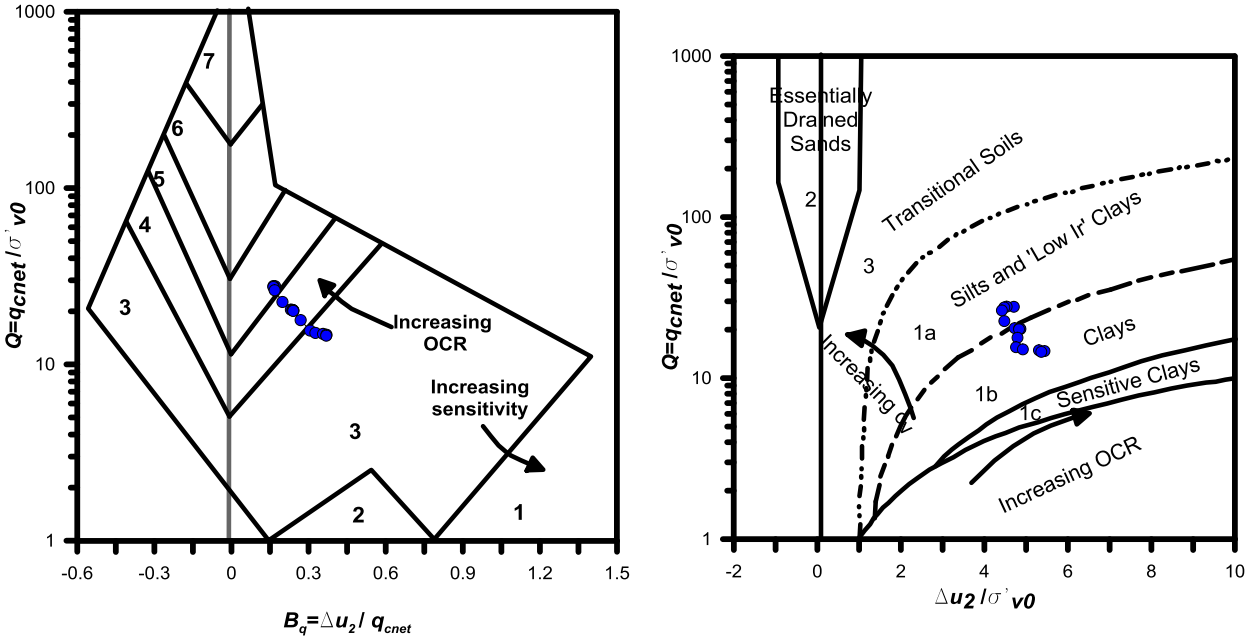

Figure 6.14: Trends of increasing *OCR* for clay data from CPTU M1 (19.35 - 20.15 m) in a) $Q - B_q$; b) $Q - \Delta u_2/\sigma'_{v0}$ space

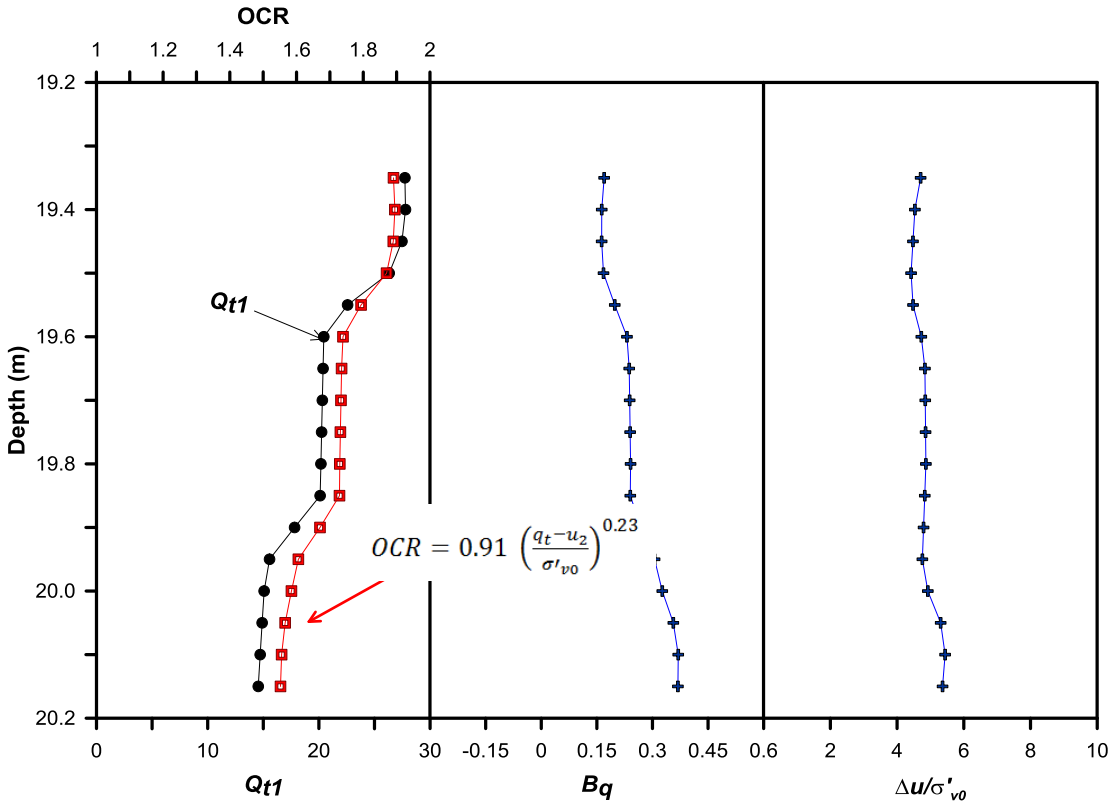

Figure 6.15: Normalized tip resistance *Q*, pore pressure ratio *Bq* and *OCR* predictions for clay data from CPTU M1

Figure 6.16 shows the percentages of soil classes predicted from CPTU M1 by three different soil classification charts. The predominance of silty sands to sandy silts (≈ 35%) can be clearly appreciated in Jefferies and Been and Robertson's approach. However percentages of sands predicted by the $Q_{tn} - F_r$ (%) chart are approximately 8% higher than those predicted by

the Jefferies and Been's chart, whereas the latter tends to predict higher percentage of organic soils and peats.

Concerning the classification chart proposed by Schneider *et al*. (2008), in the third pie chart are represented the percentages of the type of sediments predicted. As can be appreciated, the highest percentage of coarse-grained soils seems to be estimated by this approach. Transitional soils are present in 42% of data analyzed.

Despite the alternation of different grain-sized sediments, the following stratigraphic units can be identified in a Malamocco subsoil profile:

- Unit A: Alternate layers of sands, sand mixtures and silts.
- Unit B: Alternate layers of silty sand, sandy silt and clayey silt, with occasional presence of organic soils. It is clearly noticeable the presence of a dense sand (Unit B') close to the seaward edge of the breakwater.
- Unit C: Sands and sand mixtures with thin layers of silts.
- Unit D: Clays and silty clays, with occasional presence of organic soils.
- Unit E: Sands and sand mixtures.

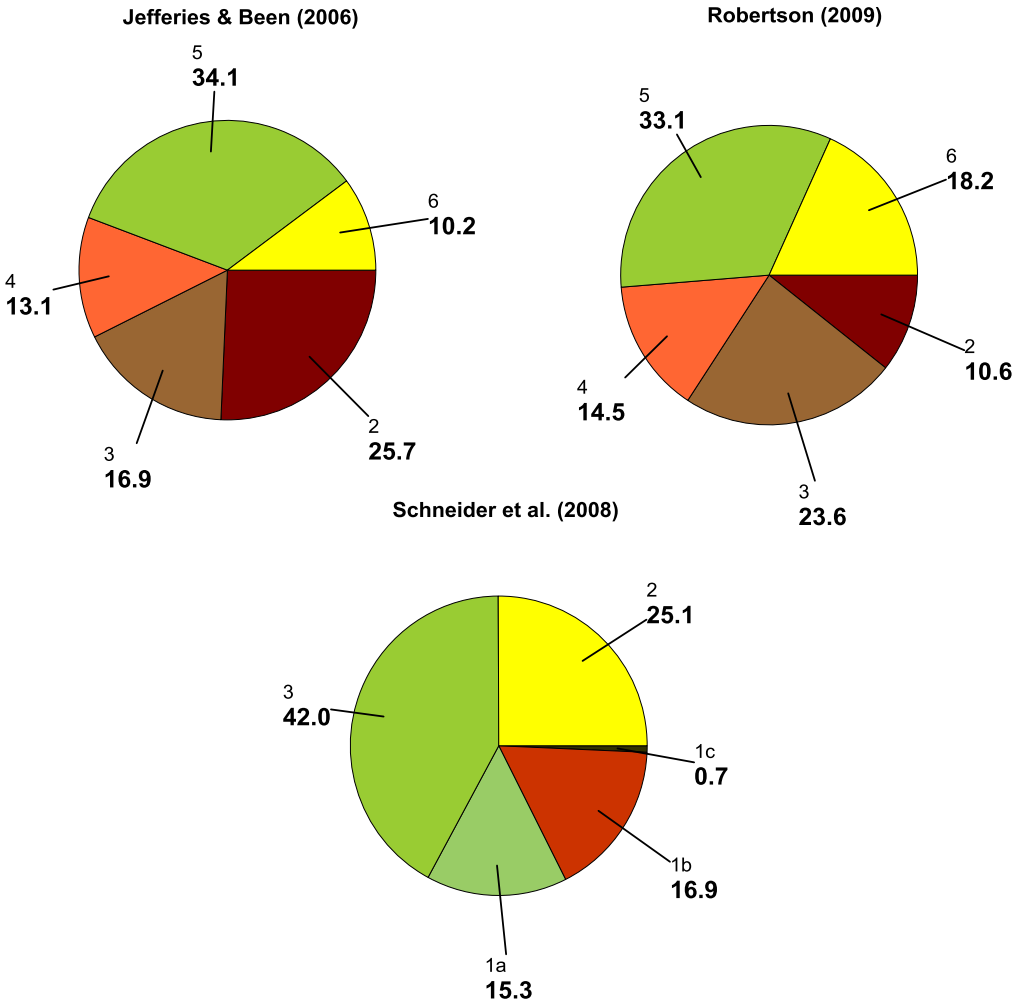

Figure 6.16: Percentages of soil types predicted by three different soil classification charts

6.4.2 Chioggia: external breakwater

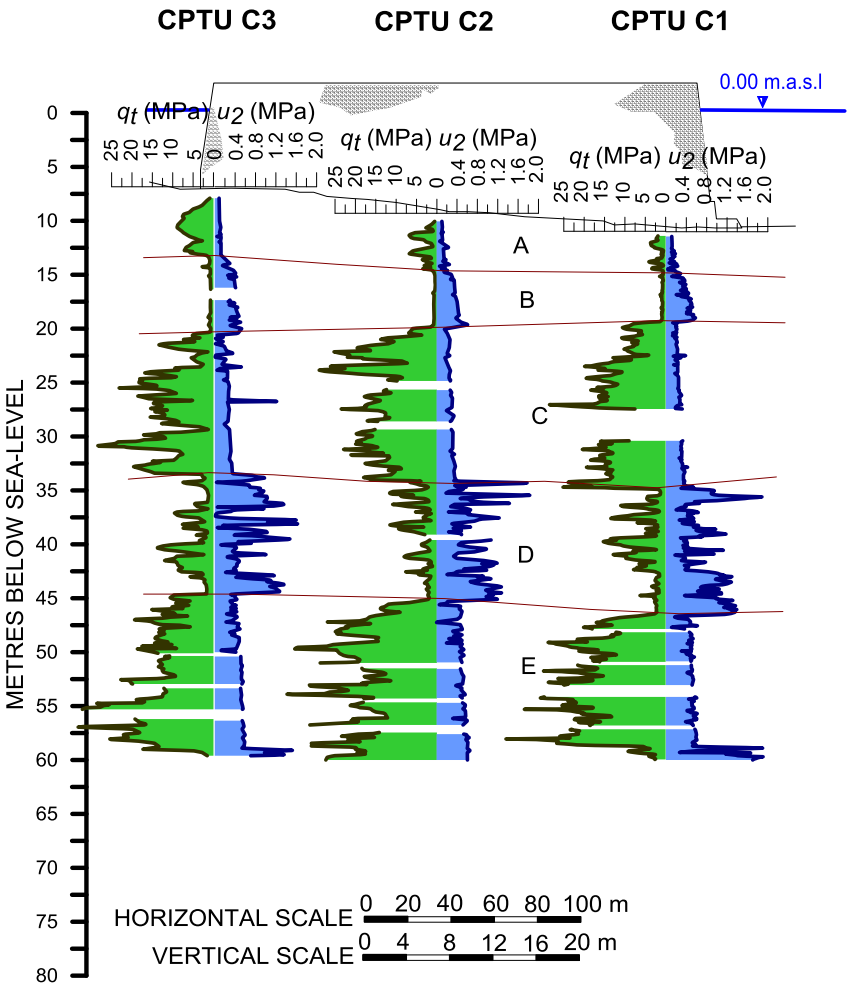

Figure 6.17: Cross section of the test-site area

For all the CPTU measurements from Chioggia the soil profile was classified using the soil classification charts already applied to Malamocco tests. Figures 6.18, 6.20 and 6.22 show the corrected cone resistance q_t, the pore pressure u_2 and the sleeve friction f_s from the three available tests CPTU C1, C2 and C3.

The application of Jefferies and Been and Robertson's charts to CPTU from Chioggia reveal that points mainly fall in zones 2 to 6. Again, comparison with the stratigraphic profiles obtained from nearby boreholes reveal a certain inaccuracy of both approaches when applied to silt mixtures, which seem to predict a more pronounced clay-like behaviour.

Cases *b* and *c* from Figures 6.19, 6.21 and 6.23 report data in terms of Q and B_q and Q and $\Delta u_2/\sigma'_{v0}$ on the classification charts proposed by Robertson (1990) and Schneider *et al.* (2008), respectively. All previous comments made for Malamocco results, comparing these classification charts, are also valid for Chioggia and for the next case of study, Lido.

- CPTU C1

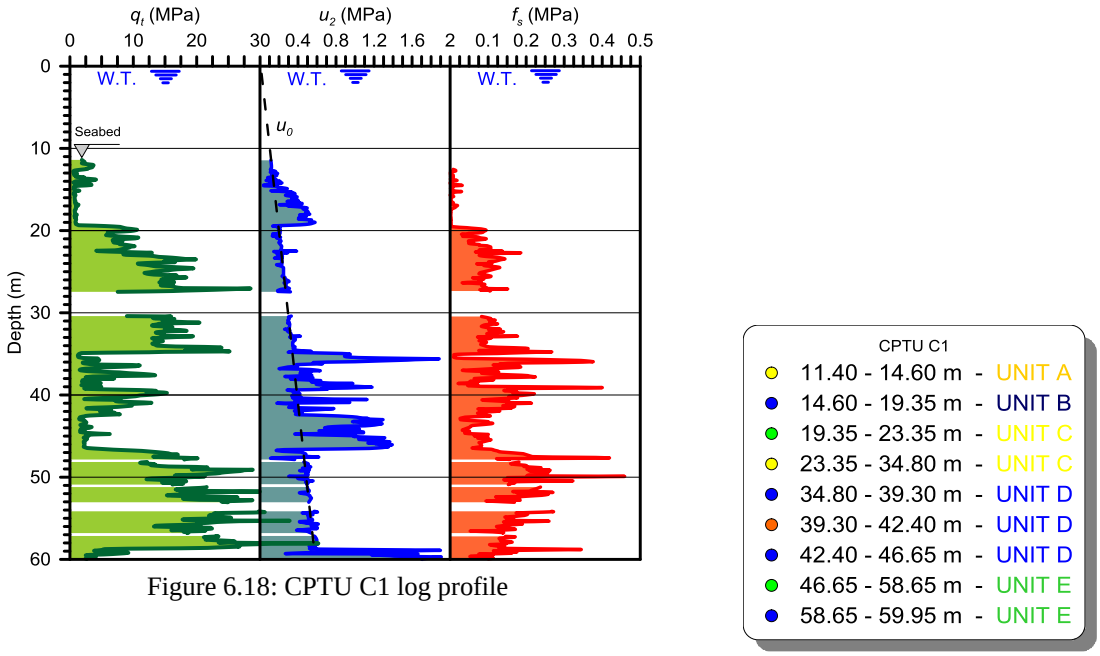

Figure 6.18: CPTU C1 log profile

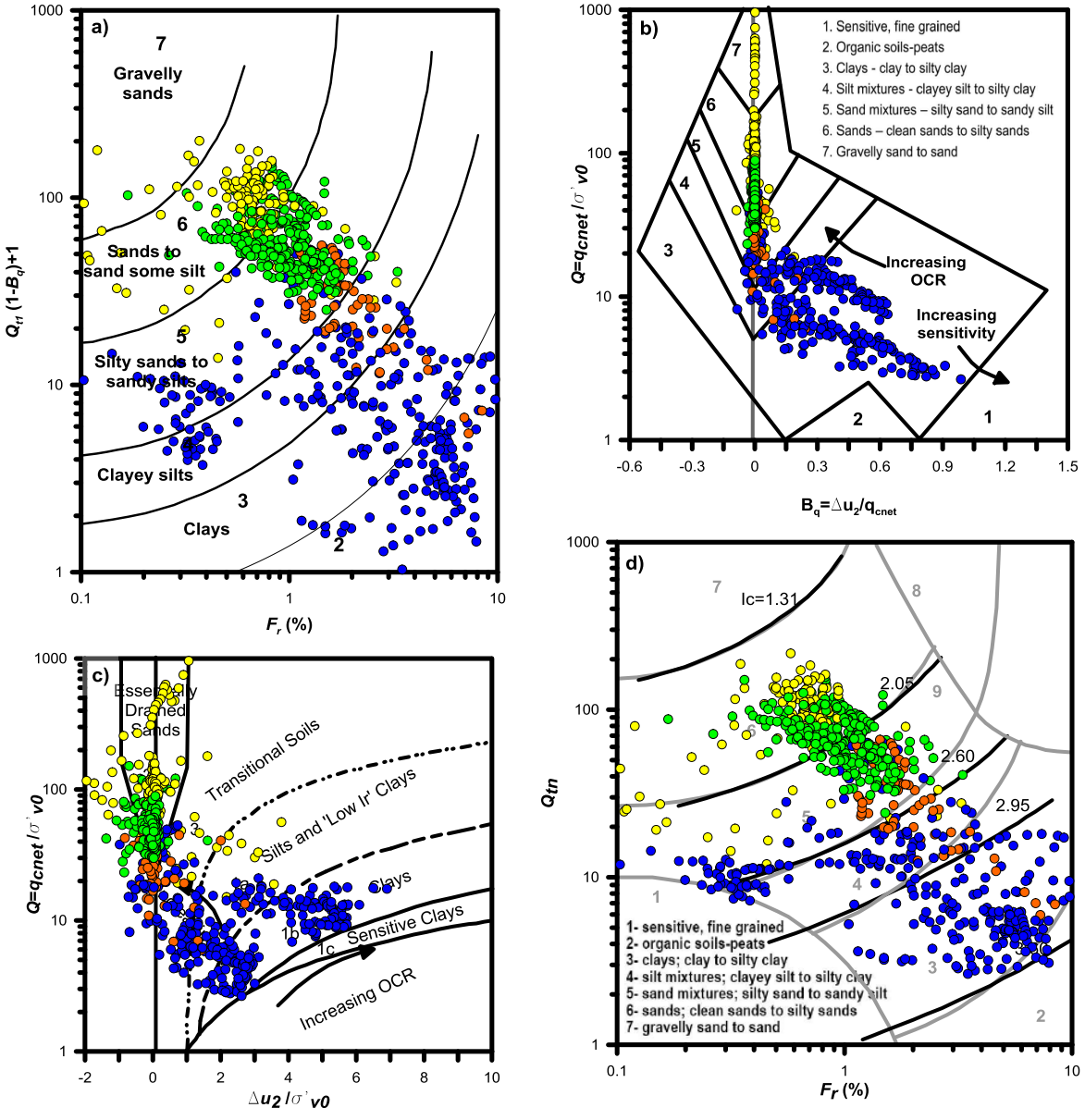

Figure 6.19: Soil classification according to the approaches proposed by: a) Jefferies and Been (2006); b) Robertson (1991); c) Schneider *et al.* (2008) and d) Robertson (2009) applied to test C1

- CPTU C2

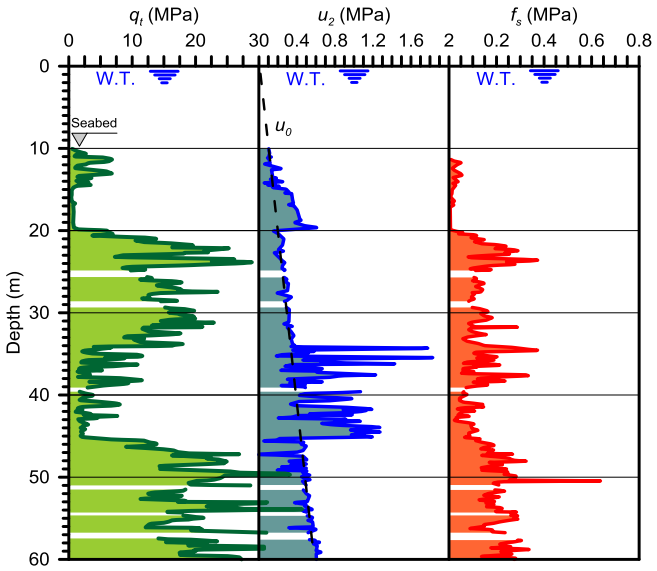

Figure 6.20: CPTU C2 log profile

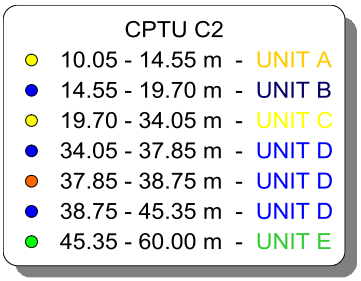

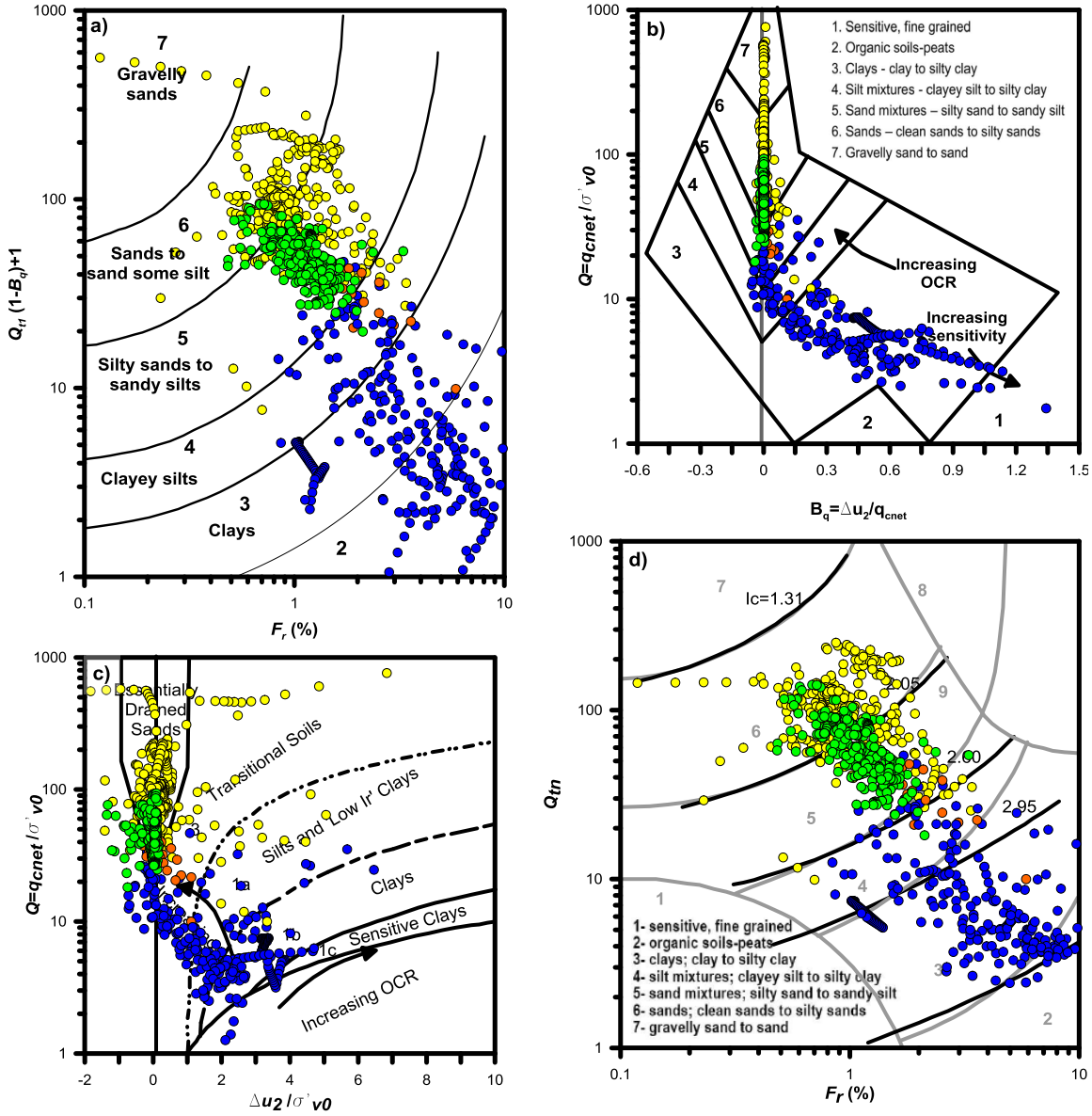

Figure 6.21: Soil classification according to the approaches proposed by: a) Jefferies and Been (2006); b) Robertson (1991); c) Schneider *et al.* (2008) and d) Robertson (2009) applied to test C2

- CPTU C3

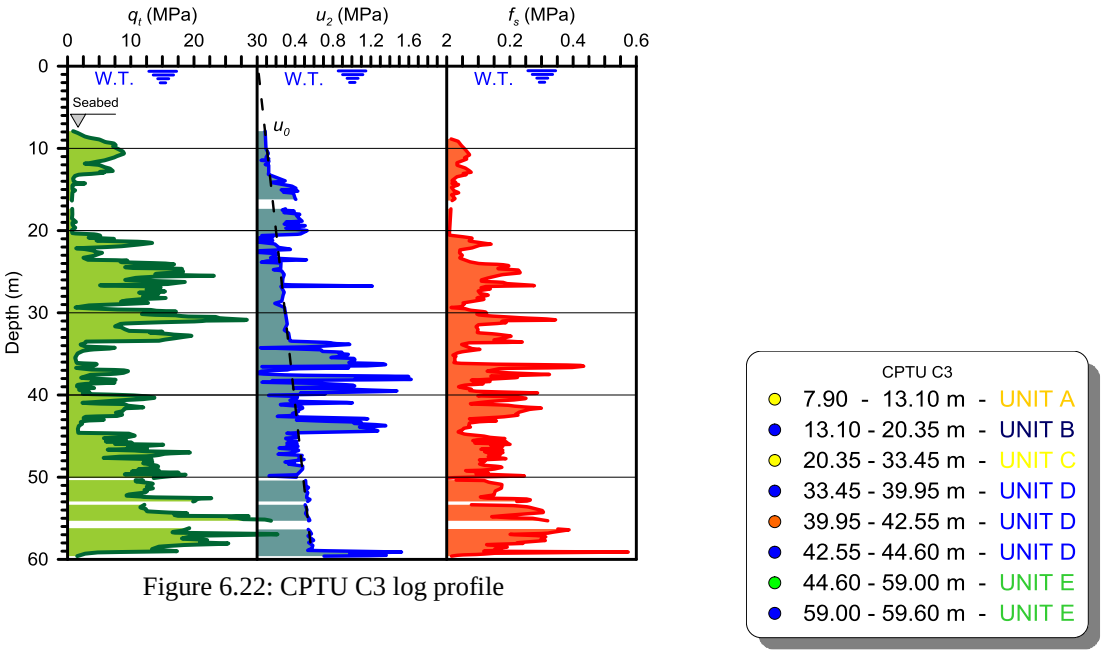

Figure 6.22: CPTU C3 log profile

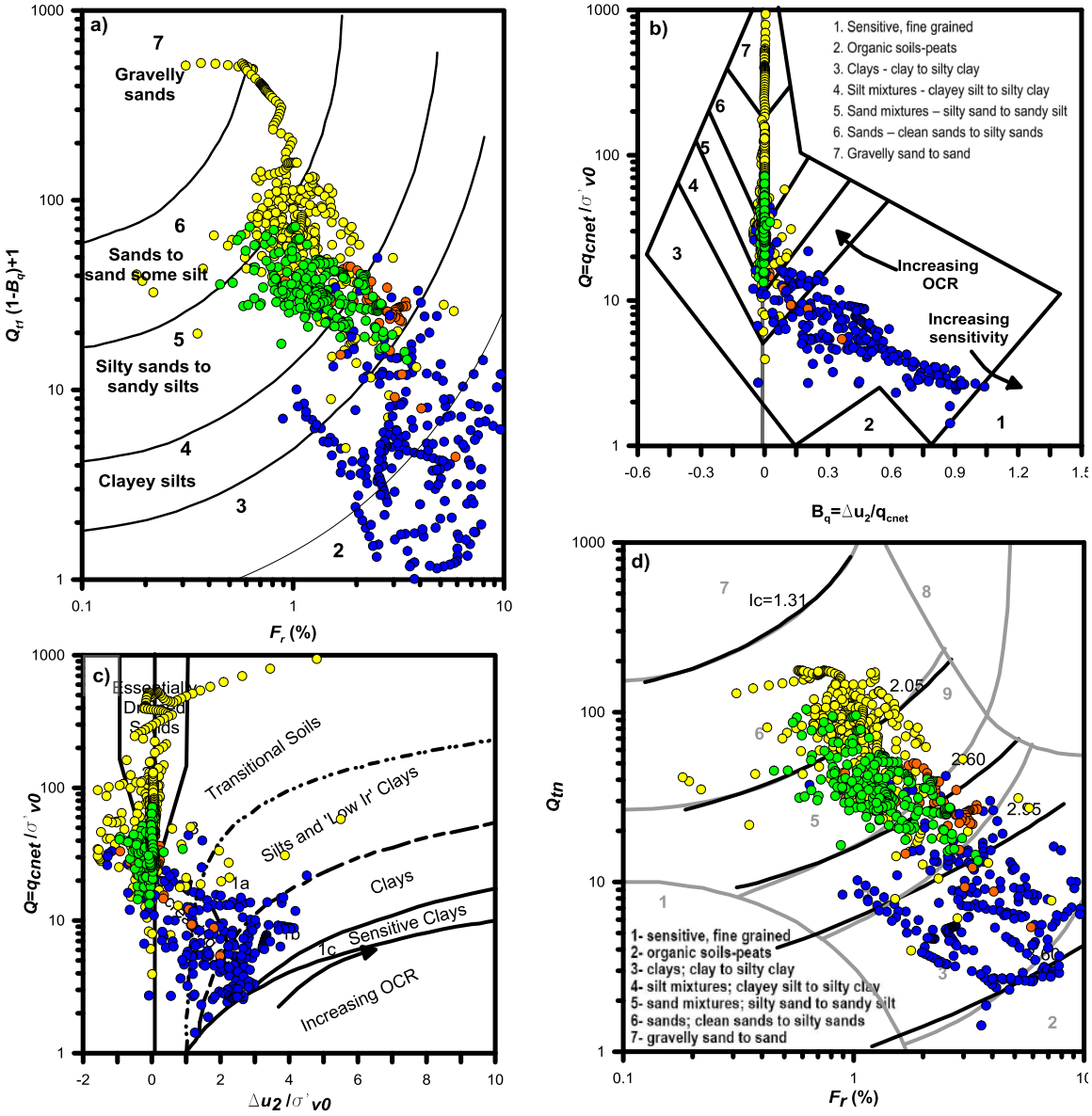

Figure 6.23: Soil classification according to the approaches proposed by: a) Jefferies and Been (2006); b) Robertson (1991); c) Schneider *et al.* (2008) and d) Robertson (2009) applied to test C3

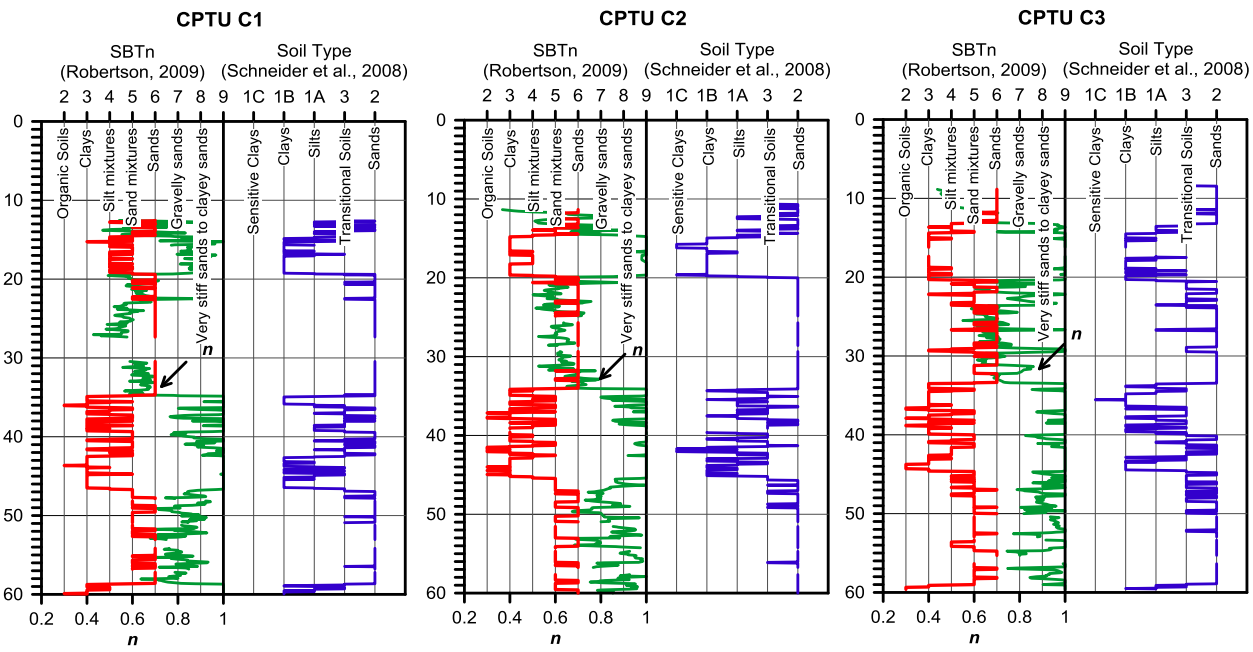

Figure 6.24: Schneider *et al*. (2008) and Robertson (2009) classification methods applied to Chioggia tests and stress exponent profiles

Soil classification charts give a good idea of the prevailing layers in this area. Five soil formations have been mainly identified (Figure 6.17). The first (formation A) and the third (formation C) soil type consist of sands and sand mixtures. Clays and silt mixtures (formation B) are mainly found in the second layer. The forth soil formation (D) consist of alternate layers of silt and sand mixtures and clays, with occasional presence of peat. Finally, sands and sandy mixtures are found in the deepest layer (E).

6.4.3 Lido: artificial island

Three piezocone tests were performed at the centre of the Lido inlet, where an artificial island was constructed in 2005. Nevertheless, no information about the exact location of the piezocone tests is available.

A view of the island is shown in Figure 6.25. This structure connects two rows of the mobile gates to be installed in the inlet which is double the width of the other two inlets.

Figure 6.25: View of the artificial island in the centre of the Lido inlet (image taken from the website salve.it)

CPTU profiles of the centre of the Lido inlet subsoil are reported in Figures 6.26, 6.28 and 6.30, showing the corrected cone resistance q_t, the pore water pressure u_2 and the sleeve friction f_s. Such profiles confirm once again the presence of a highly stratified subsoil.

Classification of the Lido inlet sediments from CPTU has been also performed using the already used four classification systems. Points mainly fall in zones 2 to 6 in Jefferies and Been and Robertson's charts. The more sophisticated chart proposed by Schneider *et al*. (2008) reveals points falling in zones 1b, 1a, 3 and 2.

Thin layers of clay plot with B_q values in excess of one, which means that points fall in zones 1c and 1 in the Schneider *et al*. (2008) and Robertson's (1991) chart, respectively.

As Robertson (2012) remarked, in shallow soft fine-grained soils, where the accuracy of the cone resistance q_t may be limited, the Schneider *et al*. (2008) chart becomes a useful check on the data. Figure 6.33 shows soils from 5.6 to 8.7 metres below sea-level (CPTU I29) plotted in the soil classification charts. Data between these depths plot in zones 5, 6 and 7 of the $Q(1\text{-}B_q)+1$ - F_r (%) chart, in zones 1, 3, 4, 5 and 6 of the Q - B_q chart, and in zones 5 and 6 of the Q_{tn} and F_r (%) chart, while points in the Q - $\Delta u_2/\sigma'_{v0}$ chart all fall in zone 1b (clays).

Despite the dense alternation of different grain-sized sediments, the soil profile below the test site can be described as follows:

- 1 – 3 m: clay and silty clay (Unit A);
- 4 – 7 m: sands and sand mixtures (Unit B);
- 20 - 25 m: alternate layers of silty sand, sandy silt, clayey silt, clays and organic soils (Unit C). Interbedded within this unit there is a sandy layer 4 - 5 m thick (Unit C'), though not everywhere;
- 6 – 8 m: silty sand to sandy silt (Unit D).

- CPTU I27

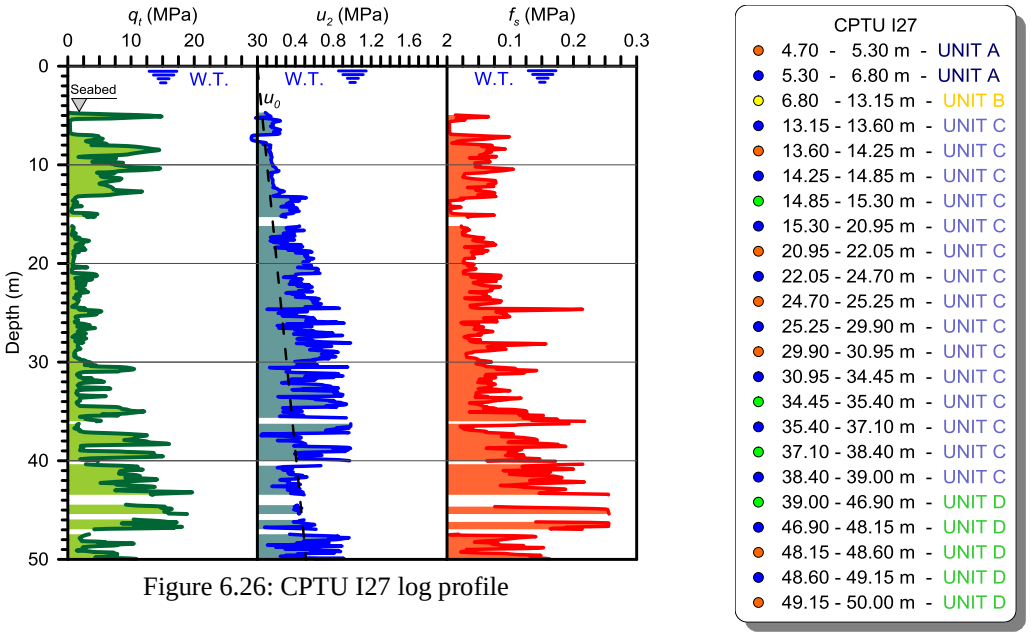

Figure 6.26: CPTU I27 log profile

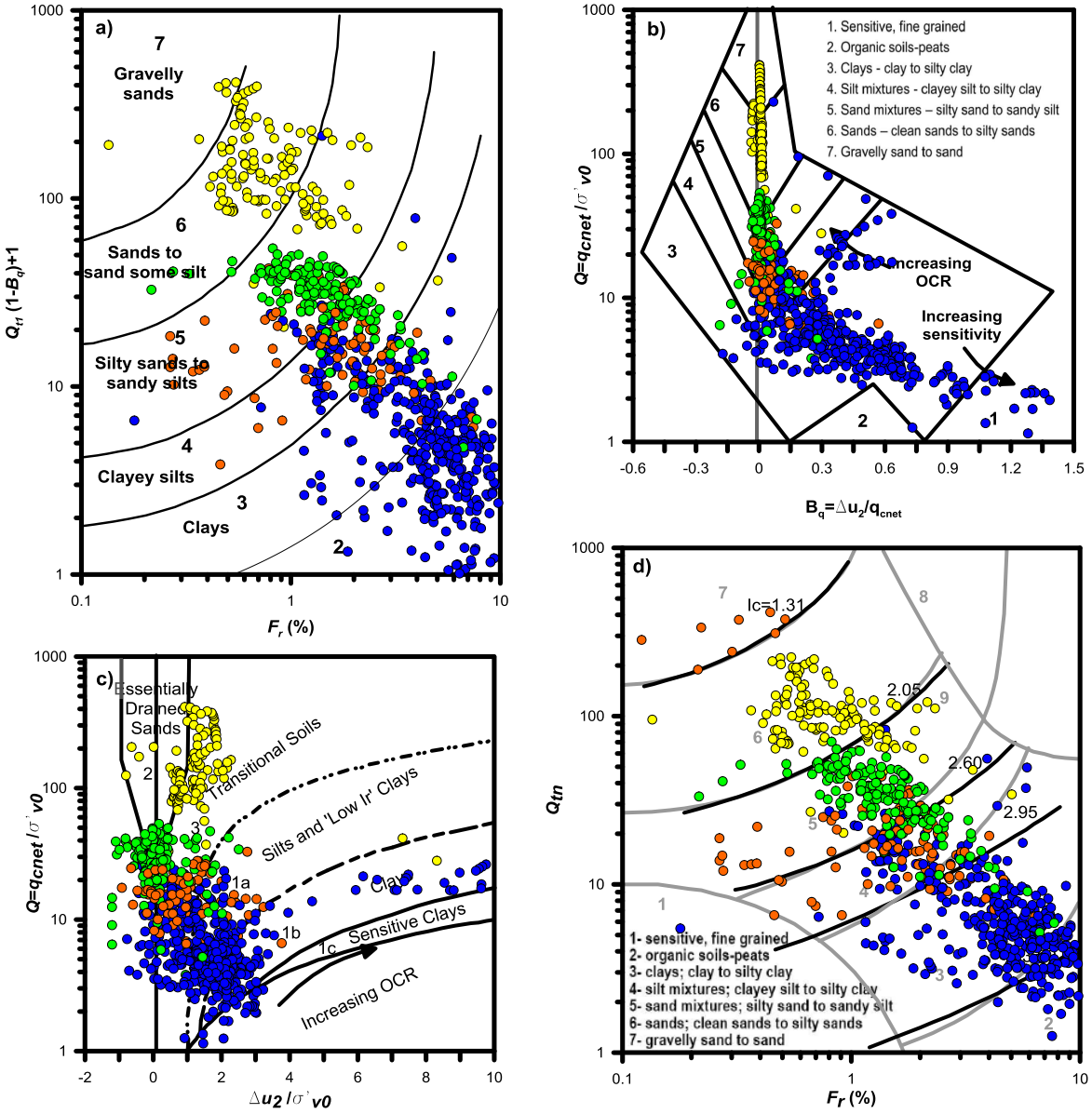

Figure 6.27: Soil classification according to the approaches proposed by: a) Jefferies and Been (2006); b) Robertson (1991); c) Schneider *et al.* (2008) and d) Robertson (2009) applied to test I27

- CPTU I29

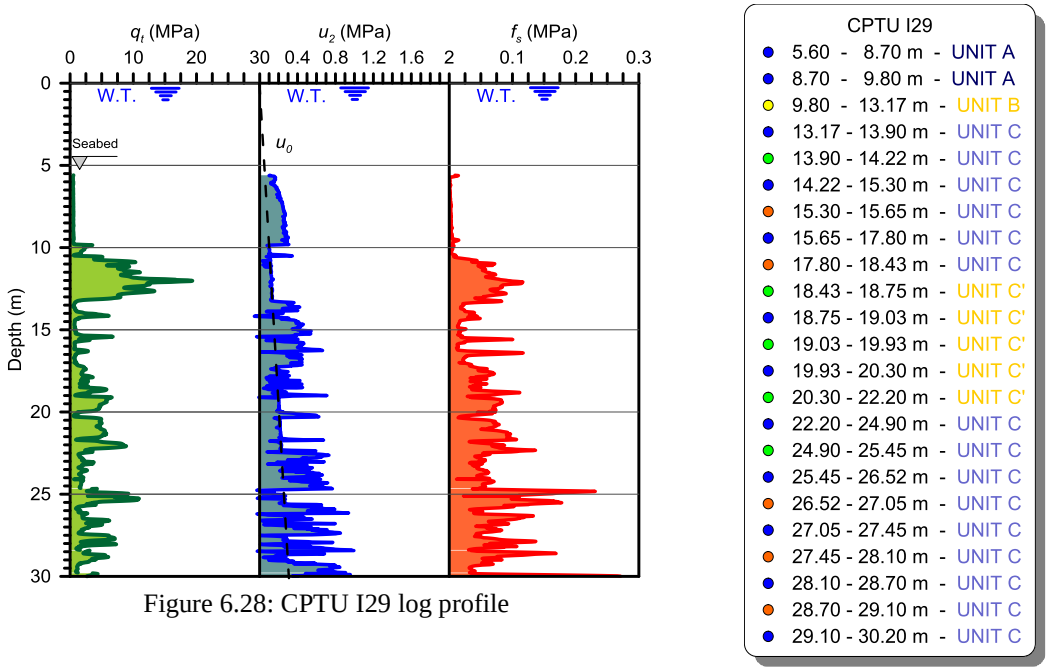

Figure 6.28: CPTU I29 log profile

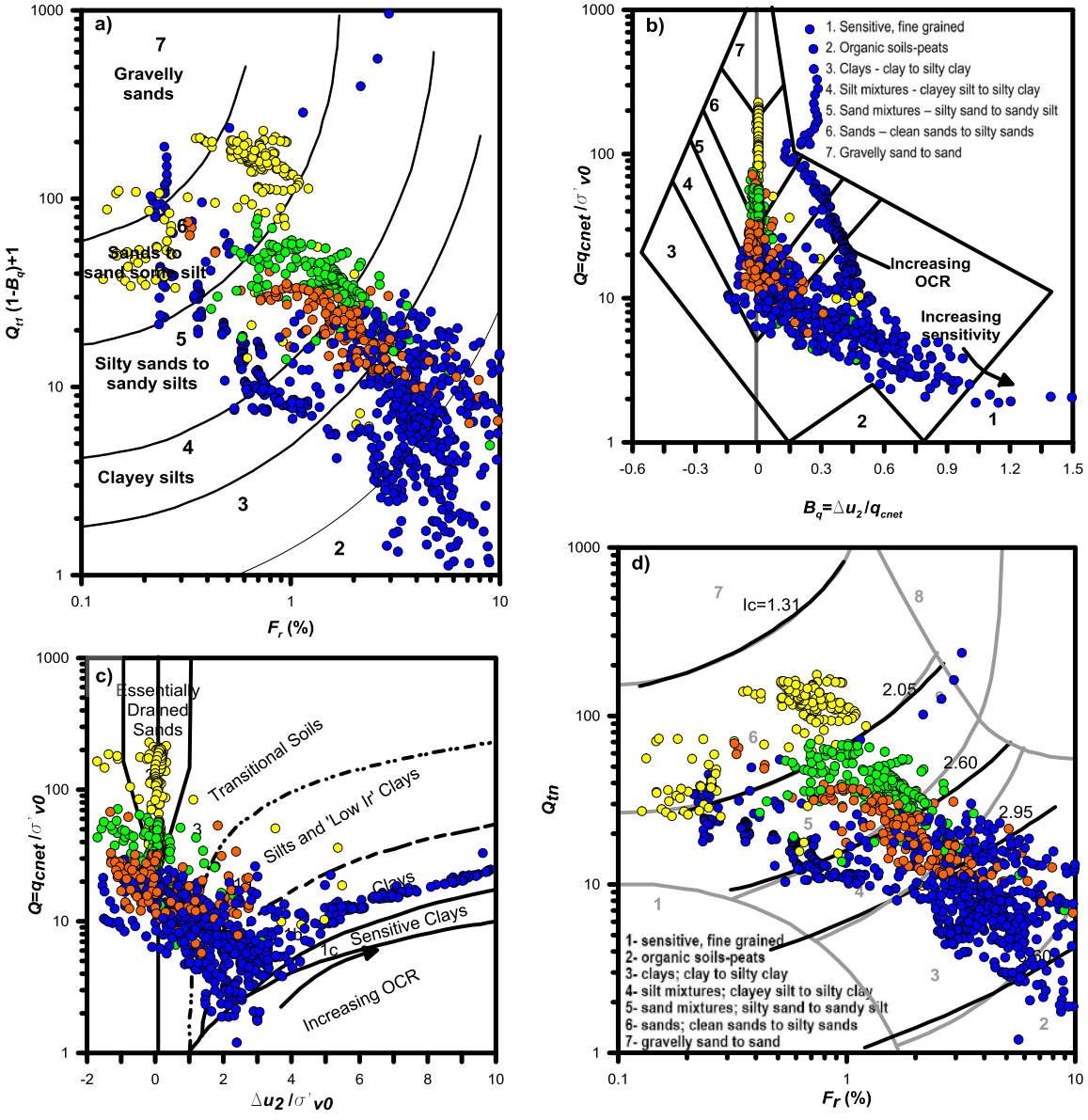

Figure 6.29: Soil classification according to the approaches proposed by: a) Jefferies and Been (2006); b) Robertson (1991); c) Schneider *et al.* (2008) and d) Robertson (2009) applied to test I29

- CPTU I30

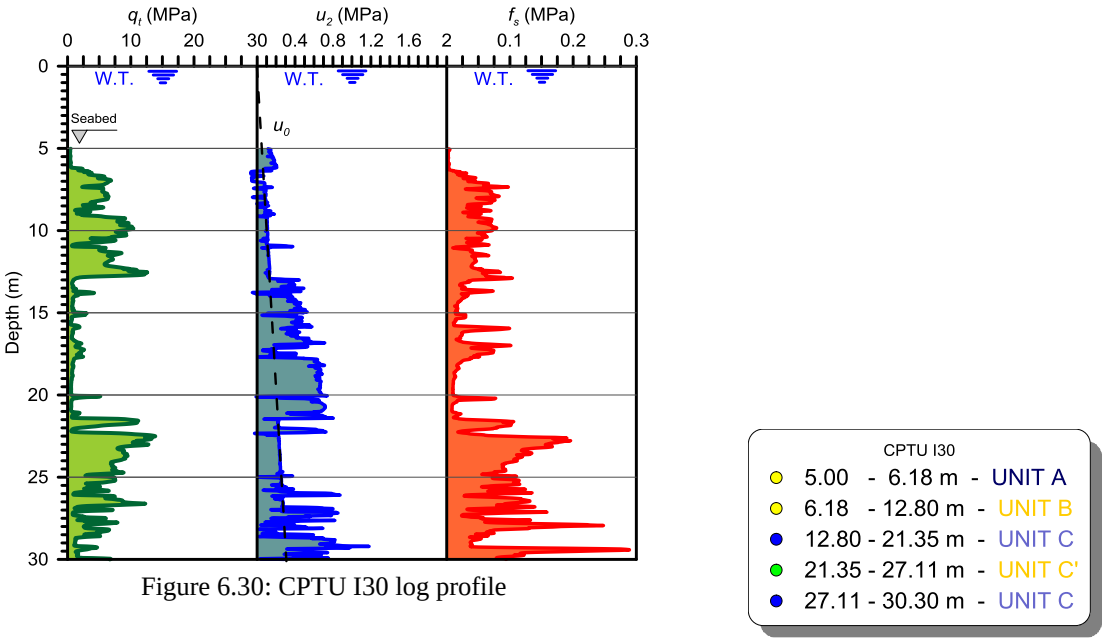

Figure 6.30: CPTU I30 log profile

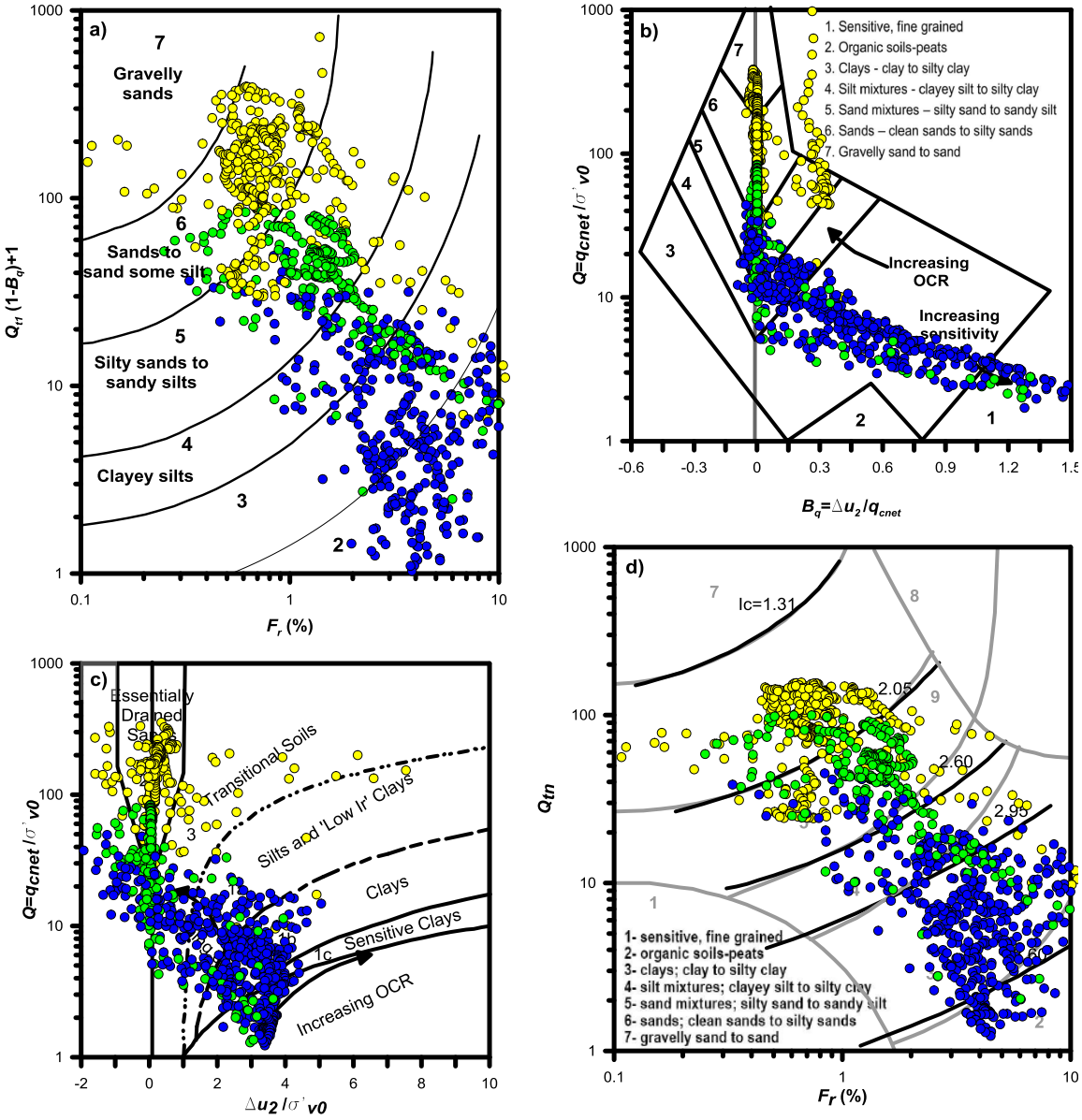

Figure 6.31: Soil classification according to the approaches proposed by: a) Jefferies and Been (2006); b) Robertson (1991); c) Schneider *et al.* (2008) and d) Robertson (2009) applied to test I30

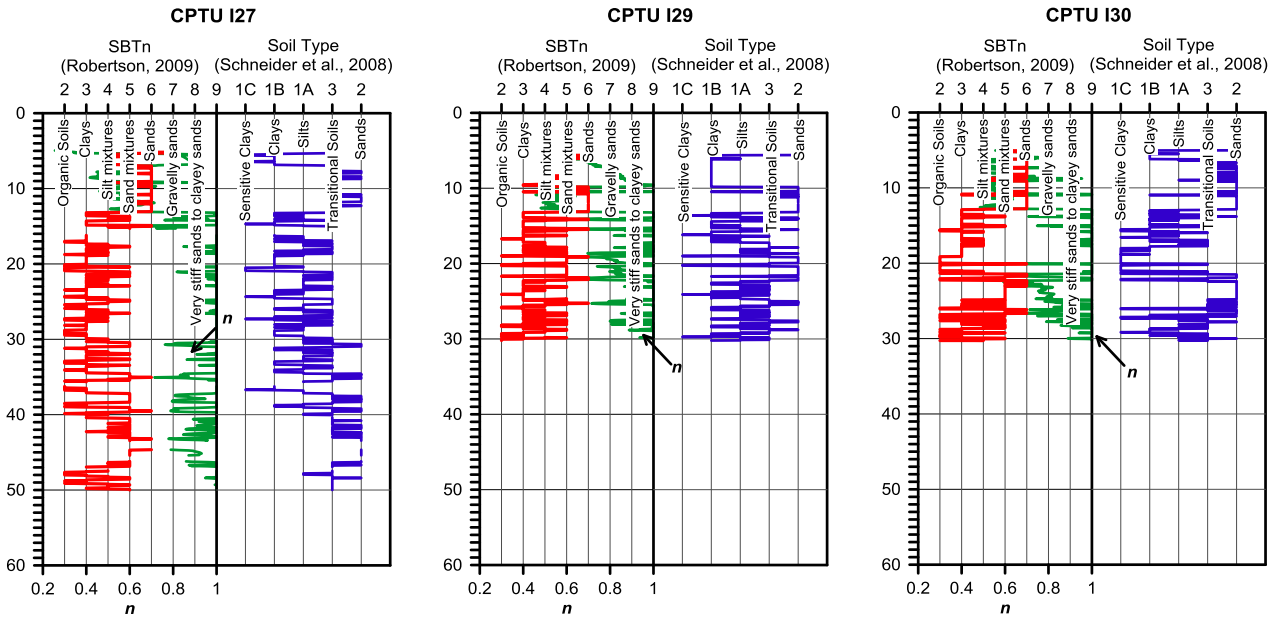

Figure 6.32: Schneider *et al*. (2008) and Robertson (2009) classification methods applied to Lido tests and stress exponent profiles

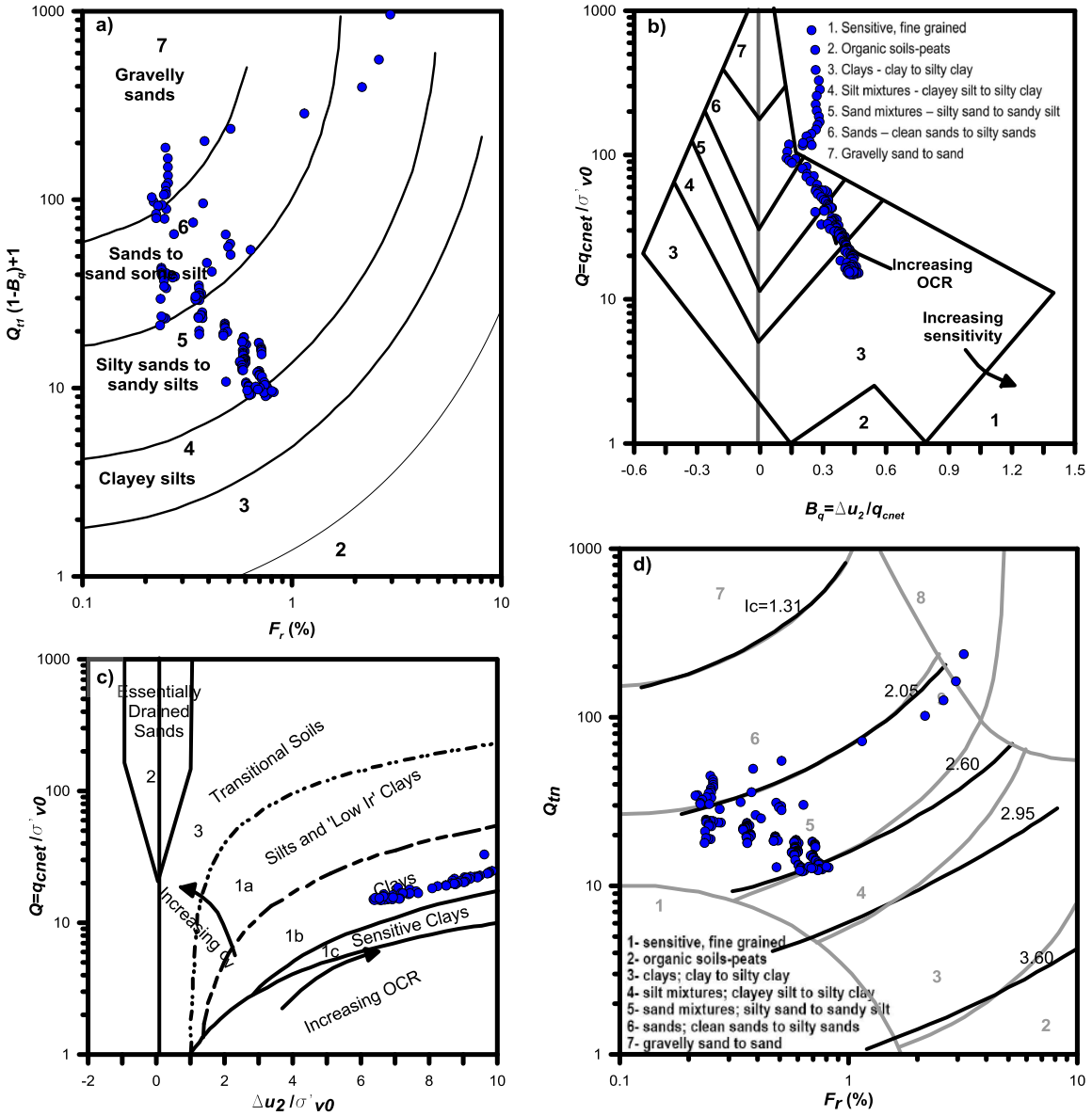

Figure 6.33: Location of shallow fine-grained soils (5.6 to 8.7 m) from CPTU I29 in four soil classification charts

6.5 Soil compressibility characteristics from CPTU

6.5.1 Constrained modulus

The two different correlations already presented in Chapter 5 for the 1D modulus have been applied to the offshore piezocone tests carried out at Malamocco, Chioggia and Lido.

$$M = 2.3(q_t - u_2) \tag{5.2}$$

$$M = 1.35 I_c (q_t - \sigma_{v0}) \tag{5.3}$$

where I_c is the soil behaviour type index (Robertson and Wride, 1998).

Predictions using Equations (5.2) and (5.3) are reported in Figures 6.34, 6.35 and 6.36. As can be observed, both result in similar values of constrained modulus, although Equation (5.2) seems to predict lower values. Typical values of M for sands generally fall in the interval 20-60 MPa, with the highest values found in the deepest layers. The constrained modulus turns out to range between 5 and 20 MPa in silt and sand mixtures and values lower than 5 MPa are generally observed in clays.

However, as Tonni and Gottardi (2011) remarked, the approaches described by Equations (5.2) and (5.3) fully disregard the complex mechanics of piezocone penetration in intermediate soils. They suggest that a more accurate interpretation of piezocone data should take into account the partial drainage phenomena during cone penetration.

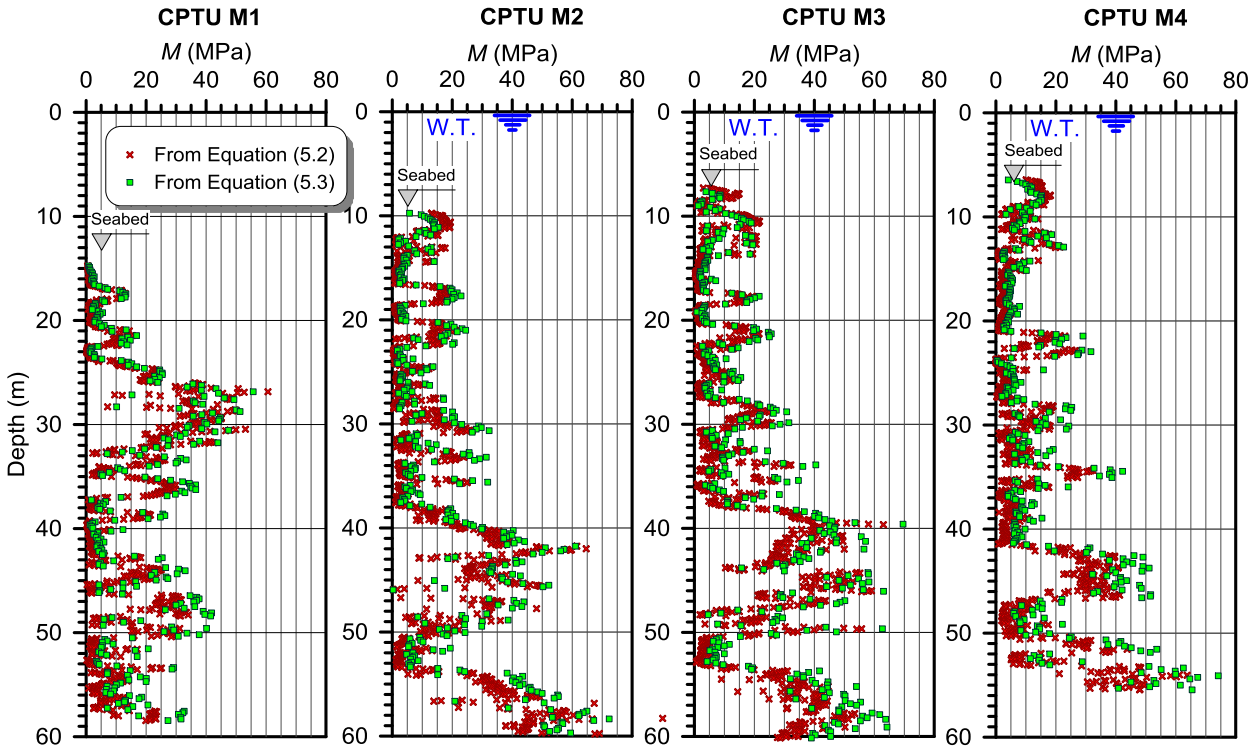

Figure 6.34: Constrained modulus predicted from Malamocco piezocone data

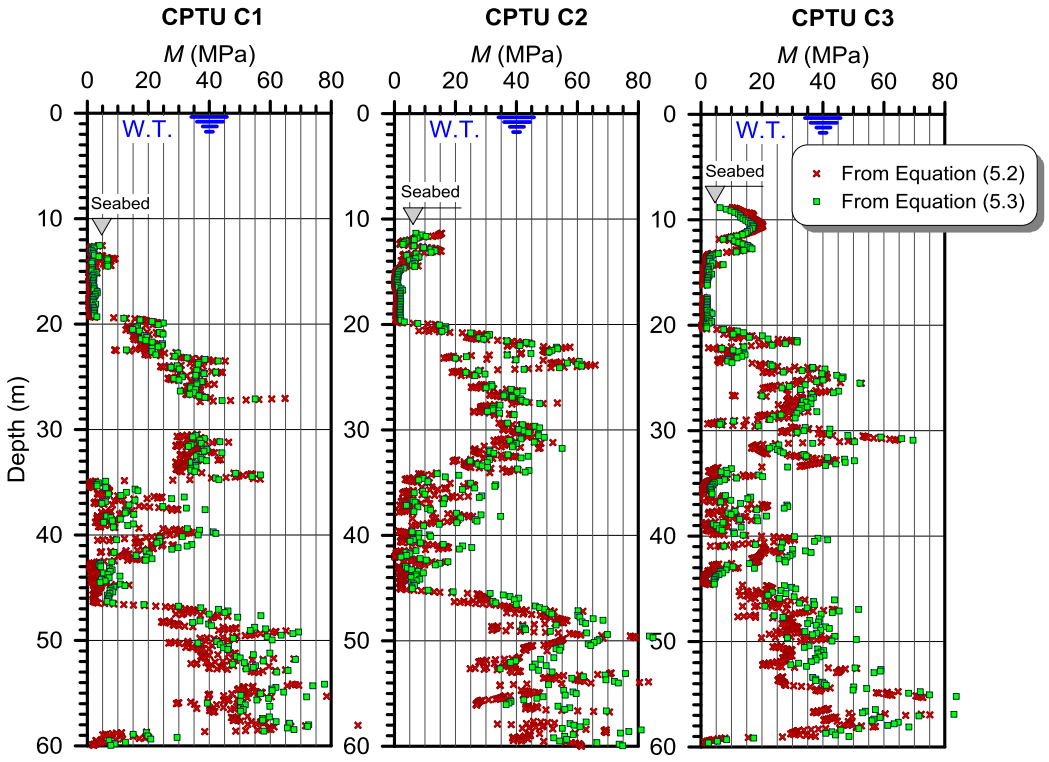

Figure 6.35: Constrained modulus predicted from Chioggia piezocone data

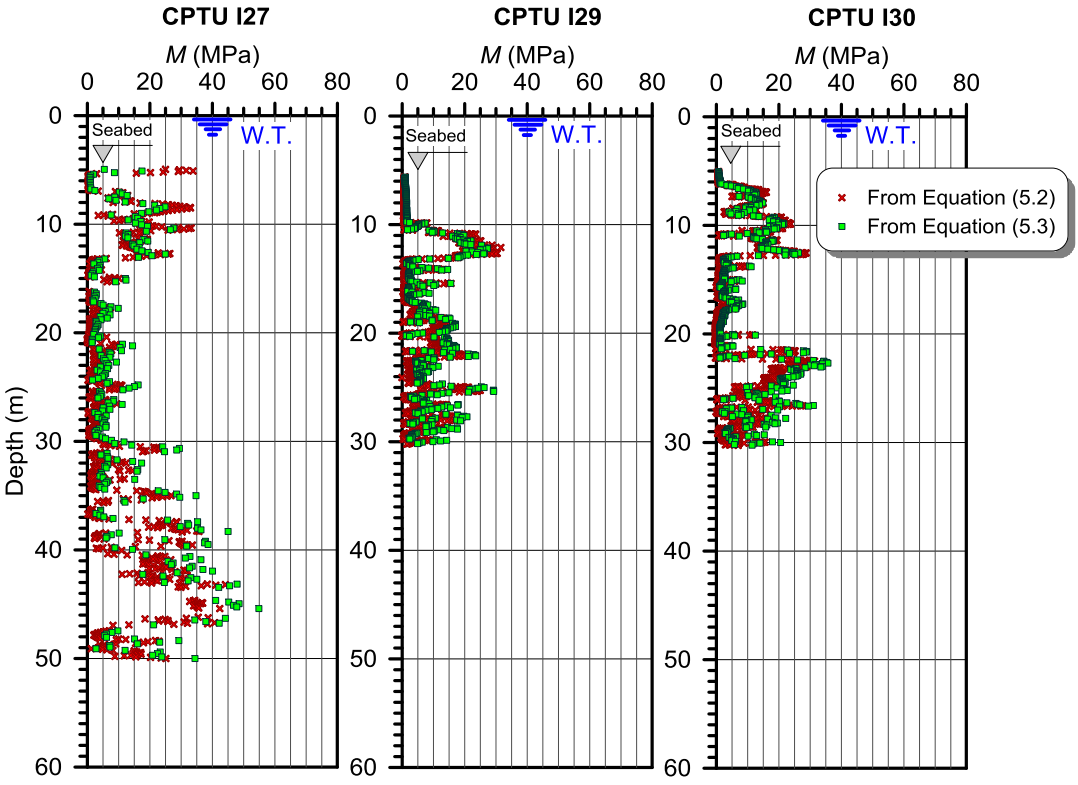

Figure 6.36: Constrained modulus predicted from Lido piezocone data

6.5.2 Coefficient of secondary compression

Empirical correlations between $C_{\alpha\varepsilon}$, and penetration test measurements, expressed in terms of the cone resistance q_t, have been obtained from calibration on the TTS field data (Bersan *et al.*, 2012; Tonni and Simonini, 2013). The approach is based on the experimental evidence that,

in Venetian soils, both cone resistance and secondary compression are governed by frictional response, therefore empirical correlations between $C_{\alpha\varepsilon}$ and q_t were taken as an alternative on the classical laboratory tests for the estimate of creep features.

Log regression analyses performed on the available data from TTS provided the following more significant relationships, both expressed in terms of the dimensionless normalized cone resistance Q_{tn}:

$$C_{\alpha\varepsilon} = 0.03 \cdot (Q_{tn})^{-0.89} \tag{5.5}$$

$$C_{\alpha\varepsilon} = 0.077 \cdot (Q_{tn})^{-1.14} \cdot \left(1 + \frac{\Delta u}{\sigma'_{v0}}\right)^{-0.74} \tag{5.6}$$

In this approach, an iterative nonlinear stress normalization procedure is applied to the corrected cone resistance q_t in order to determine Q_{tn}. It is worth mentioning that the regression including the excess pore pressure ratio $\Delta u_2/\sigma'_{v0}$ allows accounting in some way for the different pore pressure response in relation to the drainage conditions around the advancing cone.

The available piezocone data located along the Malamocco and Chioggia breakwaters and in the artificial island of the Lido inlet have been used to determine reliable values of $C_{\alpha\varepsilon}$. Figures 6.37, 6.38 and 6.39 provide the profile of the computed $C_{\alpha\varepsilon}$ obtained from Equations (5.5) and (5.6) for piezocone tests performed at three inlets.

As evident from figures, both formulations result in similar values of $C_{\alpha\varepsilon}$, although Equation (5.5) seems to estimate higher values of $C_{\alpha\varepsilon}$. However, it has been observed that Equation (5.6) predicts higher values in some isolated points, when $\Delta u_2/\sigma'_{v0}$ reach values close to -1.

In this way, the predicted mean $C_{\alpha\varepsilon}$ values for the soil classes of the Venice Lagoon include approximately the following ranges:

- sands (SBT 6) : 0.0002÷0.0009,
- sand mixtures (SBT 5) : 0.0007÷0.002,
- silt mixtures (SBT 4) : 0.001÷0.004,
- clays (SBT 3) : 0.004÷0.007.

It is worth observing that the computed values are in good agreement with the reference values of $C_{\alpha\varepsilon}$ derived from interpretation of long-term settlements observed at the Treporti Test Site.

Organic soils and peats (SBT 2) generally present $C_{\alpha\varepsilon}$ values that vary between 0.008 ÷ 0.015. Nevertheless, it has to be remarked that Equations (5.5) and (5.6) have not been calibrated on such soil class, therefore in this case the computed values of $C_{\alpha\varepsilon}$ are subject to a great deal of uncertainty.

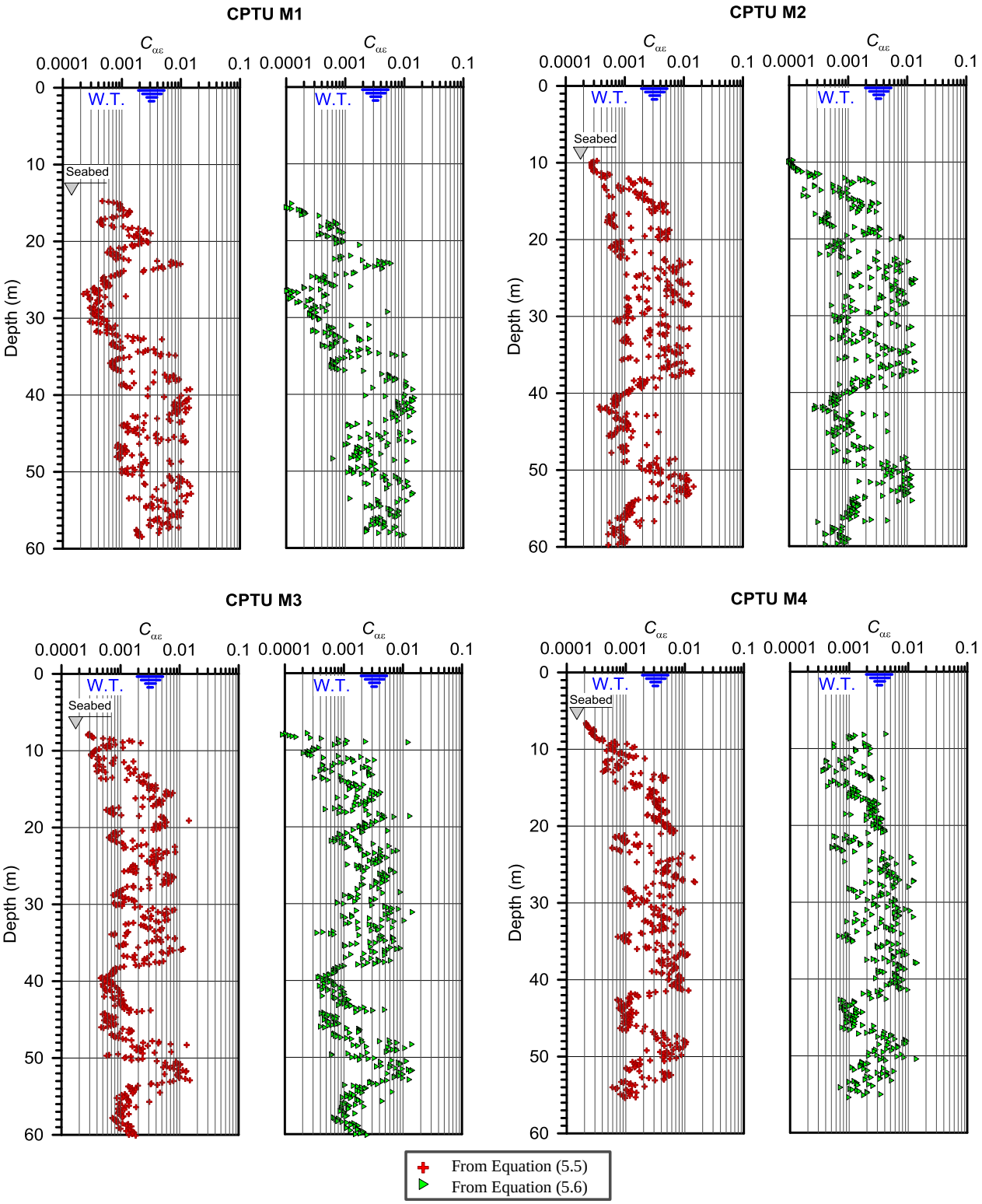

Figure 6.37: Profiles of the computed $C_{\alpha\varepsilon}$ from Malamocco piezocone data

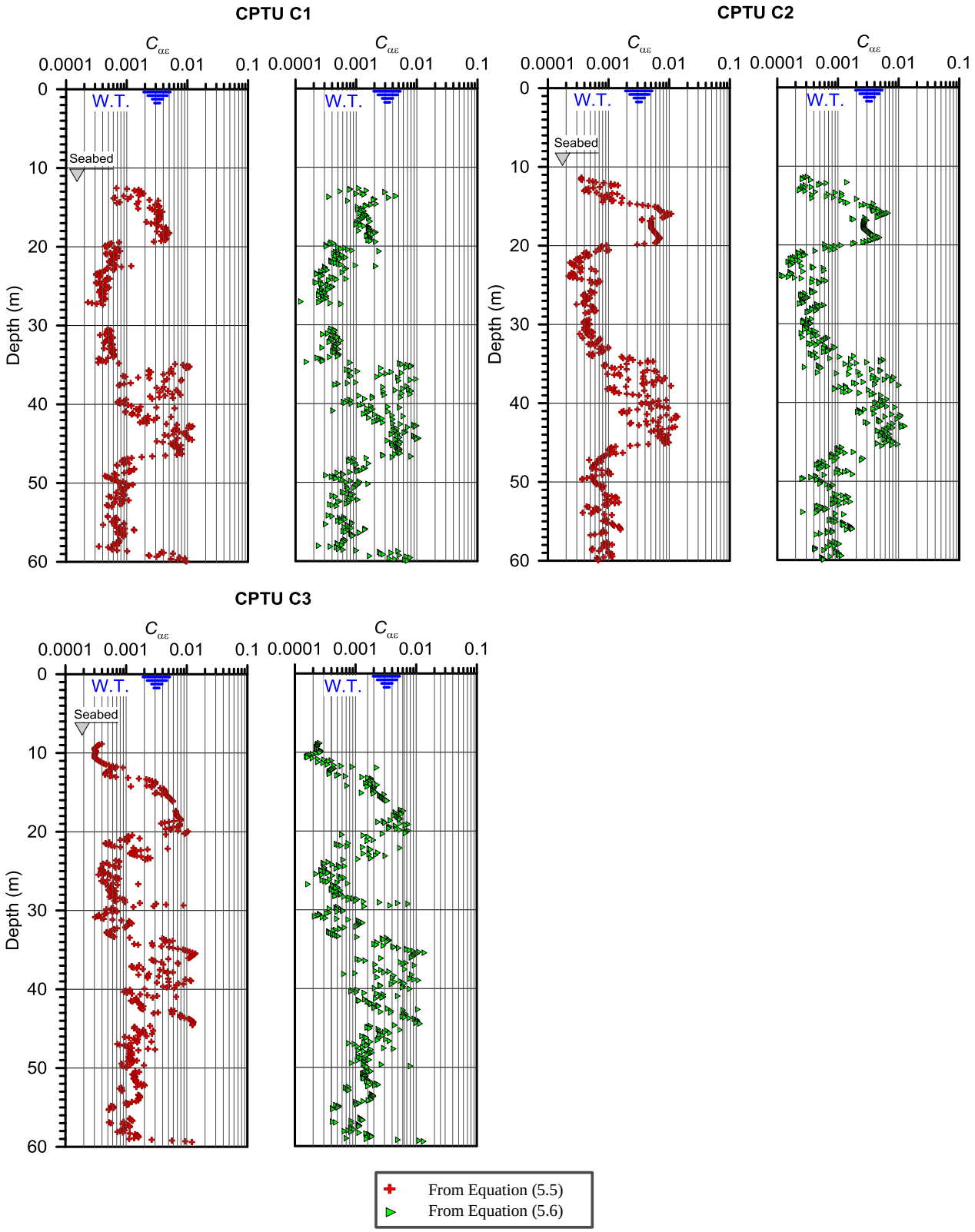

Figure 6.38: Profiles of the computed $C_{\alpha\varepsilon}$ from Chioggia piezocone data

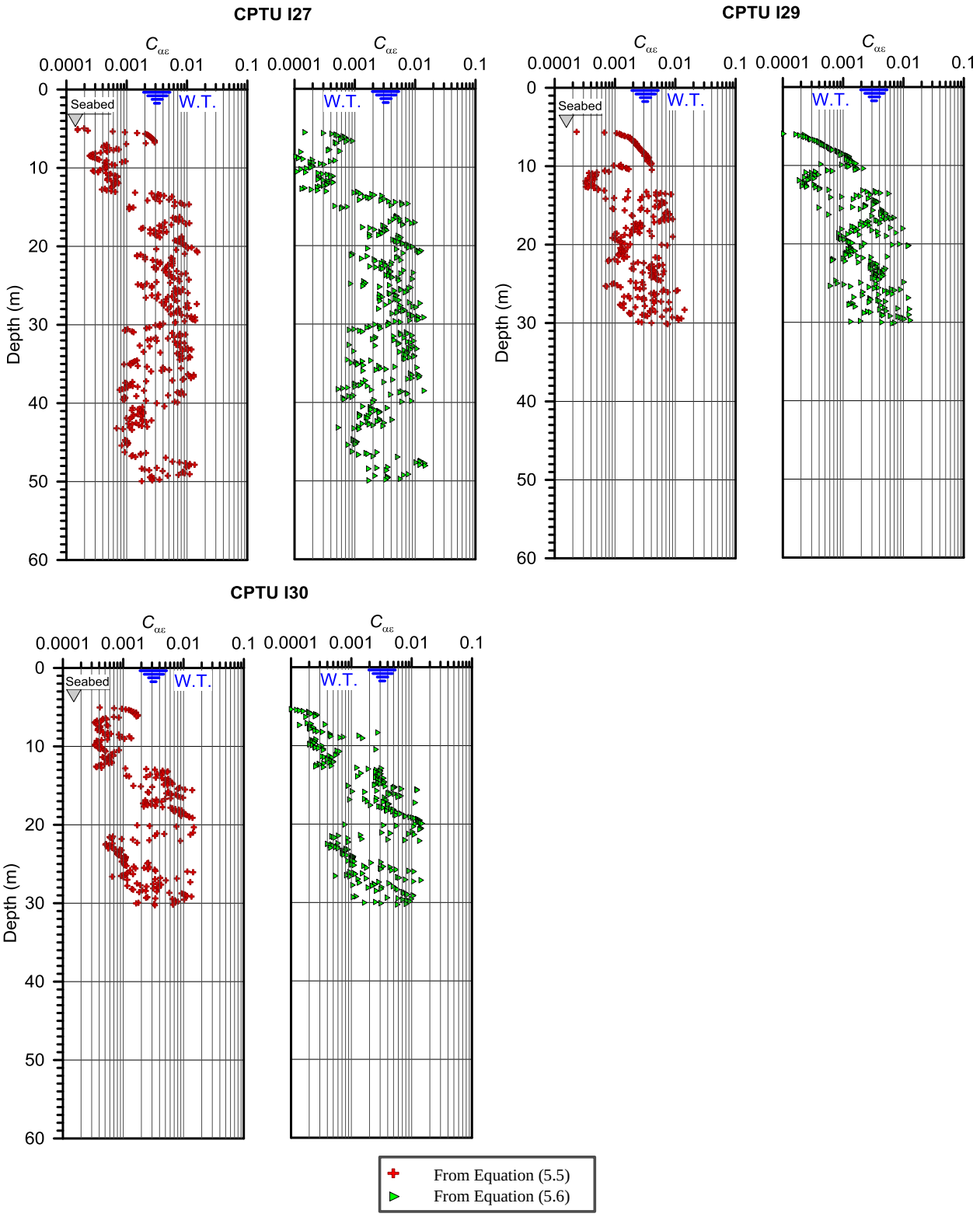

Figure 6.39: Profiles of the computed $C_{\alpha\varepsilon}$ from Lido piezocone data

6.6 Predicting long-term settlements of coastal defences

Using the secondary compression coefficient derived, the secondary compression settlement S_{sec} occurred beneath the two breakwaters and the artificial island in the period March 2008-January 2009 has been carried out, using the following equation:

$$S_{\sec} = -\sum_{1}^{n} (C_{\alpha\varepsilon})_i \cdot H_i \cdot \log_{10}\left(\frac{t}{t_{ref}}\right) \tag{6.1}$$

where n is the number of soil layers interested by the load, H_i and $C_{\alpha\varepsilon}$ are the thickness and secondary compression index of each layer, respectively, and the reference time for calculating the secondary settlement is assumed here as t_{ref} = (March 2008-*Construction Start Date*). The *Construction Start Date* has been selected for each structure from the historical photo archive found on the website *salve.it*.

Based on previous experiences on Venetian sediment behaviour, the analysis has been carried out to a depth of approximately 45-50 m from sea bottom.

Plots of the local and the total vertical displacements predicted are shown in Figures 6.40, 6.41 and 6.42. Curves have been obtained by plotting the displacements calculated using Equation (6.1) just at the end of the period of data acquisition (January 2009). Furthermore, *Prediction 1* refers to the local (or total) displacements calculated using the secondary compression index computed from Equation (5.5), and *Prediction 2* to displacements calculated using the one obtained from Equation (5.6).

The largest differences between these trends are observed in Chioggia profiles, being always the settlements from *Prediction 1* higher. Differences between the local displacements illustrated by the two trends in the clay layer (Unit B from Figure 6.17) reach values up to 1.2 mm in CPTU C2 profile.

Finally, Figures 6.43, 6.44 and 6.45 show the calculated trends of settlements versus time for Malamocco breakwater, Chioggia breakwater and Lido artificial island together with vertical displacements measured for the radar reflectors located between the available piezocone tests (see Figure 6.2). The figures clearly show that the calculated trends using Equations (5.5) and (5.6) fit fairly well the measurements detected by TerraSAR-X scenes over the period March 2008-January 2009.

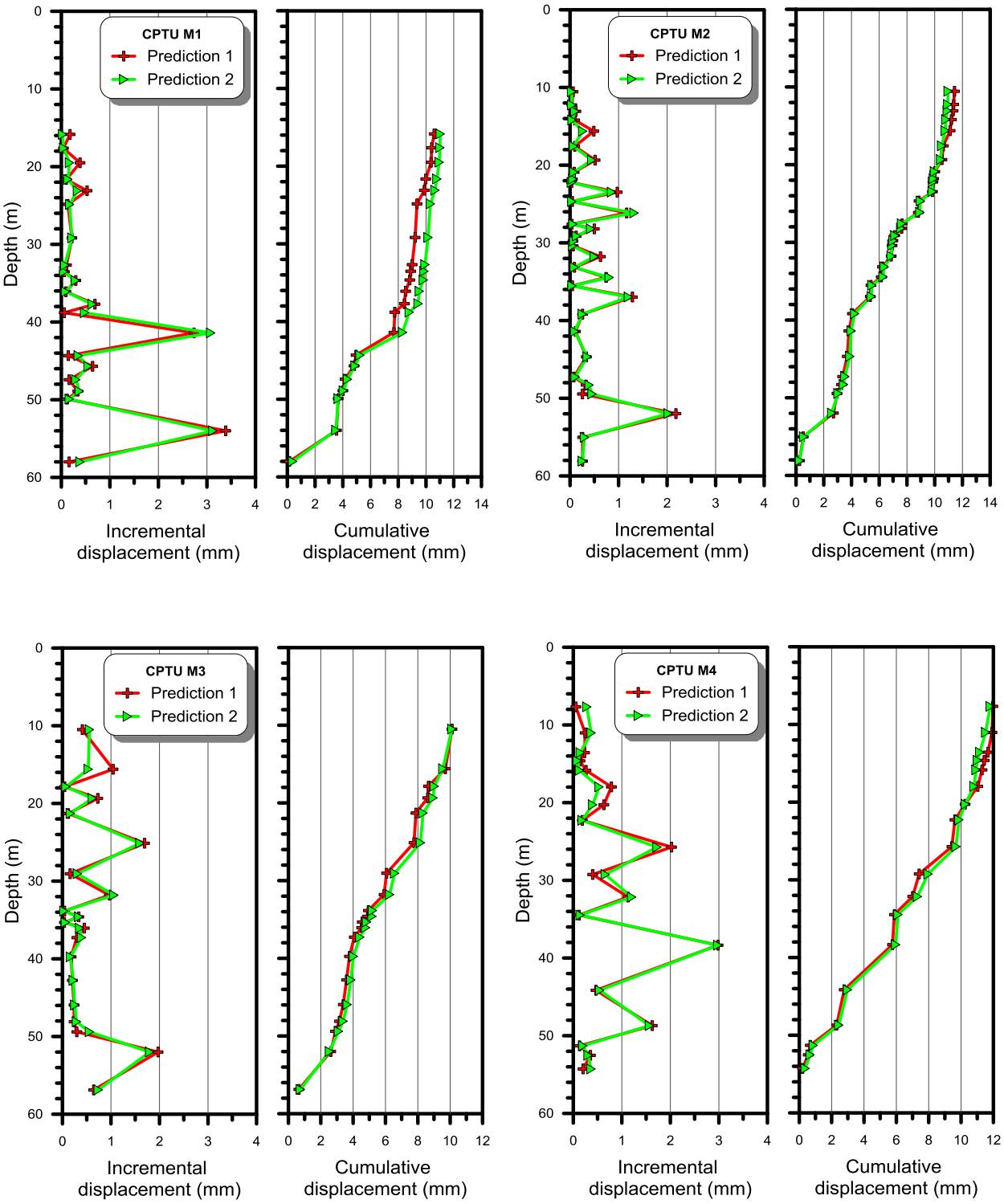

Figure 6.40: Predicted local and integral vertical displacement at the end of the period March 2008-January 2009 from Malamocco piezocone tests

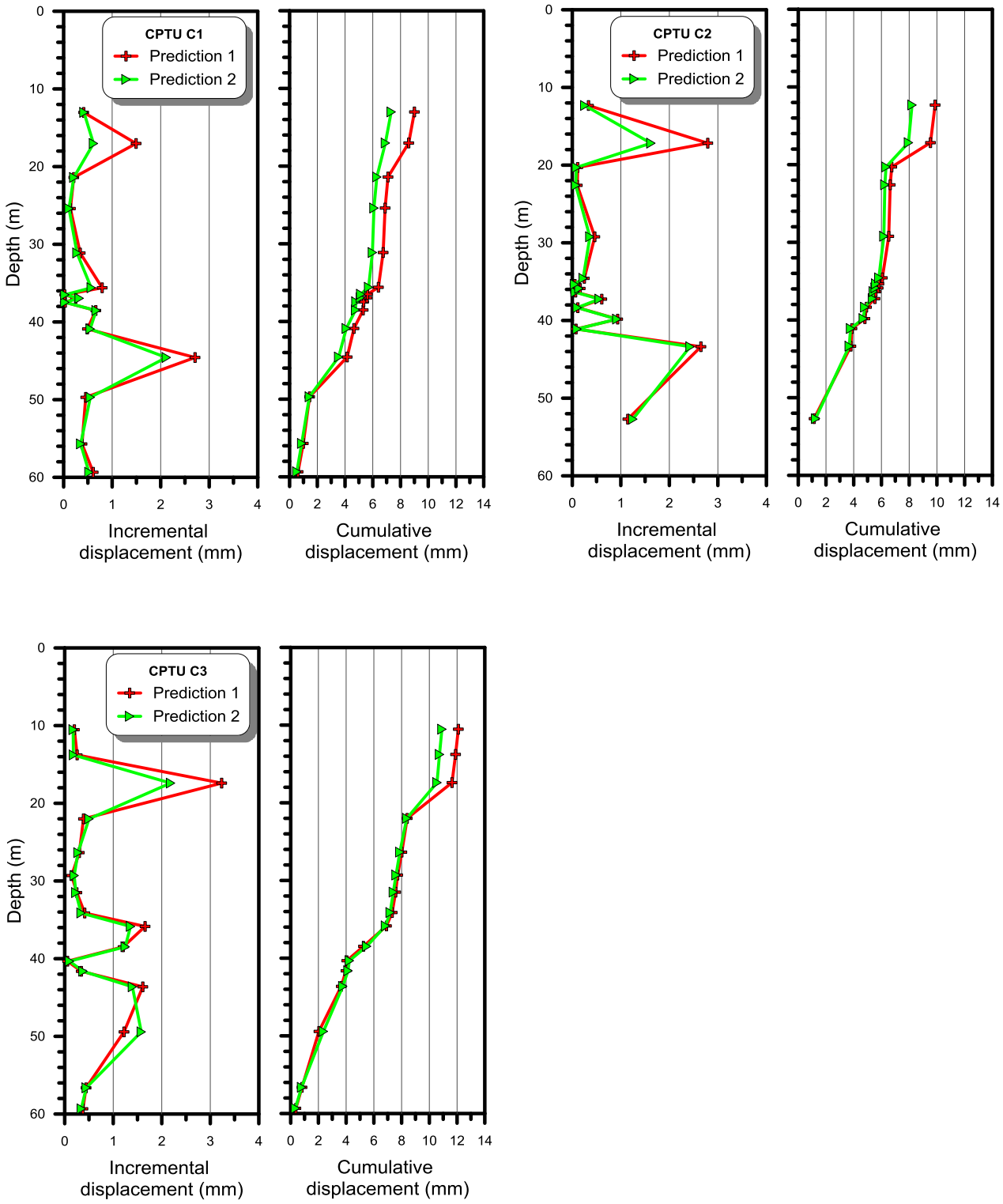

Figure 6.41: Predicted local and integral vertical displacement at the end of the period March 2008-January 2009 from Chioggia piezocone tests

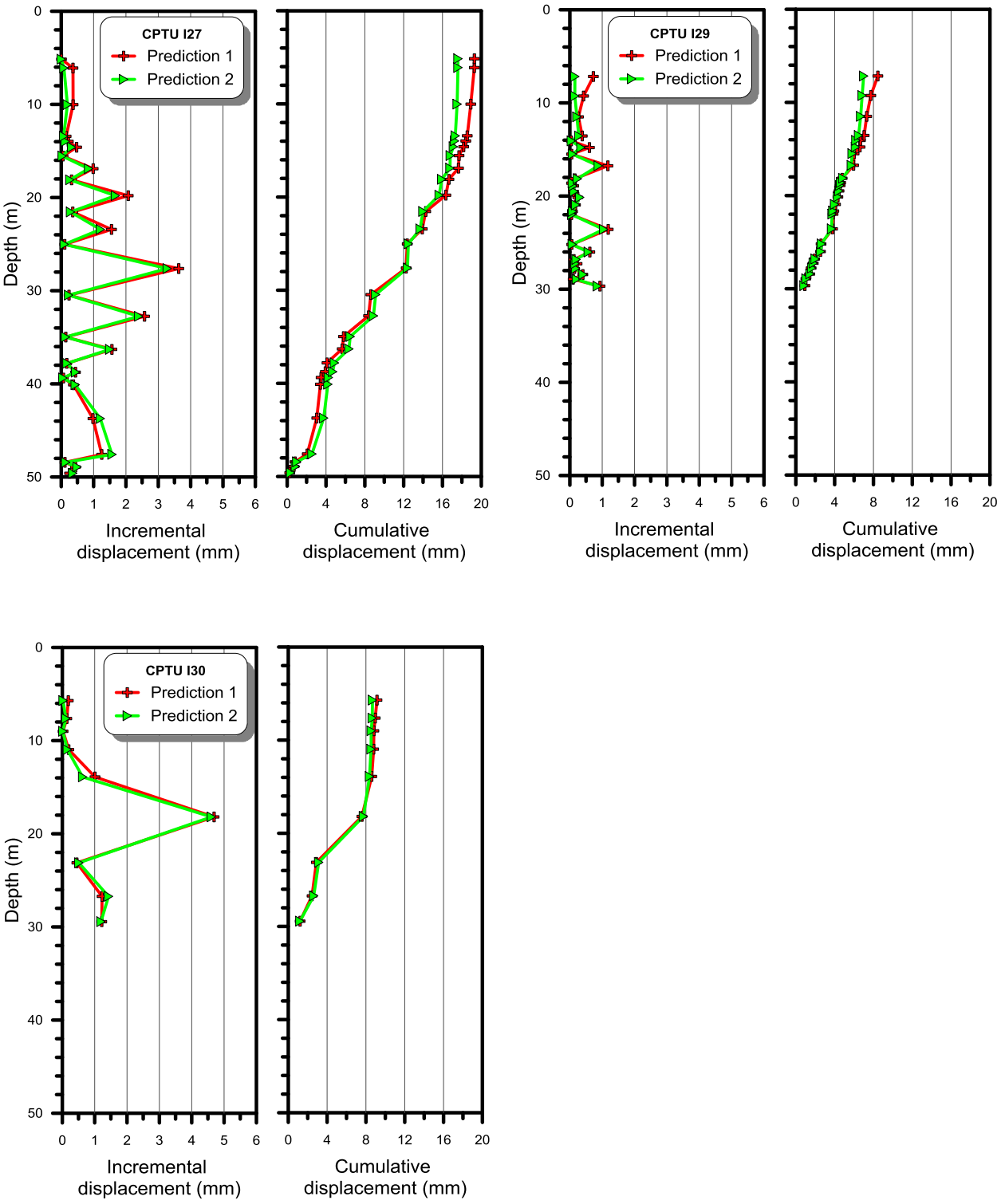

Figure 6.42: Predicted local and integral vertical displacement at the end of the period March 2008-January 2009 from Lido piezocone tests

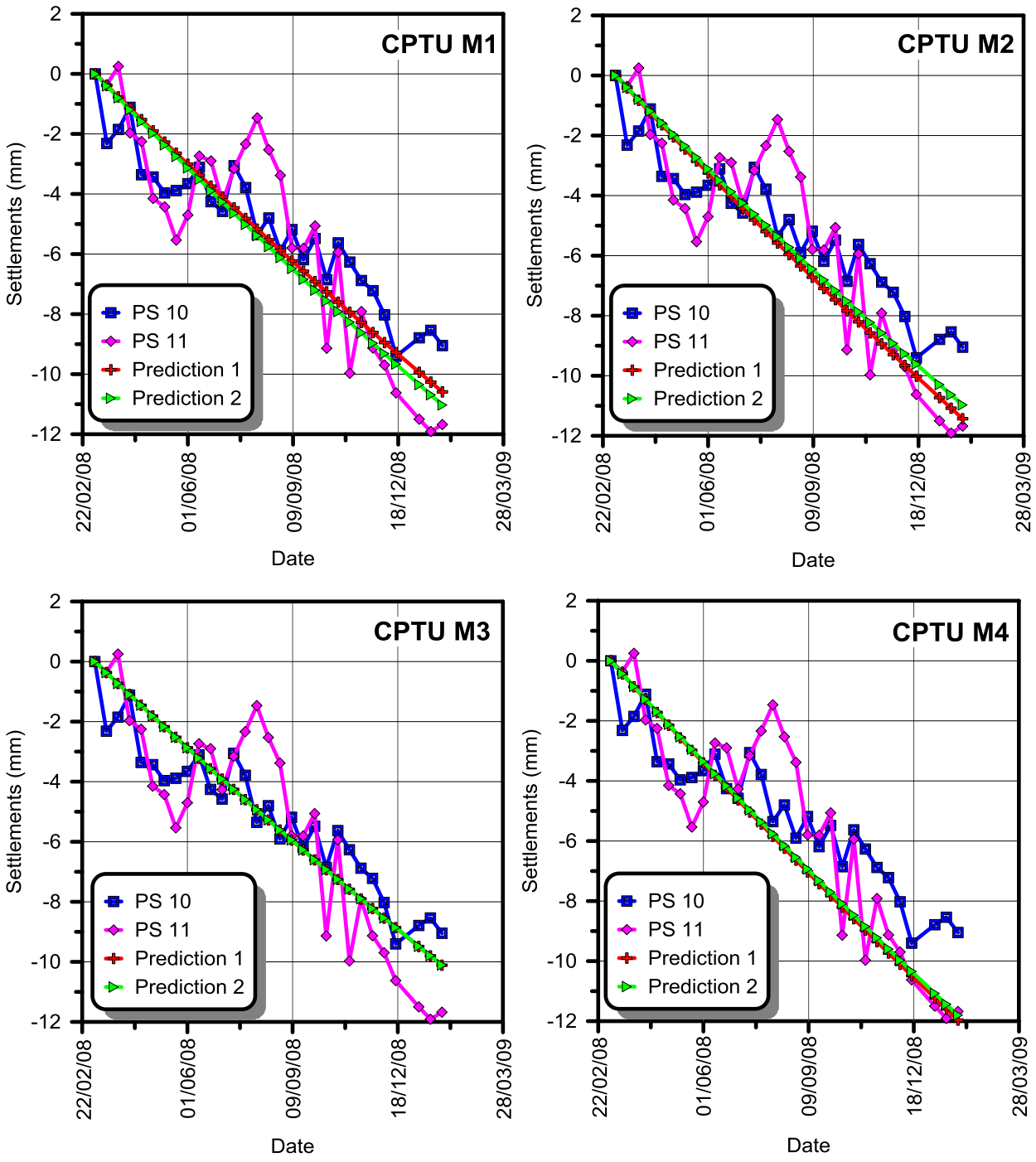

Figure 6.43: Settlement predictions using CPTU data from Malamocco

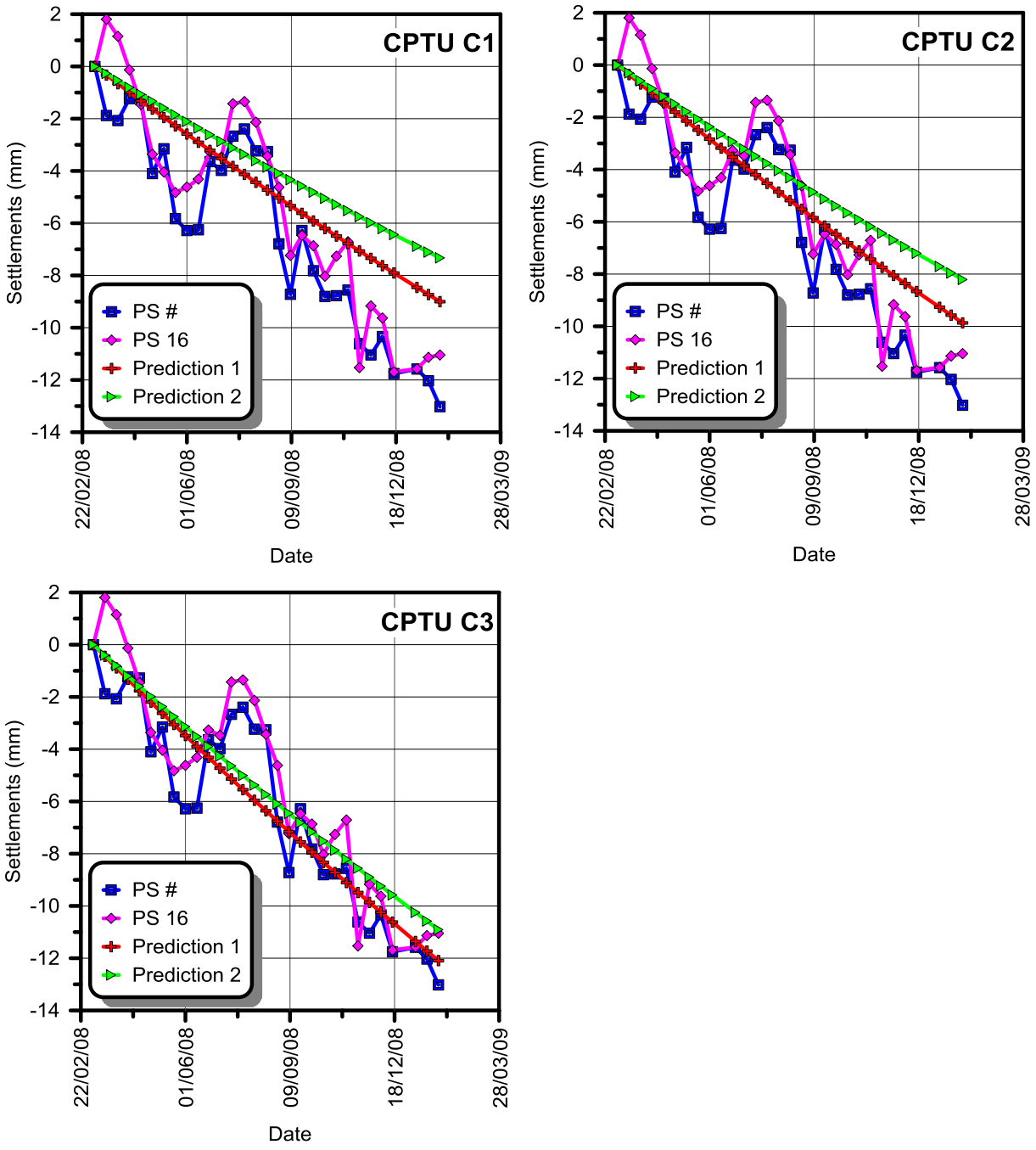

Figure 6.44: Settlement predictions using CPTU data from Chioggia

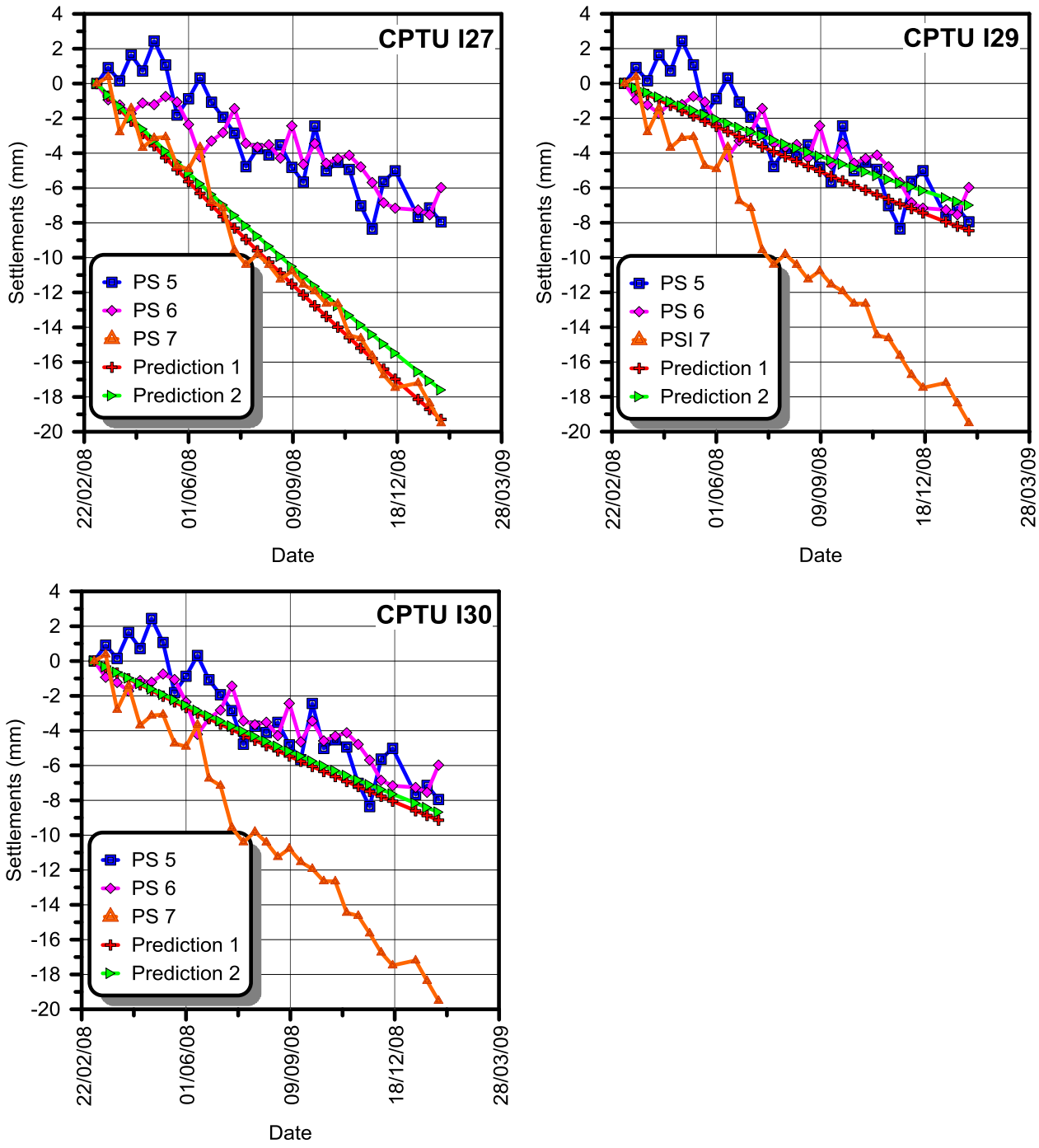

Figure 6.45: Settlement predictions using CPTU data from Lido

CHAPTER 7: NUMERICAL MODELLING OF COASTAL DEFENCES OF THE VENETIAN LAGOON

7.1 Introduction

In this Chapter, the attention has been focused on the numerical modelling of the long-term settlements of the two breakwaters built in the period 2003-2004 and 2004 at the Malamocco and Chioggia inlets respectively, using finite element code PLAXIS 2D in conjunction with a constitutive formulation specifically developed for simulating the creep behaviour of soft soils (Vermeer and Neher ,1999). However, one has to be aware that these particular soils are so heterogeneous that any material model may have intrinsic limitations in describing such soils.

Although an accurate description of the breakwater settlements would certainly require a 3D approach, especially in relation to the horizontal spatial variability of the Venetian subsoil, it was decided to first develop a 2D model in order to better understand the basic mechanisms of the soil response and verify the applicability of the numerical method to the analysis of such structures. Latter on Section 7.4, PLAXIS 3D will be used for the modelling of the long-term response of the Chioggia breakwater, whose length is smaller than the one constructed at the Malamocco Inlet.

In Chapter 6, the stratigraphic condition of the lagoon basin in this area as well as the relevant geotechnical parameters of the different soil units were derived from a number of piezocone tests carried out prior to the breakwaters construction.

The calibration of the *Soft Soil Creep* (SSC) *Model* constitutive parameters adopted in the numerical analysis, with special reference to the secondary compression coefficient, is performed by mainly using a number of piezocone-based site-specific correlations for the geotechnical characterization of Venetian soils, originally developed in the context of a comprehensive, long-lasting research project carried out at the Treporti Test Site (Tonni and Gottardi 2011). Furthermore, the SSC model was applied without distinguishing between granular and cohesive layers.

A preliminary application of the computed secondary compression coefficient $C_{\alpha\varepsilon}$ to the prediction of the long-term settlements of this coastal defence structures is shown in Chapter 6, using a simplified one-dimensional approach, and reasonable fits with the PSI-derived vertical displacements have been found (Tonni *et al.*, 2013).Finally, the whole approach is validated by comparing numerical results with settlement measurements provided by a very accurate monitoring system, based on an advanced technique known as Persistent Scatterer Interferometry. As already mentioned in Chapter 6, the long-term displacements of these coastal structures of the Venetian Lagoon were monitored by PSI from March 2008 to January 2009. These breakwaters

built at the Malamocco and Chioggia inlets have shown settlement rates that remain in the other of 5÷25 mm/year and about 15 mm/year, respectively.

7.2 Soft Soil Creep model

The Soft Soil Creep (SSC) model takes into account creep behaviour (i.e. secondary consolidation) of soft soils. As soft soils are considered near-normally consolidated clays, clayey silts or peat. A characteristic feature of these materials is their high compressibility.

Creep oedometer test is the simplest test to assess the time dependent behaviour. It consists on an axysimmetric test in which deformations occur only in the vertical direction (ε_z) whilst radial strains are constrained ($\varepsilon_r = 0$). Hence, volumetric strain coincides with axial strain ($\varepsilon_v = \varepsilon_z$). In this sense, the compression process is usually described using the void ratio $e = -\delta\varepsilon_v(1+e_0)+e_0$.

Figure 7.1 shows the main components of the oedometer apparatus: an undisturbed soil specimen is placed into a rigid metal ring that does not allow horizontal displacements or radial flow of water during compression. Porous stones at the top and bottom allow drainage during the consolidation process.

The oedometer soil stiffness is referred to as constrained modulus, $M\left(=\delta\sigma'_a/\delta\varepsilon_a\right)$, which increases as the axial stress increases (Figure 7.2). Due to lateral confinement, the critical state in oedometer test is never reached.

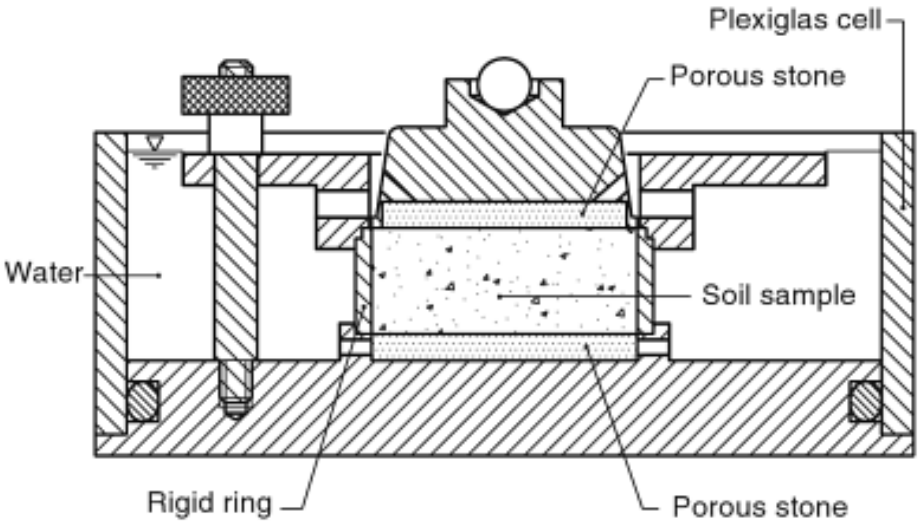

Figure 7.1: Oedometer testing apparatus (from Lancellotta, 2008)

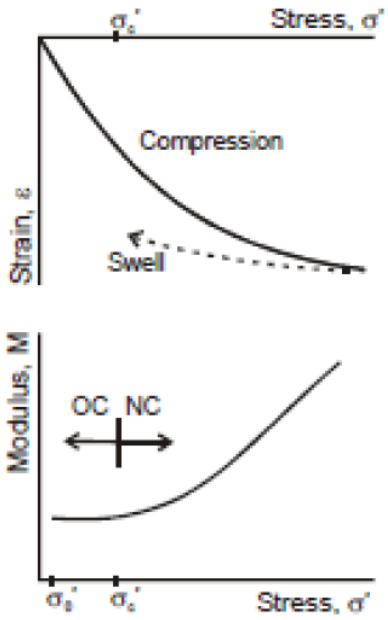

Figure 7.2: Typical stress-strain and *M*-stress curve from oedometer tests for clays (Janbu, 1969)

For the ideal normally consolidated clay, *M* increases linearly with effective stress:

$$M = m \cdot \sigma'_z \tag{7.1}$$

Hence, the strain equation can be expressed as follows:

$$d\varepsilon_z = \frac{1}{M} d\sigma'_z = \frac{1}{m} \cdot \frac{d\sigma'_z}{\sigma'_z} = \lambda^* \cdot \frac{d\sigma'_z}{\sigma'_z} \tag{7.2}$$

where λ^* is the modified compression index. Integrating Equation (7.2) between $\sigma'_{z,0}$ and σ'_z:

$$\varepsilon_z = \frac{1}{m} \cdot \ln \frac{\sigma'_z}{\sigma'_{z,0}} = \lambda^* \cdot \ln \frac{\sigma'_z}{\sigma'_{z,0}} \tag{7.3}$$

When making use of the void ratio (e) – base 10 logarithm of stress, the modified compression index λ^* is defined as:

$$\lambda^* = \frac{1}{m} = \frac{\Delta\varepsilon_z}{\Delta \ln \sigma'_z} = \frac{C_c}{\ln 10 \cdot (1 + e_0)} = \frac{C_{c\varepsilon}}{\ln 10} \tag{7.4}$$

where C_c is the compression index.

According to Janbu (1963), the most general expression for the constrained modulus is given by:

$$M = m \cdot \sigma_{ref} \left(\frac{\sigma'_z}{\sigma_{ref}} \right)^{1-n} \tag{7.5}$$

where m is the modulus number, σ_{ref} is a reference stress, σ'_z is the effective stress and n is the stress exponent. As for normally consolidated clays, the stress exponent n is equal to 0 (n = 0). Therefore:

$$M = m \cdot \sigma'_z \tag{7.6}$$

Assuming that the secondary compression is a small percentage of the primary compression, problems involving large primary compression will involve important creep deformation (Vermeer and Neher, 1999). This is for instance what happens when embankments are constructed on soft soils. On the other hand, when loading overconsolidated soils, which exhibit relative small primary settlements, a state of normal consolidation may be reached and relevant creep deformation may follow. In all these cases, computations with a creep model are advisable.

Buisman (1936) observed that soft-soil settlements could not be interpreted within the classical consolidation theory and proposed a creep law for clay. Other researchers such as Bjerrum (1967), Garlanger (1972) and Mesri and Godlewski (1977) continued Buisman's work on 1D-secondary compression. Lines of research on 3D creep modelling were followed, among others, by Sekiguchi (1977), Adachi and Oka (1982) and Borja and Kavaznjian (1985). However, as Vermeer and Neher (1999) remarked, conflicts exist. They stressed that there is a need to first formulate 1D-models as differential equations and then make an extension to a 3D-model.

The Soft Soil Creep model was proposed by Vermeer and Neher (1999). Some basic features of the SSC model are:

- Soil stiffness as a function of the effective stress
- Distinction between primary loading and unloading-reloading
- Memory of pre-consolidation stress (σ'_c)
- Time-dependent compression
- Use of the Mohr-Coulomb criterion to describe failure
- Yield surface adapt from the Modified Cam Clay model
- Associated flow rule for plastic strains

7.2.1 Soft Soil Creep model: One dimensional creep

The fundamental 1D-creep model for the Soft Soil Creep model proposed by Vermeer and Neher (1999) is constructed based on research made by Buismain (1936), Šuklje (1957), Bjerumm (1967) and Garlanger (1972). Accordingly, the total strains can be decomposed in two terms: the elastic and inelastic (visco-plastic or creep) strains. The basic idea of this visco-elastic constitutive law is that all inelastic strain are time-dependent. Furthermore, the preconsolidation stress depends on the amount of creep strain accumulated during the time (Bjerrum, 1967).

The SSC model takes into account the evolution of preconsolidation pressure with creep strain and results in an *isotache* approach model. The *isotache* model is based on the existence of a unique relationship between the current stress and strain for a given constant strain rate ($d\varepsilon'_z/dt$). The family of curves made of stress-strain point corresponding to a specific strain rate are called *isotaches*. The original model was proposed by Šuklje (1957) and later deeply investi-

gated by other authors such as Leroueil (2006). A detailed description of the *isotache* model will not be reported here.

Clays left at constant effective stress develop secondary compression strains. Figure 7.3 shows this response using *isotaches* (dashed lines). At constant stress, strain increase at a decreasing rate as the clay moves down across the family of isotaches (AB path) and this creep can be supposed to have happened over geological time for samples presently in the ground. If an oedometer test would be performed on a clay sample taken from the ground, increasing total stress would cause the strain rate to increase (BC path). Nevertheless, the rate of strain will afterward decrease (CD path) again as the creep strains dominate over the effects associated to residual pore pressures dissipation (Muir Wood, 2004). Examples of the application of the isotache model to the assessment of creep can be found in Nash (2001) and Nash and Ryde (2001).

In the following Sections a description of the compression parameters will be first provided and then a constitutive law in differential form will be formulated. Finally, the role of the overconsolidation ratio (*OCR*) in the *SSC* model will be discussed.

7.2.1.1 Compression parameters

The Janbu equation for the constrained modulus *M* (Equation (7.5)) with $n = 0$ is used to describe the oedometric virgin compression:

$$M = m\sigma_{ref}\left(\frac{\sigma'_z}{\sigma_{ref}}\right) = M_{ref}\left(\frac{\sigma'_z}{\sigma_{ref}}\right) = \frac{\sigma'_z}{\lambda^*} \tag{7.7}$$

$$\lambda^* = \frac{\sigma_{ref}}{M_{ref}} = const \tag{7.8}$$

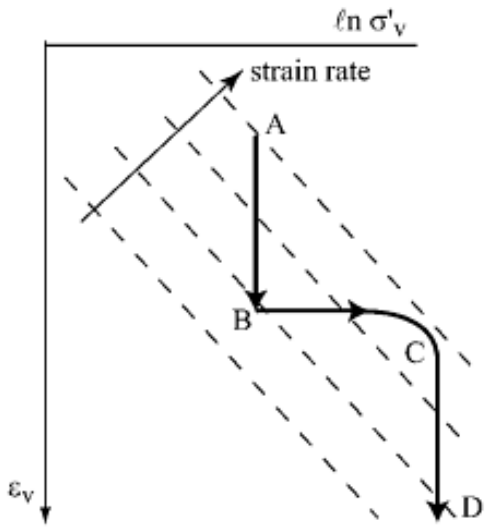

Figure 7.3: Family of isotaches for one-dimensional compression of clay (from Muir Wood, 2004)

As previously mentioned, this form of constrained modulus offers the logarithmic expression of strain in virgin compression shown in Equation (7.3). In oedometer testing, the mean stress is proportional to axial stress by means of the earth pressure coefficient at rest K_0:

$$p = \frac{(1+2K_0)\sigma'_z}{3} \tag{7.9}$$

Hence, the compression index can be expressed in terms of vertical stress and mean stress:

$$\lambda^* = \frac{\Delta\varepsilon_v}{\Delta \ln \sigma'_z} = \frac{\Delta\varepsilon_v}{\ln \frac{\sigma'_{z,2}}{\sigma'_{z,1}}} = \frac{\Delta\varepsilon_v}{\ln \frac{p'\left(3/\left(1+2K_0\right)\right)}{p'_0\left(3/\left(1+2K_0\right)\right)}} = \frac{\Delta\varepsilon_v}{\Delta \ln p'} \tag{7.10}$$

The compression index λ^* can be defined in terms of the compression index (C_c) derived from oedometer test as follows:

$$\lambda^* = \frac{C_c}{\ln 10\left(1+e_0\right)} \tag{7.11}$$

Unfortunately, the same can not be deduced for the slope of the unloading-reloading line because K_0 is not constant for overconsolidated soils. Making use of the elastic constitutive law in oedometric condition, K_0 is expressed as a function of Poisson's ratio in the unloading-reloading phase (v_{ur}):

$$\varepsilon_r = \frac{1}{E}\left(-v_{ur}\sigma'_a + \left(1-v_{ur}\right)\sigma'_r\right) = 0 \rightarrow \sigma'_r = \frac{v_{ur}}{1-v_{ur}}\sigma'_a \rightarrow K_0 = \frac{v_{ur}}{1-v_{ur}} \tag{7.12}$$

In this way, the mean stress can be expressed as:

$$dp' = \frac{1}{3}\left(1+2\frac{v}{1-v}\right)d\sigma'_z \tag{7.13}$$

Besides, for isotropic unloading/reloading situations, the modified Cam Clay model formulates the elastic volume strain as:

$$d\varepsilon_v^e = \kappa^* \frac{dp'}{p'} = \frac{dp'}{K_{ur}} \tag{7.14}$$

or by integration

$$\varepsilon_v^e = \kappa^* \ln \frac{p'}{p'_o} \tag{7.15}$$

where κ^* is the modified swelling index and K_{ur} is the bulk modulus, which is stress dependent according to the rule $K_{ur} = p'/\kappa^*$.

Substituting dp' from Equation (7.13) into (7.14):

$$\varepsilon_v^e = \kappa^* \frac{dp'}{p'} = \kappa^* \frac{\frac{(v+1)d\sigma'_z}{3(1-v)}}{\frac{(1+2K_0)\sigma'_z}{3}} = \frac{1+v}{1-v} \cdot \frac{\kappa^*}{(1+2K_0)} \cdot \frac{d\sigma'_z}{\sigma'_z} \tag{7.16}$$

where K_0 depends to a great extend on the degree of consolidation. As proposed in Vermeer and Neher (1999), the derived one-dimensional swelling index (C_r) from oedometer test in terms of void ratio and 10 base logarithm is transformed to κ^* as follows:

$$\kappa^* = \frac{C_r}{\ln 10(1+e_0)} \cdot \frac{1-v}{1+v}(1+2K_0) \tag{7.17}$$

The creep index, whose applicability will be clarified later on the next Section, does not involve stresses and it is related to the creep coefficient (C_α) obtained in 1-D compression:

$$\mu^* = \frac{C_\alpha}{\ln 10(1+e_0)} \tag{7.18}$$

It is worth observing here that all the strains used in the model are Henky strains (i.e. the strain measured incrementally with respect to the momentary dimension). Hence, the void ratio in the previous expressions should be the current value and not the initial one (Berengo, 2010).

7.2.1.2 Differential law for one-dimensional creep

As Vermeer and Neher (1999) remarked in their work, previous studies on secondary compression in oedometer tests had been concentrated on behaviour related to step loading. Several creep equations were proposed by researchers (e.g. Buisman (1936) and Garlanger (1972)). Butterfield (1979) suggested a creep equation of the form:

$$\varepsilon^H = \varepsilon_c^H + \mu^* \cdot \ln\left(\frac{\tau_c + t'}{\tau_c}\right) \tag{7.19}$$

where ε^H is the logarithmic strain (or Henky strain) defined as:

$$\varepsilon^H = -\int_{V_0}^{V} \frac{dV}{V} = -\ln\left(\frac{V}{V_0}\right) = -\ln\frac{1+e}{1+e_0} \tag{7.20}$$

and ε_c^H is the deformation during consolidation, μ^* is the modified index that describes the secondary compression per logarithmic time increment and *t'* is the effective creep time. The time τ_c is not the consolidation time t_c. This parameter depends not only on the consolidation, but also on the geometry of the sample (Neher *et al*., 2001).

By differentiating Equation (7.19) with respect to time, one obtains:

$$\dot{\varepsilon} = \frac{\mu^*}{\tau_c + t'} \tag{7.21}$$

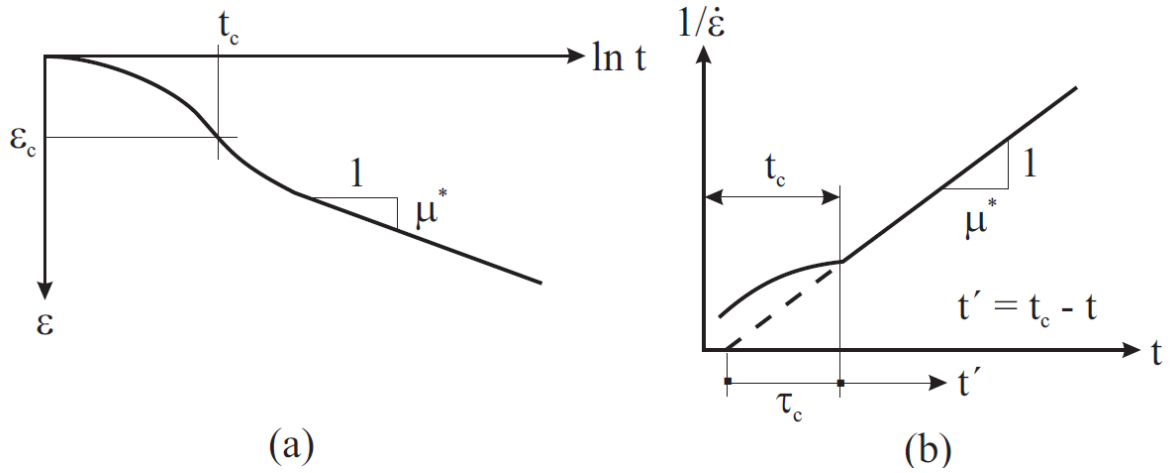

Figure 7.4: a) Consolidation curve from standard Oedometer tests, b) Janbu (1969) method

Janbu (1969) developed a method for evaluating the parameters μ^* and τ_c from experimental data. In Janbu's construction, shown in Figure 7.4*b*, τ_c is the intercept with the linear time axis of the straight creep line. For $t < t_c$, the relation between $1/\dot{\varepsilon}$ and t is not linear due to consolidation. The difference between τ_c and t_c can be also observed in the figure.

For isotropic stress states the same μ^* can be found. Considering the expressions from the modified Cam Clay model for virgin isotropic compression and isotropic unloading/reloading situations and the secondary compression part, the total volumetric strain due to an increase in mean effective stress from p'_0 to p' in a time period of $\tau = t_c + t'$ will be:

$$\varepsilon_v = \varepsilon_v^e + \varepsilon_v^{cr} = \varepsilon_{vc}^e + \varepsilon_{vc}^{cr} + \varepsilon_{vac}^{cr} = \kappa^* \ln \frac{p'}{p'_0} + \left(\lambda^* - \kappa^*\right) \ln \frac{p'_{pc}}{p'_{p0}} + \mu^* \ln \frac{\tau_c + t'}{\tau_c} \tag{7.22}$$

The elastic strain is denoted by ε_v^e and the visco-plastic creep strain by ε_v^{cr}. Besides the visco-plastic part is separated into a part during consolidation and a part after consolidation, given by the subscripts *c* and *ac* respectively.

As already mentioned, the SSC model uses the intrinsic time concept and there is still the question of how to express τ_c analytically. In order to find an analytical expression, the basic idea adopted is that all inelastic strains are time dependent. Besides, the Bjerrum's (1967) idea that preconsolidation stress totally depends on the creep strain accumulated by time is supposed. Thus, Equation (7.22) can be expressed as:

$$\varepsilon_v = \varepsilon_v^e + \varepsilon_v^{cr} = \kappa^* \ln \frac{p'}{p'_0} + \left(\lambda^* - \kappa^*\right) \ln \frac{p'_p}{p'_{p0}} \tag{7.23}$$

where

$$p'_p = p'_{p0} \exp\left(\frac{\Delta \varepsilon_v^{cr}}{\lambda^* - \kappa^*}\right) \tag{7.24}$$

The more the soil sample is left to creep, the more the preconsolidation pressure $\left(p'_p\right)$ grows. In this way, the visco-plastic part after consolidation can be written as:

$$\varepsilon_{vac}^{cr} = \varepsilon_v^{cr} - \varepsilon_{vc}^{cr} = \left(\lambda^* - \kappa^*\right)\ln\frac{p'_p}{p'_{p0}} - \left(\lambda^* - \kappa^*\right)\ln\frac{p'_{pc}}{p'_{p0}} = \left(\lambda^* - \kappa^*\right)\ln\frac{p'_p}{p'_{pc}} = \mu^* \ln\frac{\tau_c + t'}{\tau_c} \tag{7.25}$$

In conventional oedometer testing the load is increased stepwise and in each step the load is maintained for a constant period of $\tau = t_c + t'$, being τ one day. Hence, the IC-line with $p'_p = p'$ is obtained. For *OCR* = 1 and entering $p'_p = p'$ and t' = τ - t_c into Equation (7.25) it follows that:

$$\left(\lambda^* - \kappa^*\right)\ln\frac{p'}{p'_{pc}} = \mu^* \ln\frac{\tau_c + \tau - t_c}{\tau_c} \tag{7.26}$$

Assuming that $\left(\tau_c - t_c\right) << \tau$, Equation (7.26) is simplified:

$$\tau_c = \tau \cdot \left(\frac{p'_{pc}}{p'}\right)^{\frac{\lambda^* - \kappa^*}{\mu^*}} \tag{7.27}$$

Once τ_c has been derived, it is possible to formulate a constitutive law in differential form. Equation (7.22) is differentiated to obtain:

$$\dot{\varepsilon}_v = \dot{\varepsilon}_v^e + \dot{\varepsilon}_v^{cr} = \kappa^{*\cdot}\frac{\dot{p}'}{p'} + \frac{\mu^*}{\tau_c + t'} \tag{7.28}$$

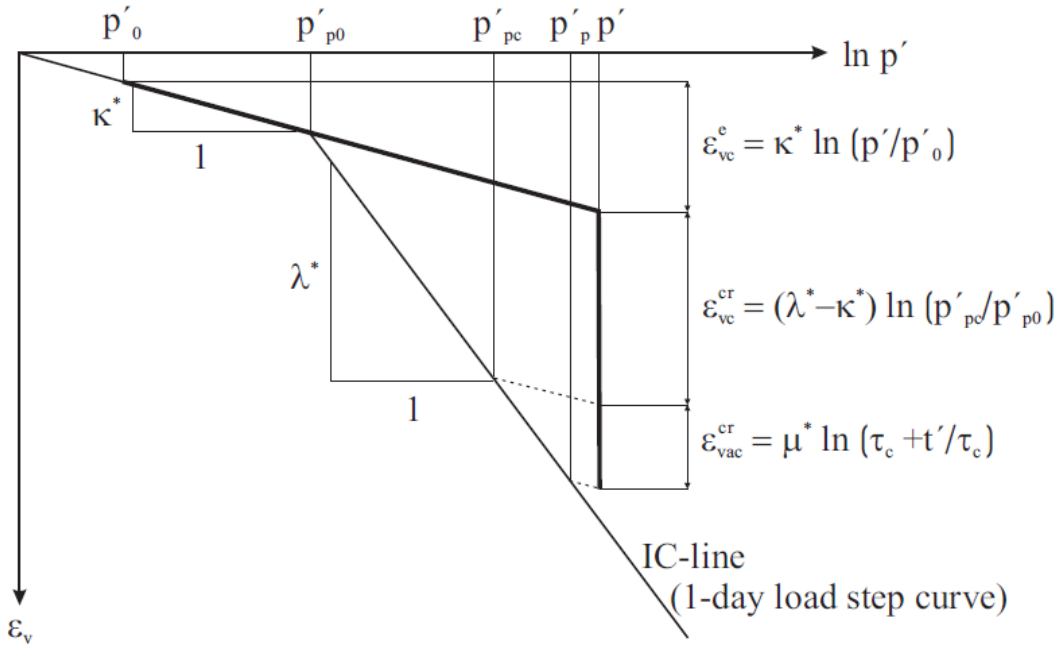

Figure 7.5: Logarithmic relationship between volumetric strain and mean stress including creep (from Neher *et al.* 2001)

Then, substituting $\tau_c + t'$ from Equation (7.25) into (7.28) one gets:

$$\dot{\varepsilon}_v = \dot{\varepsilon}_v^e + \dot{\varepsilon}_v^{cr} = \kappa^{*.} \cdot \frac{\dot{p}'}{p'} + \frac{\mu^*}{\tau_c} \cdot \left(\frac{p'_{pc}}{p'_p} \right)^{\frac{\lambda^* - \kappa^*}{\mu^*}} \tag{7.29}$$

Finally, on entering τ_c from Equation (7.27) into (7.29) it is found that:

$$\dot{\varepsilon}_v = \dot{\varepsilon}_v^e + \dot{\varepsilon}_v^{cr} = \kappa^{*.} \cdot \frac{\dot{p}'}{p'} + \frac{\mu^*}{\tau} \cdot \left(\frac{p'}{p'_p} \right)^{\frac{\lambda^* - \kappa^*}{\mu^*}} \tag{7.30}$$

7.2.1.3 The overconsolidation ratio (OCR) in the SSC model

The Soft Soil Creep model is an extension of the original Soft Soil (SS) model based on the modified Cam Clay model, but it further includes time and strain rate effects.

The SSC model distinguishes between primary loading and unloading/reloading behaviour and in this sense is similar to Soft Soil model. In the SS model, the position of the cap, i.e. the curve plane in stress space that defines the limit stress between primary loading and unloading/reloading, is initially determined by the maximum stress state that has been reached in the past. Nevertheless, in the SSC model the position of the cap it is determined not only by the preconsolidation stress, but it is also a function of time (Waterman and Broere, 2011).

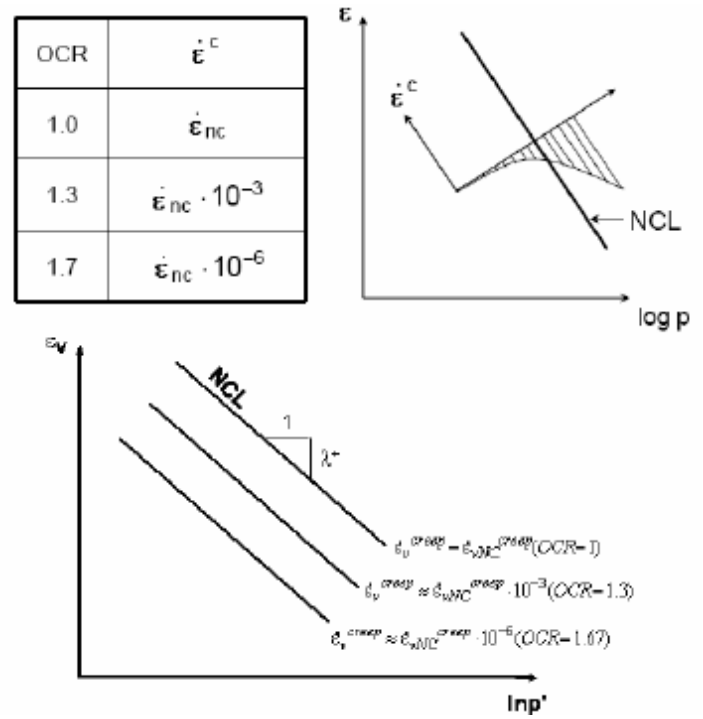

Figure 7.6: Variation of creep rate with OCR (Vermeer *et al.*, 2006; Berengo, 2010)

As already mentioned in last Section, the SSC model belongs to the isotaches family in which the overconsolidation ratio plays an important role. In fact:

$$\dot{\varepsilon}_v^{cr} = \frac{\mu^*}{\tau} \cdot \left(\frac{1}{OCR} \right)^{\beta} \tag{7.31}$$

where $\beta = \left(\lambda^* - \kappa^*\right) / \mu^*$ and $OCR = p'_p / p'$. For typical soil values, the exponent β ranges between 20 and 30.

Figure 7.6 shows the influence of *OCR* on the creep rate. It can be observed that as *OCR* increases, the creep rate decreases. If the applied load remains constant, the soil will continue to compress with time, which results in an increase of the preconsolidation pressure and *OCR* (without any change in effective stress) and the creep (strain) rate decreases.

The significant influence of the overconsolidation ratio on the creep rate has been studied by several researchers such as, for example, Brinkgreve (2001) and Waterman and Broere (2011), using the Soft Soil Creep model implemented into the finite element software PLAXIS.

7.2.2 Soft Soil Creep model: Three dimensional creep

To extend the 1-D formulation to a 3-D theory, the ellipses from the Modified Cam Clay model are considered, being the convenient way in which to write the equation of the ellipse:

$$\frac{p'}{p^{eq}} = \frac{M^2}{M^2 + \left(\frac{q}{p'} \right)^2} \tag{7.32}$$

or

$$p^{eq} = p' + \frac{q^2}{M^2 p'} \tag{7.33}$$

where *p'* and *q* are the stress invariants for isotropic stress and deviatoric stress respectively, and *M* represents the slope of the critical state line:

$$p' = \frac{1}{3}\left(\sigma'_{xx} + \sigma'_{yy} + \sigma'_{zz}\right) \tag{7.34}$$

$$q = \sqrt{\frac{1}{2}\left(\left(\sigma'_{xx} - \sigma'_{yy}\right)^2 + \left(\sigma'_{yy} - \sigma'_{zz}\right)^2 + \left(\sigma'_{zz} - \sigma'_{zz}\right)^2 + 6\left(\sigma_{xy}^2 + \sigma_{yz}^2 + \sigma_{zx}^2\right)^2\right)} \tag{7.35}$$

$$M = \frac{6 \sin \varphi_{cv}}{3 - \sin \varphi_{cv}} \tag{7.36}$$

where φ_{cv} is the critical state friction angle.

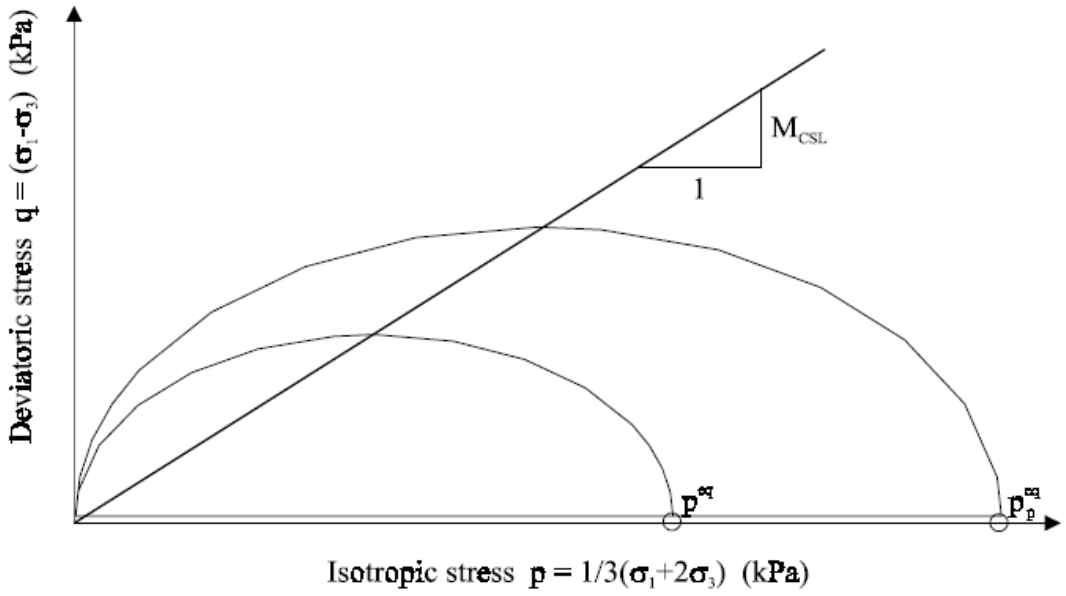

Figure 7.7: Diagram of p_{eq}-ellipse in a *p*-*q* plane (Vermeer and Neher, 1999)

The equivalent pressure p^{eq} is constant along ellipsoids in principal stress space and it is a way to project a stress state *p*'-*q* to the isotropic axis. Focusing the attention on normally consolidated states as met in oedometer that yield $\sigma'_2 = \sigma'_3 = K_0^{NC}\sigma'_1$, it follows that:

$$p^{eq} = \sigma'_1 \left[\frac{1+2K_0^{NC}}{3} + \frac{3\left(1-K_0^{NC}\right)^2}{M^2\left(1+2K_0^{NC}\right)} \right] \tag{7.37}$$

$$p_p^{eq} = \sigma'_p \left[\frac{1+2K_0^{NC}}{3} + \frac{3\left(1-K_0^{NC}\right)^2}{M^2\left(1+2K_0^{NC}\right)} \right] \tag{7.38}$$

The volumetric component of the creep strain is then defined using the 1-D formulation referred to the equivalent pressure. On the other hand, the deviatoric part has to be considered, as soft soils also exhibit deviatoric creep strains.

$$\dot{\varepsilon}_v^{cr} = \frac{\mu^*}{\tau} \cdot \left(\frac{p^{eq}}{p_p^{eq}} \right)^{\frac{\lambda^* - \kappa^*}{\mu^*}} \tag{7.39}$$

with

$$p_p^{eq} = p_{p0}^{eq} \exp\left(\frac{\Delta\varepsilon_v^{cr}}{\lambda^* - \kappa^*} \right) \tag{7.40}$$

In order to introduce general creep strains, the concept that creep strain is a simply time-dependent plastic strain is adopted. As done in plasticity theory, the 3-D model has a flow rule giving the 'direction' of the rate of creep strain. It is also assumed associated plasticity and thus ellipses are taken as plastic potentials. For defining such flow rule, vector notation and principal

directions are adopted. Using Hooke's law to relate stress rates to the elastic strain rates and a flow rule for the creep strains, one gets:

$$\underline{\dot{\varepsilon}} = \underline{\dot{\varepsilon}}^{e} + \underline{\dot{\varepsilon}}^{c} = \underline{\underline{D}}^{-1}\dot{\sigma}' + \lambda \frac{\partial g^{c}}{\partial \underline{\sigma}'} \tag{7.41}$$

where $\underline{\underline{D}}$ is the elasticity matrix and the plastic potential function $\left(g^{c}\right)$ is assumed equal to the equivalent pressure $\left(g^{c} = p^{eq}\right)$.

In this way, it follows that:

$$\dot{\varepsilon}_{v}^{c} = \dot{\varepsilon}_{1}^{c} + \dot{\varepsilon}_{2}^{c} + \dot{\varepsilon}_{3}^{c} = \lambda\left(\frac{\partial p^{eq}}{\partial \sigma'_{1}} + \frac{\partial p^{eq}}{\partial \sigma'_{2}} + \frac{\partial p^{eq}}{\partial \sigma'_{3}}\right) = \lambda \frac{\partial p^{eq}}{\partial p'} = \lambda \cdot \alpha \tag{7.42}$$

Then, making use of Equation (7.39) and (7.42), Equation (7.41) can be written as:

$$\underline{\dot{\varepsilon}} = \underline{\underline{D}}^{-1}\dot{\sigma}' + \frac{\dot{\varepsilon}_{v}^{c}}{\alpha}\frac{\partial p^{eq}}{\partial \underline{\sigma}'} = \underline{\underline{D}}^{-1}\dot{\sigma}' + \frac{1}{\alpha} \cdot \frac{\mu^{\circ}}{\tau}\left(\frac{p^{eq}}{p_{p}^{eq}}\right)^{\frac{\lambda^{*}-\kappa^{*}}{\mu^{*}}} \frac{\partial p^{eq}}{\partial \underline{\sigma}'} \tag{7.43}$$

7.3 Two-dimensional numerical modelling

7.3.1 General settings, soil layering and parameter identification

Plaxis 2D may be used to performed 2D finite element analysis. Real geotechnical problems may be modelled either by an axisymmetric or a plain strain model.

A plain strain model (Figure 7.8) is used in this study assuming geometries with a uniform cross section. Displacements and strains perpendicular to the cross section (*z*-direction) are assumed to be zero. On the other hand, a mesh of 15-noded triangular elements (Figure 7.9) was chosen, which is an accurate element that produces high quality stress results for difficult problems.

Horizontal displacements were prevented along the vertical geometry lines for which the x-coordinate is equal to the lowest or highest x-coordinate in the model, whilst both horizontal and vertical displacements were prevented along the horizontal geometry line for which the y-coordinate is equal to the lowest value in the model.

The soil layers distribution assumed in this study for numerical modelling has been retraced according to the CPTU profiles described in Chapter 6. For each piezocone profile, a single section has been defined, giving a total of 7 sections, 4 for Malamocco and·3 for Chioggia breakwaters. Following the classification profiles from the available piezocone tests, a limited number of main soil units were first identified. However, due to high heterogeneity of such layers, typically composed of a complex assortment of sands, silts and silty clays, a significant variation in the associated values of $C_{\alpha\varepsilon}$, was observed. Accordingly, each soil layer was in turn subdivided into sub-layers approximately characterized by a constant secondary compression coefficient (continuous lines in plots of Figures 7.10 and 7.11).

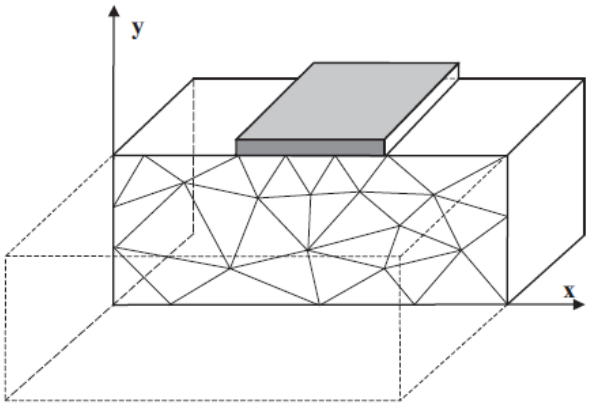

Figure 7.8: Example of a plain strain model (figure taken from Plaxis manual)

Figure 7.9: Position of nodes and stress points in a 15-node triangle (figure taken from Plaxis manual)

For all the sediments, including those having a significant sandy fraction, the isotropic SSC model has been adopted in order to describe their long-term response. A previous successful application of such constitutive formulation to Venetian sediments can be found in Berengo *et al.* (2011), in relation to the analysis of creep deformations observed at the Treporti Test Site.

The use of this formulation requires the definition of the failure parameters ϕ', c', ψ as well as of the stiffness parameters λ^*, κ^* and μ^*, corresponding to the modified compression, swelling and creep indexes respectively. Cohesion and dilation have been neglected in all layers.

As regards the stiffness parameters, the modified creep index $\mu^* = C_{\alpha\varepsilon}/\ln 10$ was derived from the selected $C_{\alpha\varepsilon}$ values plotted in Figures 7.10 and 7.11 (continuous lines) and that the secondary compression coefficient $C_{\alpha\varepsilon}$ was derived from the CPTU-based empirical relationships (Bersan *et al*. 2012; Tonni and Simonini 2013), given by:

$$C_{\alpha\varepsilon} = 0.03 \cdot (Q_{tn})^{-0.89} \tag{5.5}$$

$$C_{\alpha\varepsilon} = 0.077 \cdot (Q_{tn})^{-1.14} \cdot \left(1 + \frac{\Delta u}{\sigma'_{v0}}\right)^{-0.74} \tag{5.6}$$

In the absence of any well-established CPTU-based correlation, the modified compression index $\lambda^* = C_{c\varepsilon}/\ln 10$ was obtained using the $C_{\alpha\varepsilon}/C_{c\varepsilon}$ concept developed by Mesri and Godlewski (1977) for the analysis of secondary settlement.

Mesri and Godlewski (1977) observed that the magnitude and behaviour of C_α with time is directly related to the behaviour and magnitude of C_c with consolidation pressure. Generally, C_α decreases, remains constant, or increases with time, in the range of consolidation pressure at which C_c decreases, remains constant, or increases with σ'_v, respectively. The ratio C_α/C_c in conjunction with the end-of-primary e-logσ'_v curve totally defines the secondary compression behaviour of a soil (Mesri and Castro, 1987).

Following this concept, the relationship between $C_{\alpha\varepsilon}$ and $C_{c\varepsilon}$ was analyzed by Bersan *et al.* (2012) in relation to the different classes of the Treporti sediments. It was found that the ratio $C_{\alpha\varepsilon}/C_{c\varepsilon}$ ranged between the interval 0.02÷0.04. This value has been assumed herein equal to 0.03. Hence, reliable values of the oedometric stiffness ($\lambda^* = C_{c\varepsilon}/\ln 10$) have been obtained from the

empirical relationship $\lambda^* = \mu^*/0.03$. Finally, the modified swelling index κ^* has been taken as $\lambda^*/5$, as also proposed in Berengo *et al.* (2011).

For useful comparison, an alternative calculation of λ^* has been performed using the correlations developed by Tonni *et al*. (2010) and Tonni and Gottardi (2011) for deriving the constrained modulus *M* for the Venetian lagoon sediments:

$$M = 2.3(q_t - u_2) \tag{5.2}$$

$$M = 1.35 \cdot I_c(q_t - \sigma_{v0}) \tag{5.3}$$

where I_c is the soil behaviour type index (Robertson and Wride, 1998).

In this way, λ^* can be computed applying the Janbu's (1963) formulation for normally consolidated soils:

$$M = m\sigma_{ref}\left(\frac{\sigma'_z}{\sigma_{ref}}\right) = M_{ref}\left(\frac{\sigma'_z}{\sigma_{ref}}\right) = \frac{\sigma'_z}{\lambda^*} \tag{7.7}$$

Figure 7.12 shows the λ^* profiles derived from the application of Equation (5.5) and the relationship $\lambda^* = \mu^*/0.03$ to CPTU C3. Besides, the figure also includes the profiles of λ^* computed using Equation (5.2) and (5.3) and Janbu's formula $\left(\lambda^* = \sigma'_z / M\right)$.

It can be observed from Figure 7.12 that the application of Equation (5.3) provides the smallest values of the modified compression index, whereas higher values are obtained using Equation (5.5) and the $C_{\alpha\varepsilon}/C_{c\varepsilon}$ concept. The latter is more evident in the sandy units. On the other hand, the λ^* values computed by means of Equation (5.2) exhibit more scatter.

With regard to the friction angle ϕ', reliable estimates have been obtained by applying some well-known CPTU-based empirical correlations based on calibration chamber test results and field results. Robertson and Campanella (1983) suggested a correlation to estimate the peak friction angle (ϕ') for uncemented, unaged, moderately compressible, predominately quartz sands based on calibration chamber test results. For sands of higher compressibility, the method will tend to predict low friction angles:

$$\phi' = \arctan\left[\frac{1}{2.68}\left(\log\left(\frac{q_c}{\sigma'_{v0}}\right) + 0.29\right)\right] \tag{2.19}$$

Kulhawy and Mayne (1990) suggested an alternate relationship for clean, rounded, uncemented quartz sands, and evaluated the relationship using high quality field data:

$$\phi' = 17.6 + 11\log(q_{t1}) \tag{2.20}$$

where $q_{t1} = (q_t / p_{atm})/(\sigma'_{v0} / p_{atm})^{0.5}$.

On the other hand, for normally to lightly overconsolidated clays and silts (c'=0), the NTH solution (see Senneset et *al.*, 1989) for $20° \le \phi' \le 45°$ and $0.1 \le B_q \le 1.0$, is approximated as follows (Mayne and Campanella, 2005):

$$\phi' = 29.5 \cdot B_q^{\,0.121}\left(0.256 + 0.336 \cdot B_q + \log Q_t\right) \tag{7.44}$$

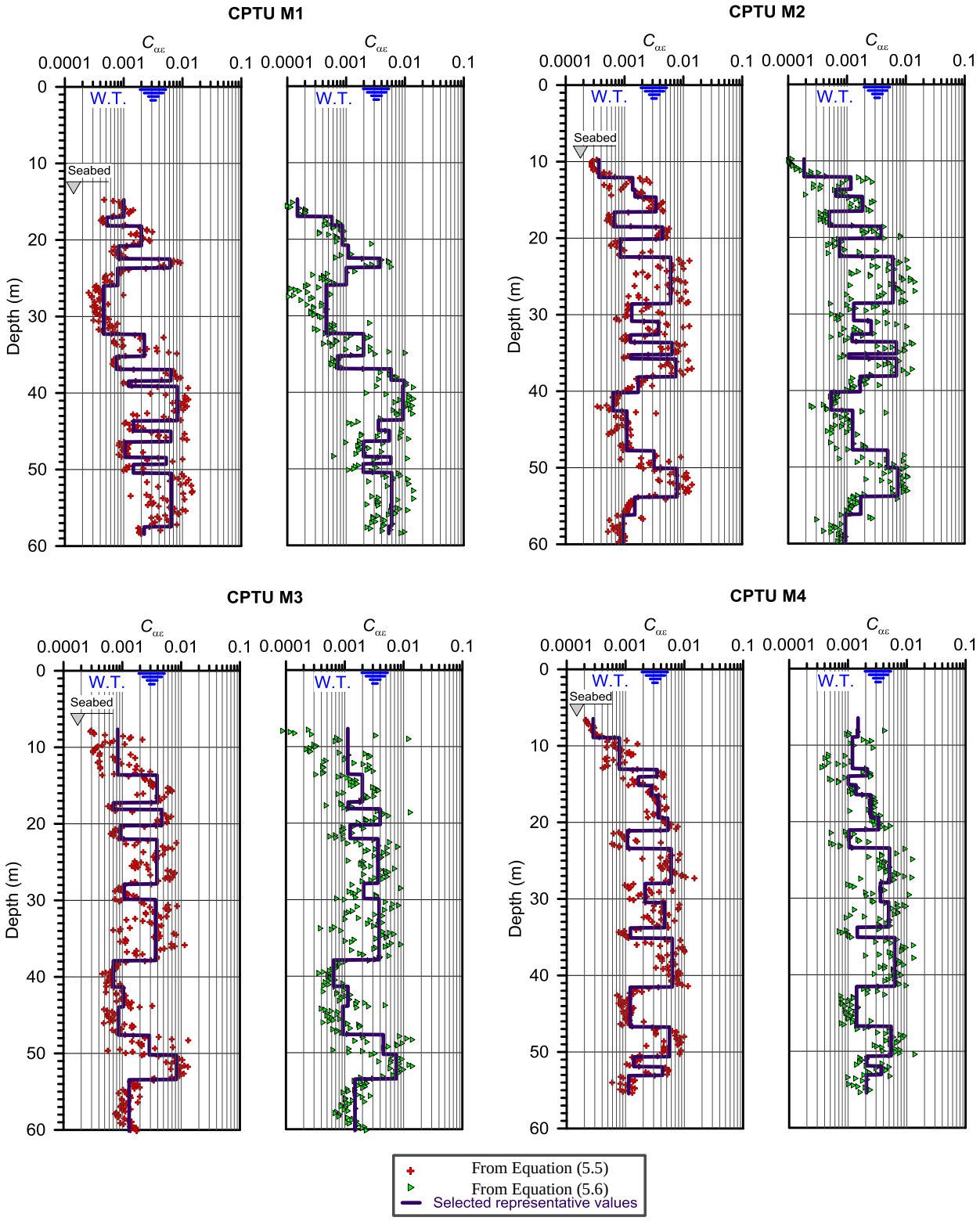

Figure 7.10: Profiles of the computed $C_{\alpha\varepsilon}$ from Malamocco CPTU data and selected values in the numerical analysis

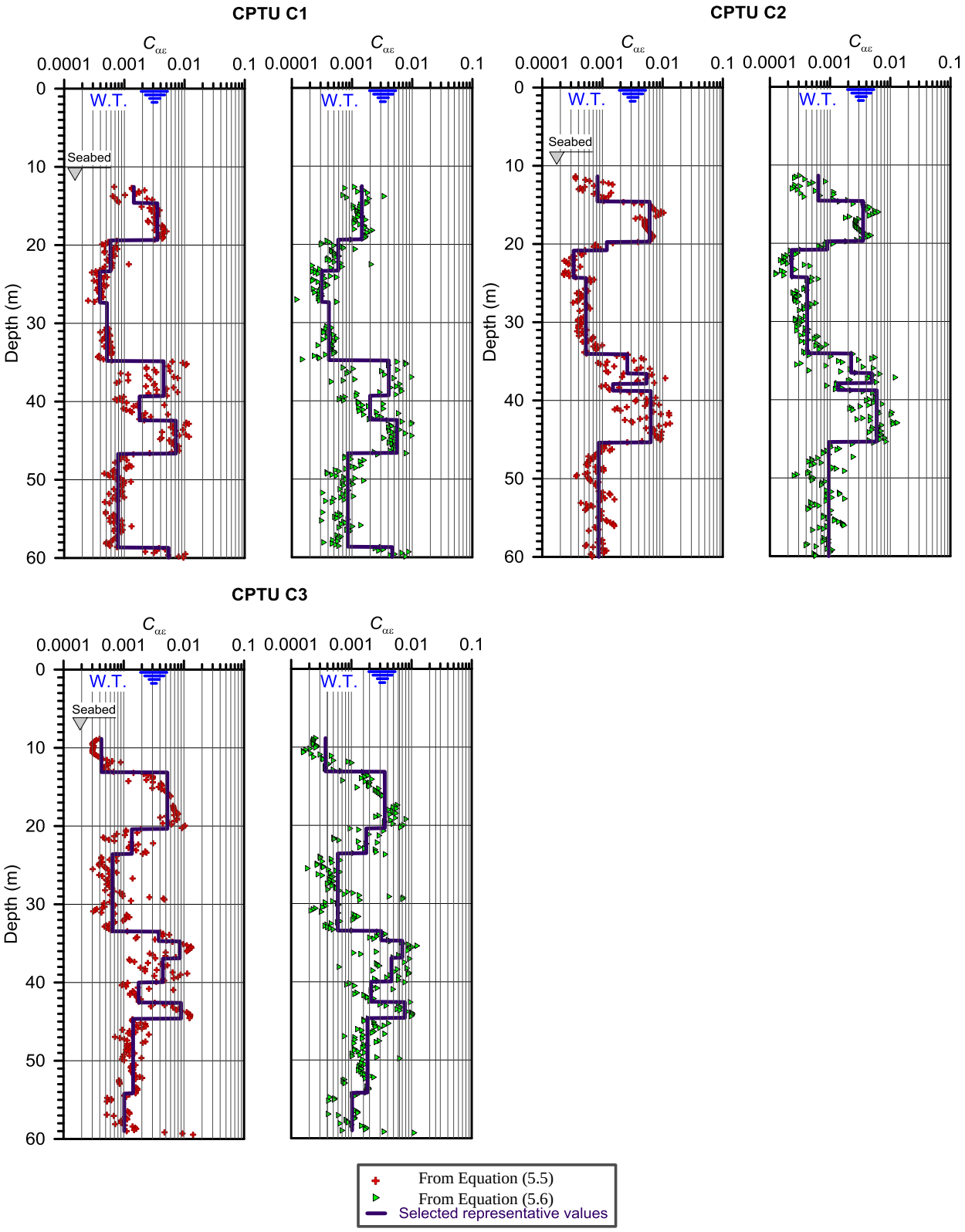

Figure 7.11: Profiles of the computed $C_{\alpha\varepsilon}$ from Chioggia CPTU data and selected values in the numerical analysis

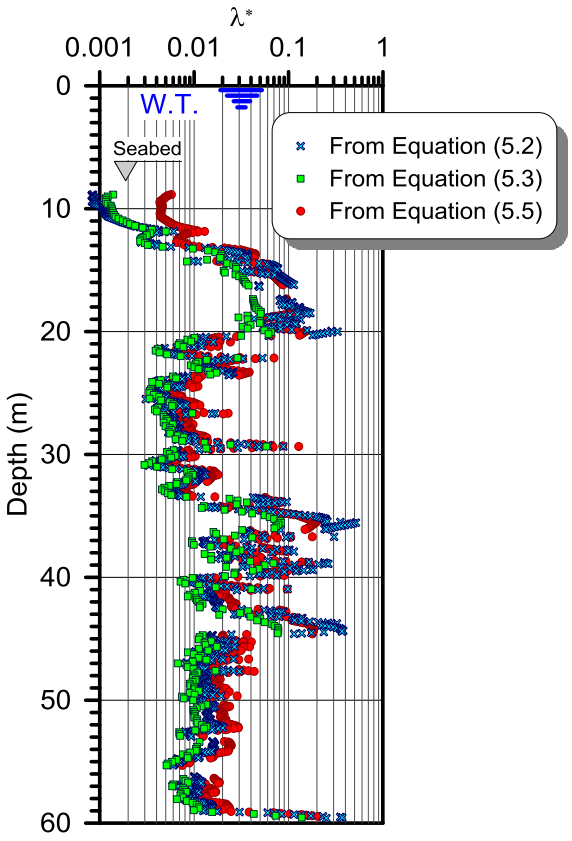

Figure 7.12: Profiles of λ^* from CPTU C3 using different approaches

Figures 7.13 and 7.14 show the profiles of friction angle estimated using the above formulas. The computed ϕ' usually range between 20÷45°, observing some drops below 20° in clay layers and some spikes showing values greater than 45° in shallow layers.

Finally, in order to properly set the initial conditions, the overconsolidation ratio (*OCR*) is necessary. As already mentioned, the *OCR*-value is defining the initial settlement velocity, the creep rate the Plaxis calculation starts. In order to properly capture the creep behaviour, the *OCR*-value has to be selected carefully. It has been observed that the use of a default initial value of 1 leads to unreasonable initial settlement velocities.

In this study, the *OCR*-values have been obtained applying the site-specific correlation developed for Treporti Test Site (Venice) by Tonni and Gottardi (2011), which showed the most realistic values:

$$OCR = 0.91\left(\frac{q_t - u_2}{\sigma'_{v0}}\right)^{0.23} \tag{5.14}$$

The computed values using Equation (5.14) turned out to generally vary between 1÷3, showing values higher than 3 in the shallowest layers. Figures 7.15 and 7.16 illustrate the profiles of the computed *OCR*-values from CPTUs.

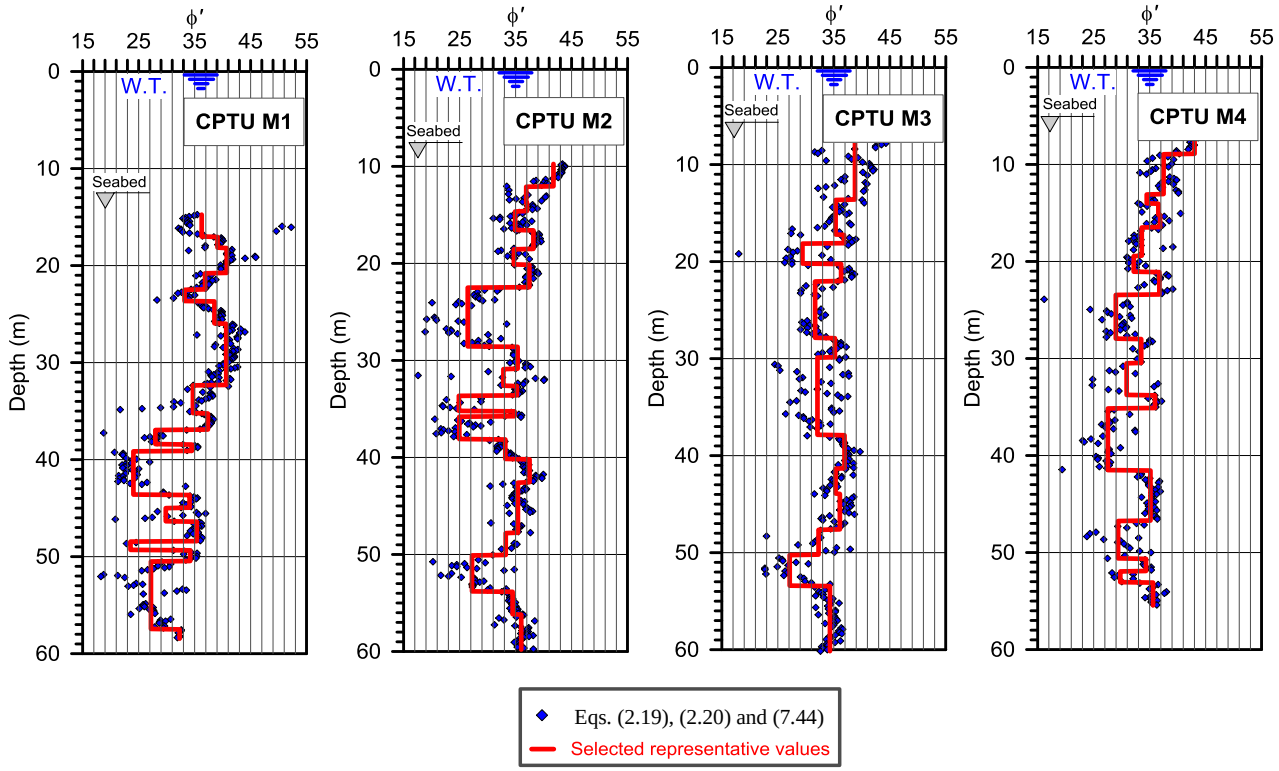

Figure 7.13: Profile of the computed ϕ′ from Malamocco CPTU data and selected values in the numerical analysis

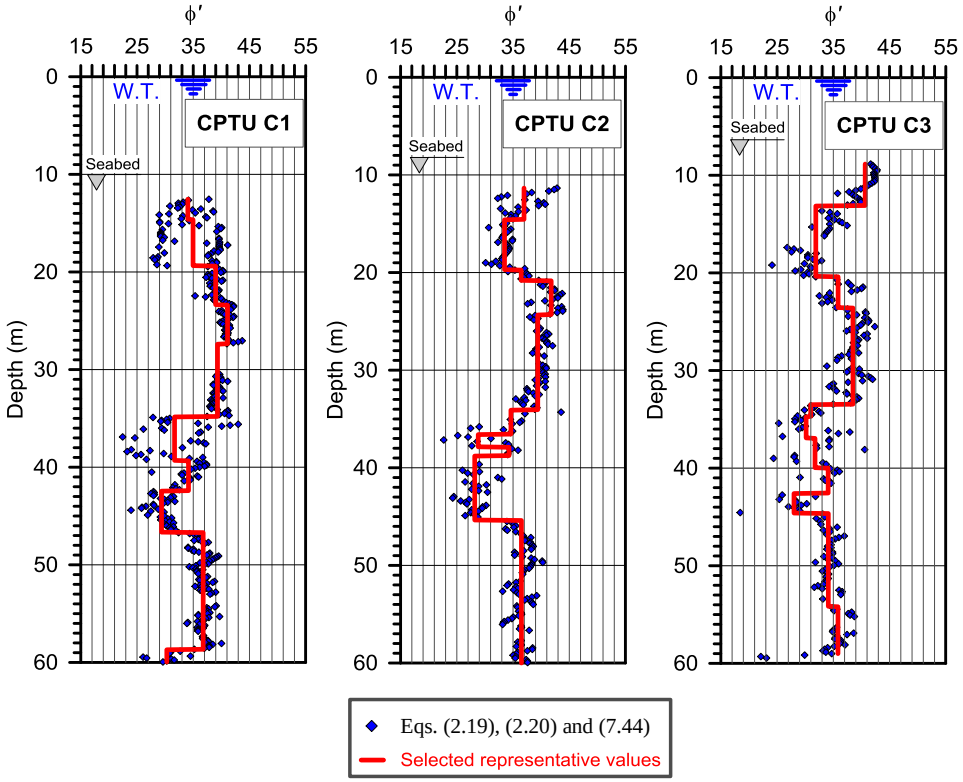

Figure 7.14: Profile of the computed ϕ′ from Chioggia CPTU data and selected values in the numerical analysis

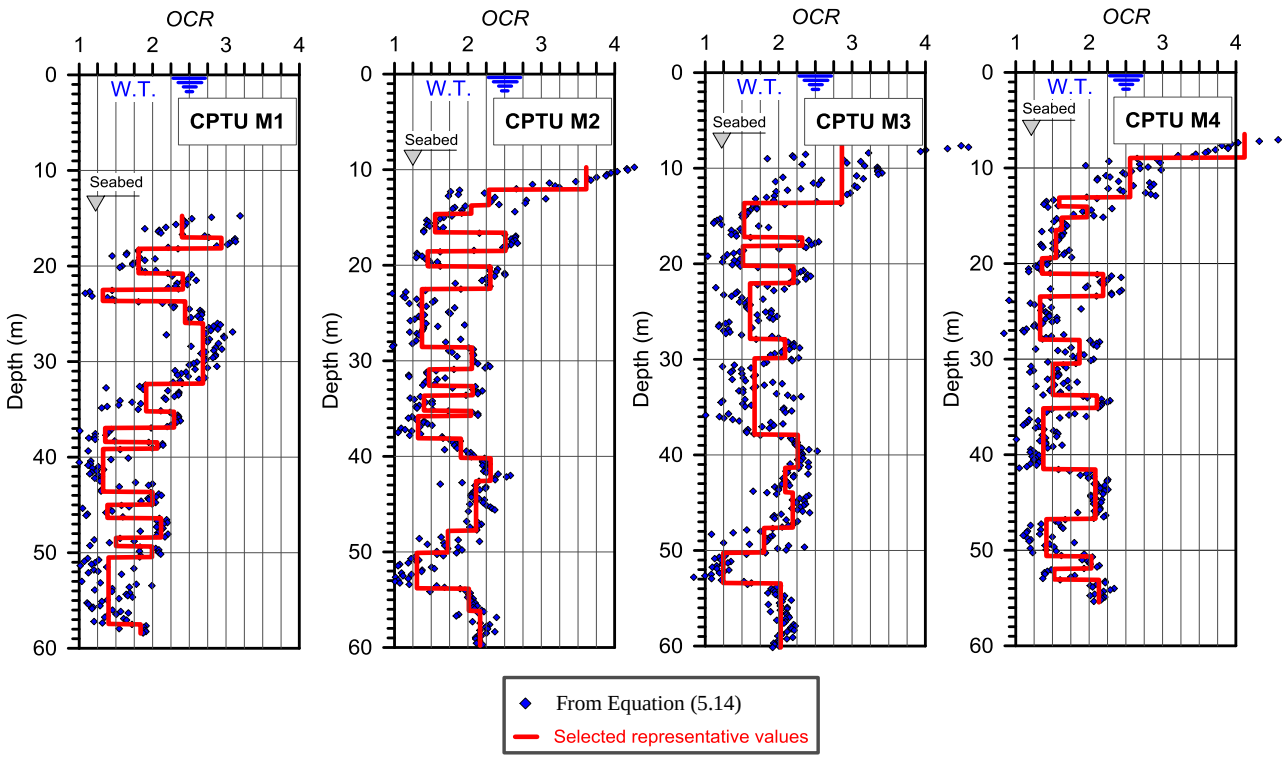

Figure 7.15: Profile of the computed *OCR* from Malamocco CPTU data and selected values in the numerical analysis

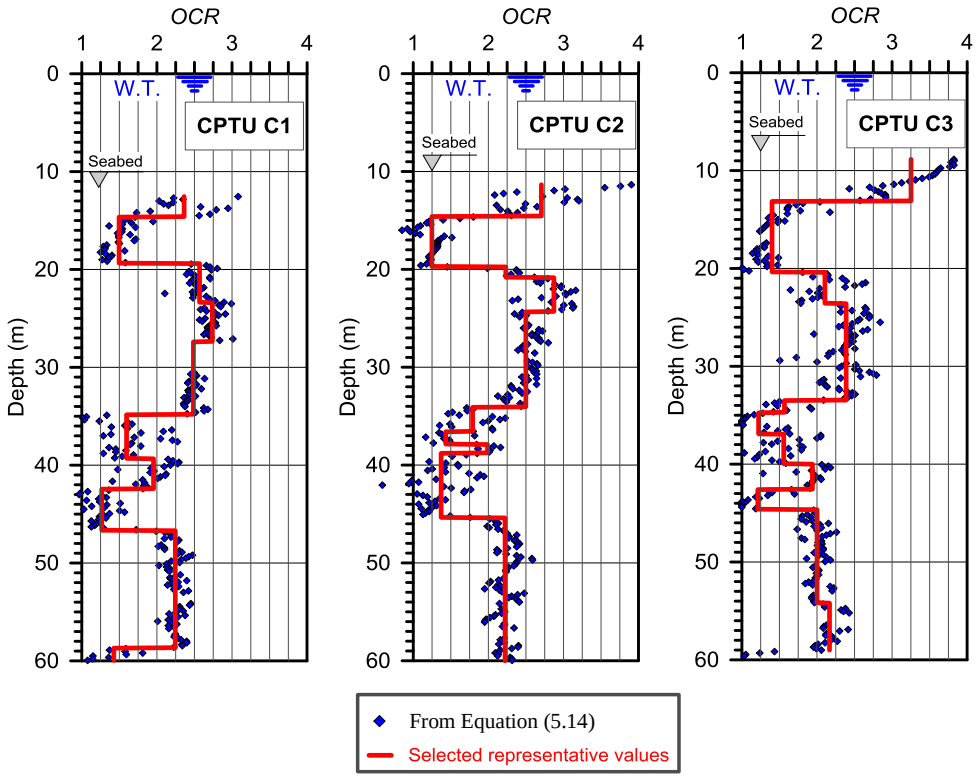

Figure 7.16: Profile of the computed *OCR* from Chioggia CPTU data and selected values in the numerical analysis

Results obtained from the application of two further correlations, Robertson (2012) and Tonni *et al*. (2010) respectively, to CPTU C3 to get the *OCR* profile, are presented in Figure 7.17, together with that obtained applying the already mentioned Equation (5.14).

The correlation suggested by Robertson (2012) for fine-grained soils is given by:

$$OCR = \left(2.625 + 1.75 \log F_r\right)^{-1.25} \left(Q_{t1}\right)^{1.25} \tag{2.37}$$

The third correlation applied was proposed by Tonni *et al.* (2010), obtained by calibrating *OCRs* on Treporti sediments:

$$OCR = 0.038 \cdot F_r \cdot \left(\frac{q_t - u_2}{\sigma'_{v0}}\right)^{1.21} \tag{5.13}$$

Figure 7.17 clearly shows that Equations (2.37) and (5.13) provide unrealistic estimates of *OCR* of coarse Venetian sediments.

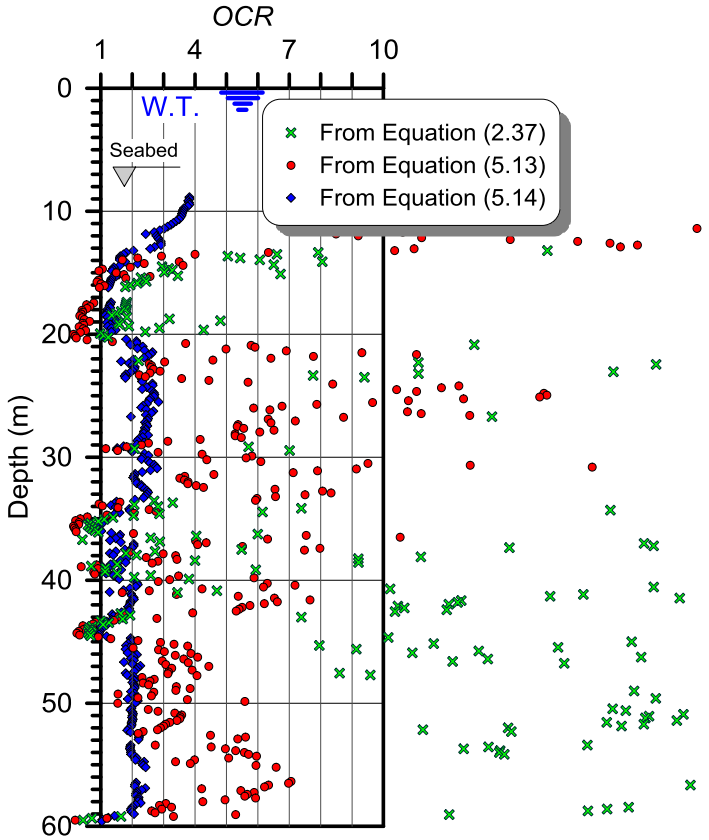

Figure 7.17: *OCR* predictions obtained applying different equations to the test CPTU C3

7.3.1.1 Malamocco: external breakwater

Figure 7.18: Construction history of the breakwater in the Malamocco Inlet (images taken from the website salve.it)

When using the *Soft Soil Creep* model, the time between the construction of the breakwater and the data of interest, in these cases March 2008, is important. In this way, the construction of the Malamocco breakwater was supposed to have started in June 2003 according to archive images from the website salve.it.

A sequence of the whole construction history of the breakwater is shown in Figure 7.18. On the other hand, Figure 7.19 indicates the 4 cross-sections selected for the 2D numerical analysis, passing through the piezocone verticals (M1, M2, M3 and M4).

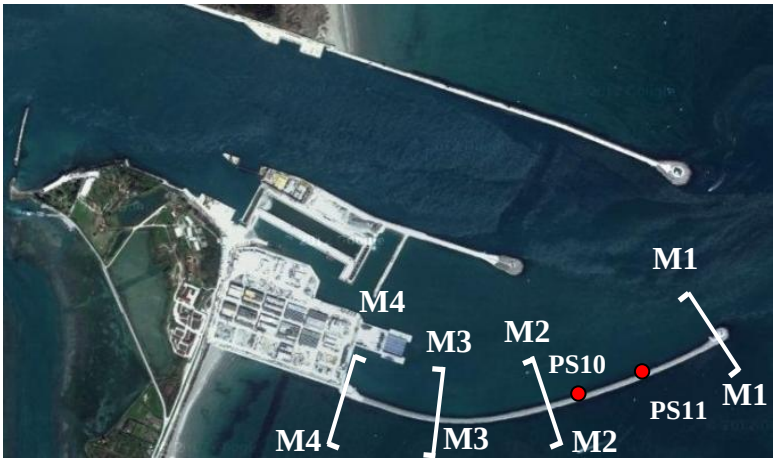

Figure 7.19: Location of the examined cross-sections in the Malamocco breakwater and location of radar reflectors (satellite view)

The soil layers distribution for the numerical analysis is shown in Figures 7.20-7.23 for each section examined. The highly stratified subsoil results in a high number of layers identified for each section.

The material parameters used in the FE analysis are summarized in Tables 7.1-7.4. As for the stiffness parameters, two alternative sets have been considered, depending on the empirical correlation initially adopted to estimate $C_{\alpha\varepsilon}$. The input stiffness parameters with subscript $_{(1)}$ have been calculated using Equation (5.5) and those with subscript $_{(2)}$, using Equation (5.6). It has to be noticed that the most compressible layers are generally identified at depths greater than 20 m below the ground surface.

The breakwater was modelled with a simple linear elastic constitutive law. This is also valid for the breakwater of Chioggia inlet. The total height of the structure and the water level for each section have been retraced from available cross-section images and from the piezocone tests. Heights of the embankment fluctuate between 9.4 and 17.65 m, corresponding to sections M4 – M4 and M1 – M1 respectively. Nevertheless, some uncertainties exist about accurate horizontal dimensions of the structures. In this regard, some simplifications were adopted.

In the numerical analysis, a drained material behaviour has been assigned to all clusters, being the attention focused on the simulation of the only long-term response. In this way, the long-term behaviour is modelled without modelling the precise sequence of undrained loading and consolidation. On the other hand this assumption is coherent with the experimental evidence that in Venetian soils the rate of consolidation is quite high, hence the decay of excess pore pressures is likely to have developed almost simultaneously with the breakwater construction.

To prevent any influence of the outer boundaries, the model has been extended in horizontal direction to a large radius. When the full geometry was defined and all material properties were assigned, the finite element mesh (*very fine* option) was generated. In areas where large deformation was expected, local mesh refinement procedure was used.

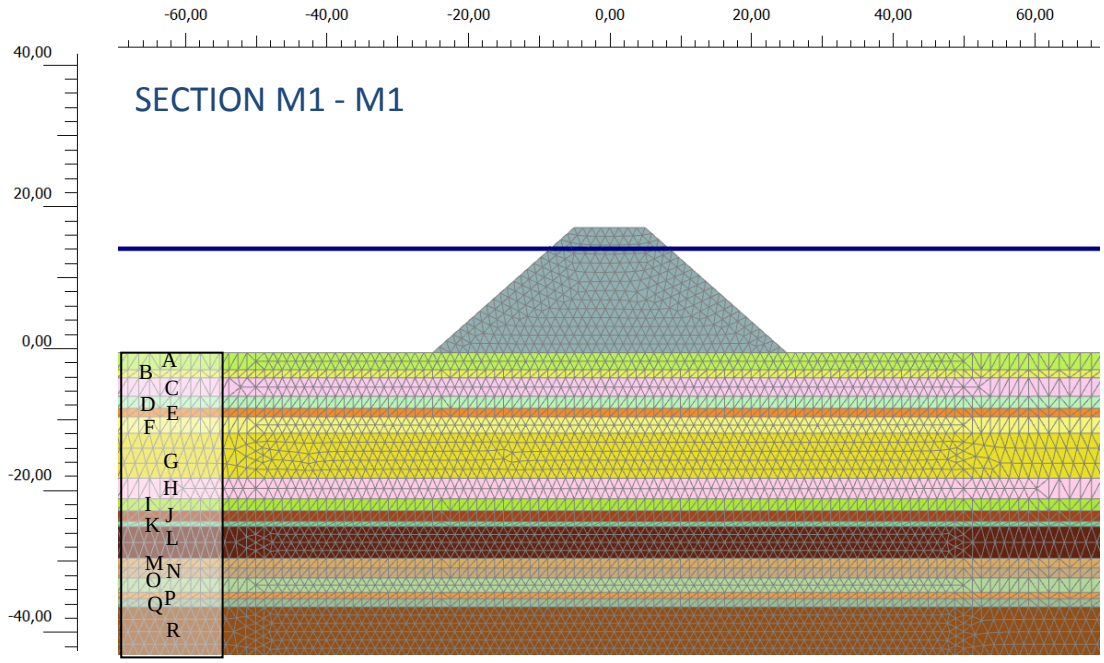

Figure 7.20: Finite element mesh for Section M1 - M1

Table 7.1: Soft Soil Creep model parameters used in Section M1 – M1

Layer	Depth (m)	Material Set 1			Material Set 2			Φ' (°)	OCR
		$\lambda^*_{(1)}$	$k^*_{(1)}$	$\mu^*_{(1)}$	$\lambda^*_{(2)}$	$k^*_{(2)}$	$\mu^*_{(2)}$		
A	0 – 2.4	0.0146	0.0029	0.00044	0.0022	0.0004	0.00006	36.3	2.4
B	2.4 – 3.55	0.0075	0.0015	0.00023	0.0083	0.0017	0.00025	39.1	2.9
C	3.55 – 6.15	0.0290	0.0058	0.00087	0.0126	0.0025	0.00038	40.7	1.8
D	6.15 – 7.85	0.0118	0.0024	0.00035	0.0158	0.0032	0.00047	36.9	2.4
E	7.85 – 9.05	0.0885	0.0177	0.00266	0.0553	0.0111	0.00166	33.2	1.3
F	9.05 – 11.35	0.0115	0.0023	0.00034	0.0146	0.0029	0.00044	38.5	2.4
G	11.35 – 17.7	0.0066	0.0013	0.00020	0.0066	0.0013	0.00020	40.6	2.7
H	17.7 – 20.6	0.0325	0.0065	0.00098	0.0286	0.0057	0.00086	34.7	1.9
I	20.6 – 22.3	0.0110	0.0022	0.00033	0.0104	0.0021	0.00031	37.4	2.3
J	22.3 – 23.8	0.0917	0.0183	0.00275	0.0844	0.0169	0.00253	28.0	1.4
K	23.8 – 24.5	0.0176	0.0035	0.00053	0.1413	0.0283	0.00424	34.5	2.1
L	24.5 - 29	0.1178	0.0236	0.00354	0.1327	0.0265	0.00398	24.1	1.3
M	29 – 30.35	0.0213	0.0043	0.00064	0.0513	0.0103	0.00154	34.1	2.0
N	30.35 – 31.75	0.0915	0.0183	0.00275	0.0783	0.0157	0.00235	29.8	1.4
O	31.75 – 33.8	0.0153	0.0031	0.00046	0.0287	0.0057	0.00086	35.4	2.1
P	33.8 – 34.7	0.0764	0.0153	0.00229	0.0835	0.0167	0.00251	23.5	1.5
Q	34.7 – 35.85	0.0212	0.0042	0.00064	0.0283	0.0057	0.00085	34.2	2.0
R	35.85 – 42.85	0.0935	0.0187	0.00281	0.0862	0.0172	0.00259	27.2	1.4

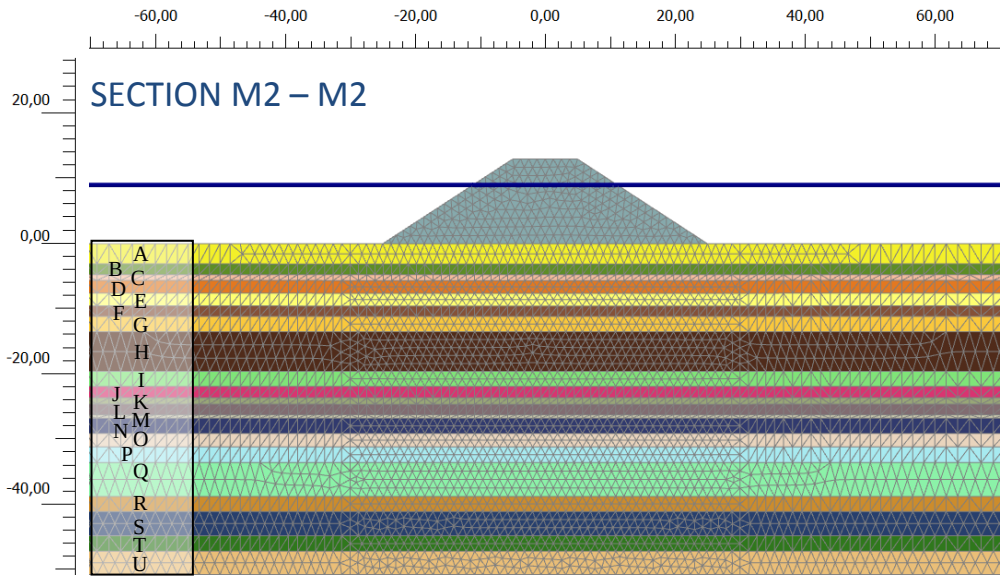

Figure 7.21: Finite element mesh for Section M2 – M2

Table 7.2: Soft Soil Creep model parameters used in Section M2 - M2

Layer	Depth (m)	Material Set 1			Material Set 2			Φ' (°)	OCR
		$\lambda^*_{(1)}$	$k^*_{(1)}$	$\mu^*_{(1)}$	$\lambda^*_{(2)}$	$k^*_{(2)}$	$\mu^*_{(2)}$		
A	0 – 3.1	0.0053	0.0011	0.00016	0.0027	0.0005	0.00008	41.8	3.6
B	3.1– 4.75	0.0199	0.0040	0.00060	0.0168	0.0034	0.00051	36.9	2.3
C	4.75 – 5.65	0.0218	0.0044	0.00065	0.0094	0.0019	0.00028	37.0	2.0
D	5.65 – 7.6	0.0495	0.0099	0.00149	0.0263	0.0053	0.00079	34.9	1.6
E	7.6– 9.55	0.0098	0.0020	0.00029	0.0072	0.0014	0.00022	38.2	2.5
F	9.55 – 11.15	0.0640	0.0128	0.00192	0.0553	0.0111	0.00166	34.7	1.5
G	11.15 – 13.5	0.0123	0.0025	0.00037	0.0107	0.0021	0.00032	37.5	2.3
H	13.5 – 19.6	0.0882	0.0176	0.00265	0.0870	0.0174	0.00261	26.5	1.4
I	19.6 – 21.9	0.0191	0.0038	0.00058	0.0188	0.0038	0.00057	35.4	2.1
J	21.9 – 23.65	0.0708	0.0142	0.00213	0.0564	0.0113	0.00169	32.8	1.5
K	23.65– 24.65	0.0182	0.0036	0.00055	0.0177	0.0035	0.00053	35.2	2.1
L	24.65 – 26.25	0.0922	0.0184	0.00277	0.0998	0.0200	0.00300	24.9	1.4
M	26.25 – 26.8	0.0184	0.0037	0.00055	0.0154	0.0031	0.00046	34.8	2.0
N	26.8 – 29.15	0.1072	0.0214	0.00322	0.1003	0.0201	0.00301	24.9	1.3
O	29.15 – 31.2	0.0247	0.0049	0.00074	0.0242	0.0048	0.00073	33.2	1.9
P	31.2 – 33.6	0.0092	0.0018	0.00028	0.0078	0.0016	0.00023	37.5	2.3
Q	33.6 – 38.8	0.0159	0.0032	0.00048	0.0180	0.0036	0.00054	35.4	2.1
R	38.8 – 41.1	0.0457	0.0091	0.00137	0.0710	0.0142	0.00213	33.2	1.7
S	41.1 - 44.85	0.1131	0.0226	0.00340	0.1049	0.0210	0.00315	27.2	1.3
T	44.85 – 47.2	0.0216	0.0043	0.00065	0.0248	0.0050	0.00074	34.5	2.0
U	47.2 – 50.8	0.0137	0.0027	0.00041	0.0135	0.0027	0.00041	36.0	2.2

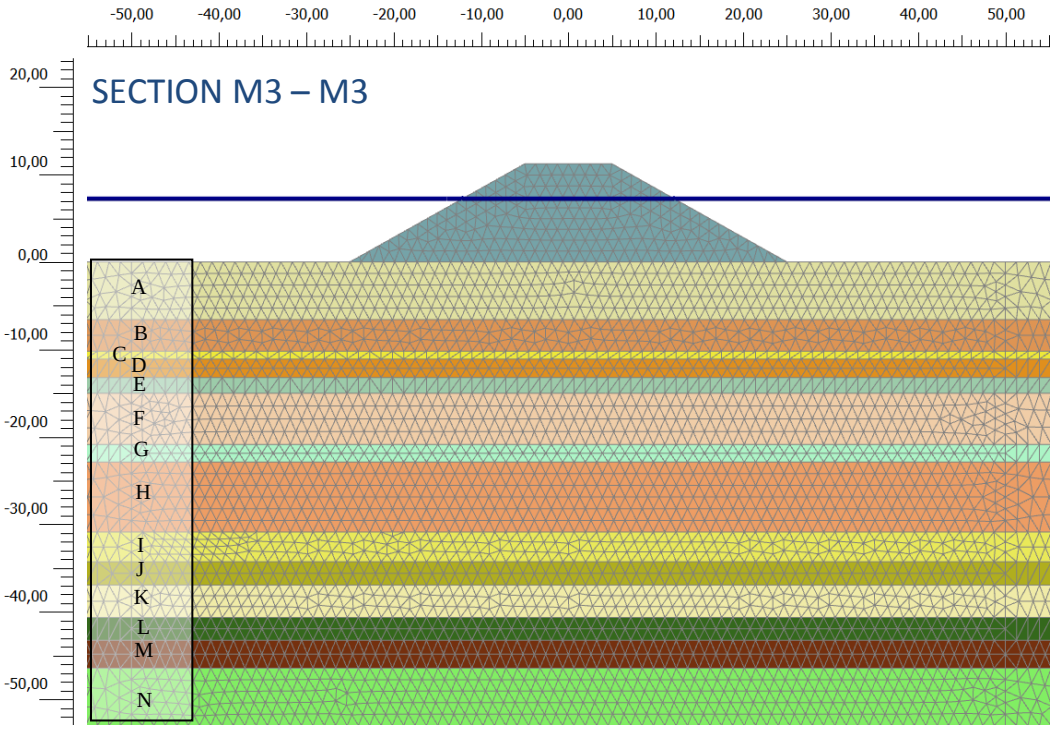

Figure 7.22: Finite element mesh for Section M3 – M3

Table 7.3: Soft Soil Creep model parameters used in Section M3 - M3

Layer	Depth (m)	Material Set 1			Material Set 2			Φ' (°)	OCR
		λ^* (1)	k^* (1)	μ^* (1)	λ^* (2)	k^* (2)	μ^* (2)		
A	0 – 6.6	0.0120	0.0024	0.00036	0.0163	0.0033	0.00049	38.8	2.9
B	6.6– 10.2	0.0564	0.0113	0.00169	0.0288	0.0058	0.00086	35.3	1.5
C	10.2 – 11.1	0.0102	0.0020	0.00031	0.0165	0.0033	0.00050	36.8	2.3
D	11.1 – 13.2	0.0682	0.0136	0.00205	0.0578	0.0116	0.00174	29.4	1.5
E	13.2– 15	0.0134	0.0027	0.00040	0.0179	0.0036	0.00054	36.3	2.2
F	15– 20.85	0.0560	0.0112	0.00168	0.0528	0.0106	0.00159	31.7	1.6
G	20.85 – 22.85	0.0156	0.0031	0.00047	0.0302	0.0060	0.00091	35.2	2.1
H	22.85 – 30.85	0.0531	0.0106	0.00159	0.0555	0.0111	0.00167	32.1	1.7
I	30.85 – 34.25	0.0102	0.0020	0.00031	0.0093	0.0019	0.00028	36.9	2.3
J	34.25 – 36.9	0.0151	0.0030	0.00045	0.0164	0.0033	0.00049	35.3	2.1
K	36.9– 40.6	0.0125	0.0025	0.00038	0.0133	0.0027	0.00040	36.1	2.2
L	40.6 – 43.2	0.0417	0.0083	0.00125	0.0655	0.0131	0.00197	32.3	1.8
M	43.2 – 46.4	0.1201	0.0240	0.00361	0.1095	0.0219	0.00329	27.1	1.2
N	46.4– 52.95	0.0189	0.0038	0.00057	0.0216	0.0043	0.00065	34.3	2.0

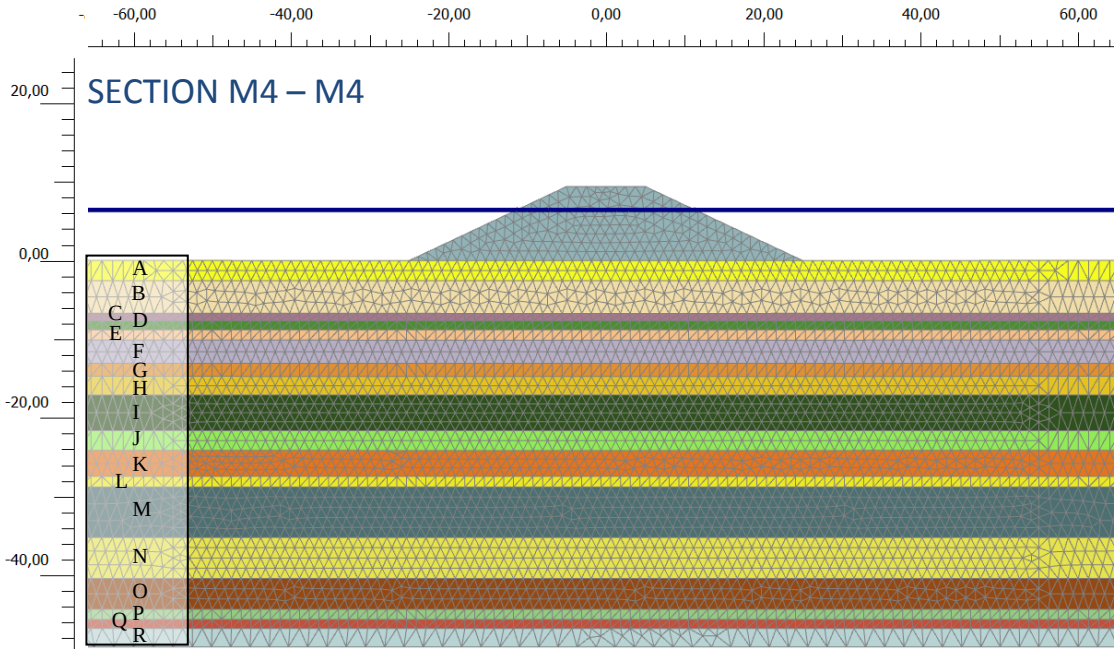

Figure 7.23: Finite element mesh for Section M4 – M4

Table 7.4: Soft Soil Creep model parameters used in Section M4 - M4

Layer	Depth (m)	Material Set 1			Material Set 2			Φ' (°)	OCR
		λ^* (1)	k^* (1)	μ^* (1)	λ^* (2)	k^* (2)	μ^* (2)		
A	0 – 2.55	0.0041	0.0008	0.00012	0.0215	0.0043	0.00064	43.0	4.1
B	2.55 – 6.7	0.0114	0.0023	0.00034	0.0172	0.0034	0.00052	37.5	2.6
C	6.7 – 7.65	0.0494	0.0099	0.00148	0.0306	0.0061	0.00092	34.5	1.6
D	7.65 – 8.8	0.0240	0.0048	0.00072	0.0147	0.0029	0.00044	36.6	2.0
E	8.8 – 10.1	0.0403	0.0081	0.00121	0.0197	0.0039	0.00059	36.9	1.6
F	10.1 – 13.05	0.0520	0.0104	0.00156	0.0351	0.0070	0.00106	33.6	1.5
G	13.05 – 14.7	0.0755	0.0151	0.00227	0.0479	0.0096	0.00144	32.2	1.4
H	14.7 – 17.05	0.0156	0.0031	0.00047	0.0151	0.0030	0.00045	36.7	2.2
I	17.05 – 21.6	0.0863	0.0173	0.00259	0.0735	0.0147	0.00221	29.0	1.3
J	21.6 – 24.1	0.0313	0.0063	0.00094	0.0516	0.0103	0.00155	33.5	1.9
K	24.1 – 27.4	0.0667	0.0133	0.00200	0.0710	0.0142	0.00213	30.9	1.5
L	27.4 – 28.75	0.0176	0.0035	0.00053	0.0208	0.0042	0.00063	35.9	2.1
M	28.75 – 35.15	0.0901	0.0180	0.00271	0.0900	0.0180	0.00270	27.5	1.4
N	35.15 – 40.35	0.0174	0.0035	0.00052	0.0203	0.0041	0.00061	35.1	2.1
O	40.35 – 44.25	0.0811	0.0162	0.00244	0.0782	0.0156	0.00235	29.4	1.4
P	44.25 – 45.55	0.0200	0.0040	0.00060	0.0302	0.0060	0.00091	34.3	2.0
Q	45.55 – 46.7	0.0615	0.0123	0.00185	0.0531	0.0106	0.00159	29.8	1.5
R	46.7 – 49.05	0.0164	0.0033	0.00049	0.0298	0.0060	0.00090	35.6	2.1

7.3.1.2 Chioggia: external breakwater

Figure 7.24: Construction history of the breakwater in the Chioggia Inlet (images taken from the website salve.it)

The construction of the approximately 550-m-long curved breakwater is assumed to have started in April 2004 according to the sequence of construction works found in the website *salve.it* (see figure above). Figure 7.25 indicates the 3 cross-sections selected for the numerical analysis passing through the piezocone verticals (C1, C2 and C3).

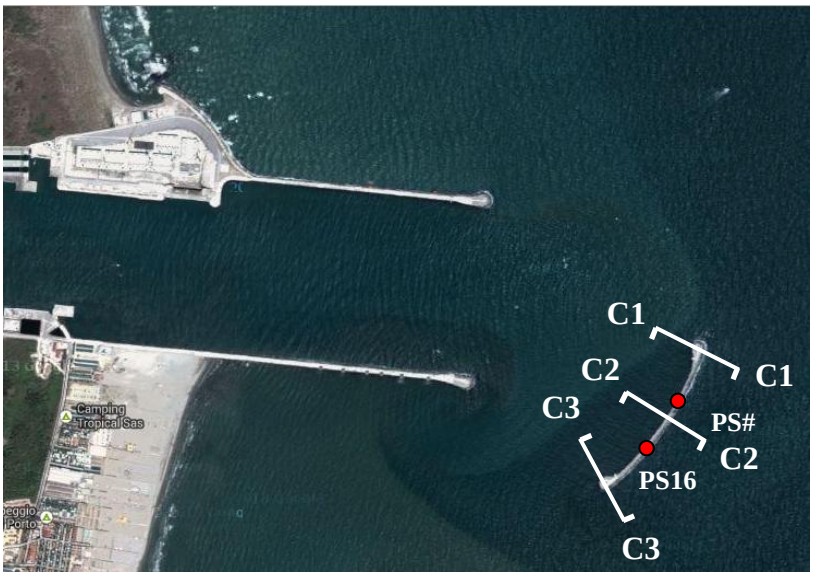

Figure 7.25: Location of the examined cross-sections in the Chioggia breakwater and location of radar reflectors (satellite view)

The different layer distribution for each section is shown in Figures 7.26-7.28. In the same way as in Malamocco sections, in order to capture more details of the variation of the $C_{\alpha\varepsilon}$ values along the depth, the subsoil was divided into several sub-layers, which vary in number from 10 to 11. It is worth to note here that the number of sub-layers identified for the Chioggia sections is smaller than that obtained for the Malamocco ones due to the less variability of the $C_{\alpha\varepsilon}$ values observed within the main units.

The input parameters for the SSC model are summarized in Tables 7.5-7.7. As in Malamocco sections, sets 1 and 2 have been considered, depending on the empirical correlation initially adopted to estimate $C_{\alpha\varepsilon}$ (Equations (5.5) or (5.6), respectively). The selected *OCR* and ϕ' for the specific range of depths are also specified.

As can be observed in these tables, the topmost soil layer (A) and the layers between approximately 10 to 25 m and 35 to 50 m represent the stiffest formations, with *OCR*-values in the range of 2÷3.3. The most compressible layers are generally identified at the second soil type (formation B) and at depths between 24 to 36 m below the seabed.

As in the Malamocco analyses, it was assumed that the material behaviour of the subsoil and the breakwater was drained. In this way, the consolidation process has been not investigated.

The total height of the breakwater and the water level for each section was retraced from available cross-section images and from the piezocone tests. Heights of the embankments fluctuate between 10.4 and 13.9 m, corresponding to sections C3 – C3 and C1 – C1 respectively. Uncertainties within the horizontal dimensions entails the assumption of some geometry simplifications.

The purpose of the analysis is to find the long-term vertical displacements in the soil from March 2008 to January 2009. To avoid any influence of the outer boundaries and to observe the settlements of the subsoil outside the loaded area, the model is extended in horizontal direction to a large radius.

When the geometry model was completed, the mesh was generated. The *Element distribution* was first set to *very fine* option in order to gain optimum performance. Afterwards a local mesh refinement procedure was used within clusters defined under the loaded area, where large deformation gradients were expected.

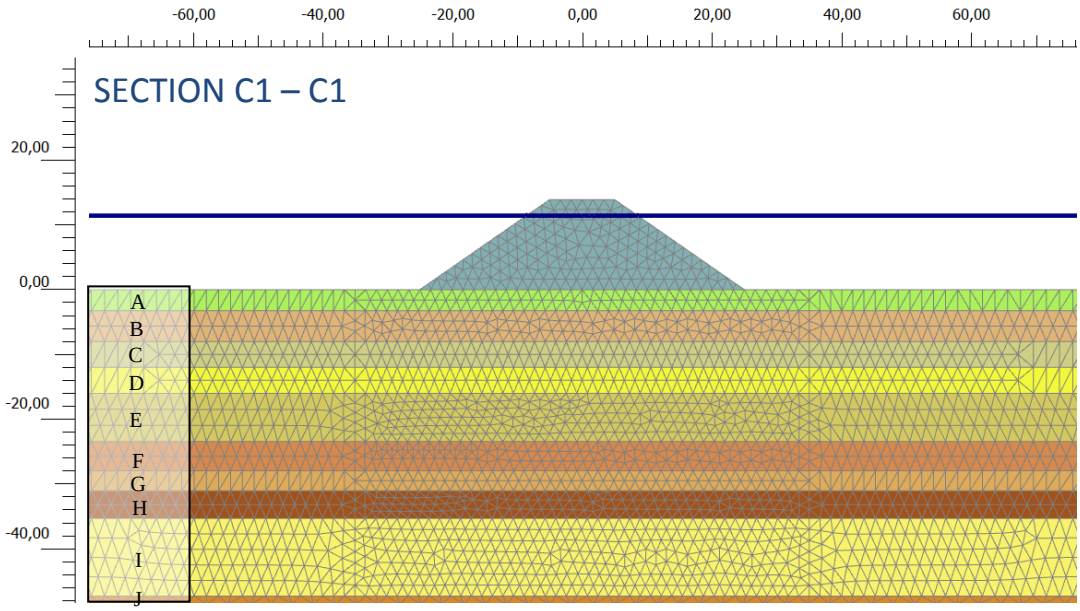

Figure 7.26: Finite element mesh for Section C1 – C1

Table 7.5: Soft Soil Creep model parameters used in Section C1- C1

Layer	Depth (m)	Material Set 1			Material Set 2			Φ' (°)	OCR
		$\lambda^*_{(1)}$	$k^*_{(1)}$	$\mu^*_{(1)}$	$\lambda^*_{(2)}$	$k^*_{(2)}$	$\mu^*_{(2)}$		
A	0 – 3.25	0.0208	0.0042	0.00062	0.0211	0.0042	0.00063	34.0	2.4
B	3.25 – 8	0.0511	0.0102	0.00154	0.0211	0.0042	0.00063	35.0	1.5
C	8 – 12	0.0085	0.0017	0.00026	0.0085	0.0017	0.00026	39.0	2.6
D	12 -16	0.0057	0.0011	0.00017	0.0045	0.0009	0.00014	41.1	2.7
E	16 – 23.45	0.0074	0.0015	0.00022	0.0060	0.0012	0.00018	39.3	2.5
F	23.45 – 27.95	0.0650	0.0130	0.00195	0.0590	0.0118	0.00177	31.7	1.6
G	27.95 – 31.05	0.0259	0.0052	0.00078	0.0289	0.0058	0.00087	34.2	2.0
H	31.05 – 35.3	0.1038	0.0208	0.00312	0.0811	0.0162	0.00244	29.4	1.3
I	35.3 – 47.3	0.0114	0.0023	0.00034	0.0124	0.0025	0.00037	36.8	2.2
J	47.3 – 48.55	0.0785	0.0157	0.00236	0.0673	0.0135	0.00202	30.3	1.4

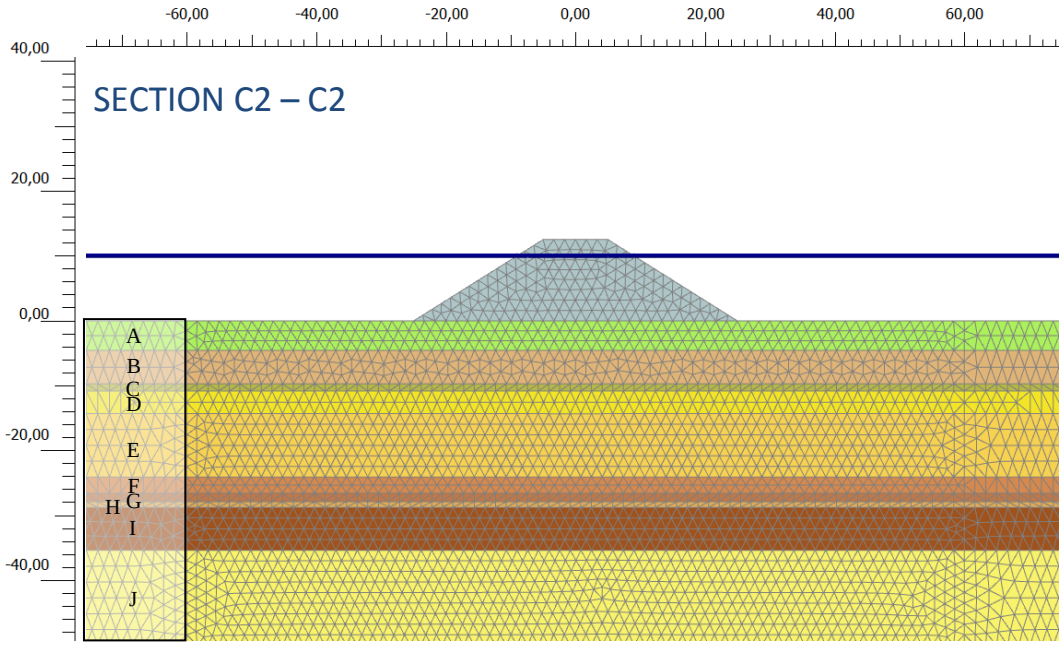

Figure 7.27: Finite element mesh for Section C2 – C2

Table 7.6: Soft Soil Creep model parameters used in Section C2- C2

Layer	Depth (m)	Material Set 1			Material Set 2			Φ' (°)	OCR
		$\lambda^*_{(1)}$	$k^*_{(1)}$	$\mu^*_{(1)}$	$\lambda^*_{(2)}$	$k^*_{(2)}$	$\mu^*_{(2)}$		
A	0 – 4.55	0.0120	0.0024	0.00036	0.0092	0.0018	0.00028	36.9	2.7
B	4.55 – 9.70	0.0881	0.0176	0.00265	0.0511	0.0102	0.00154	33.5	1.2
C	9.70 – 10.80	0.0171	0.0034	0.00051	0.0130	0.0026	0.00039	36.5	2.2
D	10.80-14.30	0.0048	0.0010	0.00014	0.0033	0.0007	0.00010	41.8	2.9
E	14.30-24.05	0.0077	0.0015	0.00023	0.0060	0.0012	0.00018	39.4	2.5
F	24.05-26.55	0.0375	0.0075	0.00113	0.0324	0.0065	0.00097	34.6	1.8
G	26.55-27.85	0.0783	0.0157	0.00235	0.0715	0.0143	0.00215	28.8	1.4
H	27.85-28.75	0.0216	0.0043	0.00065	0.0195	0.0039	0.00059	34.3	2.0
I	28.75-35.35	0.0917	0.0183	0.00275	0.0861	0.0172	0.00259	28.2	1.4
J	35.35-49.95	0.0126	0.0025	0.00038	0.0138	0.0028	0.00041	36.5	2.2

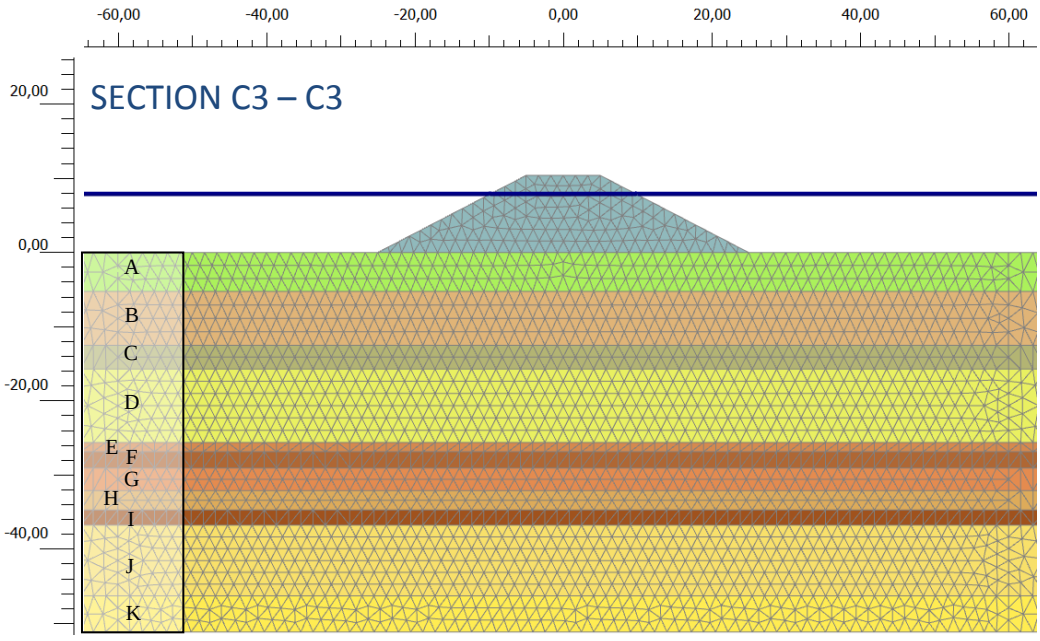

Figure 7.28: Finite element mesh for Section C3 – C3

Table 7.7: Soft Soil Creep model parameters used in Section C3- C3

Layer	Depth (m)	Material Set 1			Material Set 2			Φ' (°)	OCR
		λ^* (1)	k^* (1)	μ^* (1)	λ^* (2)	k^* (2)	μ^* (2)		
A	0 – 5.25	0.0062	0.0012	0.00018	0.0054	0.0011	0.00016	40.7	3.3
B	5.25 –12.5	0.0767	0.0153	0.00230	0.0519	0.0104	0.00156	31.9	1.4
C	12.5 – 15.7	0.0198	0.0040	0.00059	0.0256	0.0051	0.00077	35.9	2.1
D	15.7 -25.6	0.0094	0.0019	0.00028	0.0086	0.0017	0.00026	38.5	2.4
E	25.6 – 26.85	0.0554	0.0111	0.00166	0.0452	0.0090	0.00136	31.0	1.6
F	26.85 – 29.05	0.1240	0.0248	0.00372	0.1016	0.0203	0.00305	30.2	1.2
G	29.05 – 32.1	0.0646	0.0129	0.00194	0.0669	0.0134	0.00201	31.7	1.6
H	32.1 – 34.7	0.0257	0.0051	0.00077	0.0306	0.0061	0.00092	34.1	1.9
I	34.7 – 36.75	0.1295	0.0259	0.00389	0.1123	0.0225	0.00337	28.0	1.2
J	36.75 – 46.3	0.0207	0.0041	0.00062	0.0267	0.0053	0.00080	34.1	2.0
K	46.3 – 51.1	0.0148	0.0030	0.00044	0.0149	0.0030	0.00045	35.8	2.2

7.3.2 Calculation stages

Initial Phase

In PLAXIS, an *Initial Phase* is used to defined the initial conditions. The initial conditions comprise the initial groundwater conditions, the initial geometry configuration and the initial effective stress. The initial stresses in a soil are influenced by the weight of the material and its history formation. The stress state is characterized by an initial vertical effective stress, σ'_{v0} and by an effective horizontal stress, σ'_{h0}. The horizontal effective stress σ'_{v0} is related to the vertical effective stress by the coefficient of lateral earth pressure $K_0 = \sigma'_{h0} / \sigma'_{v0}$.

In this study, initial stresses were generated by using the K_0 - *procedure* available in PLAXIS. This procedure is a calculation method used to define the initial stresses for the model that takes into consideration the stress history of the soil.

The parameters required for the K_0 - procedure are defined when material properties were introduced in the material data sets. The value of K_0 for normally consolidated soils is calculated using the Jaky's formula:

$$K_0^{NC} = 1 - \sin\varphi \tag{7.45}$$

In an overconsolidated soil, K_0 would be expected to be larger than the value given by the one obtained for a normally consolidated soil. This effect is automatically taken into account for advanced soil models when generating the initial stresses using K_0 – procedure. The procedure that is followed is described in the PLAXIS MANUAL.

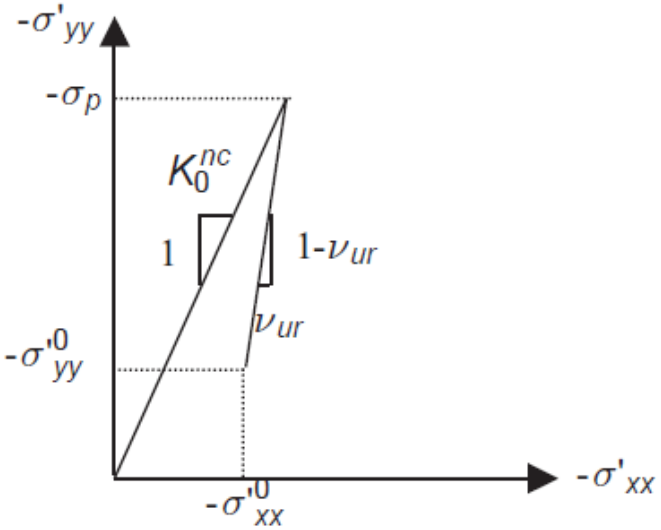

Figure 7.29: Overconsolidated stress state obtained from primary loading and subsequent unloading (figure taken from PLAXIS MANUAL)

Considering a one-dimensional compression test, preloaded to σ_p and then unloaded to σ'^{0}_{yy}. During unloading the behaviour of the sample is elastic and the incremental stress ratio, according to Hooke's law, is given by:

$$\frac{\Delta\sigma'_{xx}}{\Delta\sigma'_{yy}} = \frac{K_0^{NC}\sigma_P - \sigma'^{0}_{XX}}{\sigma_P - \sigma'^{0}_{YY}} = \frac{K_0^{NC}OCR\sigma'^{0}_{YY} - \sigma'^{0}_{XX}}{(OCR-1)\sigma'^{0}_{YY}} = \frac{\nu_{ur}}{1-\nu_{ur}} \tag{7.46}$$

Consequently the default stress ratio of the overconsolidated soil sample is given by:

$$\frac{\sigma'^{0}_{XX}}{\sigma'^{0}_{YY}} = K_0^{NC}OCR - \frac{\nu_{ur}}{1-\nu_{ur}}(OCR-1) \tag{7.47}$$

where ν_{ur}=0.15 is used if the standard setting for the SSC model parameters is selected and the *OCR*-value for each layer of the different sections here studied have been already defined in Tables 7.5-7.7.

Plastic phases

The breakwater construction would consist in a number of phases, each of them simulated by activating the different parts of the structure according to the real construction sequence. As the construction history was unknown by this author and irrelevant for this study purposes, only one phase was used to simulate the total load applied. Consequently, the calculation stage of *Phase* 1 is a *Plastic* analysis, *Staged construction*.

In this phase, the part of the geometry representing the breakwater is activated. As the *Soft Soil Creep* model is used, the *Time interval* of the calculation phase should be considered. Time intervals of 580 days (June 2003-January 2005) and 275 days (April 2004-January 2005) have been considered for Malamocco and Chioggia cases, respectively. In both of them, January 2005 has been supposed to be the date of the end of the works.

Phase 2 and *Phase* 3 are two additional phases in which no changes to the geometry were made. In *Phase* 2, a time interval of 1159 days in entered, which is the period between the end of construction (January 2005) and the start of the PS records (March 2008). Finally, *Phase* 3 is used to simulate the creep behaviour of soils in a period of 330 days (from March 2008 to January 2009). Settlements developed in this last phase were compared with those detected by PSI from March 2008 to January 2009 using TerraSAR-X images.

7.3.3 Results

In the analysis of the long-term settlements of the breakwater, the attention has been focused on the time interval March 2008 – January 2009 for which PSI measurements were available. A comparison between measured vertical displacements and predicted settlements under the centre of the breakwater are provided in Figures 7.30 and 7.31, showing the numerical results obtained

from both the parameter sets λ^*_1, μ^*_1, κ^*_1 and λ^*_2, μ^*_2, κ^*_2. Measured settlements are associated with the radar reflectors (see Figures 7.19 and 7.25), located close to the piezocone verticals assumed as a base for soil layering and geotechnical characterization.

Despite some simplified assumptions adopted in the analysis, the trend settlement at the Malamocco breakwater is generally well captured by the numerical model, with similar responses obtained from the two alternative sets of stiffness parameters. Note that the computed outcomes fit better the PS11 measurements in all sections except for M3 – M3.Besides, the prediction using *Set* 1 provides slightly higher values than *Set* 2.

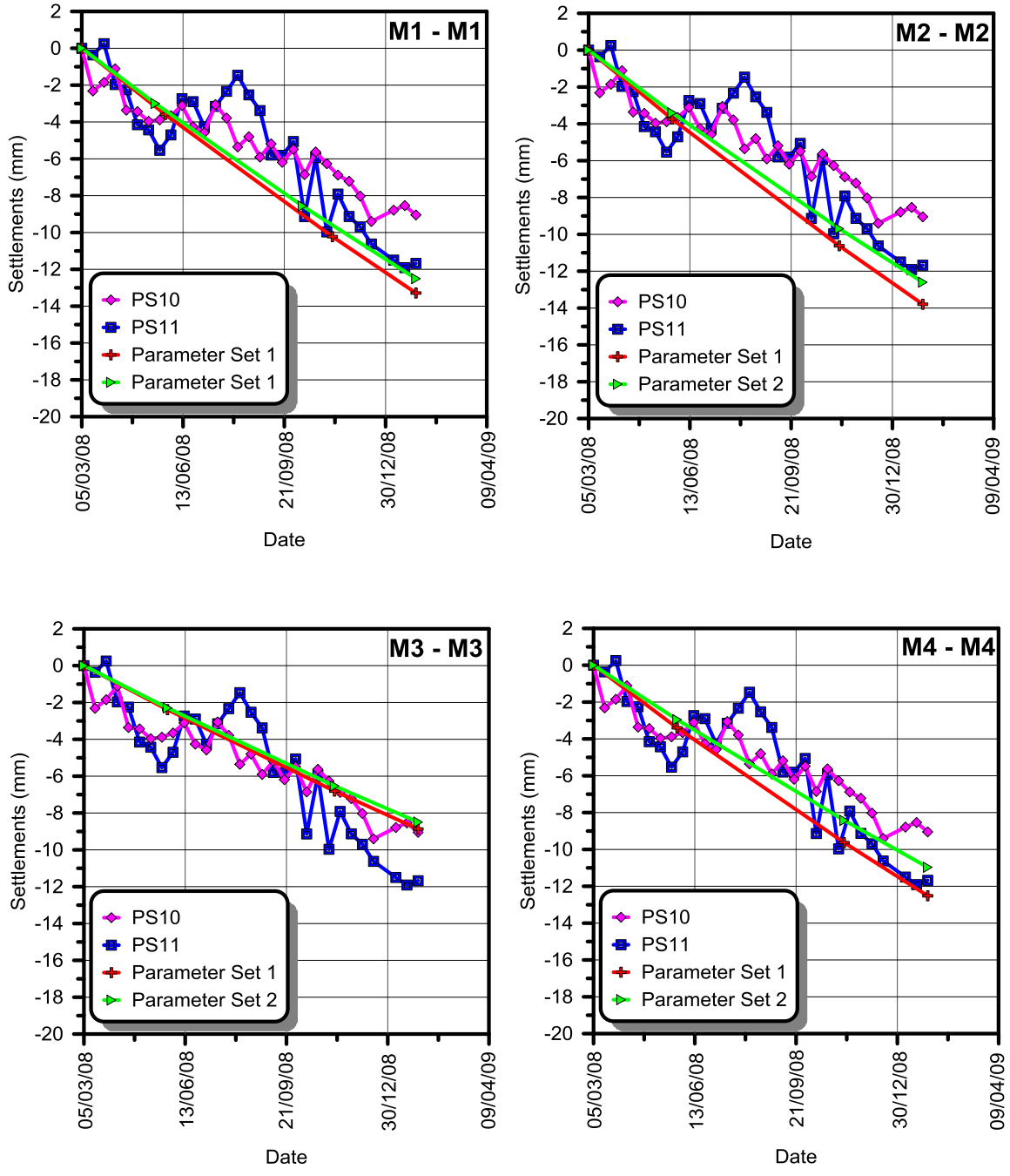

Figure 7.30: Comparison between the predicted secondary settlements and the measurements detected by PSI at the Malamocco breakwater

At the Chioggia inlet, the predicted and the recorded displacements trends of the breakwater clearly show a certain difference among them, being more evident when *Set* 2 is used. That difference increases towards the northern portion of the structure.

In order to gain a better insight into the subsoil deformation process, the profile of the integral vertical displacements computed beneath the centre of the selected sections of each breakwater is provided in Figures 7.32 and 7.33. The greatest differences between the two trends depicted (*Set 1* and *Set 2*) in each plot are observed in the fine-grained layers, particularly evident in Chioggia profiles.

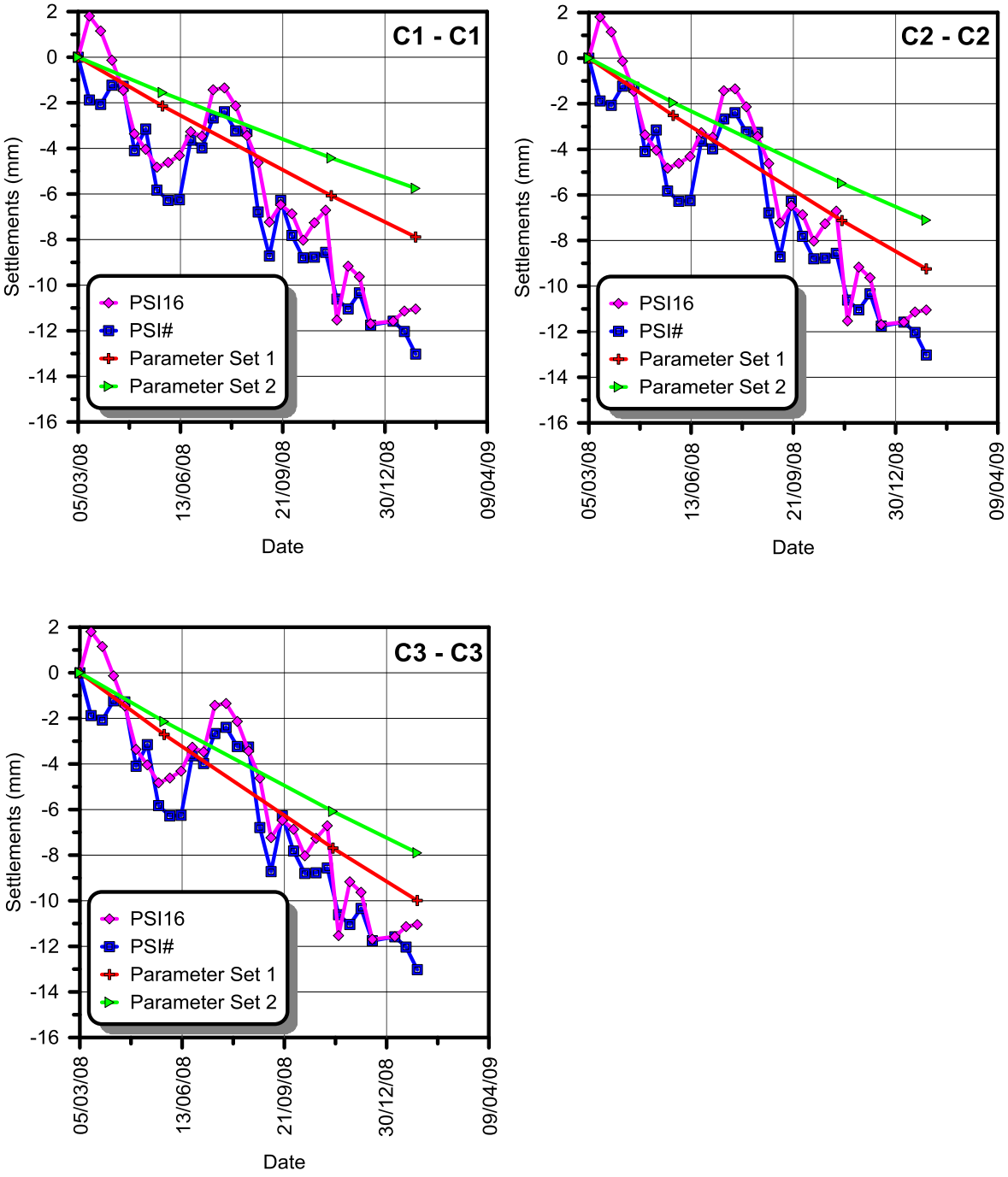

Figure 7.31: Comparison between the predicted secondary settlements and the measurements detected by PSI at the Chioggia breakwater

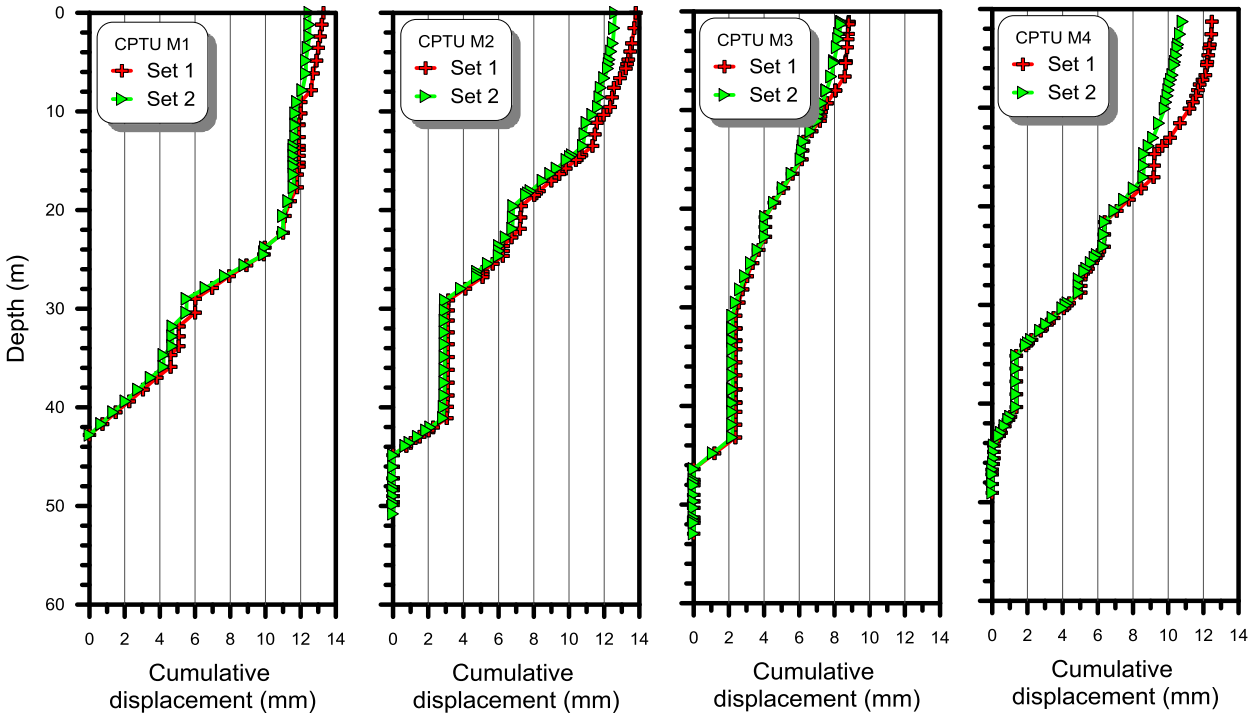

Figure 7.32: Predicted integral vertical displacement at the end of the period March 2008-January 2009 from Malamocco piezocone tests

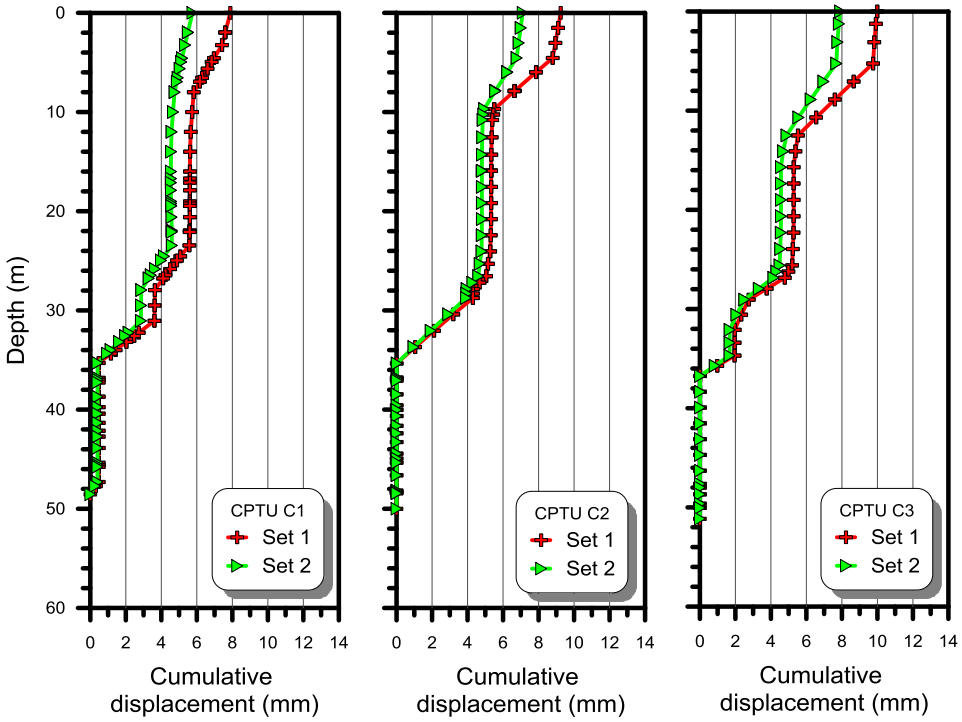

Figure 7.33: Predicted integral vertical displacement at the end of the period March 2008-January 2009 from Chioggia piezocone tests

Some remarks about drained and undrained analysis

In Section 7.3.2, calculations have been performed assuming drained conditions in order to demonstrate the time-settlement response in the long term. In this section the process is simulated by including undrained material type and consolidation analysis in all calculation stages. The section M2-M2 from Malamocco breakwater has been selected for this purpose.

In each calculation phase, the subsoil is left to consolidate for a predefined period, including the effects of changes to the geometry. The part of the geometry representing the embankment is activated in the *Construction* phase, which follows the *Initial* phase. In the next phases no changes in the geometry are made.

Figure 7.34 shows the time-settlement curve of the undrained analysis (blue line). As in the case of Treporti Test Site, primary consolidation seems to take place during the embankment construction ($t_{100} \approx 580$ days). The figure also includes the curve from the drained analysis for comparison. As evident, the predicted settlements provided by both analysis are almost the same. In particular, the vertical displacements from the drained and the undrained analysis, from March 2008 to January 2009 are, respectively, 12.62 mm and 13.46 mm.

Finally, the green line represents the settlements predicted performing a drained calculation but without any load being applied, just to let the soil creep under its self weight. From Figure 7.34, it turns out that settlement rates vary approximately from 6.5 mm/year at the beginning to 3.2 mm/year when the soil has not been disturbed for years. Differences between creep strain rates from the analyses carried out applying the bank load (red and blue lines) and that without any load (green line) are due to the dependence of the creep strain rate on the mean effective stress.

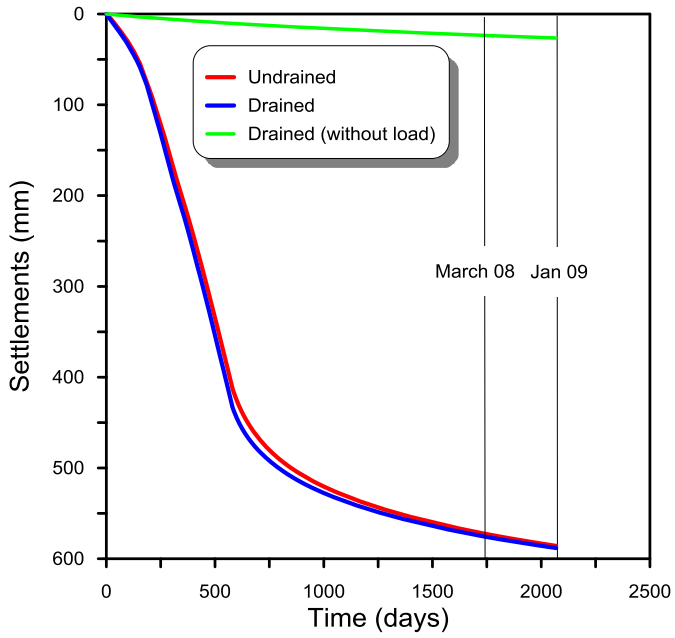

Figure 7.34: Settlement predictions at the breakwater centreline (section M2-M2)

7.4 Three-dimensional numerical modelling

In this section, the numerical analysis of the long-term performance of the Chioggia external breakwater has been carried out using the finite element code PLAXIS 3D in conjunction with the *Soft Soil Creep* model.

This could be considered a useful starting point for the three-dimensional analysis, taking into account the horizontal spatial variability of the Venetian subsoil. A crucial step at this stage consists in adopting some simplifications so as to identify soil patterns that can be described with a model. Nevertheless, difficulties in identifying trends arise when dealing with highly heterogeneous soils, such those forming the Venice lagoon basin.

The significant variability of data from CPT results, either in measured or correlated parameters, should be taken into account statistically during the selection of the characteristic values of each parameter. However, obtaining characteristic values of correlated parameters from CPT could be complicated and on this aspect not precise guidelines exist (Myftaraga and Koreta, 2013). In this way, the interpretation of the computed $C_{\alpha\varepsilon}$ values from CPTUs C1, C2 and C3, in order to select appropriate characteristic values for the soil units depicted in Figure 7.35, was a complicated task.

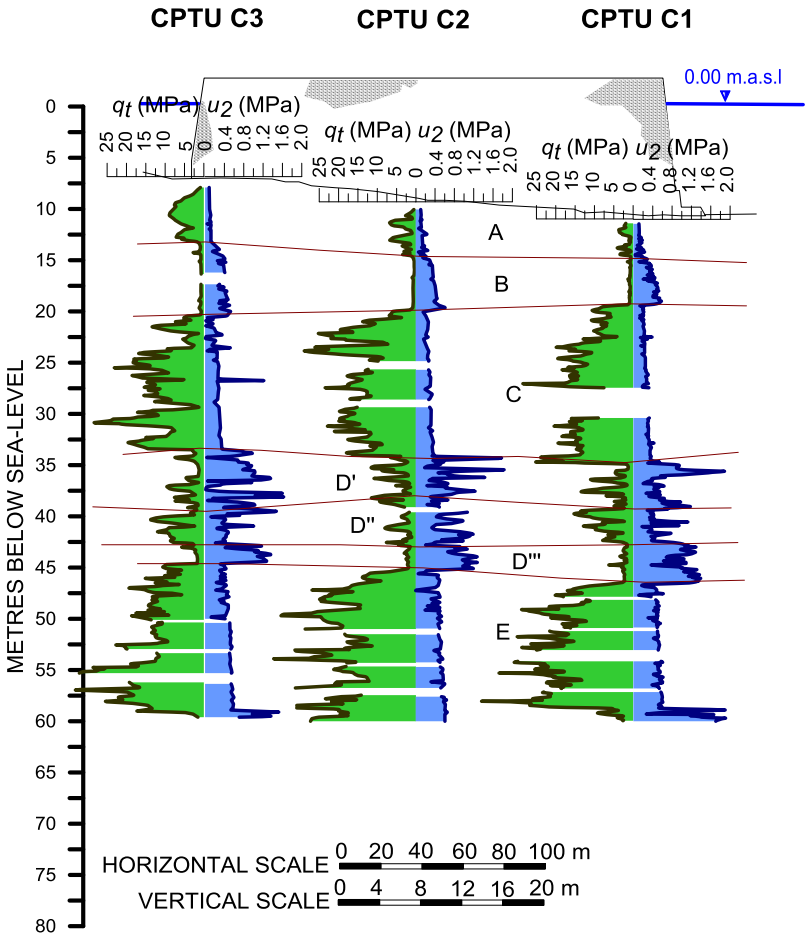

Figure 7.35: Cross section of the test-site area

The computed $C_{\alpha\varepsilon}$, obtained from the application of Equations (5.5) and (5.6) to piezocone tests C1, C2 and C3 are shown in Section 7.3.1 (Figure 7.11). The simple mean value of the $C_{\alpha\varepsilon}$ for each soil unit has been considered herein as the characteristic value and has been used to derive the stiffness parameters required in the SSC model.

The same approach applies when selecting characteristic values of the overconsolidation ratio *OCR* and the friction angle ϕ'. The correlations used to estimate these soil parameters have been already shown in Section 7.3.1.

However, it is worth remarking here that the residuals of $C_{\alpha\varepsilon}$, calculated as the difference between the predicted value for each data point and the mean value, did not show in all layers a good agreement with the theoretical normal distribution ($\bar{x} = 0$), questioning in this way the applicability of the simple mean approach.

The material parameters used in the FE analysis are summarized in Table 7.8. As in the 2D numerical analysis, two alternative sets of stiffness parameters have been considered, depending on the empirical correlation initially adopted to estimate $C_{\alpha\varepsilon}$.

A linear elastic behaviour has been assumed for the 13.8 m high breakwater. On the other hand, a horizontal seabed has been supposed and the water table has been located at 11.4 m above the seabed.

The drainage type for all clusters was set to *drained*. As in the 2D numerical analysis, the consolidation process has been not investigated.

Finally, the mesh was generated setting *Element distribution* to *very fine* option.

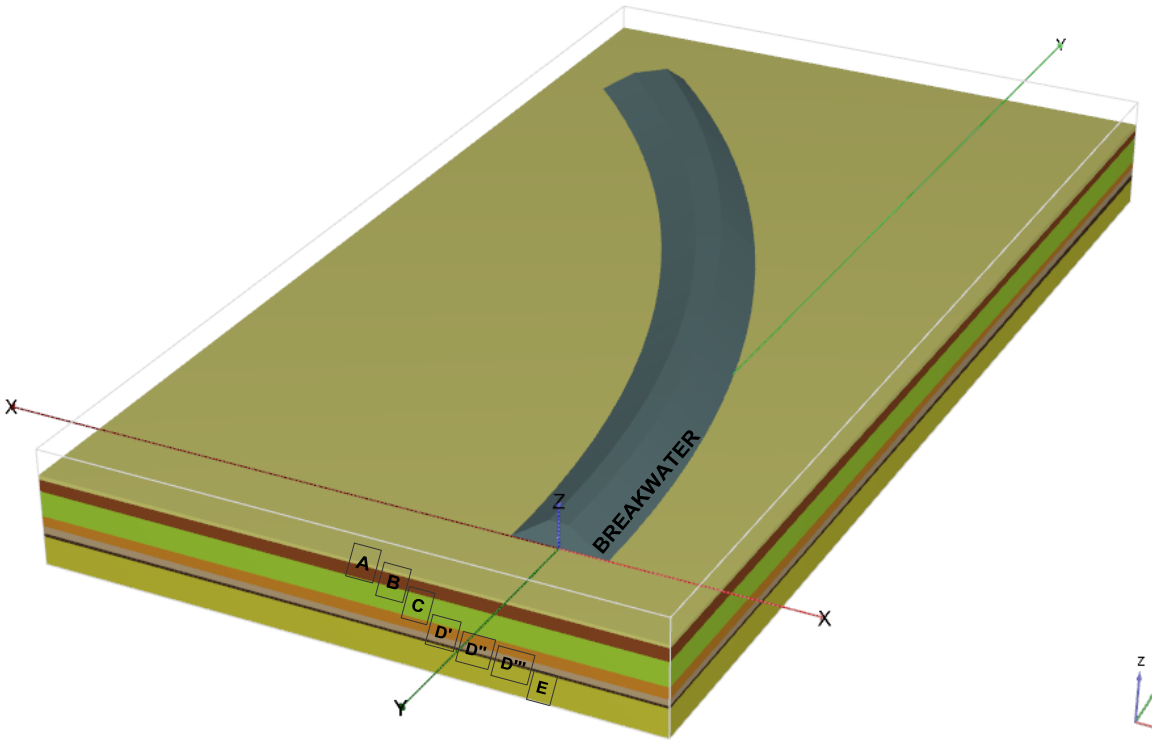

Figure 7.36: Overview of the model in PLAXIS 3D

Table 7.8: SSC Model parameters for selected soil layers

Layer	Material Set 1			Material Set 2				
	λ^* (1)	k^* (1)	μ^* (1)	λ^* (2)	k^* (2)	μ^* (2)	Φ' (°)	OCR
A	0.0113	0.0023	0.00034	0.0093	0.0019	0.00028	38.0	2.9
B	0.0734	0.0147	0.00220	0.0430	0.0086	0.00129	33.4	1.4
C	0.0094	0.0019	0.00028	0.0084	0.0017	0.00025	39.1	2.5
D'	0.0700	0.0140	0.00210	0.0628	0.0126	0.00188	31.6	1.5
D''	0.0443	0.0089	0.00133	0.0465	0.0093	0.00139	32.4	1.8
D'''	0.1178	0.0236	0.00353	0.0941	0.0188	0.00282	28.5	1.2
E	0.0162	0.0032	0.00049	0.0178	0.0036	0.00053	35.6	2.1

In the analysis of the long-term settlements of the approximately 550-m-long curved breakwater, the attention has been focused again on the time interval March 2008 – January 2009 for which PSI measurements were available, taking into account that the construction of the structure started in 2004.

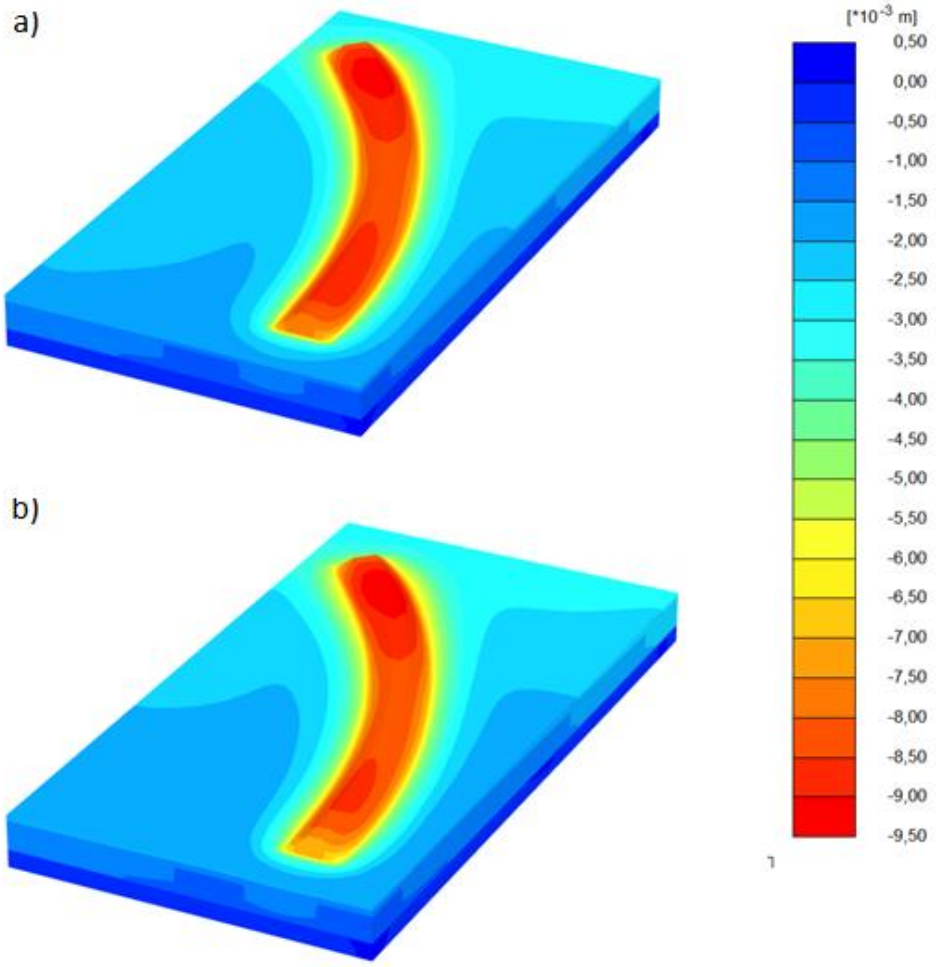

Figure 7.37: Vertical displacements at stage "January 2009" using parameters from a) Material Set 1 and b) Material Set 2

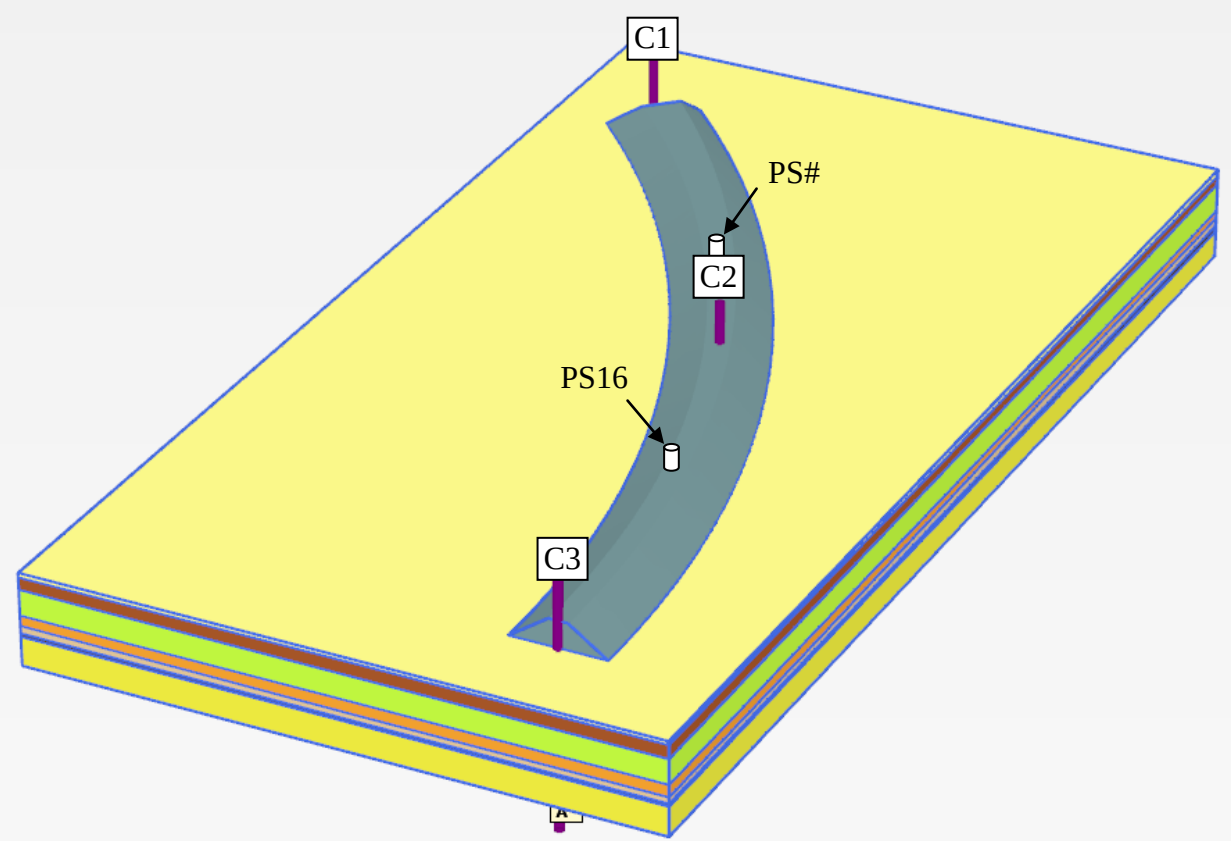

Figure 7.38: Overview of the location of the selected points and radar reflectors (Persistent Scatterer, PS)

Figure 7.39 shows the predicted settlements under the breakwater at three different points, placed close to piezocone tests locations (see Figure 7.38), and the measured vertical displacements plotted versus time. The numerical results were obtained from both parameter sets λ^*_1, μ^*_1, κ^*_1 and λ^*_2, μ^*_2, κ^*_2. Measured settlements are associated with the radar reflectors PS# and PS16, located between the piezocone soundings C1 and C2 and C2 and C3 respectively.

As in the previous two-dimensional analysis, the predicted soil response results in a stiffer behaviour compared to the recorded displacements. The settlements measured from March 2008 to January 2009 are in all cases underestimated by the isotropic soft soil creep model. Furthermore, the trends obtained using parameters from *Material Set 2* predict smaller settlements compared with those predicted using parameters from *Material Set 1*. In fact, the coefficient of variation (CoV) of the computed $C_{\alpha\varepsilon}$ using Equation (5.6) varies between high percentages, particularly in the sandy units.

In order to get a better insight into the deformation process, the profiles of the integral vertical displacements computed beneath the breakwater at the selected points are provided in Figure 7.40. Note that the contribution to total settlements of the thick silty sand layers (Unit C and E in Figure 7.35) is negligible.

Despite the differences observed between the predicted and measured trends, it should be taken into account that only a relative small period of time has been examined. In addition, the

simplified assumptions adopted in the analysis, regarding the structure dimensions, seabed position or time intervals, may have contributed to disagreement in trends.

Furthermore, Equation (5.14) seems to provide rather overestimated *OCR*-values in the coarse-grained layers. As a result, this can also have contributed to the underprediction of the secondary settlements.

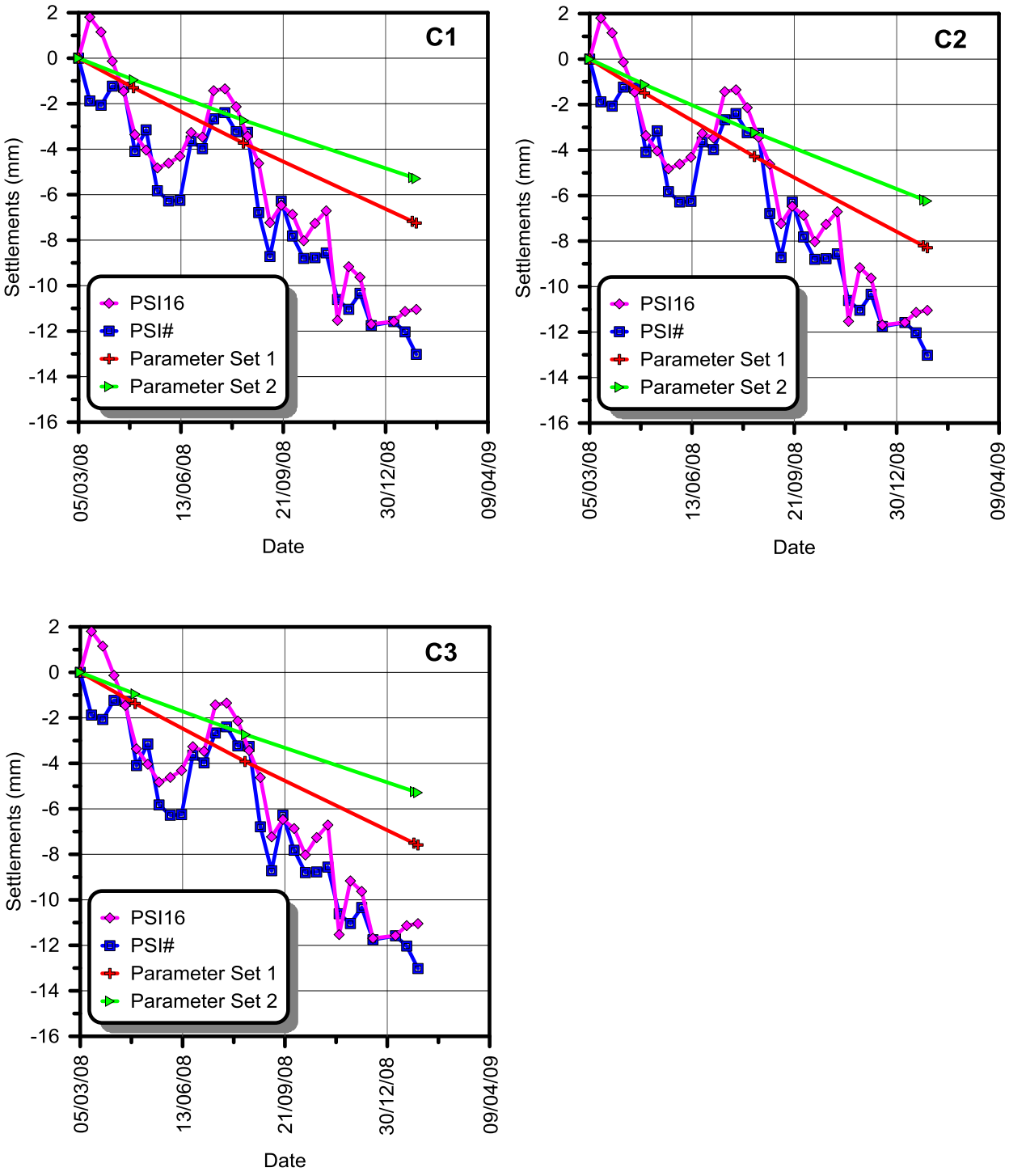

Figure 7.39: Comparison between the predicted secondary settlements and the measurements detected by PSI at the Chioggia breakwater

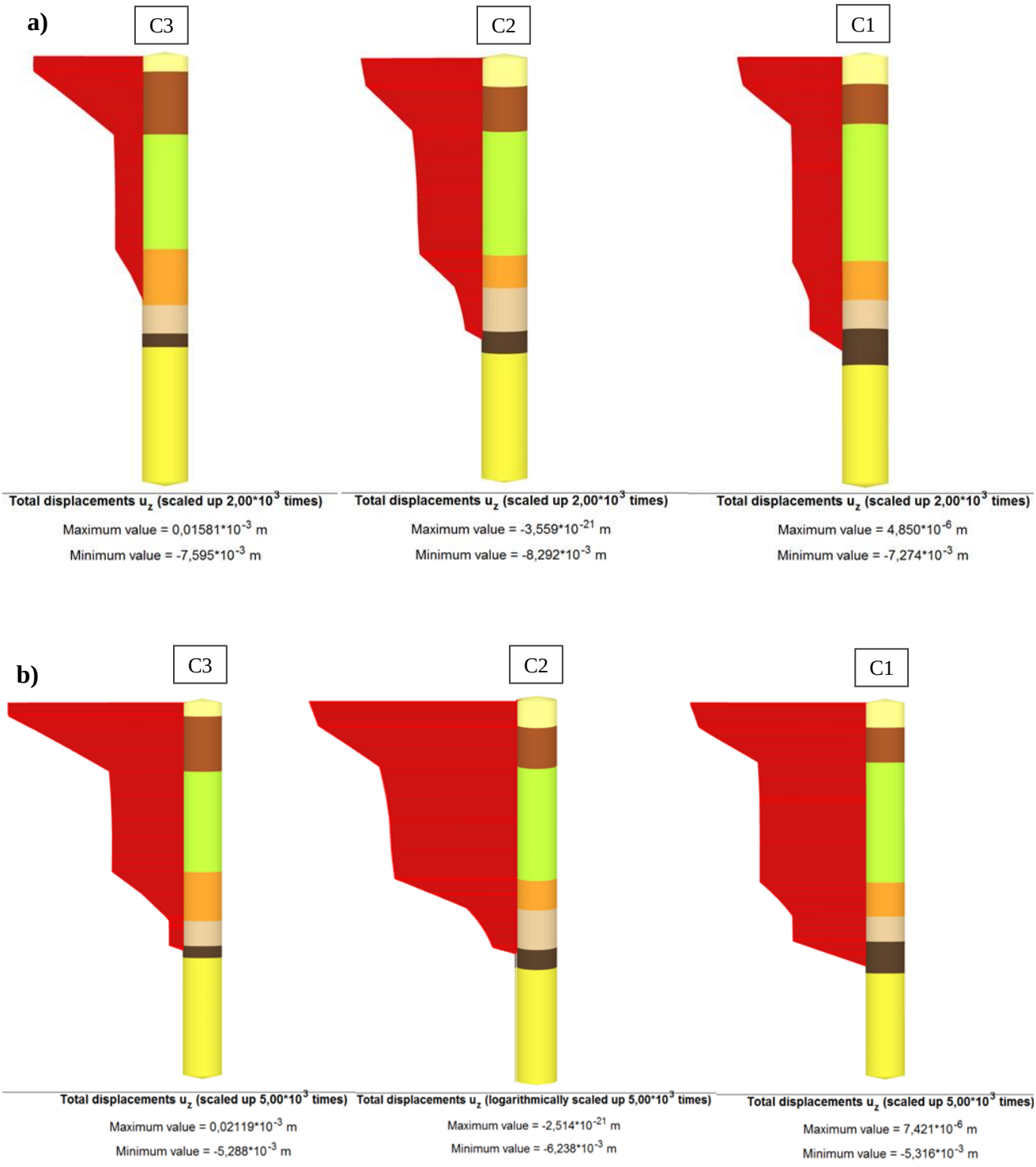

Figure 7.40: Predicted integral vertical displacement from March 2008 to January 2009 using parameters from a) Material Set 1 and b) Material Set 2 (Plaxis output)

Conclusions

Geotechnical characterization of intermediate soils (e.g. silts, silt mixtures and sand mixtures) must generally rely on in-situ testing, since in these materials undisturbed sampling is in general difficult to obtain. In the context of site investigations, cone penetration (with or without pore pressure measurements) is probably the most widely used in-situ testing technique for geotechnical characterization. However, the interpretation of cone penetration test results in intermediate soils has turned out to be rather difficult, because the experience so far gained has shown that such soils do not fit easily into existing interpretation framework.

Indeed, cone penetration at the standard penetration rate (20 mm/s) in intermediate soils is likely to be partially drained. The uncertainty with regard to the extent of partial consolidation during penetration supposes an obstacle to the estimate of the soil behaviour type and properties of such soils.

The study proposed in this thesis aims at providing a better understanding and interpretation of cone penetration data in intermediate soils. For this purpose, the thesis has been organized in two main parts. In the first part, attention has been focused on the analysis of rate effects on cone penetration measurements, taking into account some new field data obtained from piezocone tests in natural sand and silt mixtures. The main idea was to identify drainage conditions when CPTU are performed at a standard rate, since this condition is likely to strongly affect field measurements and therefore it should be taken into careful consideration in order to properly interpret the resulting data in terms of geotechnical parameters. Previous experiences in the context of variable rate CPTU tests have mainly dealt with centrifuge physical models and predominantly fine sediments, like clays or silty clays. By contrast, this study has provided a preliminary contribution in the analysis of the rate effects on natural sand and silt mixtures using a full size penetromter.

Following recent interpretation procedures proposed in the literature, the available data have been analyzed in terms of normalized CPTU measurements and normalized velocity, so as to derive trend curves of cone resistance and excess pore pressure. The transition point from undrained to partially drained and drained responses has been investigated. Although the interpretation of field tests turned out to be a difficult task because of heterogeneous soil stratigraphy, the in-situ behaviour of some data sets substantially confirmed the response already observed in laboratory test results.

A future extension of this study would require additional variable rate CPTU tests in order to get a better definition of the normalized drainage characteristic curve for these intermediate soils, with special reference to tests performed at high penetration velocities. Furthermore, difficulties in defining the normalized velocities at which drained and undrained conditions begin can be due

to the uncertainties about the evaluation of the horizontal coefficient of consolidation (c_h). The analysis has shown difficulties for deriving a suitable value of c_h and the available approaches proposed by other authors have shown significant limitations when applied to different data.

Furthermore, the study has focused on the interpretation of CPTU tests in silty sediments of the Venetian lagoon that are widely recognized as the most studied silty sediments worldwide. This part of the thesis has been developed in the context of the ambitious research project carried out in the last decade at the Treporti Test Site, with the aim of better understanding the stress-strain-time response of the predominantly silty sediments forming the Venetian lagoon basin. The experience gained on the interpretation of piezocone data in such silty sediments has revealed significant limitations of the available and well-established empirical correlations, developed for the geotechnical characterization of sands and clays and thus based on a stiff distinction between drained and undrained conditions. On the basis of the large amount of data, more suitable site-specific correlations calibrated in the context of the Trepoti research project, were proposed (e.g. Tonni *et al*., 2010; Tonni and Gottardi, 2011; Bersan *et al*., 2012; Tonni and Simonini, 2013). This study provides an attempt to validate such site-specific formulations to independent cases within the area of the Venetian lagoon, with particular reference to the assessment of the long-term response of the Venetian coastal defences. This is likely to provide a significant contribution to the geotechnical engineering practice in the area.

Accurate measurements of long-term settlements of some coastal defence structures recently constructed along the Venetian coastline have allowed evaluating the predictive capability of two slightly different empirical relationships between piezocone measurements and the secondary compression coefficient ($C_{\alpha\varepsilon}$). The application of the one-dimensional settlement method in conjunction with the $C_{\alpha\varepsilon}$ profiles provided long-term settlement predictions which agree fairly well with measured displacements, thus confirming the effectiveness of both available correlations.

Furthermore, a numerical analysis of the long-term response of two breakwaters built at inlets of the lagoon has been proposed, using a constitutive formulation specifically developed for simulating the creep behaviour of soft soils. The calibration of the constitutive parameters has been mainly performed by considering CPTU-based empirical correlations proposed for Venetian sediments, such as those for estimating $C_{\alpha\varepsilon}$ as well as the overconsolidation ratio and the oedometric stiffness.

The numerical results have proved the effectiveness of the approach in capturing the creep behaviour of Venetian soils, hence the proposed study can be considered a useful starting point for the analysis of the long-term settlements of the coastal defence structures located in the lagoon area. Nevertheless, it must be observed that a more accurate numerical study of the problem would require a constitutive formulation specifically developed for natural silt mixtures, as the Venetian soils are.

References

Adachi, T. and Oka, F. (1982). Constitutive equation for normally consolidated clays based on elasto-viscoplasticity. *Soils and Foundations,* 22, 57-70.

Augustesen, A., Liingaard, M. and Lade, P.V. (2004). Evaluation of time-dependent behaviour of soils. *Int. J. Geomechanics,* 4(3), 137-156.

Been, K. and Jefferies, M. (1985). A state parameter for sands. *Geotechnique*, 35(2), 99-112.

Been, K., Crooks, J.H.A, Becker, D.E. and Jefferies, M.G. (1986). The cone penetration tests in sand: part I, state parameter interpretation, *Géotechnique*, 36(2), 239-249.

Been, K., Jefferies, M.G., Crooks, J.H.A and Rothenburg, L. (1987). The cone penetration test in sands: part II, general inference of state. *Géotechnique*, 37(3), 285-299.

Berengo, V. (2010). *Constitutive modelling of the time-dependent behaviour of Venice heterogeneous silts*, Ph.D. thesis, University of Padova.

Berengo, V., Benz, T., Simonini, P. and Leoni, M. (2011). Site monitoring and numerical modelling of trial embankment's behaviour on Venice Lagoon soils. *ISRN Civil Engineering*, ID 378579.

Bersan, S., Cola, S., Simonini, P., Gottardi, G. and Tonni, L. (2012). Secondary compression of Venice lagoon sands and silts from CPTU. *Proc. 4th International Conference on Geotechnical and Geophysical Site Charaterization, ISC-4*, 1, 383-389.

Biscontin, G., Cola, S., Pestana, J.M. and Simonini, P. (2006). Unified compression model for Venice lagoon natural silts. *Journal of Geotechnical and Geoenvironmental Engineering*, 133 (8), 932-942.

Biscontin, G., Pestana, J.M., Cola, S. and Simonini, P. (2001). Influence of grain size on the compressibility of Venice Lagoon soils. *Proceedings of the XV International Conference on Soil Mechanics and Foundation Engineering,* Istanbul, Turkey, Vol. 4, 2801-2804.

Bjerrum, L. (1967). 7th Rankine lecture: Engineering geology of Norwegian normally-consolidated marine clays as related to settlements of buildings. *Géotechnique* 17(1), 81-118.

Bolton, M.D. (1986). The strength and dilatancy of sands. *Géotechnique*, 36(1), 65-78.

Borja, R.I. and Kavaznjian (1985). A constitutive model for the stress-strain time behaviour of 'wet' clays- *Géotechnique* 35(3), 283-298.

Brinkgreve, R.B.J. 2001. The role of OCR in the SSC Model. *Plaxis Bulletin No. 10 (March 2001)*: 12-14.

Buisman, K. (1936). Results of long duration settlement tests. *Proceeding 1st International Conference on Soil Mechanics and Foundation Engineering*, Vol. 1, Cambridge, Massachusetts, 103-107.

Butterfield, R. (1979). A natural compression law for soils (an advance on the e-logp'). Geotechnique, 29, 469-480.

Campanella, R.G. and P.K. Robertson (1988). Current Status of the Piezocone Test. *Proceedings of the First International Symposium on Penetration Testing*, 1, 93-116.

Campanella, R.G., Gillespie, D. and Robertson, P.K. (1982). Pore pressures during cone penetration testing. *Proceedings of the 2nd European Symposium on Penetration Testing*, ESPOT II, Amsterdam. A.A. Balkema, Rotterdam, the Netherlands,. 507-512.

Cetin, K.O. and Isik, N.S. (2007). Probabilistic assessment of stress normalization for CPT data. *J. Geotech. Geoenviron. Eng. ASCE*, 133(7), 887-897.

Chung, S.F., Randolph, M.F. and Schneider, J.A. (2006). Effect of cone penetration rate on penetrometer resistance in clay. *J. Geotech. Geoenviron. Eng.*, 132(9), 1188-1196.

Cola, S. and Simonini, P. (1999). Some remarks on the behaviour of Venetian silts. *Proceedings of the II Inernational Symposium on the Pre-failure Deformation Characteristics of Geomaterial*, Torino, 167-174.

Cola, S. and Simonini, P. (2002). Mecchanical behaviour of silty soils of Venice lagoon as a function of their grading properties. *Canadian Geotech. J*. 39, 879-893.

Cola, S. and Tonni, L. (2007). Adapting a generalized plasticity model to reproduce the stress-strain response of silty soils forming the Venice Lagoon basin. *Solid mechanics and its applica-*

tions, 146, 743-758.

Colombo, P. (1986). La difesa di Venezia dai fiumi e dal mare. *Rivista Italiana di Geotecnica*, 20, 73-92.

Correggiari, A., Roveri, M. and Trincardi, F. (1996). Late Pleistocene and Holocene Evolution of the North Adriatic Sea, *Quaternario*, 9, 2, 697-704.

Crosetto, M., Crippa, B., Biescas, E., Monserrat, O., Agudo, M. and Fernández, P. (2005). Land deformation monitoring using SAR interferometry: state-of-the-art. *Photogrammetr. Fernerkundung Geoinformation*, 6, 497-510.

Crosetto, M., Monserrat, O., Jungner, A. and Crippa, B. (2009). Persistent scatterer interferometry: Potential and limits. *Proceedings of the ISPRS Hannover Workshop 2009 High-Resolution Earth Imaging for Geospatial Information*.

Curzi, P.V. (1995). *Sedimentological-environmental study of the Malamocco inlet: Final report*. Consorzio Venezia Nuova, Venezia.

DeJong, J.T. and Randolph, M. F. (2012). Influence of partial consolidation during cone penetration on estimated soil behaviour type and pore pressure dissipation measurements. *J. Geotechnical and Geoenvironmental. Eng.*, 138(7), 777-788.

DeJong, J.T., Jaeger, R.A., Boulanger, R.W., Randolph, M.F. and Wahl, D.A.J. (2013). Variable penetration rate cone testing for characterization of intermediate soils. *Geotechnical and Geophysical Site Characterization 4*, 25-42. ISBN: 978-1-4665-8418-1

Donda, F., Brancolini, G., Tosi, L., Kovacevic, V., Baradello, L., Gacic, M. and Rizzetto, F. (2008). The ebb-tidal delta of the Venice Lagoon, Italy. *Holocene*, 18(2), 267-278.

Douglas, B.J. and Olsen, R.S. (1981). Soil classification using electric cone penetrometer. *Proceedings of Symposium on Cone Penetration Testing and Experience*, Geotechnical Engineering Division, ASCE. St. Louis, Missouri, October 1981, 209-227.

Eslami, A. and Fellenious, B.H. (1997). Pile Capacity by direct CPT and CPTu methods applied to 102 case histories. *Canadian Geotechnical Journal*, 34(6), 880-898.

Fahey, M. and Carter, J.P. (1993). A finite element study of the pressuremeter in sand using a nonlinear elastic plastic model. *Canadian Geotechnical Journal*, 30(2), 348-362.

Favero V., Alberotanza L. and Serandrei Barbero R. (1973). Aspetti paleoecologici, sedimentologici e geochimici dei sedimenti attraversati dal pozzo VE1bis. CNR, Laboratorio per lo studio della dinamica delle grandi masse, Rapporto tecnicon.63, Venezia.

Finnie, I.M.S. and Randolph, M.F. (1994). Punch-through and liquefaction induced failure of shallow foundations on calcareous sediments. *Proc. Int. Conf. on Behaviour of Offshore Structures, BOSS '94*, Boston, 217-230.

Garlanger, J.E. (1972). The consolidation of soils exhibiting creep under constant effective stress. *Géotechnique* 22(1), 71-78.

Gottardi, G. and Tonni, L. (2004). Use of piezocone tests to characterize the silty soils of the Venetian lagoon (Treporti test site*). Proc. ISC-2 on Geotech. And Geophysical Site Charaterization*, Porto, 1643-1650.

Gottardi, G. and Tonni, L. (2005). The Treporti test site: exploring the behaviour of the silty soils of the Venetian lagoon. *Proceedings of the 16th International Conference on Soil Mechanics and Geotechnical Engineering (ICSMGE)*, Osaka, 2, 1037-1040.

Hight, D.W., Georgiannou, V.N. and Ford, C.J. (1994). Characterization of clayey sands. Proc. Int. Conf. on Behaviour of Offshore Structures, *BOSS '94*, Boston, 321-340.

House, A., Oliveira, J. and Randolph, M.F. (2001). Evaluating the coefficient of consolidation using penetration tests. *International Journal of Geotechnical and Geonvironmental Engineering*, 134, 1142-1153.

Idriss, I.M. (1999). An update to the Seed-Idriss simplified procedure for evaluating liquefaction potential. *Proc., TRB Workshop on New Approaches to Liquefaction.* Publication No. FHWA-RD-99-165. Federal Highway Administration.

Idriss, I.M. and Boulanger, R.W. (2003). Relating K_α and K_σ to SPT Blow Count and to CPT Tip Resistance for Use in Evaluating Liquefaction potential. *Proc. of the 2003 Dam Safety Conference*, ASDSO, Minneapolis.

Idriss, I.M. and Boulanger, R.W. (2004). Semi-empirical procedures for evaluating liquefaction potential during earthquakes. *Proc. 11th International Conference on Soil Dynamics and Earthquake Engineering*, Berkeley, 32-56.

Iwasaki, T., Tokida, K., Tatsuoka, F., Watanabe, S., Yasuda, S. and Sato, H. (1982). Microzonation for soil liquefaction potential using simplified methods. *Proc. of the 3rd International Conference on Microzonation*, Seattle, 3, 1319-1330.

Jaeger, R.A., DeJong, J.T., Boulanger, R.W., Low, H.E. and Randolph, M.F. (2010). Variable penetration rate CPT in an intermediate soil. , *2nd International Symposium on Cone Penetration Testing*, CPT'10, Huntington Beach, CA, USA.

Jamiolkowski, M., Ladd, C.C., Germaine, J.T. and Lancellotta, R. (1985). New developments in field and laboratory testing of soils. *Proceedings of the 11th International Conference on Soil Mechanics and Foundation Engineering*. San Francisco, California, 57-153.

Jamiolkowski, M., Ricceri, G. and Simonini, P. (2009). Safeguarding Venice from high tides: site characterization & geotechnical problems. M. Hamza, M. Shahien and Y. El-Mossallamy, eds. *17th International Conference on Soil Mechanics and Géotechnical Engineering,* Alexandria (Egypt). Amsterdan: IOS Press, 4, 3209-3227.

Janbu, N. (1963). Soil compressibility as determined by oedometer and triaxial tests. *Proc. European Conference of Soil Mechanics and Foundation Engineering*, Wiesbaden, Vol. 1, 19-25.

Janbu, N. (1969). The resistance concept applied to deformations of soils. *Proceedings of the VII International Conference on Soil Mechanics and Foundation Engineering*, Mexico, Vol. 1, 191-196.

Jefferies, M.G. and Been, K. (2006). *Soil liquefaction – A critical state approach*. Taylor & Francis, ISBN 0-419-16170-8 478 pages.

Jefferies, M.G. and Davies, M.P. (1991). Soil Classification by the cone penetration test: discussion. *Canadian Geotechnical Journal*, 28(1), 173-176.

Jefferies, M.G. and Davies, M.P. (1993). Use of CPTU to estimate equivalent SPT N60. Geotechnical Testing Journal, 16(4), 458-468.

Kim, K., Prezzi, M., Salgado, R. and Lee, W. (2008). Effect of penetration rate on cone penetration resistance in saturated clayey soils. *J. Geotechnical and Geoenvironmental Eng.*, 134(8), 1142-1153.

Kovari, K. and Amstad, C. (1982). A new method of measuring deformations in diaphragm walls and piles. *Géotechnique*, 32(4), 402-406.

Kulhawy, F.H., and Mayne, P.H. (1990). Manual on estimating soil properties for foundation design. *Electric Power Research Institute (EPRI)*, Palo Alto, Calif.

Ladd, C.C. and Foott, R. (1974). New design procedure for stability of soft clays. *Journal of the Geotechnical Engineering Division*, 100 (GT7), 763-786.

Ladd, C.C., Foott, R., Ishihara, K., Schlosser, F. and Poulos, H.G. (1977). Stress deformation and strength characteristics, State-of-the-Art-Report. *Proc. IX Int. Conf. on Soil Mechanics and Foundations Engineering*, Tokyo. 2, 421-494.

Lancellotta, R. (2008). *Geotechnical Engineering*, Taylor and Francis, ISBN 9780415420044 499 pp.

Lehane, B.M., O'Loughlin, C.D., Gaudin, C. and Randolph, M.F. (2009). Rate effects on penetrometer resistance in kaolin. *Géotechnique*, 41(1), 41-52.

Leroueil, S. (2006) The Isotache Approach. Where are we 50 years after its development by Professor Šuklje? - 2006 Prof. Šuklje's Memorial Lecture. *Proceedings of the XIII Danube- European Conference on Geotechnical Engineering*, Ljubljana, Slovenia. 1, 55–88.

Leroueil, S., Kabbaj, M., Tavenas, F. and Bouchard, R. (1985). Stress-strain-strain rate relation for the compressibility of sensitive natural clays. *Géotechnique*, 35(2), 159-180.

Lo Presti, D.C.F., Sassu, M., Luzi, L., Castaldini, D., Tosatti, G., Meisina, C., Zizzoli, D., Zucca, F., Rossi, G., Saccorotti, G. and Piccini, D. (2013). A Preliminary Report on the 2012 Seismic Sequence in Emilia (Northern Italy). *7th Conference on case histories in Geotechnical Engineering*, Chicago.

Lunne, T. and Andersen, K.H., (2007). Soft clay shear strength parameters for deepwater geotechnical design. *Proceedings 6th International Conference, Society for Underwater Technology*,

Offshore Site Investigation and Geomechanics, London, 151-176.

Lunne, T. and Christophersen, H.P. (1983). Interpretation of cone penetrometer data for offshore sands. *Proceedings of the Offshore Technology Conference*, Richardson, Tex. Paper No. 4464.

Lunne, T., Robertson, P.K. and Powell, J.J.M. (1997). *Cone penetration testing in geotechnical practice*. Blackie Academic. EF Spon/Routledge Publ. New York, 1997, 312 pp.

Madricardo, F., Donnici, S., Buogo, S., Calicchia, P., Lezziero, A., De Carli, F. and Boccardi E. (2007). Palaeoenvironment reconstruction in the Lagoon of Venice through wide-area acoustic surveys and core sampling. *Estuar Coast Shelf Sci*, 75, 205-213.

Marchetti, S., Monaco, P., Calabrese, M. and Totani, G. (2004). DMT predicted vs. measured settlements under a full-scale instrumented embankment at Treporti (Venice, Italy). Proceedings *of the 2nd International Conference on Site Characterization, ISC'2*, Porto, 2, 1511–1518.

Marcuson, W.F., III, Hynes, M.E. and Franklin, A.G. (1990). Evaluation and use of residual strength in seismic safety analysis of embankments. *Earthquake Spectra*, 6(3), 529-572.

Mayne, P.W. (1991). Determination of OCR in clays by piezocone tests using cavity expansion and critical state concepts. *Soils and Foundations*, 31(2), 65-76.

Mayne, P.W. (2005). Integrated ground behaviour: In-situ and lab tests. *Proceedings of the International Symposium on Deformation Characteristics of Geomaterials*, Lyon, France, 22-24 September 2005. Taylor & Francis Group, London. Vol. 2, 155-177.

Mayne, P.W. (2007*a*). Cone penetration testing: A synthesis of high-way practice. Project 20-5. Transportation Research Board, Washington, D.C. NCHRP synthesis 368.

Mayne, P.W. (2007*b*). Invited overview paper: In-situ test calibrations for evaluating soil parameters. *Characterization and Engineering Prop. of Natural Soils*, 3, 1602-1652.

Mayne, P.W. and Campanella, R.G. (2005). Versatile site characterization by seismic piezocone. *Proc. XVI ICSMGE*, 2: 721-724. Rotterdam: Millpress.

Mayne, P.W. and McGillivray, A. (2004). Seismic piezocone and seismic flat dilatometer tests at Treporti. *Proceedings of the 2nd International Conference on Site Characterization, ISC'2*, Porto,

Portugal, 19–22 September 2004. Rotterdam, the Netherlands. Vol. 2, pp. 1695–1701.

Meletti, C., Galadini, F., Valensise, G., Stucchi, M., Basili, R., Barba, S., Vannucci, G. and Boschi, E. (2008). A seismic source zone model for the seismic hazard assessment of the Italian territory. *Tectonophysics*, 450, 85-108.

Mesri, G. (1987). Fourth law of soil mechanics: a law of compressibility. *Proc. Int. Symp. Geotech. Engrg. of Soft Soils*, Mexico City, 2, 179-187.

Mesri, G. (2003). Primary compression and secondary compression. *ASCE Geotechnical Special Publication* 119, 122-166.

Mesri, G. and Castro, A. (1987). C_α/C_c concept and K_0 during secondary compression. *Journal of the Geotechnical Engineering Division, ASCE*, 113, 230-247.

Mesri, G. and Godlweski, P.M. (1977). Time and stress compressibility interrelationship. Journal of the Geotechnical Engineering Division, *ASCE* 103 (GT5), 417-430.

Mesri, G., Lo, D.O.K. and Feng, T.W. (1994). Settlement of embankments on soft clays. *Proc. Settlement '94, College Station, TX, ASCE Geotechnical Special Publication (GSP 40)*, (1), 8-56.

Moss, R.E.S., Seed, R.B. and Olsen, R.S. (2006). Normalizing the CPT for overburden stress. *J. Geotech. Geoenvirom. Eng.*, 132(3), 378-387.

Muir Wood, D. (2004). *Geotechnical Modelling*. Taylor and Francis, ISBN 0419237305 496 pages.

Myftaraga, E. and Koreta, O. (2013). Characteristic shear strength parameters derived from the cone penetration test. *2nd International Balkans Conference on Challenges of Civil Engineering, BCCCEE*, 783-792.

Nash, D. (2001). Modelling the effects of surcharge to reduce long term settlement of reclamations over soft clays. - A numerical case study. *Soils and Foundations*, 41(5), 1-13.

Nash, D.F.T. and Ryde, S.J. (2001). Modelling consolidation accelerated by vertical drains in soil subject to creep. Géotechnique 51(3), 257-273.

Neher, H.P., Wehnert, M. And Bonnier, P.G. (2001). An evaluation of soft soil models based on

trial embankments Proc. of the X International Conf. on Computer Methods and Advances in Geomechanics, 1, 373-378.

Oliveira, J.R.M.S., Almeida, M.S.S., Motta, H.P.G. and Almeida, M.C.F. (2011). Influence of penetration rate on penetrometer resistance. *J. Geotechnical and Geoenvironmental Eng.*, 137(7), 695-703.

Olsen, R.S. and Mitchell, J.K. (1995). CPT stress normalization and prediction of soil classification. *Proceedings of the International Symposium on Cone Penetration Testing*. Vol. 2, Swedish Geotechnical Society, Linkoping, 257-262.

Poulsen, R., Nielsen, B.N. and Ibsen, L.B. (2013). Correlation between cone penetration rate and measured cone penetration parameters in silty soils. *Proceedings of the 18th International conference on Soil Mechanics and Geotechnical Engineering,* 1, 603-606.

Poulsen, R., Nielsen, B.N., Ibsen, L.B. (2011). Effect of Drainage Conditions on Cone Penetration Testing in Silty Soils. *Proc. 64th Canadian Geotechnical Conference and 14th Pan-American Conference on Soil Mechanics and Engineering.* Toronto, ON, Canada.

Powell, J.J.M and Quarterman, R.S.T. (1988). The interpretation of cone penetration tests in clays, with particular reference to rate effects. *Proc. Int. Symp. on Penetration Testing*, 2, 903-309.

Powell, J.J.M., Quaterman, R.S.T. and Lunne, T. (1988). Interpretation and use of piezocone test in UK clays. *Proceedings of the Geotechnology Conference: Penetration Testing in the UK*, Birmingham, UK, 151-156.

Randolph, M.F. (2004). Characterisation of soft sediments for offshore applications. *Proc. Int. Conf. Geotechnical and Geophysical Site Characterization, ISC-2*, (Porto),1, 209-232. Millpress, The Netherlands.

Randolph, M.F. and Hope, S. (2004). Effect of cone velocity on cone resistance and excess pore pressures. *Proc. Int. Symp. on Eng. Practice and Performance of Soft Deposits*, Osaka, 147-152.

Ricceri, G., Simonini, P. & Cola, S. (2002) Applicability of piezocone and dilatometer to characterize the soil of Venice lagoon. *Geotechnical and Geological Engineering*, 20, 89-121.

Robertson, P.K., Campanella, R.G., Gillespie, D. and Greig, J. (1986*a*). Use of Piezocone Cone data. *In situ'86 Use of In-situ testing in Geotechnical Engineering*, GSP 6, ASCE, Reston, VA, Specialty Publication, 1263-1280.

Robertson, P.K. (1990). Soil classification using the cone penetration test. *Canadian Geotechnical Journal*, 27(1), 151-158.

Robertson, P.K. (2009). Interpretation of cone penetration tests – a unified approach. *Canadian Geotechnical Journal*, 46(11), 1337-1355.

Robertson, P.K. (2010*a*). Soil behaviour type from the CPT: an update, *2nd International Symposium on Cone Penetration Testing*, CPT'10, Huntington Beach, CA, USA.

Robertson, P.K. (2010*b*). Estimating in-situ state parameter and friction angle in sandy soils from the CPT. *2nd international Symposium on Cone Penetration Testing*, CPT'10. Huntington Beach, CA, USA.

Robertson, P.K. (2012). Interpretation of in-situ tests – some insights. *Proceedings ISC-4: the forth international conference on site characterization*. Vol. 1. A. Balkema, CRS Taylor & Francis. 3-24.

Robertson, P.K. and Cabal, K.L (2012). *Guide to cone penetration testing*. Gregg Drilling and Testing, Inc., California.

Robertson, P.K. and Campanella, R.G. (1983). Interpretation of cone penetration tests. Part I: sand. *Canadian Geotechnical Journal*, 20(4), 718-733.

Robertson, P.K. and Campanella, R.G. (1985). Liquefaction potential of sands using the cone penetration test, *Journal of Geotechnical Engineering*, ASCE, 22(3), 298-307.

Robertson, P.K. and Fear, (1995). Liquefaction of sands and its evaluation. Keynote lecture. *IS Tokyo'95, Proc. of the 1st International Conference on Earthquake Geotechnical Engineering*. A.A. Balkema. Amsterdam.

Robertson, P.K. and Wride, C.E. (1998). Evaluating cyclic liquefaction potential using the cone penetration test. *Canadian Geotechnical Journal*, 35(3), 442-459.

Robertson, P.K., Campanella, R.G., Gillespie, D. and Rice, A. (1986*b*). Seismic CPT to measure in-situ shear wave velocity. *Journal of the Geotechnical Engineering Division*, ASCE, 112(8), 791-803.

Schmertmann, J.H. (1978). *Guidelines for cone penetration tests performance and design*. Federal Highways Administration, Washington, D.C., Report FHWA-TS-78-209.

Schnaid, F., Bedin, J. and Costa Filho, L.M. (2010). Drainage characterization of tailings from in situ test, *Proc. 2nd Int. Symp. on Cone Penetration Testing*, Huntington Beach, CA.

Schnaid, F., Lehane, B.M. and Fahey, M. 2004. Characterisation of unusual geomaterials, *Proc. Int. Conf. Geotechnical and Geophysical Site Characterization, ISC-2*, Porto (Portugal), 1, 49-73.

Schneider J.A.,Lehane, B.M. and Schnaid, F. (2007). Velocity effects on piezocone measurements in normally and overconsolidated clays. *Int. J. Physical Modelling in Geotechnics*, 2, 23-34.

Schneider, J.A., Randolph, M.F., Mayne, P.W. and Ramsey, N.R. (2008). Analysis of factors influencing soils classification using normalized piezocone tip resistance and pore pressure parameters. *Journal Geotechnical and Geoenvironmental Engrg*. 134(11), 1569-1586.

Seed, H.B. and Idriss, I.M. (1971). Simplified procedure for evaluating soil liquefaction potential. *Journal of Soil Mechanics and Foundations Division*, ASCE, 97(SM9), 1249-1273.

Seed, H.B., Tokimatsu, K., Harder, L.F. and Chung, R. (1985). Influence of SPT procedures in soil liquefaction resistance evaluations. *Journal of Geotechnical Engineering*, ASCE, 111(2), 1425-1445.

Sekiguchi, H. (1977). Rheological characteristics of clays. *Proceedings 9th International Conference on Soil Mechanics and Foundation Engineering*, Vol. 1, Tokyo, 289-292.

Senneset, K., Sandven, R. and Janbu, N. (1989). Evaluation of soil parameters from piezocone tests. *Transportation Research Record*, 1235, 24-37.

Senneset, K., Sandven, R., Lunne, T., By, T. and Amundsen, T. (1988). Piezocone tests in silty soils. *Proceedings of the First International Symposium on Penetration Testing*, ISOPT-1, Or-

lando, 2, 955-966.

Silva, M.F., White, D.J. and Bolton, M.D. (2006). An analytical study of the effect of penetration rate on piezocone tests in clay. *Int. J. Numer. Anal. Methods Geomech.*, 30(6), 501-527.

Simonini, P. (2004) Characterisation of the Venice lagoon silts from in- situ tests and the performance of a test embankment. *Proceedings of the II International Conference on Site Characterization*, Porto, 1, 187-207.

Simonini, P., Ricceri, G. and Cola, S. (2007). Geotechnical characterization and properties of Venice lagoon heterogeneous silts. *Proc. 2nd International Workshop on Characterization and Engineering Properties of Natural Soils*, Singapore. London: Taylor and Francis, 2289-2327.

Sonmez, H. (2003). Modification to the liquefaction potential index and liquefaction susceptibility mapping for a liquefaction-prone area (Inegol, Turkey). *Environ. Geology*, 44(7), 862-871

Sonmez, H. and Gokceoglu, C. (2005). A liquefaction severity index suggested for engineering practice. *Environ. Geology*, 48, 81-91.

Stark, T.D. and Olson, S.M. (1995). Liquefaction resistance using CPT and field case histories. *Journal of Geotechnical Engineering*, ASCE, 121(2), 856-869.

Strozzi, T., Teatini, P. and Tosi, L. (2009). TerraSAR-X reveals the impact of the mobile barrier works on the Venice coastal stability. *Remote Sens. Environ*. 113, 2682-2668.

Šuklje, L. (1957). The analysis of the consolidation process by the isotache method. *Proc. 4th Int. Conf. on Soil Mech. and Found. Engng.* London, 1, 200-206.

Suzuki, Y., Lehane, B.M. and Fourie, A. (2012). Effect of penetration rate on piezocone parameters in two silty deposits. *Proc. ISC'4 – Geotechnical and Geophysical Site Characterization*, 809-815.

Teatini, P., Strozzi, T., Tosi, L., Wegmüller, U., Werner, C. and Carbognin, L. (2007). Assessing short- and long-time displacements in the Venice coastland by synthetic aperture radar interferometric point target analysis. *J. Geophys. Res*. 112: F01012.

Teatini, P., Tosi, L., Strozzi, T., Carbognin L., Cecconi, G., Rosselli, R. and Libardo, S. (2010).

Resolving land subsidence within the Venice Lagoon by persistent scatterer SAR interferometry. *Phys. Chem. Earth*.

Teh, C.I. and Houlsby, G.T. (1991). An analytical study of the cone penetration test in clay. *Géotechnique*, 41(1), 17-34.

Tonni, L. and Gottardi, G. (2009). Partial drainage effects in the interpretation of piezocone tests in Venetian silty soils. *17th ICSMGE,* 5-9 October 2009 Alexandria (Egypt). Amsterdan: IOS Press, 2, 1004-1007.

Tonni, L. and Gottardi, G. (2010). Interpretation of piezocone tests in Venetian silty soils and the issue of partial drainage. R.Y. Liang, F. Zhang and K. Yang, eds. *Proc. of the 2010 GeoShanghai International Conference, Deep Foundations and Geotechnical In Situ Testing, ASCE Geotechnical Special Publication* (205 GSP), 367-374.

Tonni, L. and Gottardi, G. (2011). Analysis and interpretation of piezocone data on the silty soils of the Venetian lagoon (Treporti test site). *Can. Geotech. J*. 48, 616-633.

Tonni, L. and Simonini, P. (2013). Evaluation of secondary compression of sands and silts from CPTU. *Geomechanics and Geoengineering*, 8(3), 141-154.

Tonni, L., García Martínez, M.F. and Simonin, P. (2013). Predicting long-term settlements of coastal defences for the safeguard of the Venetian Lagoon. *Proc. 18th ICSMGE*, 3325-3328.

Tonni, L., Gottardi, G. and Simonini, P. (2011). Piezocone data and state parameter interpretation for Venetian silty soils. *5th International Symposium on Deformation Characteristics of Geomaterials, IS-Seoul 2011*, 1-3 September 2011, Seoul, Korea. Seoul: Hanrimwon Co., 1260-1267.

Tonni, L., Gottardi, G., Berengo, V. and Simonini, P. (2010). Classification, overconsolidation and stiffness of Venice lagoon soils from CPTU. P.K. Robertson and P.W. Mayne, eds. *2nd Int. Symp. On Cone Penetration Testing. CPT' 10*, 9-11 May 2010, Huntington Beach (CA). Los Angeles: Omnipress, 567-574.

Tosi, L., Rizzetto, F., Zecchin, M., Brancolini, G. and Baradello, L. (2009*a*). Morphostratigraphic framework of the Venice Lagoon (Italy) by very shallow water VHRS surveys: Evidence of radical changes triggered by human-induced river diversion. *Geophys. Res. Lett.*, 36: L09406.

Tosi, L., Teatini, P., Bincoletto, L., Simonini, P. and Strozzi, T. (2012). Integrating geotechnical and interferometric SAR measurements for secondary compressibility characterization of coastal soils. *Surveys in Geophysics*, 33(5), 907-926.

Tosi, L., Teatini, P., Carbognin, L. and Brancolini, G. (2009*b*). Using high resolution data to reveal depth-dependent mechanisms that drive land subsidence: the Venice coast, Italy. *Tectonophysics*, 474(1-2), 271-284.

Velić, J. And Malvić, T. (2011). Depositional conditions during Pliocene and Pleistocene in Northern Adriatic and possible lithostratigraphic division of these rocks. *Nafta*, 62, 1-2, 25-38.

Vermeer, P.A. and Neher, H.P. (1999). A soft soil model that accounts for creep. *Proc. Int. Symp. "Beyond 2000 in Computational Geotechnics"*, 249-261.

Vermeer, P.A., Leoni, M., Karstunen, M. and Neher, H.P. (2006) Modelling and numerical simulation of creep in soft soils. *Proceedings of the IV International Conference on Soft Soil Engineering*, Vancouver, 57-71.

Waterman, D. and Broere, W. (2011). *Practical application of the soft soil creep model.* Part I. Plaxis bulletin 15, 14-15.

Wroth, C.P. (1984). The interpretation of in-situ soil tests: Rankine Lecture. *Géotechnique*, 34(4), 449-489.

Wroth, C.P. (1988). Penetration testing – A more rigorous approach to interpretation. *First International Symposium on Penetration Testing, ISOPT-1*, 20-24 March 1988, Orlando. Rotterdam: Balkema, 1, 303-311.

Zhang, G., Robertson, P.K. and Branchman, R.W.I., (2002), Estimating Liquefaction induced Ground Settlements From CPT for Level Ground, *Canadian Geotechnical Journal*, 39(5), 1168-1180.

Zhang, Z. and Tumay, M.T. (1999). Statistical to fuzzy approach toward CPT soil classification. *Journal of Geotechnical and Geoenvironmental Engineering*, 125(3), 179-186.

Internet Sources:

Mayne, P.W. (2002). Flow Properties from Piezocone Dissipation Tests. Georgia Tech. Available at: http://geosystems.ce.gatech.edu/Faculty/Mayne/papers/. Retrieved 5 March 2014.

MOSE Project, Venice, Venetian Lagoon, Italy. water-technology.net. Available at: http://www.water-technology.net/projects/mose-project. Retrieved 25 Feb. 2014.

Mose System. Sal.ve. Available at: http://www.salve.it/uk/soluzioni/acque/f_mose.htm. Retrieved 25 Feb. 2014.

Plaxis user manual. Available at: www.plaxis.nl

Problems: High waters. Sal.ve. Available at: http://www.salve.it/uk/soluzioni/f_acquealte.htm. Retrieved 25 Feb. 2014.